Constraining Extended Theories of Gravity by Large Scale Structure and Cosmography

by

Vincenzo Salzano

Thesis submitted in satisfaction of
the final requirement for the Degree of

Philosophiæ Doctor

in

Fundamental and Applied Physics

SUPERVISOR
Salvatore Capozziello

COORDINATOR
Lorenzo Marrucci

Università degli Studi di Napoli Federico II
Dipartimento di Scienze Fisiche

December 2008

A
CiaoTatmanSakimi18agosto Panchina Alba PioggiaCavaHippoRomaTantotantotantoFirenzeG2 AltroveBacettoOrniStazionePuglia SlowAmelieVicini Vicini Masone Lorenzo Arianna Valeriollaria Girella Il sole sei tu e la luna sei tu e il vento sei tu Krauss Rifugio Dido Aaaah Risate 0909 Futuro Tu Ti Amo
R

Two monks were arguing about a flag. One said:

`"The flag is moving."`

The other said:

`"The wind is moving."`

The sixth patriarch happened to be passing by. He told them:

"Not the wind, not the flag; mind is moving."

Mumonkan - Case 29: Not the Wind, Not the Flag

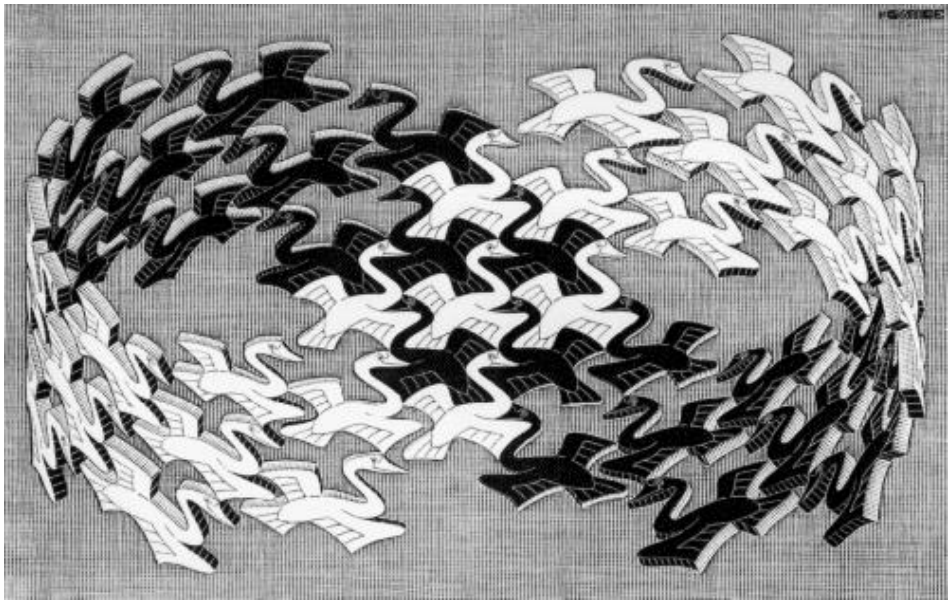

"Swans", 1956, wood engraving, Escher M.C.

Contents

Abstract

The main aim of this thesis is to show the viability of Extended Theories of Gravity in substituting General Relativity-based cosmological models in the explanation of Universe Dynamics and Origin.

After a brief review of all the questions posed by General Relativity and all the possible solutions to these ones, we start to describe deeper one of the alternative approaches to Gravity and Universe, namely the Extended Theories of Gravity.

In this context we have chosen to work with a particular class of these theories, the $f(R$-gravity models, so named because of starting from a general gravitational lagrangian, where the classical R term of the Hilbert-Einstein one is substituted by a general function $f(R)$.

We will start with a brief review of history, motivations, pros and cons of these approaches. We also review some results from literature about the cosmological mimicking of dark components as a curvature (i.e. geometrical) effect of $f(R)$ geometry and the possibility to explain rotational curves of spiral galaxies.

Then we pass to the original works presented in these pages. We think that we can extract three main characteristics of our work:

- We have never adopted a particular, well defined $f(R)$ model, in contrast with other works; we have always tried to work in the most general hypothesis it was possible. When we will show results of our analysis on clusters of galaxies, it is important to underline that they only rely on the assumption of an analytical Taylor expandable $f(R)$, without any other specification. In the case of cosmological applications, namely in the Cosmography chapter, we could say that we have worked in an even more general scenario: we chose Cosmography because it is a model independent approach to observational data, so we have no basic hypothesis not only on the mathematical form of the $f(R)$- model, but even on the nature of the universe dynamics (General Relativity or $f(R)$ one);

- Starting from previous point we have tried to give constraints to the hypothetical form of the $f(R)$-theories: we have derived values of some of the parameters that a viable $f(R)$-model should have to explain some of the question we have explored (mass profile

of clusters of galaxies). We have also explored connections between General Relativity-based (dark energy ones) and $f(R)$-based models (in cosmography) studying their mutual mimicking ability and the possibility of discriminate between them;

- Last, but not least, our analysis has the important merit of having a strong predictive power, so that it can be confirmed or confuted by comparing with some tests. From the Cosmography-based analysis, we are strongly dependent on the experimental possibilities of future surveys: if we will not have measurements within a certain sensibility range we were not be able (or we will have few possibilities) to discriminate what approach is right and what one is wrong. On the contrary, in the case of clusters of galaxies, we are able to do predicitions on results which could come from the application of $f(R)$-models to different scales of gravitational systems (galaxies, solar system). If these predictions were exact, then we would have a solid and well founded theoretical model of gravity in alternative to General Relativity.

Even if many results we had make us confident to be on the right way, it is important to underline also that our work is always built on a *conservative* hypothesis. We don't think that $f(R)$ gravity is not the theory of gravity (like General Relativity is not), but it is an important and interesting toy model which can take us nearer an effective and deeper comprehension of gravity.

List of Publications

- Capozziello, S., Cardone, V.F., **Salzano**, **V.**,
  "Cosmographic parameters in f(R) theories", Physical Review D 78, 063504 (2008)
- Capozziello, S., De Filippis, E., **Salzano**, **V.**,
  "Modelling clusters of galaxies by f(R)-gravity", Submitted to MNRAS
- Capozziello, S., Cardone, V.F., Molinaro, R., **Salzano**, **V.**,
  "The Sersic Virial Hyperplane", Submitted to MNRAS
- Capozziello, S., Lazkoz, R., **Salzano**, **V.**,
  "New insights in cosmography with Markov chains", in preparation

List of Figures

List of Tables

Part I
General Relativity vs Extended Theories of Gravity

CHAPTER 1

Introduction

1.1 Poetics of Gravity

Is there any man in the world who can affirm not knowing gravity? Surely not.
Gravity is probably the *"most fundamental"* of the fundamental forces we know to be in the universe. Even if we were not be able to find words to define it, we would have the every-day experience testifying its presence.
Why are we afraid to fall down when flying? Why cannot we touch sun and stars when jumping? And now, let's take a look to the nature: why are the highest branches of trees thinner and shorter than the lowest ones? Why is mount Everest "only" 8848 meters high and not 10000 or 100000? Why do rain drench our clothes instead of aliens' ones?
We have experience of gravity for all our life starting from our birth; after primary school we learn to say the word "gravity" and during college we learn to call with this name the hidden cause of any of the events we have spoken before... and of many many many other things...
Moreover gravity is also the most enigmatic force we know: we are not able to understand it in all its entirety just because we cannot study it from "outside", we are inside it everywhere, and probably without it man beings would not exist.
But we (who is writing) are not poets or philosophers: we are trying to be scientists.
So we need a definition for gravity; we need a mathematical description of gravity; we need to imagine experiments or places or physics where there is no gravity.
In few words: we need and want to study and understand gravity.
And how can we do this? What are our instruments?
It is obvious we cannot go in any place of the universe we want with our Cavendish balance to measure gravity. We could extrapolate our knowledge of gravity to any dimensional scale out to border of universe.
But: would be this right? Can we use "now" and "here" as synonyms of "always" and "everywhere"? What a boring universe would be if this was right! But we think that a

negative answer would be considered a wise and conservative answer by many men (and many scientists).
We will see that the story is not so linear. There are now two scientific *"thinking schools"*, or two Zen monks (like the two ones in the starting epigraph) who explain the same things in two completely different ways.
Who is right and who is wrong? Unfortunately nowadays nothing and nobody is able to discriminate between the two monks. We agree that we can make all the possible technical or theoretical disquisitions but the truth can be found only comparing theory with data from reality.
For this reason in this thesis we will propose and describe a particular view of the question we are going to face with giving also a strong correlation with what now we are able to found out from what is around us.
To start we need to start thinking to the possible answer to these questions:

What we know about gravity in a scientific way?
What can we find out from reality?
What are the possible solutions?

1.2 Brief History of Gravitational Theory

The answer to the first question is a good reason to give a brief historical summary of the evolution of gravity in science.
The XVII century was the starting milestone of gravitational theory greeting to Galileo and Newton. Galileo was the first scientist to conceive an experiment to test gravity; his pendulum and the spheres he threw down the Leaning tower of Pisa, are studied as the realization of his idea of the *experimental method*, which is now one of the principles of our scientific way of reasoning and investigating nature.
But Galileo *only* tested terrestrial gravity.
It was Newton who first formulated a *theory of gravitation* unifying terrestrial and celestial worlds, the apple falling down the tree and the Moon going around the Earth. The summa of its theoretical apparatus was the most famous *law of inverse-square gravitational force*: two massive bodies, m_1 and m_2, located in the space at positions $\vec{\mathbf{r_1}}$ and $\vec{\mathbf{r_2}}$, attract mutually each other with a gravitational force given by:

$$\vec{\mathbf{F}} = \frac{G\, m_1\, m_2}{|\vec{\mathbf{r_2}} - \vec{\mathbf{r_1}}|^3}\, (\vec{\mathbf{r_2}} - \vec{\mathbf{r_1}}) \tag{1.1}$$

where G is the notorius *gravitational constant*. All we know that any event requiring gravity in our *local* world is very well described by this mathematical law. But now we are more interested in the theoretical background of this formula: what were the key ideas of Newton? He assumed:

- Space and Time are *absolute* entities;
- the *Equivalence* of Inertial and Gravitational mass (the now-called Weak Equivalence Principle).

And we can also add another not explicit idea:

- the *numerical* factor G is a *universal constant*.

How long did Newton's conceptual basis of gravity stay untouched?
Answer to this question is historically related to another problem. We have before underlined that Newton's gravitational law is able to describe events in our *local* world.
But what does *local* mean? How large is this *local* world?
In this case Nature has joked us: in the XIX century it gave a triumph and a failure of Newtonian theory at the same time.
Using Newton's law, John Couch Adams and Urbain Le Verrier predicted the exact orbits and position of planets in Solar System. From their calculations it was possible to explain the particular motion of Uranus as depending on the presence of a new planet in the Solar System, which was later discovered and named Neptune. But with the same calculations, precessional perturbations in the orbit of Mercury were found. And these ones *could not* be described by Newton's gravitational theory without supposing another planet being in the system. But it was never found (and it doesn't exist!).

This was not the only hit to Newton's theory. At the end of XIX century Ernst Mach stated what was later called by Albert Einstein, "Mach's principle", which can be considered the *anti-formulation* of Newton's idea of Space and Time as absolute entities. Einstein stated the principle saying: *"... inertia originates in a kind of interaction between bodies..."*.
So the new idea is that the inertia of any system is given by the interaction of it with all the universe and depends on its motion with respect to all the other bodies in the universe. We have no more an inertia relative to the absolute frame of space; the local inertial frame is determined by some average of the motion of distant astronomical objects. Another interpretation of Mach's principle was given by Dicke and is related to the gravitational constant: if inertia depends on the mass distribution on the universe, is G really a constant? The gravitational coupling G can be scale-dependent and related to some scalar field. As a consequence, the concept of "inertia" and the Equivalence Principle have to be revised.

All these questions found a new re-formulation in the mirabilis XX century, with Albert Einstein and his Special Theory of Relativity and General Theory of Relativity. With the Special Relativity Einstein was intended to face with the compatibility problem between mechanics and electro-magnetism; clearly it was a non gravitational problem. But he obtained the definitive formalization of space and time as non absolute entities (and more: they have to be considered together as a *unique* coordinates system). The *new* question now was that Special Relativity was able to describe all the inertial frames but not the accelerated systems (like a gravitational one); the generalization of his ideas to these systems came with the General Relativity. At that time we were in a world where no absolute concepts existed, where inertial and gravitational mass were the same and data from observations were well fitted by the new theory. Mercury precession (already observed) and the gravitational deflection of light by Sun (predicted for the first time) were successfully verified and explained, solving the open questions of Newton's gravitational theory.

Let's take a breath now and give a brief summary of the conceptual evolution of gravity. We may say:

Newton build up the first complete theoretical apparatus of gravitational theory

$\Downarrow$

Comparing with observations there were some problems
We need a new formulation of gravity

⇓

Einstein formulated his Theory of General Relativity

⇓

General Relativity has solved previous problems
Are there other new questions fighting against General Relativity?

It is useful to remember that General Relativity contains Newton's gravity as a *limited* case: working in some range of gravitational field strength and velocities, General Relativity reduces to Newton's theory.
Then what is important to underline at this steps is that General Relativity *is* the complete theory of gravity and any result from observation has to be compared with it. Any failure in this context can be explained in two ways:

- Data are wrong, or our interpretation of data is wrong;
- General Relativity is wrong, or, in a conservative approach, it has to be *modified*.

Then we poses another dilemma:

General Relativity, or Not General Relativity: that is the question.

1.3 Shortcomings of General Relativity

Now we want to find an answer to the second question we posed in the preparatory section: What can we find out from reality?
Without doubts the weight and influence of General Relativity on history of science and on human approach to questions not only of scientific relevance but also *more than* scientific (where does universe come from? what is the fate of the universe?) is extremely powerful.
But are we sure that the General Relativity is *THE* theory of gravitation? Is it possible that it could come into problems like it happened for Newtonian formulation in the past?
The answer is positive and the found shortcomings are related both to many theoretical aspects and to observational results. In this chapter we will try to summarize these problems. An important issue has to be underlined: even if there are many problems, the reaction of scientific community is not uniform. The two Zen monks we were speaking in previous section and in the epigraph define very well the debate and the two possible answers to the breakout of General Relativity. In a very simple scheme we can summarize the guide lines of these two views:

- There are problems with General Relativity: these ones depend on some *unknown* and *invisible* ingredients which we have not yet discovered (the so called *dark energy* and *dark matter* components). But the fundamental requirement is that the General Relativity still remains the definitive gravitational theory. In this class of solutions is the so-called *Consensus Cosmological Model*, the **ΛCDM model**, the Λ Cold Dark Matter Model. It is interesting that this model is referred to as a consensus model, namely the model which picks up the greatest number of agreements in scientific community giving its greatest number of successes (with respect of other models) in comparing with observational data;

- There are problems with General Relativity: our knowledge of gravity is not complete (this one sounds like a sort of declaration of *ignorance*). We don't need to request for the existence of some unknown ingredients in the dynamics of universe; instead we investigate and study possible breakouts and extensions of General Relativity, even in a wider theoretical apparatus which contains General Relativity as a limit, such as Newton's theory is a limit in General Relativity. Some of the most fruitful alternative approaches to General Relativity are the **Extended Theories of Gravity**, which have become a sort of paradigm in the study of gravitational interaction.

This classification is simple only at a first sight; inside each view there is a plethora of competing theories and it is really difficult to orientate among them. Unfortunately we have not the possibility to discriminate among them at the moment; but it is important and useful to understand the war horses of anyone.

1.4 General Relativity and Quantum Field Theory

In the last thirty years, several shortcomings came out in the Einstein theory and people began to investigate whether General Relativity is the only fundamental theory capable of explaining the gravitational interaction. Such issues come, essentially, from cosmology and quantum field theory.
What about Quantum Field Theory? General Relativity and Quantum Field are clearly the two pillars of modern physics. Each one describing its range of physical phenomena: General Relativity is for gravitational systems and non-inertial frames from a classical point of view or on large scales, while Quantum Field Theory is valid in high energy regimes and smaller scales where a classical description is no more possible.
What happens if we have a strong gravitational field at small quantum scales? Are the two theories compatible? Of course there is no precise proof that gravity should have some quantum representation at high energies or small scales. Then the gravitational interaction is so weak that the scale where one expects non-classical behaviour of gravity is about 10^{-33} cm. Clearly, this is a non-accessible scale by our experiments and instruments now and probably in the future too.
The *unification* of these two pillars is expected and preferred for many reasons [52, 195]; but the conceptual assumptions they are based on seem to be irreconcilable. Quantum Field Theory considers time a given entity and spacetime a fixed arena where phenomena take place; for General Relativity time is dynamical and not such a relevant concept. Then in Quantum Field Theory there is the Heisenberg's uncertainty principle, which is not present in General Relativity being this one a classical theory.
Finally: General Relativity is a *classical* theory which does not work as a fundamental theory when one wants to achieve a full quantum description of spacetime (and then of gravity).

1.5 The Standard Cosmological Model

1.5.1 Overview

While things on small scales are quite doubtful, on larger scale we expect that gravitational interaction is the most important of the fundamental forces. So gravity should be the force which drives the cosmological evolution.
From a phenomenological point of view, there are some minimal requirements that any relativistic theory of gravity has to match. First of all, it has to explain the astrophysical observations (e.g. the orbits of planets, the potential of self-gravitating structures). This means that it has to reproduce the Newtonian dynamics in the weak-energy limit. Besides, it has to pass the classical Solar System tests which are all experimentally well founded.
As second step, it should reproduce galactic dynamics considering the observed baryonic constituents (e.g. luminous components as stars, sub-luminous components as planets, dust and gas), radiation and Newtonian potential which is, by assumption, extrapolated to galactic scales.
Thirdly, it should address the problem of large scale structure (e.g. clustering of galaxies) and finally cosmological dynamics, which means to reproduce, in a self-consistent way, the cosmological parameters as the expansion rate, the Hubble constant, the density parameter and so on. Observations and experiments, essentially, probe the standard baryonic matter, the radiation and an attractive overall interaction, acting at all scales and depending on distance: the gravity.
The simplest theory which try to satisfies the above requirements is the Theory of General Relativity. As we have said it is firstly based on the assumption that space and time have to be entangled into a single spacetime structure, which, in the limit of no gravitational forces, has to reproduce the Minkowski spacetime structure. Einstein profitted also of ideas earlier put forward by Riemann, who stated that the Universe should be a curved manifold and that its curvature should be established on the basis of astronomical observations.
In other words, the distribution of matter has to influence point by point the local curvature of the spacetime structure. The theory, eventually formulated by Einstein in 1915, was strongly based on three assumptions that the Physics of Gravitation has to satisfy.
The "*Principle of Relativity*", that amounts to require all frames to be good frames for Physics, so that no preferred inertial frame should be chosen a priori (if any exist).
The "*Principle of Equivalence*", that amounts to require inertial effects to be locally indistinguishable from gravitational effects (in a sense, the equivalence between the inertial and the gravitational mass).
The "*Principle of General Covariance*", that requires field equations to be "generally covariant" (today, we would better say to be invariant under the action of the group of all spacetime diffeomorphisms).
And - on the top of these three principles - the requirement that causality has to be preserved (the "*Principle of Causality*", i.e. that each point of spacetime should admit a universally valid notion of past, present and future).
Let us also recall that the older Newtonian theory of spacetime and gravitation - that Einstein wanted to reproduce at least in the limit of small gravitational forces (what is called today the "post-Newtonian approximation") - required space and time to be absolute entities, particles moving in a preferred inertial frame following curved trajectories, the curvature of which (i.e., the acceleration) had to be determined as a function of the sources (i.e., the "forces").
On these bases, Einstein was led to postulate that the gravitational forces have to be expressed by the curvature of a metric tensor field $ds^2 = g_{\mu\nu}dx^\mu dx^\nu$ on a four-dimensional spacetime

manifold, having the same signature of Minkowski metric, i.e., the so-called "Lorentzian signature", herewith assumed to be $(+,-,-,-)$. He also postulated that spacetime is curved in itself and that its curvature is locally determined by the distribution of the sources, i.e. - being spacetime a continuum - by the four-dimensional generalization of what in Continuum Mechanics is called the "matter stress-energy tensor", i.e. a rank-two (symmetric) tensor $T^m_{\mu\nu}$. Once a metric $g_{\mu\nu}$ is given, its curvature is expressed by the Riemann (curvature) tensor

$$R^{\alpha}{}_{\beta\mu\nu} = \Gamma^{\alpha}_{\beta\nu,\mu} - \Gamma^{\alpha}_{\beta\mu,\nu} + \Gamma^{\sigma}_{\beta\nu}\Gamma^{\alpha}_{\sigma\mu} - \Gamma^{\sigma}_{\beta\mu}\Gamma^{\alpha}_{\sigma\nu} \tag{1.2}$$

where the comas are partial derivatives. Its contraction

$$R^{\alpha}{}_{\mu\alpha\nu} = R_{\mu\nu}\,, \tag{1.3}$$

is the "Ricci tensor" and the scalar

$$R = R^{\mu}{}_{\mu} = g^{\mu\nu}R_{\mu\nu}\,, \tag{1.4}$$

is called the "scalar curvature" of $g_{\mu\nu}$. Einstein was led to postulate the following equations for the dynamics of gravitational forces

$$R_{\mu\nu} = \frac{\kappa}{2}T^m_{\mu\nu} \tag{1.5}$$

where $\kappa = 8\pi G$, with $c = 1$, is a coupling constant. These equations turned out to be physically and mathematically unsatisfactory.
As Hilbert pointed out, they were not of a variational origin, i.e. there was no Lagrangian able to reproduce them exactly (this is slightly wrong, but this remark is unessential here). Einstein replied that he knew that the equations were physically unsatisfactory, since they were contrasting with the continuity equation of any reasonable kind of matter. Assuming that matter is given as a perfect fluid, that is

$$T^m_{\mu\nu} = (p+\rho)u_\mu u_\nu - pg_{\mu\nu} \tag{1.6}$$

where $u_\mu u_\nu$ is a comoving observer, p is the pressure and ρ the density of the fluid, then the continuity equation requires $T^m_{\mu\nu}$ to be covariantly constant, i.e. to satisfy the conservation law

$$\nabla^\mu T^m_{\mu\nu} = 0 \tag{1.7}$$

where ∇^μ denotes the covariant derivative with respect to the metric.
In fact, it is not true that $\nabla^\mu R_{\mu\nu}$ vanishes (unless $R = 0$). Einstein and Hilbert reached independently the conclusion that the wrong field equations had to be replaced by the correct ones

$$G_{\mu\nu} = 8\pi G\, T^m_{\mu\nu} \tag{1.8}$$

where

$$G_{\mu\nu} = R_{\mu\nu} - \frac{1}{2}g_{\mu\nu}R \tag{1.9}$$

that is currently called the "Einstein tensor" of $g_{\mu\nu}$. These equations are both variational and satisfy the conservation laws since the following relation holds

$$\nabla^\mu G_{\mu\nu} = 0 \tag{1.10}$$

as a byproduct of the so-called "Bianchi identities" that the curvature tensor of $g_{\mu\nu}$ has to satisfy.

The Lagrangian that allows to obtain the field equations is the sum of a "matter Lagrangian" $\mathcal{L}_m$, the variational derivative of which is exactly $T^m_{\mu\nu}$, i.e.

$$T^m_{\mu\nu} = \frac{\delta \mathcal{L}_m}{\delta g^{\mu\nu}} \tag{1.11}$$

and of a "gravitational Lagrangian", currently called the Hilbert-Einstein Lagrangian

$$\mathcal{L}_{HE} = g^{\mu\nu} R_{\mu\nu} \sqrt{-g} = R\sqrt{-g} \tag{1.12}$$

where $\sqrt{-g}$ denotes the square root of the value of the determinant of the metric $g_{\mu\nu}$.
Under the assumptions of homogeneity and isotropy, the metric can take the form

$$ds^2 = -dt^2 + a^2(t)\left[\frac{dr^2}{1-kr^2} + r^2 d\theta^2 + r^2 \sin^2\theta d\phi^2\right], \tag{1.13}$$

known as the Friedmann-Lemaître-Robertson-Walker metric (FLRW). $k = -1, 0, 1$ according to whether the universe is hyperspherical ("closed"), spatially flat, or hyperbolic ("open") and $a(t)$ is called scale factor. Inserting this metric in Eq.(1.9) and using Eq.(1.6) one gets the following equations, the **Friedmann equations**:

$$\left(\frac{\dot{a}}{a}\right)^2 = \frac{8\pi G}{3}\rho - \frac{k}{a^2}, \tag{1.14}$$

$$\frac{\ddot{a}}{a} = -\frac{4\pi G}{3}(\rho + 3p), \tag{1.15}$$

where an overdot denotes differentiation with respect to coordinate time t. By imposing homogeneity and isotropy as unchanged characteristics of the universe, the evolution is affected by the only remaining variable: the scale factor $a(t)$. Friedmann equations are differential equations in the scale factor and tell us about the velocity and the acceleration of the expansion or contraction of the universe.
According to Big Bang theory the universe starts expanding with some initial velocity; modality of expansions depends on the quantity of matter and on the geometric properties of the universe. If $k = 0$ the universe is spatially flat and from Eq.(1.14) implies that it has to become infinite, with ρ approaching zero, in order for the expansion to halt. If $k = 1$ expansion can halt at a finite density at which the matter contribution is balanced by the k-term; in this case the universe will stop to expanding and will recollapse. For $k = -1$ even if matter is completely dissolved, curvature will drive expansion which can never halt and lasts forever.
From Eq.(1.15) we see that the acceleration of expansion is not driven by curvature, but only by matter content; it states an expected and simple intuition: gravitational interaction is always attractive (because of the ordinary matter pressure is positive).
We can say that Friedmann equations state well-defined conclusions:
If, according to Big Bang scenario, the universe is expanding, then, with General Relativity and ordinary matter considerations, the expansion should always be decelerated.

1.5.2 Problems

Are the hypothesis of homogeneity and isotropy valid for any time in cosmic evolution? Is the description of the Universe with Big Bang and Friedmann equations self-consistent and able to describe finely cosmic dynamics? There are no simple answer to these questions if even the

idea that the expansion should always be decelerated is not so strong. Why?
Given that the speed of light and consequently of any signal carrying information is finite, in the Big Bang scenario not every region of spacetime is accessible to us. If we define "particle horizon" the maximum distance from which a point in space can receive information, we define "universe" the part of the universe inside the particle horizon and which is causally connected with us. It is possible to have two different regions in the universe which are both accessible and causally-connected with us but are not causally-connected each other; they are inside our particle horizon but they are out their reciprocal particle horizons.
It is also intuitive that region which are causally connected can be homogeneous having had time to interact; at the same time homogeneity of regions which are not causally connected can only derive from some initial homogeneity of the universe giving that they had not time to interact.
Giving our knowledge of the age of the universe (giving the maximum distance that light could have walked) and the notion of causality, the universe we observe is homogeneous on scales larger than what we expect; this problem is known as the **horizon problem**. So it seems that homogeneity should be considered as an initial condition in studying the evolution of the universe. The problem is taken to points of extreme relevance if one considers also that actually the microwave background is not perfectly isotropic, but instead exhibits small fluctuations. These irregularities are thought to represent the seeds from which structures in the Universe grow. For the same reason that one cannot have thermalize separated regions, one cannot also create an irregularity; so in the standard Big Bang theory one cannot have a theory allowing the generation of the seed perturbations, which have to be there already.
Another problem is the so called **flatness problem**. Consider the Eq.(1.14); the Hubble parameter H is defined as

$$H \equiv \dot{a}/a\,. \tag{1.16}$$

We can use it to define the critical density

$$\rho_c = \frac{3H^2}{8\pi G}, \tag{1.17}$$

which is the density which would make the 3-geometry flat. From critical density we can define the dimensionless parameters

$$\Omega = \frac{\rho}{\rho_c}, \tag{1.18}$$

$$\Omega_k = -\frac{k}{a^2H^2}. \tag{1.19}$$

With these one Eq.(1.14) becomes

$$\Omega + \Omega_k = 1 \tag{1.20}$$

The dimensionless quantities Ω and Ω_k are measurable, and it is known that Ω is very close to 1. Extrapolating in the past this means that Ω would have had to be even closer to 1, making the contribution of Ω_k (and k) exponentially small. The fact that Ω seems to be so close to 1 is not a dynamical consequence of evolution but it appears as a strange coincidence deriving from some fine tuning of the initial conditions.
A possible solution to all these problems is the **inflationary cosmology**; it is not a replacement of Big Bang cosmology but an add-on that occurs at very early times without disturbing any of its successes and solving all its puzzles. The precise definition of inflation is simply an epoch during which the scale factor of the Universe is accelerating

$$\ddot{a} > 0 \tag{1.21}$$

or in a more physical definition

$$\frac{d}{dt}\frac{1}{aH} < 0 \tag{1.22}$$

If inflation occurs then we solve the flatness problem, because from

$$\Omega - 1 = \Omega_k = \frac{k}{a^2 H^2} \tag{1.23}$$

the condition for inflation is precisely the condition that Ω is driven toward 1 rather than away from it. Also the horizon problem is solved: during inflation the comoving Hubble length (aH) decreases dramatically allowing our entire present observable region to lie within a region that was well inside the Hubble radius at the start of inflation. Any initial inhomogeneities finish up on scales vastly larger than our observable universe.
Assuming that we work within General Relativity, the condition for inflation can be rewritten as a requirement on the material driving the expansion. Directly from Eq.(1.15) we find

$$\rho + 3p < 0 \tag{1.24}$$

Because we always assume ρ to be positive, it is necessary for p to be negative to satisfy this condition, given that Eq.(1.15) is independent of the curvature of the Universe. But it seems impossible for ordinary baryonic matter to satisfy this condition; so inflation can be only achieved within the framework of General Relativity if some new form of matter field with special characteristics is introduced.

1.5.3 Observations

While inflation gives a possible theoretical solution to some of the problems of Standard Cosmological Model, we need to find proofs of this hypothesis. Nowadays we have different independent instrument of investigation:

- **Cosmic Microwave Background Radiation** (CMBR): in the early universe, baryons, photons and electrons formed a hot plasma, in which the mean free path of a photon was very short due to constant interactions of the photons with the plasma through Thompson scattering. However, due to the expansion of the universe and the subsequent decrease of the temperature, it subsequently became energetically favourable for electrons to combine with protons to form hydrogen (recombination epoch). This allowed photons to travel freely through the space. This decoupling of photons from matter is supposed to have taken place at a redshift $z \approx 1089$, when the age of the universe was about 380,000 years, or approximately 13.7 billion years ago. The photons which left the last scattering surface at that time, then travelled freely through space and have continued cooling since then. CMB was first detected in 1965 by Penzias and Wilson: using a radiometer for radio astronomy observations and satellite communication experiments they found an excess of 3.5 K antenna temperature which they could not explain. It was the CMBR theoretically predicted by Gamow in 1948. More recent measurements of CMBR show that it has a black body spectrum corresponding to approximately 2.7 K. In the first experiments (and until a good sensitivity was not reached by instruments), CMBR appeared to be isotropous. However it was soon realized that attention should be paid not to the overall isotropy, but on the small fluctuations present in the CMBR, which reveal density fluctuations. The density fluctuations indicated by the small anisotropies in the temperature of CMBR are believed to act as seeds for gravitational collapse, leading to gravitationally bound systems which

constitute the large scale matter structures of actual universe. This allows us to build a coherent scenario about how these structure were formed and to explain the current small inhomogeneities and anisotropies;

- Large Scale Structure (LSS): reading the standard evolutionary history of the universe considering matter as the main character (and not photons just like in CMBR), one obtains another observable quantity to understand universe: the Baryonic Acoustic Oscillations (BAO). The key ingredients are: plasma (photons and gas-baryonic matter), neutrinos and dark matter (non baryonic component). Let's consider a small initial perturbation (detectable as inhomogeneity in CMBR). Each one of the components has a different behaviour with respect of perturbation:

  – neutrinos don't interact gravitationally so they are free to stream away from the initial perturbation;

  – dark matter moves only in response to gravity and has no intrinsic motion (it is cold dark matter) so it sits in the perturbation location;

  – photons and gas are mixed in plasma and are the dominant part of density perturbation.

  While universe is expanding and cooling gas and photons are submitted to matter oscillations: photons are hot and numerous, so the photon-gas fluid has a great internal pressure; the initial perturbation is also an initial overpressure. This pressure tries to equalize itself with the surroundings resulting in an expanding spherical wave. The result is that gas and photons perturbation is carried outward. As time goes on, the spherical shell of gas and photons continues to expand, neutrinos spread out and dark matter collects in the overall density perturbation (attracting the background material in that region), which is now considerably bigger because the photons and neutrinos have left the center. Hence, the peak in the dark matter remains centrally concentrated but with an increasing width. When we arrive at recombination epoch, photons begin to slip past the gas particles: sound speed begins to drop and pressure wave slows down and this continues until the photons have completely leaked out of the gas perturbation. The photon perturbation begins to smooth itself out at the speed of light (just like the neutrinos did). The photons travel (mostly) unimpeded until the present-day, where we can record them as CMBR. At this point, the sound speed in the gas has dropped to much less than the speed of light, so the pressure wave stalls. We are left with a dark matter perturbation around the original center and a gas perturbation in a shell about 150 Mpc (500 million light-years) in radius. As time goes on, however, these two species gravitationally attract each other and both perturbations grow quickly in response to the combined gravitational forces of both the dark matter and the gas. At the end the spherical shell of the gas perturbation has imprinted itself in the dark matter. This is known as the baryonic acoustic peak (BAO). At late times, galaxies form in the regions that are overdense in gas and dark matter. For the most part, this is driven by where the initial overdensities were, since we see that the dark matter has clustered heavily around these initial locations. However, there is a 1% enhancement in the regions 150 Mpc away from these initial overdensities. Currently there are many surveys determining the distribution of galaxies and confirming the expected theoretical peak;

- Type Ia Supernovae (SNeIa): these exploding stellar objects are believed to be approximately standard candles, namely astronomical objects with known luminosity and

absolute magnitude. Therefore they can be used to reveal distances, leading to the possibility of forming a redshift-distance relation and thereby measuring the expansion of the universe at different redshifts. The Hubble diagram measured by both the Supernova Cosmology Project and the High-z Team up to redshift $z \sim 1 \div 2$, has been the first evidence that the Universe is undergoing a phase of accelerated expansion.

What are the most important results coming from the mixed use of these observational instruments of investigation? First of all the most recent CMBR data set coming from the Five-Years WMAP (Wilkinson Microwave Anisotropy Prove experiment) observations gives a 95% confidence limit on deviation from the simple ΛCDM model (flat, gaussian, adiabatic, power-law) on Ω_k:

$$-0.063 < \Omega_k < 0.017 \tag{1.25}$$

while combining CMBR with BAO and SNeIa:

$$-0.0728 < \Omega_k < 0.0087 \tag{1.26}$$

From this we derive that Ω is very close to unity and the universe appears to be spatially flat, $\Omega_k \sim 0$,while the power spectrum of CMBR appears to be consistent with gaussianity and adiabaticity. Both these results are in perfect agreement with the inflationary predictions.
But observational data take also other important results: even tough Ω is very close to unity, the contribution of matter is only

$$\Omega_m \approx 0.25 \tag{1.27}$$

which means that matter contributes to universe for only the 25%. And the remaining 75% what is made of? We need to introduce (in a General Relativity built model) an unknown form of energy called **dark energy**. If one tries to model dark energy as a perfect fluid with equation of state $p = w\rho$ then

$$w_{de} = -0.972^{+0.061}_{-0.060} \qquad (68\% \text{ limit}), \tag{1.28}$$

so that dark energy satisfies Eq.(1.23). Since it is the dominant energy component today, this implies that the universe should be undergoing an accelerated expansion as well. This result is also confirmed in an independent way by SNeIa surveys.
Between the two period of acceleration (inflation and the current one) there is the conventional era of evolutionary cosmology: after inflation we have Big Bang nucleosynthesis with the production of nuclei other than hydrogen. There are very strict bound on the abundances of primordial light elements coming from observation and which don't seem to allow significant deviations from standard cosmology. Certainly nucleosynthesis took place during the so called radiation dominated era, namely a period in which radiation was the most important contribution to the energy of the universe. As it is well known the formation of structure, on the contrary, requests the transition from a radiation-dominated to a matter-dominated era. This transition is natural giving that matter density is inversely proportional to the volume, so it is proportional to a^{-3}, while radiation is proportional to a^{-4}, so it decreases faster than the matter energy density while universe expands.

At the end, we can summarize the current picture of evolution of universe giving the next phases:

- Pre-Inflationary Era (probably a Quantum Gravity Era);
- Inflationary Era (we need it to solve some problems coming out the application of Friedmann Equation, namely General Relativity, to the expansion of Universe);

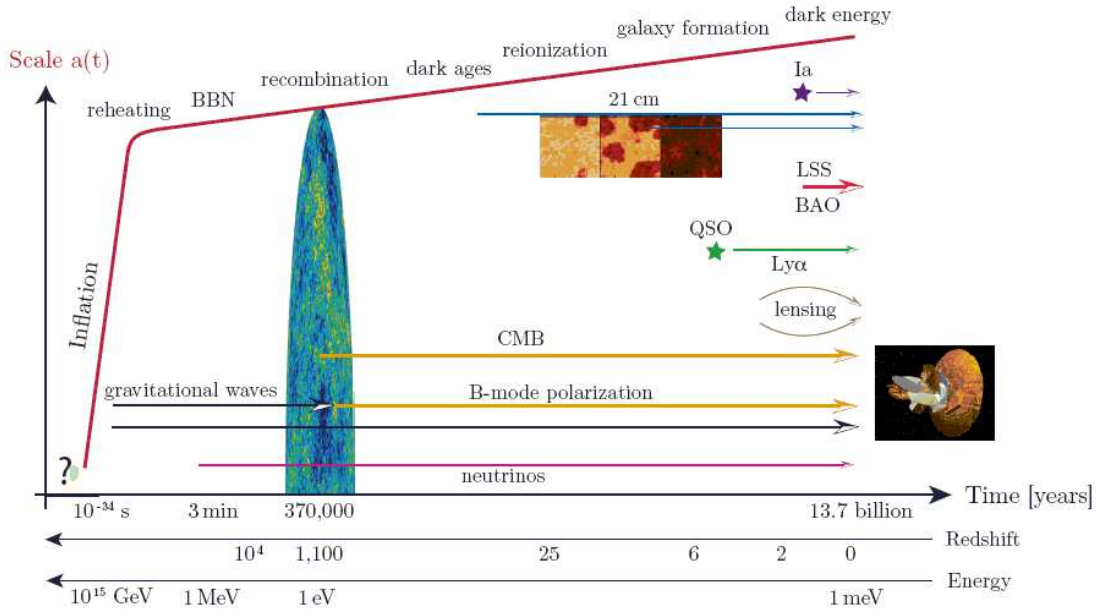

Figure 1.1: History of the Universe. In this schematic key events in the history of universe and their associated time and energy scales are presented. There are also illustrated several cosmological probes that provide us with information about the structure and the evolution of the universe. *Acronyms*: BBN (Big Bang Nucleosynthesis), LSS (Large Scale Structure), BAO (Baryonic Acoustic Oscillations), QSO (Quasi Stellar Objects; Quasars), Lyα (Lyman-Alpha), CMB (Cosmic Microwave Background), Ia (Type Ia Supernovae), 21 cm (hydrogen 21 cm-transition).

- Radiation-dominated Era (for Nucleosynthesis);
- Matter-dominated Era (for the formation of gravitationally bound structures);
- Dark Energy Era (in the present the expansion of Universe is accelerating and not decelerating as we expect from General Relativity and the attractive nature of gravitational interaction).

If at cosmological scales we have had to introduce dark energy, on astrophysical scales there is a similar puzzle: even if the matter contribution is stated at 25%, observations indicate the ordinary baryonic matter has a smaller contribute:

$$\Omega_b = 0.0462 \pm 0.0015 \tag{1.29}$$

which means that only the 4% of all the matter in the universe is made of our similar matter, or the only known kind of matter, the baryonic one! This unknown kind of matter has been defined **dark matter**; the definition *dark* comes from the possibility to detect it only via its gravitational interaction with ordinary matter and not the electromagnetic one with photons, so that it is *optically* invisible. So we cannot directly observe it and we can trace it only analyzing dynamics of gravitational systems. It is interesting underline that this undetectable component of the universe was already postulated, in an epoch were precision cosmological

measurements were not possible: in 1933 Fritz Zwicky posed the *"missing mass"* question for cluster of galaxies. Using the virial theorem he computed the mass of the Coma galaxy cluster needed to account for the motion of galaxies near its edges, and compared it with the mass obtained from galaxy counts and the total brightness of cluster. The virial mass turned out to be larger by a factor of almost 400. And this was not the only case where the presence of invisible matter was requested; the first compelling evidence for the existence of dark matter came from the rotation curves of spiral galaxies. The velocity curves of stars as functions of the radius did not appear to have the expected shapes: while from Newtonian dynamics we expect to see them decreasing at large distances, they appear almost flat. Assuming Newton's gravitational theory right, this implies that there should be more matter than the luminous one and this additional invisible matter has a different distribution within the galaxy (the *dark halo*).

1.6 The ΛCDM model

What is the problem now? We have a cosmological scenario which has surely many strange properties, but in our era of precision cosmology is also almost *clear*; in a brief summary we have that:

- The Universe is spatially flat ($\Omega_k \approx 0$);
- The Universe is undergoing a phase of *accelerated* expansion ($w_{de} = -0.972$);
- The Universe is now composed by a dominant unknown kind of energy, the dark energy ($\Omega_{DE} = 0.75$), while matter is splitted in dark matter (non ordinary matter) ($\Omega_{DM} \approx 0.25$) and baryonic matter ($\Omega_b = 0.0462$).

What is the simplest model that agree with these data? It is defined ΛCDM model because the key ingredient is the **cosmological constant** Λ which one needs to drive accelerated expansion.
The cosmological constant has an history longer than our knowledge of the previous parameters; it was first introduced by Einstein early after his formulation of General Relativity, for deriving a solution of the field equations describing a static universe. The idea of a static universe was later rapidly abandoned when Hubble discovered that the Universe is expanding. Considering our actual necessities to explain the accelerated expansion, the cosmological constant results to be extremely useful; if we allow the cosmological constant to be present in the field equations, the Friedmann equations will be modified:

$$\left(\frac{\dot{a}}{a}\right)^2 = \frac{8\pi G}{3}\rho + \frac{\Lambda}{3} - \frac{k}{a^2}, \tag{1.30}$$

$$\frac{\ddot{a}}{a} = \frac{\Lambda}{3} - \frac{4\pi G}{3}(\rho + 3p). \tag{1.31}$$

From Eq.(1.30) one infers that the universe can now enter a phase of accelerated expansion once the cosmological constant term dominates over the matter term on the right side. On the other hand if we define

$$\Omega_k = \frac{\Lambda}{3H^2} \tag{1.32}$$

than Eq.(1.19) now is

$$\Omega_m + \Omega_k + \Omega_\Lambda = 1 \tag{1.33}$$

In this sense the observations can be interpreted to mean that

$$\Omega_\Lambda \approx 0.72 \tag{1.34}$$

With these requirements and solutions the ΛCDM model is more than a phenomenological fit to data: it is the simplest model that can fit the cosmic microwave background observations as well the large scale structure observations and supernovae observations of accelerating expansion of the universe with a remarkable agreement. As a phenomenological model, however, it gives no insight about the nature of dark matter, or the reason of the presence of the cosmological constant, neither does it justify the value of the latter. For a deeper inspection we can consider the Eq.(1.8)

$$G_{\mu\nu} = 8\pi G\, T^m_{\mu\nu}; \tag{1.35}$$

the insertion of cosmological constant (and eventually dark matter) only modify the right member but not the left one. So we add new ingredients but we still consider General Relativity as the right gravitational theory. Putting it into the form of a stress-energy tensor $T^\mu_\nu = \mathrm{diag}(\Lambda, -\Lambda, -\Lambda, -\Lambda)$ it resembles a perfect fluid with equation of state $p = -\rho$, or $w = -1$ which is in very good agreement with the value of $w_{de} = -0.972$.
Once the cosmological term is considered to be a matter term, we could think of it as representing the vacuum energy associated with matter fields. From field theory one can effectively associate cosmological constant to a non-vanishing vacuum density:

$$\Lambda = 8\pi G < \rho >, \tag{1.36}$$

and using the standard model of particle physics it is possible estimate its value. Because of some divergence problem from high-frequencies modes it is not possible to derive an exact value for it. Considering as cutoff scale the Planck scale ($M_{Planck} = 10^{18}\,\mathrm{Gev}$), which is a typical scale at which the validity of classical gravity is becoming questionable, we have

$$\rho_\Lambda \approx (10^{27}\ \mathrm{eV})^4. \tag{1.37}$$

On the other hand observations give

$$\rho_\Lambda \approx (10^{-3}\ \mathrm{eV})^4. \tag{1.38}$$

There is a difference of 120 orders of magnitude which is too large to be attributed to a rough approximation. This is the so called **cosmological constant problem**.
And this is not the only one. Another problem is defined as the **coincidence problem**. It is apparent from data that $\Omega_\Lambda \approx 0.72$ and $\Omega_m \approx 0.28$ have comparable values today. However, as the universe expands their fractional contributions change rapidly since

$$\frac{\Omega_\Lambda}{\Omega_m} = \frac{\rho_\Lambda}{\rho_m} \propto a^3. \tag{1.39}$$

Since Λ is constant, ρ_Λ should once have been negligible compared to the energy densities of matter and radiation and it will come to dominate completely at some point in the late time universe. However, the striking fact is that the period of transition between matter domination and cosmological constant domination is very short compared to cosmological time scales (in the presence of a positive cosmological constant there is an infinite future in which Λ is dominating). The problem is that we live *exactly* in this era; obviously the transition from matter domination to cosmological constant domination, or, alternatively, from deceleration to acceleration, would happen eventually. But why now?

1.7 Solutions to ΛCDM model?

First of all let's face with a problem: inflation solves many problems but how can we give a well motivated theoretical background to it? This is an interesting question also because we know that the inflation is characterized by an accelerated expansion; possible solutions to it could be extended also to the actual acceleration and being substitutes of cosmological constant.
To obtain inflation, as long as one is convinced that gravity is well described by General Relativity, we need material with the unusual property of a negative pressure. Such a material is a **scalar field**, describing scalar particles. Although there has yet been no direct observation of a fundamental scalar particle, such particles proliferate in modern particle physics.
A scalar field minimally coupled to gravity satisfies the Klein-Gordon equation

$$\nabla^2\phi + V'(\phi) = 0 \tag{1.40}$$

The term $V(\phi)$ is the potential of the scalar field, which we might hope to derive from some particle physics motivation. The prime denotes partial differentiation with respect the variable. Assuming an homogeneous scalar field $\phi \equiv \phi(t)$ we can derive expressions for the energy density and pressure

$$\rho_\phi = \frac{1}{2}\dot{\phi}^2 + V(\phi), \tag{1.41}$$

$$p_\phi = \frac{1}{2}\dot{\phi}^2 - V(\phi). \tag{1.42}$$

The equations of motion can be derived directly by substituting these relations into the Friedmann and continuity equations; assuming a spatially flat Universe, and that the scalar dominates over both matter and radiation, we obtain

$$H^2 \approx \frac{8\pi G}{3}\left(\frac{1}{2}\phi^2 + V(\phi)\right) \tag{1.43}$$

and

$$\ddot{\phi} + 3H\dot{\phi} = -V'(\phi). \tag{1.44}$$

From the forms of the effective energy density and pressure, the condition for inflation is satisfied, provided that $\dot{\phi}^2 < V(\phi)$; in fact $w_\phi = p_\phi/\rho_\phi$ approaches minus one when $\dot{\phi}^2 \ll V(\phi)$. The scalar field responsible for inflation is often called *inflaton*.
The standard approximation technique for analyzing inflation is the **slow-roll approximation**, namely together with the condition $\dot{\phi}^2 < V(\phi)$ we add $\ddot{\phi}$ negligible. They are equivalent to assess that the potential terms are dominant with respect to the kinetic terms, causing the scalar to roll slowly from one value to another. With these conditions previous two relations are

$$H^2 \simeq \frac{8\pi G}{3}V(\phi)\,, \tag{1.45}$$

$$3H\dot{\phi} \simeq -V'(\phi)\,. \tag{1.46}$$

For this approximation to be valid, it is necessary for two conditions to hold

$$\epsilon(\phi) \ll 1\,, \tag{1.47}$$

$$|\eta(\phi)| \ll 1\,, \tag{1.48}$$

where the *slow-roll parameters* ϵ and $\eta$are defined by

$$\epsilon(\phi) = 4\pi G\left(\frac{V'}{V}\right)^2, \tag{1.49}$$

$$\eta(\phi) = 8\pi G \frac{V''}{V} \,. \tag{1.50}$$

That these conditions are necessary for the slow-roll approximation to be valid can be found easily by substitution; but they are not sufficient conditions because they only restrict the form of the potential. What is important to note is that one can start with a scalar that initially satisfies the slow-roll conditions but, after some period, ϕ can be driven to such a value so as to violate them. For example, for $V(\phi) = m^2\phi^2/2$, they are satisfied provided that $\phi^2 > 16\pi G$. For such a potential, inflation proceeds until the scalar field gets too close to the minimum for the slow-roll conditions to be maintained, and inflation come to end. In definitive: an inflation model consists of a potential and a way of ending inflation.

Now let's face with the dark energy problems. There are two possible way of investigation: one can try to find direct solutions to the cosmological constant and the coincidence problems and consequently attempt to provide an appealing theoretical explanation for the presence and value of the cosmological constant, or one can abandon the idea of cosmological constant altogether and attempt to find alternative ways to explain acceleration.
The first approach resorts to High Energy Physics: for example from supersimmetry (SUSY) one can derive a value for vacuum energy matter density which is "only" 60 orders of magnitude smaller than the observed value. This is an improvement with respect to the 120 orders of magnitude but it is still too different. Other approaches can come from string theory of loop quantum gravity, but it is not possible to solve the cosmological constant problem without a fine tuning of the initial conditions. Moreover the coincidence problem is not solved.
The second approach refers to "anthropic principle" which can be given in at least three version. First, "our mere existence can potentially serve as an experimental tool": this sounds like a philosophical more than scientific solution, and is not very useful for answering our questions. Second, "the laws of nature are by themselves incomplete and become complete only if one adds the requirement that conditions should allow intelligence to arise, for only in the presence of intelligent life does science become meaningful": this looks like a new Ptolemaic model, where is not the Earth at the center of the Universe, but Intelligent Life or Science. Third, "observers will only observe condition which allow for observers": this one is the most discussed in scientific world and acquires meaning if one invokes probability theory. It states that, since the existence of intelligent observers requires certain conditions, it is not possible for them in practice to observe any other conditions, something that introduces a bias in any probabilistic analysis. This requires an extra assumption: that parts of the universe, either in space or time, might be in alternative conditions. Unfortunately we cannot conclude at this point whether this statement is true or not. Assuming that it is, one could put constrains on the value of the cosmological constant by requiring that it should be small enough for galaxies to form and arrive at the conclusion that the currently observed value of the cosmological constant is by no means unlikely. Some modern theories do allow such alternative states of the universe to co-exist (multiverse), and for this reason it has recently been argued that the anthropic principle could even be placed on firm ground by using the ideas of string theory. However, admitting that there are limits on our ability to unambiguously and directly explain the observable universe inevitably comes into disappointment.

As an indirect approach to solve the question of cosmological constant, one could dismiss the constant at all and assume that there is some form of dynamical dark energy. In this sense there is no more connection with the question of vacuum energy, and there are no more problems of orders of magnitude. But, being the cosmological constant in great agreement with data, we have a constraint on dynamical model: they have to be able to mimic precisely a constant at present times. One of the simplest and probably the most common alternative

to cosmological constant in this field is **quintessence**, a scalar field inspired by inflationary model. It has an equation of state $p_q = w\rho_q$ where w is equal to the equation of state of the energy component dominating the universe (i.e. equal to $1/3$ during radiation domination and 0 during matter domination) until w undergoes a transition to less than -$1/3$ which initiates the accelerated expansion of the universe. Quintessence is dynamic, and generally has a density and equation of state that varies through time and space.
If the scalar field is taken to be spatially homogeneous, its equation of motion in a Friedmann-Lemaître-Robertson-Walker spacetime will be given by Eq.(1.42) and its energy density and pressure by Eqs.(1.39)-(1.40) respectively, just like inflaton. A viable candidate for dark energy shoud have an effective equation of state with w very close to minus one. As we have seen for inflation, this condition can be achieved if the condition $\dot{\phi}^2 \ll V(\phi)$ holds (this is intended to be different from the slow-roll condition for inflaton field).
The value given in Eq.(1.36) for the energy density of the cosmological constant now becomes the current value of the energy density of the scalar ρ_ϕ. Since we have asked that the potential term should be very dominant with respect of the kinetic terms, this value for the energy density effectively constrains the current value of the potential. What is more, the equation of motion of the scalar field, Eq.(1.42), is that of a damped oscillator, $3H\dot{\phi}$ being the friction term. This implies that, for ϕ to be rolling slowly enough so that $\dot{\phi}^2 \ll V(\phi)$ could be satisfied, then $H \approx \sqrt{V''(\phi)}$. Consequently, this means that the current value of $V''(\phi)$ should be that of the observed cosmological constant or, taking also into account that $\sqrt{V''(\phi)}$ represents the effective mass of the scalar m_ϕ, that

$$m_\phi \approx 10^{-33}\ \mathrm{eV}. \tag{1.51}$$

Such a small value for the mass of the scalar field raises doubts about whether quintessence really solves the cosmological constant problem; actually it only transfers the problem from the domain of cosmology to the domain of particle physics: generally scalar fields usually present in quantum field theory have masses many orders of magnitude larger than this value (Higgs field, for example, should have a mass of 10^{11} eV). We have to consider also that the coincidence problem remains unresolved.

About dark matter, even in this case if we accept that General Relativity describes gravity correctly, then an explanation for the nature of dark matter as some form of matter yet to be observed in the universe or laboratory should be given. The baryonic candidates for dark matter are mostly quite conventional astrophysical objects such as brown dwarfs, massive black holes and cold diffuse gas. However, there is a precise evidence from observations that only a small fraction of dark matter can be baryonic. So the real problem is to find a candidate in the non-baryonic particles family. Generally there are two major categories:

- hot dark matter, namely non baryonic ultra-relativistic particles, such as neutrinos. But this kind of candidates are generally not preferred because of giving that dark matter should have driven the formation of structures, it cannot consist of particles with too high velocities, since there would be problems in clustering;
- cold dark matter, namely non baryonic non-relativistc particles. There are many candidates for this family such as Weakly Interacted Massive Particles (WIMPS) predicted by supersymmetry theories (neutralino, gravitino).

It is important to underline that to nowadays no valid candidate for dark matter has been experimentally detected, even if there are many experiments realized for direct or indirect detection of any kind of dark matter candidates. The most recent and ambitious is the Large Hadronic Collider (LHC) which should give some answers to the high energy particle physics phenomenology and, so, also for dark matter and cosmology.

1.8 Final remarks on General Relativity

What is the main goal of this chapter?

We have first done a very brief and fast review of gravity theory and challenges it has to face with during science history. We have seen that until now any theory of gravity has gone in a systematic trend: first, someone has depicted a theoretical building, then data have proposed problems and new challenges. After any step more and more general theories of gravity have been defined.

What is the problem today? We could say that we have some difficulties to *"objectively analyze"* General Relativity, the most recent and *successful* theory of gravity.

General Relativity is a comprehensive theory of spacetime, gravity and matter. Its formulation implies that space and time are not "absolute" entities, as in Classical Mechanics, but dynamical quantities strictly related to the distribution of matter and energy. As a consequence, this approach gave rise to a new conception of the Universe itself which, for the first time, was considered as a dynamical system. In other words, Cosmology has been enclosed in the realm of Science and not only of Philosophy, as before the Einstein work. On the other hand, the possibility of a scientific investigation of the Universe has led to the formulation of the Standard Cosmological Model [386] which, quite nicely, has matched with observations.

Despite of these results, in the last thirty years, several shortcomings came out in the Einstein theory and people began to investigate whether General Relativity is the only fundamental theory capable of explaining the gravitational interaction. Such issues come, essentially, from quantum field theory and cosmology. In the first case, problems arise because of General Relativity is a *classical* theory which does not work as a fundamental theory, when one wants to achieve a full quantum description of spacetime (and then of gravity). On the other hand, the presence of the Big Bang singularity, the flatness and horizon problems [182] led to the statement that Cosmological Standard Model, based on the General Relativity and the Standard Model of Particle Physics, is inadequate to describe the Universe at extreme regimes.

As we have seen in previous pages, due to these facts, solutions have been searched. An inflation era has been theoretically supposed to solve flatness and horizon problems, and it seems to work good and some of its predictions are verified by recent observations (anisotropies in the cosmic microwave background). As we have said, the extension of the Hubble diagram of Type Ia Supernovae to redshifts higher than one [312] has been the first evidence that the Universe is undergoing a phase of accelerated expansion; balloon born experiments, such as BOOMERanG [119] and MAXIMA [356] and recent precise measurements of the CMBR spectrum, due to the WMAP experiment [349, 351, 186, 350], determined the location of the first and second peak in the anisotropy spectrum of the cosmic microwave background radiation strongly pointing out that the geometry of the Universe is spatially flat. If combined with constraints coming from galaxy clusters on the matter density parameter Ω_M, these data indicate that the Universe is dominated by a non-clustered fluid with negative pressure, generically dubbed dark energy, which is able to drive the accelerated expansion.

After these observational evidences, an overwhelming flood of papers has appeared: they present a great variety of models trying to explain this phenomenon. In any case, the simplest explanation is claiming for the well known cosmological constant Λ [319]. Although it is the best fit to most of the available astrophysical data [351], the ΛCDM model fails in explaining why the inferred value of Λ is so tiny (120 orders of magnitude lower!) if compared with the typical vacuum energy values predicted by particle physics and why its energy density is today comparable to the matter density (the coincidence problem). As a tentative solution, many authors have replaced the cosmological constant with a scalar field rolling down its potential and giving rise to the model now referred to as quintessence [286, 112]. Even if successful in

fitting the data, the quintessence approach to dark energy is still plagued by the coincidence problem since the dark energy and matter densities evolve differently and reach comparable values for a very limited portion of the Universe evolution coinciding at present era. To be more precise, the quintessence dark energy is tracking matter and evolves in the same way for a long time. But then, at late time, somehow it has to change its behavior into no longer tracking the dark matter but starting to dominate as a cosmological constant. This is the coincidence problem of quintessence. And many other theoretical problems are living now...
At the end we can say that Universe and Gravity are...under construction!

CHAPTER 2

Extended Theories of Gravity

As we have pointed out in the previous chapter, nowadays we can't be more sure the General Relativity is the only fundamental theory capable of explaining the gravitational interaction. To be more exact, we can take a look to the field equations

$$R_{\mu\nu} - \frac{1}{2} g_{\mu\nu} R = 8\pi G \, T^{m}_{\mu\nu} \tag{2.1}$$

All the solutions to the shortcomings of Einstein theory we have shown starts from considering General Relativity as the right gravity theory and modify the *right* member of these equations, adding new and invisible (up to now) ingredients, such as dark energy, dark matter, scalar fields, and so on.
But what happen if we consider only the known and visible components and change the visual to the *left* member? Why can't we modify General Relativity?
This is the approach of **Alternative theories of gravity**.

2.1 Dimensional considerations on General Relativity

Let's start with some considerations on typical dimensions and scales where General Relativity is applied. We want to underline that these considerations are approximate and only quantitative; but they can be useful to show some misunderstandings in applying General Relativity which are not generally considered with the right paying attention. Taking a review of all the necessary ingredients in gravitational theory and their dimensional nature[1], we have:

[1]We will use: L for length, M for mass and t for time

- the metric:
$$ds^2 = g_{\mu\nu} dx^\mu dx^\nu \,,$$
where:
$$\begin{aligned} g_{\mu\nu} &\rightarrow \text{adimensional}\,, \\ x^\mu &\rightarrow L\,; \end{aligned}$$

- the scalar curvature:
$$R = R^\mu_\nu \rightarrow L^{-2}\,;$$

- the gravitational Hilbert-Einstein action:
$$S = \int d^4x\sqrt{-g}\left(\frac{c^3 R}{16\pi G} - \frac{2c^3\Lambda}{16\pi G} + \frac{\mathcal{L}_m}{c}\right) \,,$$
where:
$$\begin{aligned} G &\rightarrow L^3\, M^{-1}\, t^{-2} \\ \Lambda &\rightarrow L^{-2} \\ \mathcal{L}_m &\rightarrow L^{-1}\, M\, t^{-2} \quad \text{(matter energy density)} \\ S &\rightarrow L^2\, M\, t^{-1} \end{aligned}$$

- Einstein's equations:
$$G_{\mu\nu} + g_{\mu\nu}\Lambda = \frac{8\pi G}{c^4} T_{\mu\nu}\,,$$
where
$$T_{\mu\nu} \rightarrow L^{-1}\, M\, t^{-2}$$

Now we can try to answer to this question:

Where does General Relativity is well tested?

Two situations where this happens are:

- Solar System and Binary Pulsars whose scale is tipically
$$r \approx 10^9 \div 10^{12}\ \mathrm{m}$$

- Nucleosynthesis; we can do some approximative quantitative considerations about it. Typical temperatures of nucleosynthesis are
$$T \approx 10^8 \div 10^9\ \mathrm{K}\,.$$
Friedmann equations in this era are
$$3H_N^2 = \frac{8\pi G}{c^2}\rho_N + \Lambda - \frac{k}{a^2}\,,$$
where the last two terms are supposed to be negligible so that we have
$$3H_N^2 = \frac{8\pi G}{c^2}\frac{4}{c}\sigma T^4\,,$$

with σ being Boltzmann's equation. Hubble radius at nucleosynthesis can be estimated to be

$$r_N \approx \frac{c}{H_N} = \sqrt{\frac{3c^5}{32\pi\sigma G T^4}}$$

which means:

$$r_N \approx 10^{11}\ \mathrm{m}$$

And what about scalar curvature's values in these two cases? We can try to estimate it:

- for Solar System and Binary Pulsars we have to consider the Schwartzchild metric:

$$ds^2 = \left(1 - \frac{2GM}{c^2 r}\right)\, dt^2 - \left(1 - \frac{2GM}{c^2 r}\right)^{-1}\, dl^2$$

from which we obtain

$$R = 0$$

- at Nucleosynthesis: we have a Friedmann-Robertson-Walker metric and we are in a radiation-dominated epoch so that the scale factor $a(t) \propto t^{1/2}$. Using the definition of the scalar curvature

$$R = -\frac{6}{c^2}(2H^2 + \dot{H})$$

we obtain

$$R = 0$$

So we can conclude that the only known examples where General Relativity works good, namely Solar System and Nucleosynthesis, invoke the same scale ($r \approx 10^{11}$ m) and the same value of scalar curvature ($R \sim 0$).

Now let's growing up in scale and consider galaxies and clusters, whose typical dimensional distance scale are

$$r = 10 \div 100\ \mathrm{kpc} = \begin{cases} 10^{19}\ \mathrm{m} & \text{for galaxies} \\ 10^{21} \div 10^{22}\ \mathrm{m} & \text{for clusters} \end{cases}$$

We know that these ones are also the first scales where we need to consider the dark matter ingredient to explain, for example, rotation curves of spiral galaxies, or discrepancies in dynamics of clusters of galaxies. But dark matter is also needed for structures formation. Given the equation for the evolution of the perturbations (i.e. seeds of gravitational structures)

$$\ddot{\delta}_k + 2H\dot{\delta}_k - 4\pi G\rho_B\delta_k = 0$$

where δ_k is the density contrast $\delta\rho/\rho$. After the decoupling we have $a \propto t^{2/3}$ and baryon density $\rho_B \propto a^{-3}$ so that the growing solution of perturbation equation is $\delta_k \propto t^{2/3}$. At decoupling we have $\delta_k \approx 10^{-5}$ and $a_{dec}/a_0 \approx 10^{-3}$, so there is no time for gravitational structures to form with only baryonic matter.
While if we assume that dark matter is decoupled from radiation it can drive the evolution of perturbations. If we consider this period pre-decoupling, between equivalence and decoupling, we have

$$T \approx 10^3 \div 10^4\ \mathrm{K}$$

which means

$$r \approx 10^{19} \div 10^{22}\ \mathrm{m}$$

This is the same scale of galaxies and clusters.
What can we say about scalar curvature? While it is difficult to estimate it for galaxies and clusters, we can estimate it for equivalence and decoupling time. From cosmology we can write the scalar curvature as a redshift function

$$R = -\frac{3H_0^2}{c^2}[4 + (z^3 + 3z^2 + 3z - 3)\Omega_{0,M}]$$

At equivalence we have $z \approx 10^5$ while at decoupling $z \approx 10^3$ so that

$$R = -\frac{3H_0^2}{c^2} z^3 \Omega_{0,M} \approx \frac{z^3}{r_{H_0}^2}$$

and estimating the Hubble radius, $r_{H_0}^2 = 13 \cdot 10^9$ light years, at the end we have

$$R \approx 10^{-37} \div 10^{-31} \text{ m}^{-2}$$

Let's grow up in scale again reaching Hubble radius

$$r \approx 100 \text{ Mpc} \sim 10^{24} \div 10^{26} \text{ m}$$

At these scales we know we need something driving the accelerated expansion, the Cosmological Constant, Λ, or Quintessence. Evaluating scalar curvature

$$R_0 \approx -\frac{9H_0^2}{c^2} \approx 10^{-51} \text{ m}^{-2}$$

It is worthy to consider that the Cosmological Constant

$$\Lambda \approx \frac{H_0^2}{c}^2$$

so that $\Lambda \sim R_0$.

It is useful to consider also the smallest scales. If we consider the inflationary epoch, Hubble factor is quite constant; we can consider it from the e-folding number, $N \approx 60 \approx H_{inf}\Delta t$:

$$H_{inf} \approx 10^{34} \div 10^{35} \text{ s}^{-1}$$

so that

$$r_{inf} = \frac{c}{H} \approx 10^{-27} \text{ m}$$

While for the scalar curvature, being $\dot{H} = 0$, we have

$$R = -12\frac{H_{inf}^2}{c^2} \approx 10^{55} \text{ m}^{-2}$$

Finally at Planck scale:

$$r \sim l_P \approx 10^{-35} \text{ m}$$
$$R \sim r^{-2} \approx 10^{70} \text{ m}^{-2}$$

What do we want to say with all these estimations? Clearly General Relativity can be considered the *right* gravity theory only in a really narrow scale range (Solar System and Nucleosynthesis). The tests span a range of four in scale; but we apply (or we are supposing to apply in the right way) General Relativity on a range of scale of 60 orders of magnitude and a range of curvature of 120.

Is it correct this kind of working?

2.2 Tassonomy and Motivations

Due to the problems of Standard Cosmological Model and to the problems of the solution found to solve them, and, first of all, to the lack of a definitive quantum gravity theory, alternative theories have been considered in order to attempt, at least, a semi-classical scheme where General Relativity and its positive results could be recovered. One of the most fruitful approaches has been that of **Extended Theories of Gravity** which have become a sort of paradigm in the study of gravitational interaction. They are based on corrections and enlargements of the Einstein theory. The paradigm consists, essentially, in adding higher-order curvature invariants and minimally or non-minimally coupled scalar fields into dynamics which come out from the effective action of quantum gravity [59].

Another motivation to modify General Relativity, and which we have not underlined well in the previous sections, comes from the issue of a full recovering of the Mach principle which leads to assume a varying gravitational coupling. As we have said, the principle states that the local inertial frame is determined by some average of the motion of distant astronomical objects [47]. This fact implies that the gravitational coupling can be scale-dependent and related to some scalar field. As a consequence, the concept of "inertia" and the Equivalence Principle have to be revised. For example, the Brans-Dicke theory [51] is a serious attempt to define an alternative theory to the Einstein gravity: it takes into account a variable Newton gravitational coupling, whose dynamics is governed by a scalar field non-minimally coupled to the geometry. In such a way, Mach's principle is better implemented [51, 67, 325].

Besides, every unification scheme as Superstrings, Supergravity or Grand Unified Theories, takes into account effective actions where non-minimal couplings to the geometry or higher-order terms in the curvature invariants are present. Such contributions are due to one-loop or higher-loop corrections in the high-curvature regimes near the full (not yet available) quantum gravity regime [59]. Specifically, this scheme was adopted in order to deal with the quantization on curved spacetimes and the result was that the interactions among quantum scalar fields and background geometry or the gravitational self-interactions yield corrective terms in the Hilbert-Einstein Lagrangian [44]. Moreover, it has been realized that such corrective terms are inescapable in order to obtain the effective action of quantum gravity at scales closed to the Planck one [376]. All these approaches are not the *"full quantum gravity"* but are needed as working schemes toward it.

In summary, higher-order terms in curvature invariants (such as R^2, $R^{\mu\nu}R_{\mu\nu}$, $R^{\mu\nu\alpha\beta}R_{\mu\nu\alpha\beta}$, $R\Box R$, or $R\Box^k R$) or non-minimally coupled terms between scalar fields and geometry (such as $\phi^2 R$) have to be added to the effective Lagrangian of gravitational field when quantum corrections are considered. For instance, one can notice that such terms occur in the effective Lagrangian of strings or in Kaluza-Klein theories, when the mechanism of dimensional reduction is used [168].

On the other hand, from a conceptual viewpoint, there are no *a priori* reason to restrict the gravitational Lagrangian to a linear function of the Ricci scalar R, minimally coupled with matter [240]. Furthermore, the idea that there are no "exact" laws of physics could be taken into serious account: in such a case, the effective Lagrangians of physical interactions are "stochastic" functions. This feature means that the local gauge invariances (*i.e.* conservation laws) are well approximated only in the low energy limit and the fundamental physical constants can vary [31].

Besides fundamental physics motivations, all these theories have acquired a huge interest in cosmology due to the fact that they "naturally" exhibit inflationary behaviors able to overcome the shortcomings of Cosmological Standard Model (based on General Relativiy). The related cosmological models seem realistic and capable of matching with the CMBR observations

[352, 139, 218]. Furthermore, it is possible to show that, via conformal transformations, the higher-order and non-minimally coupled terms always correspond to the Einstein gravity plus one or more than one minimally coupled scalar fields [362, 239, 383, 68, 174].

More precisely, higher-order terms appear always as contributions of order two in the field equations. For example, a term like R^2 gives fourth order equations [318], $R\,\Box R$ gives sixth order equations [174, 16], $R\,\Box^2 R$ gives eighth order equations [33] and so on. By a conformal transformation, any 2nd-order derivative term corresponds to a scalar field: for example, fourth-order gravity gives Einstein plus one scalar field, sixth-order gravity gives Einstein plus two scalar fields and so on [174, 326].

Furthermore, it is possible to show that the $f(R)$-gravity is equivalent not only to a scalar-tensor one but also to the Einstein theory plus an ideal fluid [82]. This feature results very interesting if we want to obtain multiple inflationary events since an early stage could select "very" large-scale structures (clusters of galaxies today), while a late stage could select "small" large-scale structures (galaxies today) [16]. The philosophy is that each inflationary era is related to the dynamics of a scalar field. Finally, these extended schemes could naturally solve the problem of "graceful exit" bypassing the shortcomings of former inflationary models [218, 15].

In addition to the revision of Standard Cosmology at early epochs (leading to the Inflation), a new approach is necessary also at late epochs. Extended Theories could play a fundamental role also in this context. In fact, the increasing bulk of data that have been accumulated in the last few years have paved the way to the emergence of a new cosmological model usually referred to as the *Concordance Model*.

As we have said, to solve problems coming from observations (such as an accelerated expansion), many candidates have been defined: a cosmological constant, or a scalar field like quintessence which is in definitive a dynamical cosmological constant.

Moreover, it is not clear where this scalar field originates from, thus leaving a great uncertainty on the choice of the scalar field potential. The subtle and elusive nature of dark energy has led many authors to look for completely different scenarios able to give a quintessential behavior without the need of exotic components. To this aim, it is worth stressing that the acceleration of the Universe only claims for a negative pressure dominant component, but does not tell anything about the nature and the number of cosmic fluids filling the Universe.

This consideration suggests that it could be possible to explain the accelerated expansion by introducing a single cosmic fluid with an equation of state causing it to act like dark matter at high densities and dark energy at low densities. An attractive feature of these models, usually referred to as *Unified Dark Energy* (UDE) or *Unified Dark Matter* (UDM) models, is that such an approach naturally solves, al least phenomenologically, the coincidence problem. Some interesting examples are the generalized Chaplygin gas [204], the tachyon field [285] and the condensate cosmology [32]. A different class of UDE models has been proposed [91, 74] where a single fluid is considered: its energy density scales with the redshift in such a way that the radiation dominated era, the matter era and the accelerating phase can be naturally achieved. It is worth noticing that such class of models are extremely versatile since they can be interpreted both in the framework of UDE models and as a two-fluid scenario with dark matter and scalar field dark energy. The main ingredient of the approach is that a generalized equation of state can be always obtained and observational data can be fitted.

Actually, there is still a different way to face the problem of cosmic acceleration. As stressed in [236], it is possible that the observed acceleration is not the manifestation of another ingredient in the cosmic pie, but rather the first signal of a breakdown of our understanding of the laws of gravitation (in the infra-red limit).

From this point of view, it is thus tempting to modify the Friedmann equations to see whether it is possible to fit the astrophysical data with models comprising only the standard matter. Interesting examples of this kind are the Cardassian expansion [160] and the DGP gravity [140]. Moving in this same framework, it is possible to find alternative schemes where a quintessential behavior is obtained by taking into account effective models coming from fundamental physics giving rise to generalized or higher-order gravity actions [69, 275, 96, 11], [273].

For instance, a cosmological constant term may be recovered as a consequence of a non - vanishing torsion field thus leading to a model which is consistent with both SNeIa Hubble diagram and Sunyaev - Zel'dovich data coming from clusters of galaxies [70]. SNeIa data could also be efficiently fitted including higher-order curvature invariants in the gravity Lagrangian [72, 226, 276, 227]. It is worth noticing that these alternative models provide naturally a cosmological component with negative pressure whose origin is related to the geometry of the Universe thus overcoming the problems linked to the physical significance of the scalar field.

It is evident, from this short overview, the high number of cosmological models which are viable candidates to explain the observed accelerated expansion. This abundance of models is, from one hand, the signal of the fact that we have a limited number of cosmological tests to discriminate among rival theories, and, from the other hand, that a urgent degeneracy problem has to be faced. To this aim, it is useful to remark that both the SNeIa Hubble diagram and the angular size - redshift relation of compact radio sources [102, 297] are distance based methods to probe cosmological models so then systematic errors and biases could be iterated. From this point of view, it is interesting to search for tests based on time-dependent observables.

For example, one can take into account the *lookback time* to distant objects since this quantity can discriminate among different cosmological models. The lookback time is observationally estimated as the difference between the present day age of the Universe and the age of a given object at redshift z. Such an estimate is possible if the object is a galaxy observed in more than one photometric band since its color is determined by its age as a consequence of stellar evolution. It is thus possible to get an estimate of the galaxy age by measuring its magnitude in different bands and then using stellar evolutionary codes to choose the model that reproduces the observed colors at best.

Coming to the weak-field-limit approximation, which essentially means considering Solar System scales, Extended Theories are expected to reproduce General Relativity which, in any case, is firmly tested only in this limit [388]. This fact is matter of debate since several relativistic theories *do not* reproduce exactly the Einstein results in the Newtonian approximation but, in some sense, generalize them. As it was firstly noticed by Stelle [355], a R^2-theory gives rise to Yukawa-like corrections in the Newtonian potential. Such a feature could have interesting physical consequences. For example, some authors claim to explain the flat rotation curves of galaxies by using such terms [322]. Others [242] have shown that a conformal theory of gravity is nothing else but a fourth-order theory containing such terms in the Newtonian limit. Besides, indications of an apparent, anomalous, long-range acceleration revealed from the data analysis of Pioneer 10/11, Galileo, and Ulysses spacecrafts could be framed in a general theoretical scheme by taking corrections to the Newtonian potential into account [19, 41].

In general, any relativistic theory of gravitation yields corrections to the Newton potential (see for example [306]) which, in the post-Newtonian (PPN) formalism, could be a test for the same theory [388]. Furthermore the newborn *gravitational lensing astronomy* [333] is giving rise to additional tests of gravity over small, large, and very large scales which soon will provide direct measurements for the variation of the Newton coupling [215], the potential of galaxies, clusters of galaxies and several other features of self-gravitating systems.

Such data will be, very likely, capable of confirming or ruling out the physical consistency

of General Relativity or of any Extended Theory. In summary, the general features of Extended Theories are that the Einstein field equations result to be modified in two senses: $i)$ geometry can be non-minimally coupled to some scalar field, and/or $ii)$ higher than second order derivative terms in the metric come out. In the former case, we generically deal with scalar-tensor theories of gravity; in the latter, we deal with higher-order theories. However combinations of non-minimally coupled and higher-order terms can emerge as contributions in effective Lagrangians. In this case, we deal with higher-order-scalar-tensor theories of gravity.

Considering a mathematical viewpoint, the problem of reducing more general theories to Einstein standard form has been extensively treated; one can see that, through a "Legendre" transformation on the metric, higher-order theories, under suitable regularity conditions on the Lagrangian, take the form of the Einstein one in which a scalar field (or more than one) is the source of the gravitational field (see for example [240, 345, 153, 241]); on the other side, as discussed above, it has been studied the mathematical equivalence between models with variable gravitational coupling with the Einstein standard gravity through suitable conformal transformations (see [132, 125]).

In any case, the debate on the physical meaning of conformal transformations is far to be solved ([149]). Several authors claim for a true physical difference between Jordan frame (higher-order theories and/or variable gravitational coupling) since there are experimental and observational evidences which point out that the Jordan frame could be suitable to better match solutions with data. Others state that the true physical frame is the Einstein one according to the energy theorems [241]. However, the discussion is open and no definitive statement has been formulated up to now.

The problem should be faced from a more general viewpoint and the Palatini approach to gravity could be useful to this goal. The Palatini approach in gravitational theories was firstly introduced and analyzed by Einstein himself [144]. It was, however, called the Palatini approach as a consequence of an historical misunderstanding [60, 154].

The fundamental idea of the Palatini formalism is to consider the (usually torsion-less) connection Γ, entering the definition of the Ricci tensor, to be independent of the metric g defined on the spacetime $\mathcal{M}$. The Palatini formulation for the standard Hilbert-Einstein theory results to be equivalent to the purely metric theory: this follows from the fact that the field equations for the connection Γ, firstly considered to be independent of the metric, give the Levi-Civita connection of the metric g. As a consequence, there is no reason to impose the Palatini variational principle in the standard Hilbert-Einstein theory instead of the metric variational principle.

However, the situation completely changes if we consider the Extended Theories, depending on functions of curvature invariants, as $f(R)$, or non-minimally coupled to some scalar field. In these cases, the Palatini and the metric variational principle provide different field equations and the theories thus derived differ [241, 155]. The relevance of Palatini approach, in this framework, has been recently proven in relation to cosmological applications [**?**, 273, 381, 228, 229].

It has also been studied the crucial problem of the Newtonian potential in alternative theories of Gravity and its relations with the conformal factor [255]. From a physical viewpoint, considering the metric g and the connection Γ as independent fields means to decouple the metric structure of spacetime and its geodesic structure (being, in general, the connection Γ not the Levi-Civita connection of g). The chronological structure of spacetime is governed by g while the trajectories of particles, moving in the spacetime, are governed by Γ.

This decoupling enriches the geometric structure of spacetime and generalizes the purely metric formalism. This metric-affine structure of spacetime is naturally translated, by means of the same (Palatini) field equations, into a bi-metric structure of spacetime. Beside the

physical metric g, another metric h is involved. This new metric is related, in the case of $f(R)$-gravity, to the connection. As a matter of fact, the connection Γ results to be the Levi-Civita connection of h and thus provides the geodesic structure of spacetime.

If we consider the case of non-minimally coupled interaction in the gravitational Lagrangian (scalar-tensor theories), the new metric h is related to the non-minimal coupling. The new metric h can be thus related to a different geometric and physical aspect of the gravitational theory. Thanks to the Palatini formalism, the non-minimal coupling and the scalar field, entering the evolution of the gravitational fields, are separated from the metric structure of spacetime. The situation mixes when we consider the case of higher-order-scalar-tensor theories. Due to these features, the Palatini approach could greatly contribute to clarify the physical meaning of conformal transformation [13].

Let's start our description of basic ideas of Extend Theories from the action of the General Relativity:

$$\mathcal{A} = \int d^4x\sqrt{-g}[R + \mathcal{L}_m] \tag{2.2}$$

where the gravitational part is given by Eq.(1.12)

$$\mathcal{L}_g = g^{\mu\nu}R_{\mu\nu}\sqrt{-g} = R\sqrt{-g} \tag{2.3}$$

The choice of Hilbert and Einstein for the gravitational lagrangian term was completely arbitrary (as it became clear a few years later), but it was certainly the simplest one both from the mathematical and the physical viewpoint. As it was later clarified by Levi-Civita in 1919, curvature is not a "purely metric notion" but, rather, a notion related to the "linear connection" to which "parallel transport" and "covariant derivation" refer [224].

In a sense, this is the precursor idea of what in the sequel would be called a "gauge theoretical framework" [210], after the pioneering work by Cartan in 1925 [98]. But at the time of Einstein, only metric concepts were at hands and his solution was the only viable.

It was later clarified that the three principles of relativity, equivalence and covariance, together with causality, just require that the spacetime structure has to be determined by either one or both of two fields, a Lorentzian metric g and a linear connection Γ, assumed to be torsionless for the sake of simplicity.

The metric g fixes the causal structure of spacetime (the light cones) as well as its metric relations (clocks and rods); the connection Γ fixes the free-fall, i.e. the locally inertial observers. They have, of course, to satisfy a number of compatibility relations which amount to require that photons follow null geodesics of Γ, so that Γ and g can be independent, *a priori*, but constrained, *a posteriori*, by some physical restrictions. These, however, do not impose that Γ has necessarily to be the Levi-Civita connection of g [288].

This justifies - at least on a purely theoretical basis - the fact that one can envisage the so-called "Alternative Theories of Gravitation", that we prefer to call "Extended Theories of Gravitation" since their starting points are exactly those considered by Einstein and Hilbert: theories in which gravitation is described by either a metric (the so-called "purely metric theories"), or by a linear connection (the so-called "purely affine theories") or by both fields (the so-called "metric-affine theories", also known as "first order formalism theories"). In these theories, the Lagrangian is a scalar density of the curvature invariants constructed out of both g and Γ.

The choice Eq.(2.3) is by no means unique and it turns out that the Hilbert-Einstein Lagrangian is in fact the only choice that produces an invariant that is linear in second derivatives of the metric (or first derivatives of the connection). A Lagrangian that, unfortunately, is

rather singular from the Hamiltonian viewpoint, in much than same way as Lagrangians, linear in canonical momenta, are rather singular in Classical Mechanics (see e.g. [23]).

A number of attempts to generalize General Relativity (and unify it to Electromagnetism) along these lines were followed by Einstein himself and many others (Eddington, Weyl, Schrodinger, just to quote the main contributors; see, e.g., [20]) but they were eventually given up in the fifties of XX Century, mainly because of a number of difficulties related to the definitely more complicated structure of a non-linear theory (where by "non-linear" we mean here a theory that is based on non-linear invariants of the curvature tensor), and also because of the new understanding of Physics that is currently based on four fundamental forces and requires the more general "gauge framework" to be adopted (see [203]).

Still a number of sporadic investigations about "alternative theories" continued even after 1960 (see [388] and refs. quoted therein for a short history). The search of a coherent quantum theory of gravitation or the belief that gravity has to be considered as a sort of low-energy limit of string theories (see, e.g., [180]) - something that we are not willing to enter here in detail - has more or less recently revitalized the idea that there is no reason to follow the simple prescription of Einstein and Hilbert and to assume that gravity should be classically governed by a Lagrangian linear in the curvature.

Further curvature invariants or non-linear functions of them should be also considered, especially in view of the fact that they have to be included in both the semi-classical expansion of a quantum Lagrangian or in the low-energy limit of a string Lagrangian.

Moreover, it is clear from the recent astrophysical observations and from the current cosmological hypotheses that Einstein equations are no longer a good test for gravitation at Solar System, galactic, extra-galactic and cosmic scale, unless one does not admit that the matter side of Eq.(1.8) contains some kind of exotic matter-energy which is the "dark matter" and "dark energy" side of the Universe.

The idea which we propose here is much simpler and is what we have anticipated at the beginning of this chapter. Instead of changing the matter side of Einstein Equations Eq.(1.8) in order to fit the "missing matter-energy" content of the currently observed Universe (up to the 95% of the total amount!), by adding any sort of inexplicable and strangely behaving matter and energy, we claim that it is simpler and more convenient to change the gravitational side of the equations, admitting corrections coming from non-linearities in the Lagrangian. However, this is nothing else but a matter of taste and, since it is possible, such an approach should be explored. Of course, provided that the Lagrangian can be conveniently tuned up (i.e., chosen in a huge family of allowed Lagrangians) on the basis of its best fit with all possible observational tests, at all scales (solar, galactic, extragalactic and cosmic).

Something that - in spite of some commonly accepted but disguised opinion - can and should be done before rejecting a priori a non-linear theory of gravitation (based on a non-singular Lagrangian) and insisting that the Universe has to be necessarily described by a rather singular gravitational Lagrangian (one that does not allow a coherent perturbation theory from a good Hamiltonian viewpoint) accompanied by matter that does not follow the behavior that standard baryonic matter, probed in our laboratories, usually satisfies.

2.3 Apparatus

With the above considerations in mind, let us start with a general class of higher-order-scalar-tensor theories in four dimensions given by the action

$$\mathcal{A} = \int d^4x\sqrt{-g}\left[F(R,\Box R,\Box^2 R,..\Box^k R,\phi) - \frac{\varepsilon}{2}g^{\mu\nu}\phi_{;\mu}\phi_{;\nu} + \mathcal{L}_m\right], \tag{2.4}$$

where F is an unspecified function of curvature invariants and of a scalar field ϕ. The term $\mathcal{L}_m$, as above, is the minimally coupled ordinary matter contribution. We shall use physical units $8\pi G = c = \hbar = 1$; ε is a constant which specifies the theory. Actually its values can be $\varepsilon = \pm 1, 0$ fixing the nature and the dynamics of the scalar field which can be a standard scalar field, a phantom field or a field without dynamics (see [150, 317] for details).

In the metric approach, the field equations are obtained by varying (2.4) with respect to $g_{\mu\nu}$. We get

$$\begin{aligned} G^{\mu\nu} &= \frac{1}{\mathcal{G}}\left[T^{\mu\nu} + \frac{1}{2}g^{\mu\nu}(F - \mathcal{G}R) + (g^{\mu\lambda}g^{\nu\sigma} - g^{\mu\nu}g^{\lambda\sigma})\mathcal{G}_{;\lambda\sigma}\right. \\ &+\frac{1}{2}\sum_{i=1}^{k}\sum_{j=1}^{i}(g^{\mu\nu}g^{\lambda\sigma} + g^{\mu\lambda}g^{\nu\sigma})(\Box^{j-i})_{;\sigma}\left(\Box^{i-j}\frac{\partial F}{\partial \Box^i R}\right)_{;\lambda} \\ &\left.-g^{\mu\nu}g^{\lambda\sigma}\left((\Box^{j-1}R)_{;\sigma}\Box^{i-j}\frac{\partial F}{\partial \Box^i R}\right)_{;\lambda}\right], \end{aligned} \tag{2.5}$$

where $G^{\mu\nu}$ is the above Einstein tensor and

$$\mathcal{G} \equiv \sum_{j=0}^{n}\Box^j\left(\frac{\partial F}{\partial \Box^j R}\right). \tag{2.6}$$

The differential Eqs.(2.5) are of order $(2k+4)$. The stress-energy tensor is due to the kinetic part of the scalar field and to the ordinary matter:

$$T_{\mu\nu} = T^m_{\mu\nu} + \frac{\varepsilon}{2}[\phi_{;\mu}\phi_{;\nu} - \frac{1}{2}\phi^{\alpha}_{;}\phi_{;\alpha}]\,. \tag{2.7}$$

The (eventual) contribution of a potential $V(\phi)$ is contained in the definition of F. From now on, we shall indicate by a capital F a Lagrangian density containing also the contribution of a potential $V(\phi)$ and by $F(\phi)$, $f(R)$, or $f(R, \Box R)$ a function of such fields without potential.

By varying with respect to the scalar field ϕ, we obtain the Klein-Gordon equation

$$\varepsilon\Box\phi = -\frac{\partial F}{\partial \phi}\,. \tag{2.8}$$

Several approaches can be used to deal with such equations. For example, as we said, by a conformal transformation, it is possible to reduce an ETG to a (multi) scalar-tensor theory of gravity [**?**, 383, 68, 174, **?**].

The simplest extension of General Relativiy is achieved assuming

$$F = f(R)\,, \qquad \varepsilon = 0\,, \tag{2.9}$$

in the action (2.4); $f(R)$ is an arbitrary (analytic) function of the Ricci curvature scalar R. We are considering here the simplest case of fourth-order gravity but we could construct such kind of theories also using other invariants in $R_{\mu\nu}$ or $R^{\alpha}_{\beta\mu\nu}$. The standard Hilbert-Einstein action is, of course, recovered for $f(R) = R$. Varying with respect to $g_{\alpha\beta}$, we get the field equations

$$f'(R)R_{\alpha\beta} - \frac{1}{2}f(R)g_{\alpha\beta} = f'(R)^{;\mu\nu}\left(g_{\alpha\mu}g_{\beta\nu} - g_{\alpha\beta}g_{\mu\nu}\right), \tag{2.10}$$

which are fourth-order equations due to the term $f'(R)^{;\mu\nu}$; the prime indicates the derivative with respect to R. Eq.(2.10) is also the equation for $T_{\mu\nu} = 0$ when the matter term is absent.

By a suitable manipulation, the above equation can be rewritten as:

$$G_{\alpha\beta} = \frac{1}{f'(R)}\left\{\frac{1}{2}g_{\alpha\beta}\left[f(R) - Rf'(R)\right] + f'(R)_{;\alpha\beta} - g_{\alpha\beta}\Box f'(R)\right\}, \tag{2.11}$$

where the gravitational contribution due to higher-order terms can be simply reinterpreted as a stress-energy tensor contribution. This means that additional and higher-order terms in the gravitational action act, in principle, as a stress-energy tensor, related to the form of $f(R)$. Considering also the standard perfect-fluid matter contribution, we have

$$G_{\alpha\beta} = \frac{1}{f'(R)}\left\{\frac{1}{2}g_{\alpha\beta}\left[f(R) - Rf'(R)\right] + f'(R)_{;\alpha\beta} - g_{\alpha\beta}\Box f'(R)\right\} + \frac{T^m_{\alpha\beta}}{f'(R)} = T^{curv}_{\alpha\beta} + \frac{T^m_{\alpha\beta}}{f'(R)}, \tag{2.12}$$

where $T^{curv}_{\alpha\beta}$ is an effective stress-energy tensor constructed by the extra curvature terms. In the case of General Relativity, $T^{curv}_{\alpha\beta}$ identically vanishes while the standard, minimal coupling is recovered for the matter contribution. The peculiar behavior of $f(R) = R$ is due to the particular form of the Lagrangian itself which, even though it is a second order Lagrangian, can be non-covariantly rewritten as the sum of a first order Lagrangian plus a pure divergence term. The Hilbert-Einstein Lagrangian can be in fact recast as follows:

$$L_{HE} = \mathcal{L}_{HE}\sqrt{-g} = \left[p^{\alpha\beta}(\Gamma^\rho_{\alpha\sigma}\Gamma^\sigma_{\rho\beta} - \Gamma^\rho_{\rho\sigma}\Gamma^\sigma_{\alpha\beta}) + \nabla_\sigma(p^{\alpha\beta}u^\sigma{}_{\alpha\beta})\right] \tag{2.13}$$

where:

$$p^{\alpha\beta} = \sqrt{-g}g^{\alpha\beta} = \frac{\partial\mathcal{L}}{\partial R_{\alpha\beta}} \tag{2.14}$$

Γ is the Levi-Civita connection of g and $u^\sigma_{\alpha\beta}$ is a quantity constructed out with the variation of Γ [**?**]. Since $u^\sigma_{\alpha\beta}$ is not a tensor, the above expression is not covariant; however a standard procedure has been studied to recast covariance in the first order theories [**?**]. This clearly shows that the field equations should consequently be second order and the Hilbert-Einstein Lagrangian is thus degenerate.

From the action (2.4), it is possible to obtain another interesting case by choosing

$$F = F(\phi)R - V(\phi), \qquad \varepsilon = -1. \tag{2.15}$$

In this case, we get

$$\mathcal{A} = \int d^4x\,\sqrt{-g}\left[F(\phi)R + \frac{1}{2}g^{\mu\nu}\phi_{;\mu}\phi_{;\nu} - V(\phi)\right] \tag{2.16}$$

$V(\phi)$ and $F(\phi)$ are generic functions describing respectively the potential and the coupling of a scalar field ϕ. The Brans-Dicke theory of gravity is a particular case of the action (2.16) for $V(\phi)$=0 [**?**]. The variation with respect to $g_{\mu\nu}$ gives the second-order field equations

$$F(\phi)G_{\mu\nu} = F(\phi)\left[R_{\mu\nu} - \frac{1}{2}Rg_{\mu\nu}\right] = -\frac{1}{2}T^\phi_{\mu\nu} - g_{\mu\nu}\Box_g F(\phi) + F(\phi)_{;\mu\nu}, \tag{2.17}$$

here $\Box_g$ is the d'Alembert operator with respect to the metric g The energy-momentum tensor relative to the scalar field is

$$T^\phi_{\mu\nu} = \phi_{;\mu}\phi_{;\nu} - \frac{1}{2}g_{\mu\nu}\phi_{;\alpha}\phi^{;\alpha} + g_{\mu\nu}V(\phi) \tag{2.18}$$

The variation with respect to ϕ provides the Klein - Gordon equation, i.e. the field equation for the scalar field:

$$\Box_g\phi - RF_\phi(\phi) + V_\phi(\phi) = 0 \tag{2.19}$$

where $F_\phi = dF(\phi)/d\phi$, $V_\phi = dV(\phi)/d\phi$. This last equation is equivalent to the Bianchi contracted identity [**?**]. Standard fluid matter can be treated as above.

2.4 Extended Theories at cosmological scales

2.4.1 Dark Energy as a curvature effect

In [77], it is shown that the most popular quintessence (dark energy) models can be reproduced, in principle, only considering "curvature effects" i.e. only generalizing the theory of gravity to some $f(R)$ which is not supposed to be simply linear in R. From our point of view, this approach seems "economic" and "conservative" and does not claim for unknown fundamental ingredients, up to now not detected, in the cosmic fluid. As it is clear, from Eq.(2.12), the curvature stress - energy tensor formally plays the role of a further source term in the field equations so that its effect is the same as that of an effective fluid of purely geometric origin. Let us rewrite it here for convenience:

$$T^{curv}_{\alpha\beta} = \frac{1}{f'(R)}\left\{\frac{1}{2}g_{\alpha\beta}\left[f(R) - Rf'(R)\right] + f'(R)^{;\mu\nu}(g_{\alpha\mu}g_{\beta\nu} - g_{\alpha\beta}g_{\mu\nu})\right\} . \tag{2.20}$$

It is possible to show that such a quantity provides all the ingredients we need to tackle with the dark side of the Universe. In fact, depending on the scales, such a curvature fluid can play, in principle, the role of dark matter and dark energy. To be more precise, also the coupling $1/f'(R)$ in front of the matter stress energy tensor, see Eqs.(2.12), plays a fundamental role in the dynamics since it affects, in principle, all the physical processes (e.g. the nucleo- synthesis) and the observable (luminous, clustered, baryonic) quantities. This means that the whole problem of the dark side of the Universe could be addressed considering a comprehensive theory where the interplay between the geometry and the matter has to be reconsidered assuming non-linear contributions and non-minimal couplings in curvature invariants.

From the cosmological point of view, in the standard framework of a spatially flat homogenous and isotropic Universe, the cosmological dynamics is determined by its energy budget through the Friedmann equations. In particular, the cosmic acceleration is achieved when the r.h.s. of the acceleration equation remains positive. Specifically the Friedmann equation, in physical units, is

$$\frac{\ddot{a}}{a} = -\frac{1}{6}\left(\rho_{tot} + 3p_{tot}\right) . \tag{2.21}$$

The subscript tot denotes the sum of the curvature fluid and the matter contribution to the energy density and pressure. From the above relation, the acceleration condition, for a dust dominated model, leads to :

$$\rho_{curv} + \rho_m + 3p_{curv} < 0 \rightarrow w_{curv} < -\frac{\rho_{tot}}{3\rho_{curv}} \tag{2.22}$$

so that a key role is played by the effective quantities :

$$\rho_{curv} = \frac{1}{f'(R)}\left\{\frac{1}{2}\left[f(R) - Rf'(R)\right] - 3H\dot{R}f''(R)\right\} , \tag{2.23}$$

and

$$w_{curv} = -1 + \frac{\ddot{R}f''(R) + \dot{R}\left[\dot{R}f'''(R) - Hf''(R)\right]}{\left[f(R) - Rf'(R)\right]/2 - 3H\dot{R}f''(R)} , \tag{2.24}$$

deduced from Eq.(2.20). As a first simple choice, one may neglect ordinary matter and assume a power - law form $f(R) = f_0R^n$, with n a real number, which represents a straightforward generalization of Einstein GR in the limit $n = 1$. One can find power - law solutions for $a(t)$

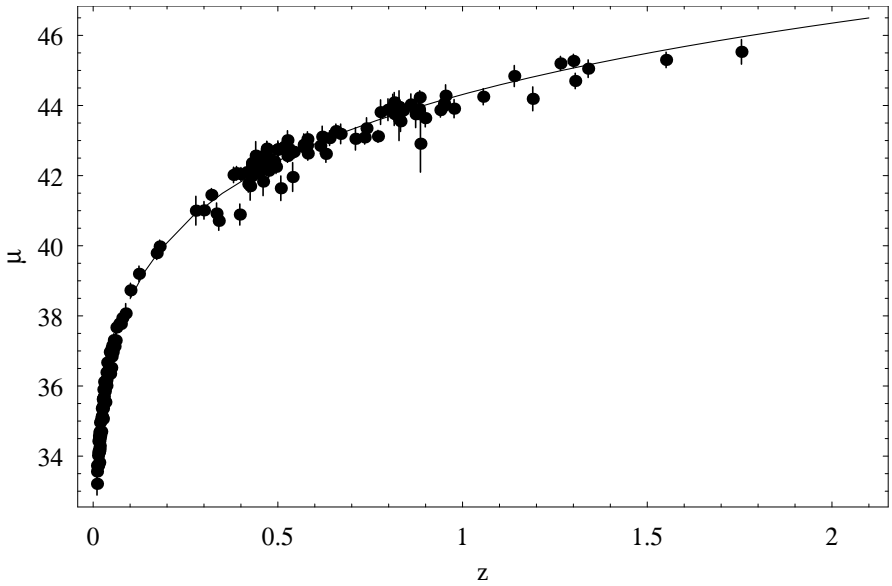

Figure 2.1: Best fit curve to the SNeIa Hubble diagram for the power law Lagrangian model. Only data of "Gold" sample of SNeIa have been used.

providing a satisfactory fit to the SNeIa data and a good agreement with the estimated age of the Universe in the range $1.366 < n < 1.376$ [76, 72]. On the other side, one can develop the same analysis in presence of the ordinary matter component, although in such a case, one has to solve numerically the field equations. Then, it is still possible to confront the Hubble flow described by such a model with the Hubble diagram of SNeIa using the above mentioned methods. The data fit turns out to be significant (see Fig. 2.2) improving the χ^2 value and it fixes the best fit value at $n = 3.46$ when it is accounted only the baryon contribute $\Omega_b \approx 0.04$ (according with BBN prescriptions). It has to be remarked that considering dark matter does not modify the result of the fit, as it is evident from Fig. 2.2, in some sense positively supporting the assumption of no need for dark matter in this model. A part the simplicity of the power law model, the theoretical implications of the best fit values found for n are telling us that dynamics related to cosmological constant (whose theoretical shortcomings are well known) could be seriously addressed by finding a reliable $f(R)$ gravity model (see also [353]).

From the evolution of the Hubble parameter in term of redshift, one can even calculate the age of Universe. In Fig. 2.3, it is sketched the age of the Universe as a function of the correlation between the deceleration parameter q_0 and the model parameter n. The best fit value $n = 3.46$ provides $t_{univ} \approx 12.41$ Gyr.

It is worth noticing that considering $f(R) = f_0 R^n$ gravity is only the simplest generalization of the Einstein theory. In other words, it has to be considered that R^n - gravity represents just a working hypothesis as there is no overconfidence that such a model is the correct final gravity theory. In a sense, we want only to suggest that several cosmological and astrophysical results can be well interpreted in the realm of a power law extended gravity model.

As matter of fact, this approach gives no rigidity about the value of the power n, although it would be preferable to determine a model capable of working at different scales. Furthermore, one does not expect to be able to reproduce the whole cosmological phenomenology by means of a simple power law model, which has been demonstrated to be not sufficiently versatile

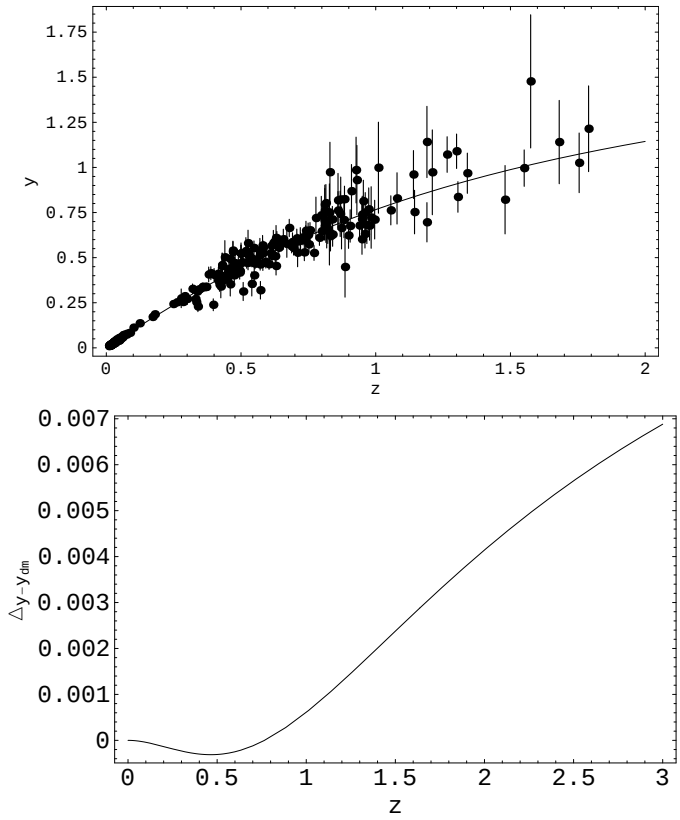

Figure 2.2: The Hubble diagram of 20 radio galaxies together with the "Gold" sample of SNela, in term of the redshift as suggested in [124]. The best fit curve refers to the R^n - gravity model without dark matter (left), while in the *right* panel it is shown the difference between the luminosity distances calculated without dark matter and in presence of this component in term of redshift. It is evident that the two behaviors are quite indistinguishable.

[83, 18, 17].

For example, it can be easily demonstrated that this model fails when it is analyzed with respect to its capability of providing the correct evolutionary conditions for the perturbation spectra of matter overdensity. This point is typically addressed as one of the most important issues which suggest the need for dark matter. In fact, if one wants to discard this component, it is crucial to match the experimental results related to the Large Scale Structure of the Universe and the CMBR which show, respectively at late time and at early time, the signature of the initial matter spectrum.

As important remark, we notice that the quantum spectrum of primordial perturbations, which provides the seeds of matter perturbations, can be positively recovered in the framework of R^n - gravity. In fact, $f(R) \propto R^2$ can represent a viable model with respect to CMBR data and it is a good candidate for cosmological Inflation (see [192, 193] and references therein).

In order to develop the matter power spectrum suggested by this model, we resort to the equation for the matter contrast obtained in [392] in the case of fourth order gravity (see even [260] for a review on cosmological perturbations in $f(R)$ - theories). This equation can

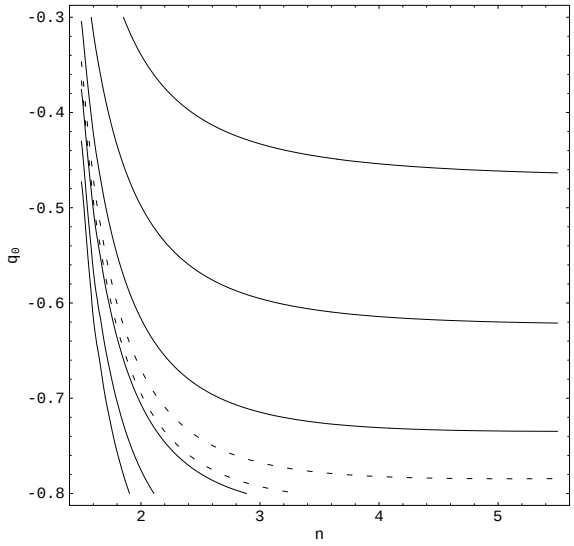

Figure 2.3: Contour plot in the plane $(q_0\,,\ n)$ describing the Universe age as induced by R^n - gravity model without dark matter. The contours refer to age ranging from 11 Gyr to 16 Gyr from up to down. The dashed curves define the $1-\sigma$ region relative to the best fit Universe age suggested by the last WMAP release ($13.73^{+0.13}_{-0.17}$ Gyr) in the case of Λ-CDM model [350]. At the best fit $n \simeq 3.5$ for SNeIa, the measured $q_0 \simeq -0.5$ gives a rather short age (about 11.5 Gyr) with respect to the WMAP constraint. This is an indication that the $f(R)$ model has to be further improved.

be deduced considering the conformal Newtonian gauge for the perturbed metric [392]:

$$ds^2 \,=\, (1+2\psi)dt^2 \,-\, a^2(1+2\phi)\Sigma_{i=1}^{3}(dx^i)\,. \tag{2.25}$$

where ψ and ϕ are now gravitational perturbation potentials. In GR, it is $\phi = -\psi$, since there is no anisotropic stress; in ETGs, this relation breaks, in general, and the $i \neq j$ components of field equations give new relations between ϕ and ψ.

In particular, for $f(R)$ gravity, due to the non-vanishing derivatives $f_{R;i;j}$ (with $i \neq j$), the $\phi - \psi$ relation becomes scale dependent. Instead of the perturbation equation for the matter contrast δ, we provide here its evolution in term of the growth index $\mathcal{F} = d\ln\delta/d\ln a$, which is the directly measured quantity at $z \sim 0.15$:

$$\mathcal{F}'(a) - \frac{\mathcal{F}(a)^2}{a} + \left[\frac{2}{a} + \frac{1}{a}E'(a)\right]\mathcal{F}(a) - \frac{1-2Q}{2-3Q}\cdot\frac{3\Omega_m\, a^{-4}}{n\,E(a)^2\tilde{R}^{n-1}} \,=\, 0\,, \tag{2.26}$$

(the prime, in this case, means the derivative with respect to a, n is the model parameter, being $f(R) \propto R^n$), $E(a) = H(a)/H_0$, $\tilde{R}$ is the dimensionless Ricci scalar, and

$$Q \,=\, -\frac{2f_{RR}\,k^2}{f_R\,a^2}\,. \tag{2.27}$$

For $n = 1$ the previous expression gives the ordinary growth index relation for the Cosmological Standard Model. It is clear, from Eq.(2.26), that such a model suggests a scale dependence

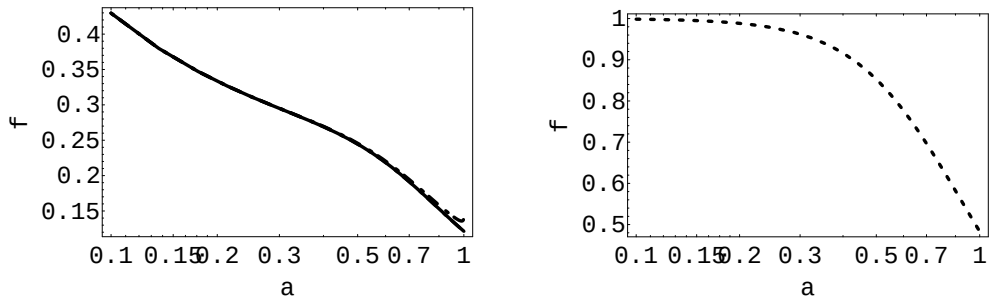

Figure 2.4: Scale factor evolution of the growth index : (*left*) modified gravity, in the case $\Omega_m = \Omega_{bar} \sim 0.04$, for the SNela best fit model with $n = 3.46$, (*right*) the same evolution in the case of a ΛCDM model. In the case of R^n - gravity it is shown also the dependence on the scale k. The three cases $k = 0.01,\ 0.001,\ 0.0002$ have been checked. Only the latter case shows a very small deviation from the leading behavior. Clearly, the trend is that the growth law saturates to $\mathcal{F} = 1$ for higher redshifts (i.e. $a \sim 0.001$ to 0.01). This behavior agrees with observations since we know that comparing CMB anisotropies and LSS, we need roughly $\delta \propto a$ between recombination and $z \sim 5$ to generate the present LSS from the small fluctuations at recombination seen in the CMB.

of the growth index which is contained into the corrective term Q so that, when $Q \to 0$, this dependence can be reasonably neglected.

In the most general case, one can resort to the limit $aH < k < 10^{-2} h\, Mpc^{-1}$, where Eq.(2.26) is a good approximation, and non-linear effects on the matter power spectrum can be neglected. Studying numerically Eq.(2.26), one obtains the growth index evolution in term of the scale factor; for the sake of simplicity, one can assume the initial condition $\mathcal{F}(a_{ls}) = 1$ at the last scattering surface as in the case of matter-like domination. The results are summarized in Fig.(2.4) - (2.5), where they have been displayed, in parallel, the growth index evolution in R^n - gravity and in the ΛCDM model. In the case of $\Omega_m = \Omega_{bar} \sim 0.04$, one can observe a strong disagreement between the expected rate of the growth index and the behavior induced by power law fourth order gravity models.

This negative result is evidenced by the predicted value of $\mathcal{F}(a_{z=0.15})$, which has been observationally estimated by the analysis of the correlation function for 220000 galaxies in 2dFGRS dataset sample at the survey effective depth $z = 0.15$. The observational result suggests $\mathcal{F} = 0.58 \pm 0.11$ [222], while previous model gives $\mathcal{F}(a_{z=0.15}) \sim 0.117\ (k = 0.01),\ 0.117\ (k = 0.001),\ 0.122\ (k = 0.0002)$.

Although this result seems frustrating with respect to the underlying idea to discard the dark matter component from the cosmological dynamics, it does not give substantial improvement in the case of R^n - gravity model plus dark matter. In fact, as it is possible to observe from Fig.(2.5), even in this case the growth index prediction is far to be in agreement with the ΛCDM model and again, at the observational scale $z = 0.15$, there is not enough growth of perturbations to match the observed Large Scale Structure. In such a case one obtains : $\mathcal{F}(a_{z=0.15}) \sim 0.29\ (k = 0.01),\ 0.29\ (k = 0.001),\ 0.31\ (k = 0.0002)$, which are quite increased with respect to the previous case but still very far from the experimental estimate.

It is worth noticing that no significant different results are obtained if one varies the power n. Of course in the case of $n \to 1$, one recovers the standard behavior if a cosmological constant contribution is added. These results seem to suggest that an ETG model which considers a simple power law of Ricci scalar, although cosmologically relevant at late times, is

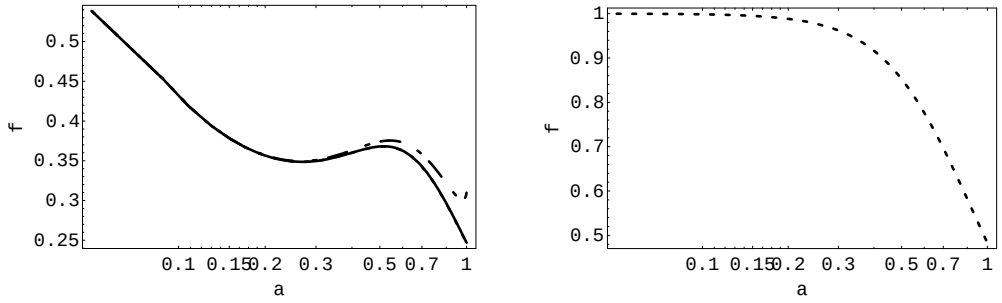

Figure 2.5: The evolution of the growth index in terms of the scale factor when dark matter is included in the whole energy budget. Again, the *left* plot shows the modified gravity evolution for the SNeIa best fit model with $n = 3.46$, while the *right* one refers to ΛCDM model.

not viable to describe the evolution of Universe at all scales.

In other words such a scheme seems too simple to give account of the whole cosmological phenomenology. In fact, in [392] a gravity Lagrangian considering an exponential correction to the Ricci scalar, $f(R) = R + A\exp(-B\,R)$ (with $A,\ B$ two constants), gives a grow factor rate which is in agreement with the observational results at least in the dark matter case. To corroborate this point of view, one has to consider that when the choice of $f(R)$ is performed starting from observational data (pursuing an inverse approach) as in [77], the reconstructed Lagrangian is a non - trivial polynomial in term of the Ricci scalar, as we shall see below.

A result which directly suggests that the whole cosmological phenomenology can be accounted only by a suitable non - trivial function of the Ricci scalar rather than a simple power law function. In this case, cosmological equations, coming from an $f(R)$ action, can be reduced to a linear third order differential equation for the function $f(R(z))$, where z is the redshift. The Hubble parameter $H(z)$ inferred from the data and the relation between z and R can be used to finally work out $f(R)$.

This scheme provides even another interesting result. Indeed, one may consider the expression for $H(z)$ in a given dark energy model as the input for the reconstruction of $f(R)$ and thus work out a $f(R)$ theory giving rise to the same dynamics as the input model.

This suggests the intriguing possibility to consider observationally viable dark energy models (such as ΛCDM and quintessence) only as effective parameterizations of the curvature fluid [77, 83]. As matter of fact, the results obtained with respect to the study of the matter power spectra in the case of R^n - gravity do not invalidate the whole approach, since they can be referred to the too simple form of the model. Similar considerations can be developed for cosmological solutions derived in Palatini approach (see [75] for details).

An important remark is in order at this point. If the power n is not a natural number, R^n models could be not analytic for $R \to 0$. In this case, the Minkowski space is not a solution and, in general, the post-Minkowskian limit of the theory could be bad defined. Actually this is not a true shortcoming if we consider R^n-gravity as a toy model for a (still unknown) self-consistent and comprehensive theory working at all scales.

However, the discussion is not definitely closed since some authors support the point of view that no $f(R)$ theories with $f = R + \alpha R^n$, $n \neq 1$ can evolve from a matter-dominated epoch $a(t) \propto t^{2/3}$ to an accelerated phase [17]. This result could be the end of such theories, if the phase space analysis of cosmological solutions is not correctly faced.

In [94], and recently in [95], it is shown that transient matter-dominated evolutions evolving

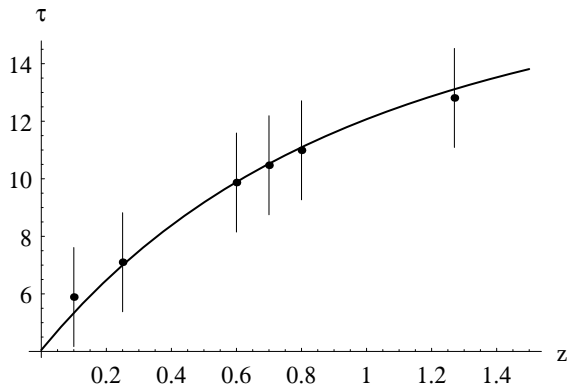

Figure 2.6: Comparison between predicted and observed values of $\tau = t_L(z) + \Delta f$ for the best fit ΛCDM model. Data in Table I have been used.

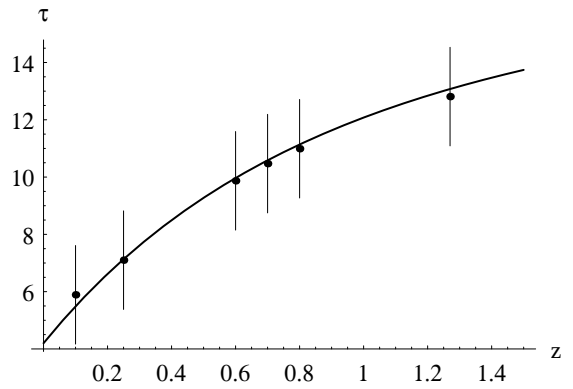

Figure 2.7: Comparison between predicted and observed values of $\tau = t_L(z) + \Delta f$ for the best fit $f(R)$ power-law model as in Fig.2.2. Data in Table I have been used. Also for this test, it is evident the strict concordance with ΛCDM model in Fig.2.6.

toward accelerated phases are actually possible and the lack of such solutions in [17] depends on an incomplete parameterization of the phase space.

In general, by performing a conformal transformation on a generic $f(R)$ gravity theory, it is possible to achieve, in the Einstein frame, dust matter behaviors which are compatible with observational prescriptions. In addition, by exploiting the analogy between the two frames and between modified gravity and scalar-tensor gravity, one can realize that physical results, in the two conformally related frames, could be completely different. In other words one can pass from a non - phantom phase behavior (Einstein frame) to a phantom regime (Jordan frame) [82].

Now, we can suppose to change completely the point of view. In fact, we can rely directly with the Jordan frame and we can verify if a dust matter regime is intrinsically compatible with modified gravity.

As a first example, one can cite the exact solution provided in [72], which has been deduced working only in the Jordan Frame (FRW Universe). In particular, one is able to find a power

law regime for the scale factor whose rate is connected with the power n of the Lagrangian $f(R) = f_0 R^n$.

In other words, one has $a(t) = a_0 t^\alpha$ with $\alpha = \dfrac{2n^2 - 3n + 1}{2 - n}$. Such an exact solution is found out when only baryonic matter is considered [78, 84]. It is evident that such a solution allows to obtain an ordinary matter behavior ($\alpha = 2/3$) for given values of the parameter n (i.e. $n \sim -0.13,\ n \sim 1.29$).

Such solutions are nevertheless stable and no transition to acceleration phase then occurs. In general, it is possible to show that solutions of the type

$$a = a_0 (t - t_0)^{\frac{2n}{3(1+w)}}\,, \tag{2.28}$$

where w is the barotropic index of standard perfect fluid, arises as a transient phase, and this phase evolves into an accelerated solution representing an attractor for the system [94]. In any case, a single solution exactly matching, in sequence, radiation, matter and accelerated phases is unrealistic to be found out in the framework of simple $f(R)$-power law theories. The discussion can be further extended as follows.

2.4.2 Reconstructing f(R) model

Modified gravity can span a wide range of analytic functions of the Ricci scalar where $f(R) = f_0 R^n$ only represents the simplest choice. In general, one can reverse the perspective and try to derive the form of gravity Lagrangian directly from the data or mimicking other cosmological models.

Such an approach has been developed in [77], and allows to recover modified gravity Lagrangians by the Hubble flow dynamics $H(z)$: in particular, it is possible to show that wide classes of dark energy models worked out in the Einstein frame can be consistently reproduced by $f(R)$-gravity as quintessence models with exponential potential [71].

Clearly the approach works also for the case of coupled quintessence scalar fields. In other words, the dynamics of $H(z)$, considered in the Jordan frame, is reconstructed by observational data considered in the Einstein frame then assuming one of the two frames as the "physical frame" could be misleading. Here we further develop this approach with the aim to show, in general, the viability of $f(R)$ gravity to recover a matter-dominated phase capable of evolving in a late accelerating phase.

From a formal point of view, the reconstruction of the gravity Lagrangian from data is based on the relation which expresses the Ricci scalar in terms of the Hubble parameter:

$$R = -6\left(\dot{H} + 2H^2 + \frac{k}{a^2}\right)\,. \tag{2.29}$$

Now, starting from the above the $f(R)$ field equations (2.12) one can reconstruct the form of $f(R)$ from the Hubble parameter as a function of the redshift z exploiting the relation (2.29) after this expression has been rewritten in term of the redshift itself.

A key role in this discussion is played by the conservation equation for the curvature and the matter fluids which, in the case of dust matter, (i.e. $p_m = 0$) gives:

$$\begin{aligned} \dot{\rho}_{curv} + 3H(1 + w_{curv})\rho_{curv} &= -\frac{1}{f'(R)}(\dot{\rho}_m + 3H\rho_m) \\ &\quad -\rho_m \frac{df'(R)}{dt}\,. \end{aligned} \tag{2.30}$$

In particular, one may assume that the matter energy density is conserved :

$$\rho_m = \Omega_M \rho_{crit} a^{-3} = 3H_0^2 \Omega_M (1+z)^3 \tag{2.31}$$

with $z = 1/a - 1$ the redshift (having set $a(t_0) = 1$), Ω_M the matter density parameter (also here, quantities labelled with the subscript 0 refers to present day ($z = 0$) values). Eq.(2.31) inserted into Eq.(2.30), allows to write a conservation equation for the effective curvature fluid :

$$\begin{aligned} \dot{\rho}_{curv} + 3H(1+w_{curv})\rho_{curv} &= 3H_0^2 \Omega_M (1+z)^3 \\ &\times \frac{\dot{R} f''(R)}{[f'(R)]^2} \, . \end{aligned} \tag{2.32}$$

Actually, since the continuity equation and the field equations are not independent [77], one can reduce to the following single equation

$$\begin{aligned} \dot{H} &= -\frac{1}{2f'(R)} \left\{ 3H_0^2 \Omega_M (1+z)^3 + \ddot{R} f''(R) + \right. \\ &\left. + \dot{R} \left[\dot{R} f'''(R) - H f''(R) \right] \right\} , \end{aligned} \tag{2.33}$$

where all quantities can be expressed in term of redshift by means of the relation $\frac{d}{dt} = -(1+z)H\frac{d}{dz}$. In particular, for a flat FRW metric, one has :

$$R = -6 \left[2H^2 - (1+z)H \frac{dH}{dz} \right] , \tag{2.34}$$

$$f'(R) = \left(\frac{dR}{dz} \right)^{-1} \frac{df}{dz} \, , \tag{2.35}$$

$$f''(R) = \left(\frac{dR}{dz} \right)^{-2} \frac{d^2 f}{dz^2} - \left(\frac{dR}{dz} \right)^{-3} \frac{d^2 R}{dz^2} \frac{df}{dz} \, , \tag{2.36}$$

$$\begin{aligned} f'''(R) &= \left(\frac{dR}{dz} \right)^{-3} \frac{d^3 f}{dz^3} + 3 \left(\frac{dR}{dz} \right)^{-5} \left(\frac{d^2 R}{dz^2} \right)^2 \frac{df}{dz} + \\ &- \left(\frac{dR}{dz} \right)^{-4} \left(3 \frac{d^2 R}{dz^2} \frac{d^2 f}{dz^2} + \frac{d^3 R}{dz^3} \frac{df}{dz} \right) \, . \end{aligned} \tag{2.37}$$

Now, one has all the ingredients to reconstruct the shape of $f(R)$ by data or, in general, by the definition of a suitable $H(z)$ viable with respect to observational results. In particular, one can show that a standard matter regime (necessary to cluster large scale structure) can arise, in this scheme, before the accelerating phase arises as, for example, in the so called *quiessence* model.

A quiessence model is based on an ordinary matter fluid plus a cosmological component whose equation of state w is constant but can scatter from $w = -1$. This approach represents the easiest generalization of the cosmological constant model, and it has been successfully tested against the SNeIa Hubble diagram and the CMBR anisotropy spectrum so that it allows to severely constraint the barotropic index w [183, 184, 253].

It is worth noticing that these constraints extend into the region $w < -1$, therefore models (phantom models) violating the weak energy condition are allowed. From the cosmological dynamics viewpoint, such a model, by definition, has to display an evolutionary rate of expansion which moves from the standard matter regime to the accelerated behavior in relation to the value of w. In particular, this quantity parameterizes the transition point to the accelerated epoch.

Actually, if it is possible to find out a $f(R)$-gravity model compatible with the evolution of the Hubble parameter of the quiessence model, this result suggests that modified gravity is compatible with a phase of standard matter domination. To be precise, let us consider the Hubble flow defined by this model, where, as above :

$$H(z) = H_0\sqrt{\Omega_M(1+z)^3 + \Omega_X(1+z)^{3(1+w)}} \tag{2.38}$$

with $\Omega_X = (1-\Omega_M)$ and w the constant parameter defining the dark energy barotropic index. This definition of the Hubble parameter implies:

$$R = -3H_0^2\left[\Omega_M(1+z)^3 + \Omega_X(1-3w)(1+z)^{3(1+w)}\right] . \tag{2.39}$$

The ansatz in Eq.(2.38) allows to obtain from Eq.(**??**) a differential relation for $f(R(z))$ which can be solved numerically by choosing suitable boundary conditions. In particular we choose :

$$\left(\frac{df}{dz}\right)_{z=0} = \left(\frac{dR}{dz}\right)_{z=0} , \tag{2.40}$$

$$\left(\frac{d^2f}{dz^2}\right)_{z=0} = \left(\frac{d^2R}{dz^2}\right)_{z=0} . \tag{2.41}$$

$$f(z=0) = f(R_0) = 6H_0^2(1-\Omega_M) + R_0 . \tag{2.42}$$

A comment is in order here. We have derived the present day values of df/dz and d^2f/dz^2 by imposing the consistency of the reconstructed $f(R)$ theory with *local* Solar System tests. One could wonder whether tests on local scales could be used to set the boundary conditions for a cosmological problem. It is easy to see that this is indeed meaningful.

Actually, the isotropy and homogeneity of the Universe ensure that the present day value of a whatever cosmological quantity does not depend on where the observer is. As a consequence, hypothetical observers living in the Andromeda galaxy and testing gravity in his planetary system should get the same results. As such, the present day values of df/dz and d^2f/dz^2 adopted by these hypothetical observers are the same as those we have used, based on our Solar System experiments. Therefore, there is no systematic error induced by our method of setting the boundary conditions.

Once one has obtained the numerical solution for $f(z)$, inverting again numerically Eq.(2.39), we may obtain $z = z(R)$ and finally get $f(R)$ for several values of w.

It turns out that $f(R)$ is the same for different models for low values of R and hence of z. This is a consequence of the well known degeneracy among different quiessence models at low z that, in the standard analysis, leads to large uncertainties on w. This is reflected in the shape of the reconstructed $f(R)$ that is almost w - independent in this redshift range.

An analytic representation of the reconstructed fourth order gravity model, can be obtained considering that the following empirical function

$$\ln(-f) = l_1\left[\ln(-R)\right]^{l_2}\left[1+\ln(-R)\right]^{l_3} + l_4 \tag{2.43}$$

approximates very well the numerical solution, provided that the parameters (l_1, l_2, l_3, l_4) are suitably chosen for a given value of w. For instance, for $w = -1$ (the cosmological constant) it is:

$$(l_1, l_2, l_3, l_4) = (2.6693, 0.5950, 0.0719, -3.0099) \ .$$

At this point, one can wonder if it is possible to improve such a result considering even the radiation, although energetically negligible. Rather than inserting radiation in the (2.38), a more general approach in this sense is to consider the Hubble parameter descending from a unified model like those discussed in [91]. In such a scheme one takes into account energy density which scales as:

$$\rho(z) = A \ \left(1 + \frac{1+z}{1+z_s}\right)^{\beta-\alpha} \ \left[1 + \left(\frac{1+z}{1+z_b}\right)^{\alpha}\right] \tag{2.44}$$

having defined:

$$z_s = 1/s - 1 \ , \qquad z_b = 1/b - 1 \ . \tag{2.45}$$

This model, with the choice $(\alpha, \beta) = (3, 4)$, is able to mimic a Universe undergoing first a radiation dominated era (for $z \gg z_s$), then a matter dominated phase (for $z_b \ll z \ll z_s$) and finally approaching a de Sitter phase with constant energy.

In other words, it works in the way we are asking for. In such a case, the Hubble parameter can be written, in natural units, as $H = \sqrt{\frac{\rho(z)}{3}}$ and one can perform the same calculation as in the quiessence case.

As a final result, it is again possible to find out a suitable $f(R)$-gravity model which, for numerical reasons, it is preferable to interpolate as $f(R)/R$:

$$\begin{aligned}\frac{f(R)}{R} \ = \ 1.02 \times \frac{R}{R_0} \Bigg[1 + \Bigg(-0.04 \times (\frac{R}{R_0})^{0.31} \\ +0.69 \times (\frac{R}{R_0})^{-0.53}\Bigg) \times \ln(\frac{R}{R_0})\Bigg] \ ,\end{aligned} \tag{2.46}$$

where R_0 is a normalization constant. This result once more confutes issues addressing modified gravity as incompatible with structure formation prescriptions. In fact, also in this case, it is straightforward to show that a phase of ordinary matter (radiation and dust) domination can be obtained and it is followed by an accelerated phase.

Furthermore, several recent studies are pointing out that large scale structure and CMBR anisotropy spectrum are compatible with $f(R)$ gravity as discussed in details in [346, 366] for the metric approach and in [214] for the Palatini approach.

In particular, in [346], it is shown that several classes of $f(R)$ theories can tune the large-angle CMB anisotropy, the shape of the linear matter power spectrum, and qualitatively change the correlations between the CMB and galaxy surveys. All these phenomena are accessible with current and future data and will soon provide stringent tests for such theories at cosmological scales [48, 151, 281, 393].

2.5 Toy models

Are there some f(R) models which satisfies all the right requirements to be considered as good starting point of an Extended Theory of Gravity? We are now going to consider some f(R) models which don't contain a cosmological constant and are explicitly designed to satisfy

cosmological and Solar System constraints in given limits of the parameter space. Practically we choose a class of functional forms of f(R) which are able to match, in principle, observational data. In definitive:

- they have to reproduce CMBR constraints in the high redshift regime which agree with the presence of a effective cosmological constant;
- they should give rise to an accelerated expansion, at low redshift, according to ΛCDM;
- they need to have a sufficient number of degrees of freedom in the parameterization in order to encompass low redshift phenomena, as large scale structure, according to the observations;
- small deviations from the General Relativity should be consistent with Solar System tests.

All these requirements suggest that we can assume the limits

$$\lim_{R\to\infty} f(R) = \text{ constant} \tag{2.47}$$

and

$$\lim_{R\to 0} f(R) = 0\ . \tag{2.48}$$

Recently an interesting f(R) model has been proposed in [190]. Starting with a gravity action

$$\mathcal{A} = \int d^4x\sqrt{-g}\left[\frac{R+f(R)}{16\pi G} + \mathcal{L}_m\right] \tag{2.49}$$

in this model[2] f(R) is given by

$$f_{HS}(R) = -m^2\frac{c_1\left(R/m^2\right)^n}{c_1\left(R/m^2\right)^n + 1} \tag{2.50}$$

where $n > 0$, c_1 and c_2 are dimensionless parameters and m is a mass scale taken for convenience being equal to

$$m^2 \equiv \frac{8\pi G}{3}\overline{\rho_0} = (8315\ \mathrm{Mpc})^{-2}\left(\frac{\Omega_m h^2}{0.13}\right) \tag{2.51}$$

where $\overline{\rho_0}$ is the average density today. The sign of f(R) is chosen so that its second derivative

$$f_{RR} \equiv \frac{\mathrm{d}^2 f(R)}{\mathrm{d}R^2} > 0 \tag{2.52}$$

for $R \ll m^2$ to ensure that, at high density, the solution is stable at high curvature. This condition also implies that cosmological tests at high redshift remain the same as in General Relativity. This model clearly satisfies the conditions

$$\lim_{R\to\infty} f_{HS}(R) = \text{ constant} \tag{2.53}$$

$$\lim_{R\to 0} f_{HS}(R) = 0\ . \tag{2.54}$$

[2] HS is for authors' names, Hu and Sawicki

The second condition means that there could be a flat spacetime solution, i.e. vanishing cosmological constant. There is no true cosmological constant introduced in this class; however, at curvatures high compared with m^2 (R is large even in the present universe), $f_{HS}(R)$ may be expanded as

$$\lim_{m^2/R\to 0} f_{HS}(R) \approx -\frac{c_1}{c_2}m^2 + \frac{c_1}{c_2^2}m^2\left(\frac{m^2}{R}\right)^n . \tag{2.55}$$

Thus the limiting case of $c_1/c_2^2 \to 0$ at fixed c_1/c_2 is a cosmological constant in both cosmological and local tests of gravity. Moreover it shows an "effective" cosmological constant $-m^2c_1/c_2$ and generates late-time accelerating expansion. One can show that

$$H^2 \sim \frac{8\pi G m^2 c_1}{c_2} \sim (70\ \mathrm{km/s}\cdot\ \mathrm{pc})^2 \sim (10^{-33}\ \mathrm{eV})^2 \tag{2.56}$$

At the intermediate epoch, where the matter density ρ is larger than the effective cosmological constant,

$$\rho > \frac{m^2 c_1}{c_2}, \tag{2.57}$$

there appears the matter dominated phase and the universe expands with deceleration. Hence, the above model describes an effective ΛCDM cosmology.

Although the model from [190] is very successfull, the early time inflation is not included there. But it is possible to modify the f(R) gravity model to treat the inflation and the late-time accelerating expansion in a unified way. In order to include the inflation at the early universe, the simplest extention may require

$$\lim_{R\to\infty} f(R) = -\Lambda_i. \tag{2.58}$$

Here Λ_i is an effective cosmological constant at early universe and therefore we assume $\Lambda_i \ll (10^{-33}\ \mathrm{eV})^2$. For instance, it could be $\Lambda_i \sim 10^{20\div 38}$.

In order that the accelerating expansion in the present universe could be generated, let us consider that f(R) could be a small constant at present universe, that is,

$$f(R_0) = -2\widetilde{R}_0\ ,\ f'(R_0) \sim 0. \tag{2.59}$$

Here R_0 is the present curvature, $R_0 \sim (10^{-33}\ \mathrm{eV})^2$. The last condition corresponding to the second one in Eq.(2.54):

$$\lim_{R\to 0} f(R) = 0\ . \tag{2.60}$$

In the above class of models, the universe starts from the inflation driven by the effective cosmological constant, Eq.(2.58) at the early stage, where curvature is very large. As curvature becomes smaller, the effective cosmological constant also becomes smaller. After that the radiation/matter dominates. When the density of the radiation and the matter becomes small and the curvature goes to the value R_0, there appears the small effective cosmological constant Eq.(2.59). Hence, the current cosmic expansion could start. An example satisfying Eqs.(2.58)-(2.59)-(2.60) is

$$f(R) = -\frac{(R-R_0)^{2n+1} + R_0^{2n+1}}{f_0 + f_1\left[(R-R_0)^{2n+1} + R_0^{2n+1}\right]} = -\frac{1}{f_1} + \frac{f_0/f_1}{f_0 + f_1\left[(R-R_0)^{2n+1} + R_0^{2n+1}\right]} \tag{2.61}$$

Here n is a positive integer, and

$$\frac{R_0^{2n+1}}{f_0 + f_1 R_0^{2n+1}} = 2R_0 \ , \ \frac{1}{f_1} = \Lambda_i \tag{2.62}$$

that is

$$f_0 = \frac{R_0^{2n}}{2} - \frac{R_0^{2n+1}}{\Lambda_i} \sim \frac{R_0^{2n}}{2} \ , \ f_1 = \frac{1}{\Lambda_i}. \tag{2.63}$$

By introducing the auxiliary field A in the gravitational part of the action Eq.(2.49), one can rewrite

$$\mathcal{A}_\} = \frac{1}{8\pi G} \int d^4x \sqrt{-g} \left\{ (1 + f'(A))(R - A) + A + f(A) \right\} \tag{2.64}$$

As it is clear, if $F'(R) = 1 + f'(R) < 0$, the effective coupling $(8\pi G)/F'(A)$ becomes negative and the theory enter the anti-gravity regime. This is not the case for General Relativity. The action can be again recast in a scalar-tensor form by using the conformal scale transformation $g_{\mu\nu} \to e^\sigma g_{\mu\nu}$ with the scalar field σ given as $\sigma = -\ln(1 + f'(A))$. In general, an effective mass for the scalar field σ is defined as

$$m_\sigma^2 = \frac{1}{2} \left[\frac{A}{F'(A)} - \frac{4F(A)}{(F'(A))^2} + \frac{1}{F''(A)} \right] \tag{2.65}$$

which, in the weak field limit, could introduce corrections to the Newton law. Naively, one expect the order of mass m_σ could be that of the Hubble rate, that is, $m_\sigma \sim H \sim 10^{-33}$ eV, which is very light and the correction could be very large. We should note, however, that the mass m_σ depends on the curvature. The curvature on the earth, R_{earth}, is much larger than the average curvature R_{solar} in the solar system, and R_{solar} is also much larger than the average curvature in the universe, whose order whose order is given by the square of the Hubble rate, H^2, that is, $R_{earth} \gg R_{solar} \gg H^2$. Then if the mass becomes large when the curvature is large, the correction to the Newton law could be small. In air on the earth, the scalar curvature could be given by $A = R \sim 10^{-50}$ eV^2. On the other hand, in the solar system, we find $A = R \sim 10^{-61}$ eV^2. In the model Eq.(2.61) if $n \leq 3$ in the air or $n \leq 10 \sim 12$ (if $\Lambda_i \sim 10^{20 \div 38}$) in the solar system, we find

$$f_0 \ll f_1 \left\{ \ (R - R_0)^{2n+1} + R_0^{2n+1} \right\} \sim f_1 R^{2n+1} \tag{2.66}$$

and

$$F(R) = R + f(R) \sim R - \frac{1}{f_1} + \frac{f_0}{f_1^2 R^{2n+1}} \sim \frac{1}{f_1}. \tag{2.67}$$

Furthermore, if $n > 6 \sim 7$ (if $\Lambda_i \sim 10^{20 \div 38}$) in the air, we find $F'(R) \sim 1$ and

$$m_\sigma^2 \sim \frac{F(A)}{F'(A)^2} \sim \frac{2}{f_1} \sim 10^{38 \div 56} \text{ eV}^2, \tag{2.68}$$

which is very large and there is no observable correction to the Newton law. On the other hand, in the Solar System, if $n \gg 10 \sim 12$ (if $\Lambda_i \sim 10^{20 \div 38}$)

$$m_\sigma^2 \sim \frac{1}{2F''(A)} \sim \frac{f_0}{f_1 R^{2n+3}} \sim 10^{239 \div 295 - 10n} \text{ eV}^2, \tag{2.69}$$

which is large enough since the radius of the earth is about 10^7 m $\sim 10^{-14}$ eV and there is no visible correction to the Newton law.

As condition that inflation occurs one may impose the condition

$$\lim_{R\to\infty} f(R) = \alpha R^m \tag{2.70}$$

instead of Eq.(2.58). A simplest model which satisfies this condition and the Eqs.(2.59)-(2.60) is

$$f(R) = \alpha R^m - \beta R^n \ . \tag{2.71}$$

Here α and β are positive constants and m and n are positive integers satisfying the condition $m > n$. Since

$$f'(R) = \alpha m R^{m-1} - \beta n R^{n-1} \ , \tag{2.72}$$

we find

$$R_0 = \left(\frac{\beta n}{\alpha m}\right)^{1/(m-n)} \ , \ f(R_0) = -\beta\left(1-\frac{n}{m}\right)\left(\frac{\beta n}{\alpha m}\right)^{n/(m-n)} < 0 \tag{2.73}$$

Since

$$f(R_0) = -2\widetilde{R}_0 \sim R_0 \sim (10^{-33}\ \mathrm{eV}^2), \tag{2.74}$$

one gets $\alpha \sim R_0^{1-m}$ and $\beta \sim R_0^{1-n}$. This show that f(R) becomes larger than R, $f(R) \gg R$, even in the solar system where $R \sim 10^{-61}\ \mathrm{eV}^2$, which could be inconsistent.

Another more realistic proposal is

$$f(R) = \frac{\alpha R^{m+l} - \beta R^n}{1+\gamma R^l} \ . \tag{2.75}$$

Here α, β and γ are positive constants while n, m and l are positive integers satisfying the condition $m + l > n$. For simplicity we now choose

$$n = m = l \tag{2.76}$$

$$f(R) = \frac{\alpha R^{2n} - \beta R^n}{1+\gamma R^n} \tag{2.77}$$

Then since

$$f'(R) = \frac{nR^{n-1}(\alpha\gamma R^{2n} - 2\alpha R^n - \beta)}{(1+\gamma R^n)^2} \tag{2.78}$$

one gets R_0 satisfying Eq.(2.59) is given by

$$R_0 = \left\{\frac{1}{\gamma}\left(1+\sqrt{1+\frac{\beta\gamma}{\alpha}}\right)\right\}^{1/n} \ , \tag{2.79}$$

and therefore

$$f(R_0) \sim -2\widetilde{R}_0 = \frac{\alpha}{\gamma^2}\left(1+\frac{(1-\beta\gamma/\alpha)\sqrt{1+\beta\gamma/\alpha}}{2+\sqrt{1+\beta\gamma/\alpha}}\right) \ . \tag{2.80}$$

Let us check if we can choose parameters to reproduce realistic cosmological evolution. As a working hypothesis we assume $\beta\gamma/\alpha \gg 1$, then

$$R_0 \sim (\beta/\alpha\gamma)^{1/2n} \ , \ f(R_0) = -2\widetilde{R}_0 \sim -\beta/\gamma \tag{2.81}$$

We also assume

$$f(R_I) \sim (\alpha/\gamma)R_I^n \sim R_I \ , \tag{2.82}$$

where R_I is the curvature in the inflationary epoch which is $R_I \sim (10^{15}\,\mathrm{GeV})^2 = (10^{24}\,\mathrm{eV})^2$. As a result one obtains

$$\alpha \sim 2\widetilde{R}_0 R_0^{-2n}\ ,\ \beta \sim 4\widetilde{R}_0^2 R_0^{-2n} R_I^{n-1}\ ,\ \gamma \sim 2\widetilde{R}_0 R_0^{-2n} R_I^{n-1}\ . \tag{2.83}$$

Hence we can confirm the assumption $\beta\gamma/\alpha \gg 1$ if $n > 1$ as

$$\frac{\beta\gamma}{\alpha} \sim 4\widetilde{R}_0^2 R_0^{-2n} R_I^{2n-2} \sim 10^{228(n-1)} \tag{2.84}$$

It is also possible to investigate the above correction to the Newton law in the model Eq.(2.77) with conditions Eq.(2.83). In the Solar System where $R \sim (10^{-61}\,\mathrm{eV})^2$, or in the air on earth, where $R \sim (10^{-50}\,\mathrm{eV})^2$, we find

$$F(R) = R + f(R) \sim R - 2R_0 \sim R\,, \tag{2.85}$$

$$F'(R) = 1 + f'(R) \sim 1 + \frac{n\alpha}{\gamma} R^{n-1} \sim 1 + n\left(\frac{R}{R_I}\right)^{n-1} \sim 1\,, \tag{2.86}$$

$$F''(R) = f''(R) \sim \frac{n(n-1)}{R_I}\left(\frac{R}{R_I}\right)^{n-2}\ . \tag{2.87}$$

Then in the solar system the mass m_σ of the scalar field σ is given by $m_\sigma^2 \sim 10^{-160+109n}\ \mathrm{eV}^2$ and in the air on the earth, $m_\sigma^2 \sim 10^{-144+98n}\ \mathrm{eV}^2$. In both cases, the mass m_σ is very large if $n \geq 2$ and the correction to the Newton law is very small. Thus, it is proposed a viable modified gravity model which unifies curvature-induced R^m inflation with effective ΛCDM cosmology. There is no violation of Newton law in such theory while the known universe expansion history is reproduced.

2.6 Final lesson on Extended theories of Gravity

Astrophysical observations are pointing out huge amounts of "dark matter" and "dark energy" needed to explain the observed large scale structure and cosmic dynamics. The emerging picture is a spatially flat, homogeneous Universe undergoing the today observed accelerated phase. Despite of the good quality of astrophysical surveys, commonly addressed as *Precision Cosmology*, the nature and the nurture of dark energy and dark matter, which should constitute the bulk of cosmological matter-energy, are still unknown. Furthermore, up to now, no experimental evidence has been found, at fundamental level, to explain such mysterious components.

The problem could be completely reversed considering dark matter and dark energy as "shortcomings" of General Relativity in its simplest formulation (a linear theory in the Ricci scalar R, minimally coupled to the standard perfect fluid matter) and claiming for the "correct" theory of gravity as that derived by matching the largest number of observational data, without imposing any theory *a priori*. As a working hypothesis, accelerating behavior of cosmic fluid, large scale structure, potential of galaxy clusters, rotation curves of spiral galaxies could be reproduced by means of *extending* the standard theory of General Relativity. In other words, gravity could acts in different ways at different scales and the above "shortcomings" could be due to incorrect extrapolations of the Einstein gravity, actually tested at short scales and low energy regimes.

We have done an historical and technical survey of what is intended for *Extended Theories of Gravity* in the so called "metric" approaches, and we have discussed some cosmological

applications where the issues related to the dark components are addressed by enlarging the Einstein theory to more general $f(R)$ Lagrangians, where $f(R)$ is a generic function of Ricci scalar R, not assumed simply linear. Obviously, this is not the final answer to the problem of "dark-components" but it can be considered as an operative scheme whose aim is to avoid the addition of unknown exotic ingredients to the cosmic pie.

Part II
Gravitational systems in $\mathrm{f(R)}$

CHAPTER 3

Galaxies without Dark Matter

3.1 Galaxies

In this chapter(based on [84, 162, 78]) we are now going to start our investigation on the possibility to successfully applying the approach of Extended Theories of Gravity to gravitational systems on different scales.
In a cosmological framework, such an approach lead to modified Friedmann equations that can be formally written in the usual form by defining an effective *curvature fluid* giving rise to a negative pressure which drives the cosmic acceleration [69, 87, 96, 272, 88]. Also referred to as $f(R)$ theories, this approach is recently extensively studied both from the theoretical and the observational point of view (see e.g. [72, 75, 49]). Moreover, this same approach has been also proposed, in early cosmology, as a mechanism giving rise to an inflationary era without the need of any inflaton field [352].

All this amount of work has been, essentially, concentrated on the cosmological applications and have convincingly demonstrated that extended theories of gravity (in particular $f(R)$ gravity) are indeed able to explain the cosmic speed up and fairly fit the available data-sets and, hence, represents a viable alternative to the dark energy models [77].

Changing the gravity sector could have consequences not only at cosmological scales, but also at the galactic and cluster scales so that it is mandatory to investigate the low energy limit of such theories. A strong debate is open with different results arguing in favor [131, 347, 101, 268, 12, 89] or against [135, 104, 284] such models. It is worth noting that, as a general result, higher order theories of gravity cause the gravitational potential to deviate from its Newtonian $1/r$ scaling [355, 212, 331, 107, 343, 254] even if such deviations may be vanishing.

We are now going to focus on the problem of rotation curves of spiral galaxies, historically considered one of the most important evidences for the existence of dark matter haloes; while we are going to interpret it as a signal of the breakdown of General Relativity.

W are first going to investigate the Newtonian limit of power law $f(R) = f_0 R^n$ theories, assuming that the metric in the low energy limit ($\Phi/c^2 << 1$) may be taken as Schwarzschild - like. It turns out that a power law term $(r/r_c)^\beta$ has to be added to the Newtonian $1/r$ term in order to get the correct gravitational potential. While the parameter β may be expressed analytically as a function of the slope n of the $f(R)$ theory, r_c sets the scale where the correction term starts being significant. Nevertheless, the simple power law $f(R)$ gravity is nothing else but a toy-model which fail if one tries to achieve a comprehensive model for all the cosmological dynamics, ranging from the early universe, to the large scale structure up to the late accelerated era [78, 216].

We will consider spiral galaxies splitted in two families starting from their different physical properties:

- Low Surface Brightness Galaxies (LSB). There are many *photometric* definitions for them, the most general and qualitative being that they are galaxies in which the contrast with respect to the background sky brightness is low (at least one magnitude fainter). Tipically, LSB galaxies are described as having the morphology of late-type/irregular spiral galaxies. This description certainly holds true for a significant percentage of LSB galaxies, but there are also LSB systems which have diffuse yet well defined outer disks and occasionally bulges. What we are more interested in is that LSB and dwarf galaxies are supposed to be dark matter dominated at all radii so that the details of the visible matter distribution are less important. In particular, LSB galaxies have an unusually high gas content, representing up to 90% of their baryonic content [**?**, 334], which makes it possible to measure the rotation curve well beyond the optical radius $R_{opt} \simeq 3.2 R_d$. Moreover, combining 21 - cm HI lines and optical emission lines such as Hα and [NII] makes it possible to correct for possible systematic errors due to beam smearing in the radio. As a result, LSB rotation curves are nowadays considered a useful tool to put severe constraints on the properties of the dark matter haloes (see, e.g., [121] and references therein). Then it becomes clear that being this family of galaxies dark matter dominated, they are a greatly consistent test for the application of Extended Theories;

- High Surface Brightness Galaxies (HSB): their photometric characterizing is clearly opposite to the previous class one. But in the choice of samples what we were more interested on are some other properties, for example:

  - they have rotation curves which are smooth, symmetric and extended to large radii;
  - they have very small bulges so that these ones can be neglected in the mass model to a good approximation;
  - their luminosity profiles are well measured and present a smooth behaviour;
  - data are uniform in quality up to maximal radii of each galaxy.

  Their main importance is to expand to bigger and various elements of the same family (spiral galaxies) the sample where we can apply our approach.

3.2 Low energy limit of $f(R)$ gravity

As just stated in the introduction, $f(R)$ theories of gravity represent a straightforward generalization of the Einstein General Relativity. To this aim, one considers the action :

$$\mathcal{A} = \int d^4x\sqrt{-g}\,[f(R) + \mathcal{L}_m] \tag{3.1}$$

where $f(R)$ is a generic analytic function of the Ricci scalar curvature R and $\mathcal{L}_m$ is the standard matter Lagrangian. The choice $f(R) = R + 2\Lambda$ gives the General Relativity including the contribution of the cosmological constant Λ. Varying the action with respect to the metric components $g_{\mu\nu}$, one gets the generalized Einstein equations that can be more expressively recast as [69, 77] :

$$\begin{aligned} G_{\mu\nu} &= \frac{1}{f'(R)}\left\{\frac{1}{2}g_{\mu\nu}\left[f(R) - Rf'(R)\right] + f'(R)_{;\mu\nu}\right. \\ &- \left. g_{\mu\nu}\Box f'(R)\right\} + \frac{T^{(m)}_{\mu\nu}}{f'(R)} \end{aligned} \tag{3.2}$$

where $G_{\mu\nu} = R_{\mu\nu} - (R/2)g_{\mu\nu}$ is the Einstein tensor and the prime denotes derivative with respect to R. The two terms $f'(R)_{;\mu\nu}$ and $\Box f'(R)$ imply fourth order derivatives of the metric $g_{\mu\nu}$ so that these models are also referred to as *fourth order gravity*. Starting from Eq.(3.2) and adopting the Robertson - Walker metric, it is possible to show that the Friedmann equations may still be written in the usual form provided that an *effective curvature fluid* (hence the name of *curvature quintessence*) is added to the matter term with energy density and pressure depending on the choice of $f(R)$. As a particular case, it is possible to consider power - law $f(R)$ theories, i.e. setting :

$$f(R) = f_0 R^n \tag{3.3}$$

with n the slope of the gravity Lagrangian ($n = 1$ being the Einstein theory) and f_0 a constant with the dimensions chosen in such a way to give $f(R)$ the right physical dimensions. It has been shown that the choice (3.3), with $n \neq 1$ and standard matter, is able to properly fit the Hubble diagram of Type Ia Supernovae without the need of dark energy [72, 94] and could also be reconciled with the constraints on the PPN parameters [89].

Here we are going to review the study of the low energy limit[1] of this class of $f(R)$ theories. Let us consider the gravitational field generated by a pointlike source and solve the field equations (3.2) in the vacuum case. Under the hypothesis of weak gravitational fields and slow motions, it is possible to write the spacetime metric as :

$$ds^2 = A(r)dt^2 - B(r)dr^2 - r^2 d\Omega^2 \tag{3.4}$$

where $d\Omega^2 = d\theta^2 + \sin^2\theta d\varphi^2$ is the line element on the unit sphere. It is worth noting that writing Eq.(3.4) for the weak field metric is the same as assuming implicitly that the Jebsen - Birkhoff theorem holds. While this is true in standard General Relativity, it has never been definitively proved for $f(R)$ theories. Actually, since for a general $f(R)$ theory the field equations are fourth order, it is quite difficult to show that the only stationary spherically symmetric vacuum solution is Schwarzschild like. However, that this is indeed the case has

[1] Although not rigourously correct, in the following we will use the terms *low energy limit* and *Newtonian limit* as synonymous.

been demonstrated for $f(R)$ theories involving terms like $R + R^2$ with $R^2 = R^{\alpha}{}_{\beta}{}^{\mu\nu} R_{\alpha}{}^{\beta}{}_{\mu\nu}$ with torsion [307] and for the case of any invariant of the form R^2 also in the case of null torsion [270]. Moreover, the Jebsen - Birkhoff theorem has been shown to hold also for more complicated theories as multidimensional gravity and Einstein - Yang - Mills theories [53, 54]. Therefore, although a rigorous demonstration is still absent, it is likely that this theorem is still valid for power - law $f(R)$ theories, at least in an *approximated* weak version[2] that is enough for our aims.

To find the two unknown functions $A(r)$ and $B(r)$, one first combines the 00 - vacuum component and the trace of the field equations (3.2) in absence of matter :

$$3\Box f'(R) + Rf'(R) - 2f(R) = 0 \ ,$$

to get a single equation :

$$f'(R)\left(3\frac{R_{00}}{g_{00}} - R\right) + \frac{1}{2}f(R) - 3\frac{f'(R)_{;00}}{g_{00}} = 0 \ . \tag{3.5}$$

Eq.(3.5) is completely general and holds whatever is $f(R)$. It is worth stressing, in particular, that, even if the metric is stationary so that $\partial_t g_{\mu\nu} = 0$, the term $f'(R)_{;00}$ is not vanishing because of the non-null Christoffel symbols entering the covariant derivative. Using Eq.(3.3), Eq.(3.5) reduces to :

$$R_{00}(r) = \frac{2n-1}{6n}\ A(r)R(r) - \frac{n-1}{2B(r)}\frac{dA(r)}{dr}\frac{d\ln R(r)}{dr} \ , \tag{3.6}$$

while the trace equation reads :

$$\Box R^{n-1}(r) = \frac{2-n}{3n}R^n(r) \ . \tag{3.7}$$

Note that for $n = 1$, Eq.(3.7) reduces to $R = 0$, which, inserted into Eq.(3.6), gives $R_{00} = 0$ and the standard Schwarzschild solution is recovered. In general, expressing R_{00} and R in terms of the metric (3.4), Eqs.(3.6) and (3.7) become a system of two nonlinear coupled differential equations for the two functions $A(r)$ and $B(r)$. A physically motivated hypothesis to search for solutions is

$$A(r) = \frac{1}{B(r)} = 1 + \frac{2\Phi(r)}{c^2} \tag{3.8}$$

with $\Phi(r)$ the gravitational potential generated by a pointlike mass m at the distance r. With the above hypothesis, the vacuum field equations reduce to a system of two differential equations in the only unknown function $\Phi(r)$. To be more precise, one can solve Eq.(3.6) or (3.7) to find out $\Phi(r)$ and then use the other relation as a constraint to find solutions of physical interest. To this aim, let us remember that, as well known, $f(R)$ theories induces modifications to the gravitational potential altering the Newtonian $1/r$ scaling [**?**, 212, 331, 107]. We thus look for a solution for the potential that may be written as :

$$\Phi(r) = -\frac{Gm}{2r}\left[1 + \left(\frac{r}{r_c}\right)^{\beta}\right] \tag{3.9}$$

[2] It is, for instance, possible that the metric (3.4) solves the field equations only up to terms of low order in Φ/c^2 with Φ the gravitational potential. For the applications we are interested in, $\Phi/c^2 << 1$, such weak version of the Jebsen - Birkhoff theorem should be verified.

so that the gravitational potential deviates from the usual Newtonian one because of the presence of the second term on the right hand side. Note that, when $\beta = 0$, the Newtonian potential is recovered and the metric reduces to the classical Schwarzschild one. On the other hand, as we will see, it is just this term that offers the intriguing possibility to fit galaxy rotation curves without the need of dark matter.

In order to check whether Eq.(3.9) is indeed a viable solution, one first inserts the expression for $\Phi(r)$ into Eqs.(3.6) and (3.7) which are both solved if :

$$\begin{aligned} &(n-1)(\beta-3)\left[-\beta(1+\beta)V_1\eta^{\beta-3}\right]^{n-1} \\ &\times\left[1+\frac{\beta V_1\mathcal{P}_0}{\mathcal{P}_1\eta}\right]\mathcal{P}_1\eta = 0 \end{aligned} \tag{3.10}$$

with $\eta = r/r_c$, $V_1 = Gm/c^2r_c$ and

$$\begin{aligned} \mathcal{P}_0 &= 3(\beta-3)^2n^3 - (5\beta^2-31\beta+48)n^2 \\ &- (3\beta^2-16\beta+17)n - (\beta^2-4\beta-5)\ , \end{aligned} \tag{3.11}$$

$$\begin{aligned} \mathcal{P}_1 &= 3(\beta-3)^2(1-\beta)n^3 + (\beta-3)^2(5\beta-7)n^2 \\ &- (3\beta^3-17\beta^2+34\beta-36)n + (\beta^2-3\beta-4)\beta\ . \end{aligned} \tag{3.12}$$

Eq.(3.10) is identically satisfied for particular values of n and β. However, there are some simple considerations allow to exclude such values. First, $n = 1$ must be discarded since, when deriving Eq.(3.6) from Eq.(3.5), we have assumed $R \neq 0$ which is not the case for $n = 1$. Second, the case $\beta = 3$ may also be rejected since it gives rise to a correction to the Newtonian potential scaling as η^2 so that the total potential diverges quadratically which is quite problematic. Finally, the case $\beta = -1$ provides a solution only if $n > 1$. Since we are interested in a solution which works whatever n is, we discard also this case. However, in the limit we are considering, it is $V_1 << 1$. For instance, it is $V_1 \simeq v_c^2/c^2 \sim 10^{-6} \div 10^{-3}$ ranging from Solar System to galactic scales, with v_c the circular velocity. As a consequence, we can look for a further solution of Eq.(3.10) solving :

$$\mathcal{P}_1(n,\beta)\eta + \beta V_1\mathcal{P}_0(n,\beta) \simeq \mathcal{P}_1(n,\beta)\eta = 0\ . \tag{3.13}$$

since the second term of Eq.(3.13) is always negligible for the values of n and β in which we are interested. Eq.(3.13) is an algebraic equation for β as function of n with the following three solutions :

$$\beta = \begin{cases} \dfrac{3n-4}{n-1} \\ \dfrac{12n^2-7n-1-\sqrt{p(n)}}{q(n)} \\ \dfrac{12n^2-7n-1+\sqrt{p(n)}}{q(n)} \end{cases} \tag{3.14}$$

with :

$$\begin{aligned} p(n) &= 36n^4+12n^3-83n^2+50n+1\ , \\ q(n) &= 6n^2-4n+2\ . \end{aligned}$$

It is easy check that, for $n = 1$, the second expression gives $\beta = 0$, i.e. the approximate solution reduces to the Newtonian one as expected. As a final check, one has to inserte back into the vacuum field equations (3.5) and (3.7) the modified gravitational potential (3.9) with

$$\beta = \frac{12n^2-7n-1-\sqrt{36n^4+12n^3-83n^2+50n+1}}{6n^2-4n+2} \tag{3.15}$$

finding out that the approximated solution solve the field equations up to 10^{-6} which is more than sufficient in all astrophysical applications which we are going to consider.

Armed with Eqs.(3.9) and (3.15), one can, in principle, set constraints on n by imposing some physically motivated requirements to the modified gravitational potential. However, given the nonlinear relation between n and β, in the following it is better to consider β and use Eq.(3.15) to infer n from the estimated β.

As a first condition, it is reasonable to ask that the potential does not diverge at infinity. To this aim, one imposes:

$$\lim_{r\to\infty} \Phi(r) = 0$$

which constraints $\beta - 1$ to be negative. A further constraint can be obtained considering the Newtonian potential $1/r$ as valid at Solar System scales. As a consequence, since the correction to the potential scales as $r^{\beta-1}$, one must impose $\beta - 1 > -1$ in order to avoid increasing Φ at the Solar System scales. In order to not evade these constraints, in the following, we will only consider solutions with

$$0 < \beta < 1 \tag{3.16}$$

that, using Eq.(3.15), gives $n > 1$ as lower limit on the slope n of the gravity Lagrangian.

While β controls the shape of the correction term, the parameter r_c controls the scale where deviations from the Newtonian potential sets in. Both β and r_c have to be determined by comparison with observations at galactic scales. An important remark is in order here. Because of Eq.(3.15), β is related to n which enters the gravity Lagrangian. Since this is the same for all gravitating systems, as a consequence, β must be the same for all galaxies. On the other hand, the scale length parameter r_c is related to the boundary conditions and the mass of the system. In fact, considering the generalization of Eq.(3.9) to extended systems, one has to take care of the mass distribution and the geometrical configurations which can differ from one galaxy to another. As a consequence, r_c turns out to be not a universal quantity, but its value must be set on a case-by-case basis.

Before considering the generalization to extended systems, it is worth evaluating the rotation curve for the pointlike case, i.e. the circular velocity $v_c(r)$ of a test particle in the potential generated by the point mass m. For a central potential, it is $v_c^2 = r d\Phi/dr$ that, with Φ given by Eq.(3.9), gives:

$$v_c^2(r) = \frac{Gm}{2r}\left[1 + (1-\beta)\left(\frac{r}{r_c}\right)^{\beta}\right] . \tag{3.17}$$

As it is apparent, the corrected rotation curve is the sum of two terms. While the first one equals half the Newtonian curve Gm/r, the second one gives a contribution that may also be higher than the half classical one. As expected, for $\beta = 0$, the two terms sum up to reproduce the classical result. On the other hand, for β in the range (3.16), $1 - \beta > 0$ so that the the corrected rotation curve is higher than the Newtonian one. Since measurements of spiral galaxies rotation curves signal a circular velocity higher than what is predicted on the basis of the observed mass and the Newtonian potential, the result above suggests the possibility that our modified gravitational potential may fill the gap between theory and observations without the need of additional dark matter.

It is worth noting that the corrected rotation curve is asymptotically vanishing as in the Newtonian case, while it is usually claimed that observed rotation curves are flat (i.e., asymptotically constant). However, such a statement should be not be taken literally. Actually, observations do not probe v_c up to infinity, but only up to a maximum radius R_{max} showing that the rotation curve is flat within the measurement uncertainties. However, this by no way excludes the possibility that v_c goes to zero at infinity. Considering Eq.(3.17), if the exponent

of the correction term is quite small, the first term decreases in a Keplerian way, while the second one approaches its asymptotically null value very slowly so that it can easily mimic an approximately flat rotation curve in agreement with observations.

3.3 Extended systems

The solution (3.9) has been obtained in the case of a pointlike source, but may be easily generalized to the case of extended systems. To this aim, we may simply divide the system in infinitesimal elements with mass dm and add the different contributions. In the continuous limit, the sum is replaced by an integral depending on the mass density and the symmetry of the system spatial configuration. Once the gravitational potential has been obtained, the rotation curve may be easily evaluated and then compared with observations.

3.3.1 Spherically symmetric systems

The generalization of Eq.(3.9) to a spherically symmetric system is less trivial than one would expect. In the case of the Newtonian gravitational potential, the Gauss theorem ensures us that the flux of the gravitational field generated by a point mass m through a closed surface only depends on the mass m and not on the position of the mass inside the surface. Moreover, the force on a point inside the surface due to sources outside the surface vanishes. As a result, we may imagine that the whole mass of the system is concentrated in its center and, as a consequence, the gravitational potential has the same formal expression as for the pointlike case provided one replaces m with $M(r)$, being this latter quantity the mass within a distance r from the centre.

From a mathematical point of view, one can write in the Newtonian case :

$$\begin{aligned}\Phi_N(r) &= -G\int \frac{\rho(\mathbf{x}')}{|\mathbf{x}-\mathbf{x}'|}d^3x' \\ &= -\frac{4\pi G}{r}\int_0^\infty \rho(r')r'^2dr' \\ &= -\frac{GM(r)}{r}\end{aligned}$$

where, in the second row, it has been used the Gauss theorem to take the $|\mathbf{x}-\mathbf{x}'|^{-1}$ outside the integral sign (considering all the mass concentrated in the point $\mathbf{x}'=0$) and then limited the integral to r since points with $r'>r$ do not contribute to the gravitational force.

It is quite easy to show that the Gauss theorem for the gravitational field is a consequence of the scaling $1/r^2$ of the Newtonian force. Since this scaling is lost in the case of the modified potential (3.9), the Gauss theorem does not hold anymore. However, apart from the multiplicative factor $1/2$, one can split the modified gravitational potential as the sum of two terms, the first one scaling as in the Newtonian case. For this term, the Gauss theorem holds and we recover the classical results so that the total gravitational potential of a spherically symmetric system may be written as :

$$\Phi(r) = \frac{\Phi_N(r)+\Phi_c(r)}{2} = -\frac{GM(r)}{2r} + \frac{\Phi_c(r)}{2} \tag{3.18}$$

with :

$$\Phi_c(r) = -G\int_0^\infty \rho(r')r'^2dr' \int_{-\pi/2}^{\pi/2}\sin\theta' d\theta' \int_0^{2\pi}\psi_c d\phi' \tag{3.19}$$

with ψ_c the non-Newtonian part of the modified gravitational potential for the pointlike case. In order to be more general, one can consider the calculation for a generic modified potential of the type :

$$\psi = -\frac{Gm}{2r}\left[1+\alpha\left(\frac{r}{r_c}\right)^{\beta}\right] \tag{3.20}$$

so that :

$$\psi_c(r) = -\frac{\alpha G m}{r_c}\left(\frac{r}{r_c}\right)^{\beta-1} \tag{3.21}$$

with α and β two parameters depending on the particular theory of gravity one is considering. While for R^n gravity $\alpha = 1$, in general, α could also be negative. Inserting the above ψ_c into Eq.(3.19), we replace r' with

$$|\mathbf{x}-\mathbf{x}'| = (r^2 + r'^2 - 2rr'\cos\theta')^{1/2}$$

where the spherical symmetry of the system has been used so that the potential in the point $\mathbf{x} = (r,\theta,\phi)$ only depends on r and one can set $\theta = \phi = 0$. Integrating over the angular variables (θ',ϕ'), we finally get :

$$\Phi_c(r) = -\frac{\pi G\alpha r_c^2}{3}\left[\mathcal{I}_1(r) + \mathcal{I}_2(r)\right] \tag{3.22}$$

with :

$$\begin{aligned}\mathcal{I}_1 &= 3\pi\int_0^\infty (\xi^2+\xi'^2)^{(\beta-1)/2}\rho(\xi')\xi'^2 d\xi' \\ &\times \ {}_2F_1\left[\left\{\frac{1-\beta}{4},\frac{3-\beta}{4}\right\},\{2\},\frac{4\xi^2\xi'^2}{(\xi^2+\xi'^2)^2}\right] ,\end{aligned} \tag{3.23}$$

$$\begin{aligned}\mathcal{I}_2 &= 4(1-\beta)\xi\int_0^\infty (\xi^2+\xi'^2)^{(\beta-3)/2}\rho(\xi')\xi'^2 d\xi' \\ &\times \ {}_3F_2\left[\left\{1,\frac{3-\beta}{4},\frac{5-\beta}{4}\right\},\left\{\frac{3}{2},\frac{5}{2}\right\},\frac{4\xi^2\xi'^2}{(\xi^2+\xi'^2)^2}\right] ,\end{aligned} \tag{3.24}$$

and we have generically defined $\xi = r/r_c$ and used the notation ${}_pF_1[\{a_1,\ldots,a_p\},\{b_1,\ldots,b_q\},x]$ for the hypergeometric functions.

Eqs.(3.23) and (3.24) must be evaluated numerically for a given expression of the mass density $\rho(r)$. Once $\Phi_c(r)$ has been evaluated, one can compute the rotation curve as :

$$v_c^2(r) = r\frac{\partial\Phi}{\partial r} = \frac{v_{c,N}^2(r)}{2} + \frac{r}{2}\frac{\partial\Phi_c}{\partial r} \tag{3.25}$$

with $v_{c,N}^2(r) = GM(r)/r$ the Newtonian rotation curve. Since we are mainly interested in spiral galaxies without any spherical component, we only note that, since Φ_c has to be evaluated numerically, in order to avoid numerical derivatives, it is better to first differentiate analytically the expressions for $\mathcal{I}_1$ and $\mathcal{I}_2$ and then integrate numerically the corresponding integrals. It is easy to check that the resulting rotation curve is typically slowly decreasing so that it vanishes asymptotically as in the Newtonian case. However, the rate of decline is slower than the Keplerian one so that the total rotation curve turns out to be higher than the Newtonian one: this fact allows to fit galaxy rotation curves without the need of any dark matter halo[3].

[3]It is worth stressing, at this point, that general conservation laws are guaranteed by

3.3.2 Thin disk

The case of a disk - like system is quite similar to the previous one and, indeed, the gravitational potential may be determined following the same method as before simply taking care of the cylindrical rather than spherical symmetry of the mass configuration. In order to simplify computations, but still dealing with realistic systems, we will consider a circularly symmetric and infinitesimally thin disk and denote by $\Sigma(R)$ its surface mass density[4] and by R_d its scale length. Note that a thin circular disk is the standard choice in describing spiral galaxies so that the model we consider is indeed the most realistic one.

Adopting cylindrical coordinates (R, ϕ, z), the gravitational potential may be evaluated as :

$$\Phi(R,z) = \int_0^\infty \Sigma(R')R'dR' \int_0^{2\pi} \psi(|\mathbf{x}-\mathbf{x}'|)d\phi' \tag{3.26}$$

with ψ the pointlike potential and :

$$|\mathbf{x}-\mathbf{x}'|^2 = \left[(R+R')^2+z^2\right]\left[1-k^2\cos^2\left(\phi'/2\right)\right] \ , \tag{3.27}$$

$$k^2 \equiv \frac{4RR'}{\left[(R+R')^2+z^2\right]} \ . \tag{3.28}$$

Inserting Eq.(3.20) into Eq.(3.26), one gets an integral that can be split into two additive terms. The first one is half the usual Newtonian one that can be solved using standard procedure [43] and therefore will not be considered anymore. The second one is the correction term Φ_c that reads[5] :

$$\begin{aligned}\Phi_c(R,z) &= -\alpha G\Sigma_0 r_c \int_0^\infty \tilde{\Sigma}(\xi')\left[(\xi+\xi')^2+\zeta^2\right]^{\frac{\beta-1}{2}}\xi' d\xi' \\ &\times \int_0^{2\pi}\left[1-k^2\cos^2\left(\phi'/2\right)\right]^{\frac{\beta-1}{2}}d\phi'\end{aligned} \tag{3.29}$$

with $\Sigma_0 = \Sigma(R=0)$, $\tilde{\Sigma} = \Sigma/\Sigma_0$, $\xi = R/r_c$ and $\zeta = z/r_c$. Integrating over $d\phi'$ and using Eq.(4.20), one finally gets :

$$\begin{aligned}\Phi_c(R,z) &= -2^{\beta-2}\pi\alpha G\Sigma_0 r_c \xi^{\frac{\beta-1}{2}}\int_0^\infty d\xi'\tilde{\Sigma}(\xi')\xi'^{\frac{1+\beta}{2}} \\ &\times \ {}_2F_1\left[\left\{\frac{1}{2},\frac{1-\beta}{2}\right\},\{1\},k^2\right]k^{1-\beta} \ .\end{aligned} \tag{3.30}$$

Eq.(3.30) makes it possible to evaluate the corrective term to the gravitational potential generated by an infinitely thin disk given its surface density $\Sigma(\xi)$. As a useful application, we consider the case of the exponential disk [**?**] :

$$\Sigma(R) = \Sigma_0 \exp\left(-R/R_d\right) \tag{3.31}$$

Bianchi identities which hold for generic $f(R)$, so the non-validity of Gauss theorem is not a shortcoming since we are considering the low energy limit of the theory.

[4]Here, R is the cylindrical coordinate in the plane of the disk (i.e., $R^2 = x^2+y^2$) to be not confused with the Ricci scalar curvature.

[5]As in the previous paragraph, it is convenient to let apart the multiplicative factor $1/2$ and inser it only in the final result so that the total potential reads $\Phi(R,z) = \left[\Phi_N(R,z)+\Phi_c(R,z)\right]/2$.

with R_d the scale radius. With this expression for the surface density, the corrective term in the gravitational potential may be conveniently written as :

$$\begin{aligned}\Phi_c(R,z) &= -2^{\beta-2}\eta_c^{-\beta}\pi\alpha G\Sigma_0 R_d \eta^{\frac{\beta-1}{2}} \int_0^\infty d\eta' \mathrm{e}^{-\eta'}\ \eta'^{\frac{\beta+1}{2}} \\ &\times\ {}_2F_1\left[\left\{\frac{1}{2},\frac{1-\beta}{2}\right\},\{1\},k^2\right] k^{1-\beta} \end{aligned} \tag{3.32}$$

with $\eta = R/R_d$ and $\eta_c = r_c/R_d$ and k is still given by Eq.(4.20) replacing (R, R', z) with $(\eta, \eta', z/R_d)$. The rotation curve for the disk may be easily computed starting from the usual relation [43] :

$$v_c^2(R) = R\frac{\partial\Phi(R,z)}{\partial R}\bigg|_{z=0} = \eta\frac{\partial\Phi(R,z)}{\partial\eta}\bigg|_{z/R_d=0} . \tag{3.33}$$

Inserting the total gravitational potential into Eq.(3.33), one may still split the rotation curve in two terms as :

$$v_c^2(R) = \frac{v_{c,N}^2(R) + v_{c,corr}^2(R)}{2} \tag{3.34}$$

where the first term is the Newtonian one, which for an exponential disk reads [**?**] :

$$\begin{aligned} v_{c,N}^2(R) &= 2\pi G\Sigma_0 R_d (\eta/2)^2 \\ &\times\ [I_0(\eta/2)K_0(\eta/2) - I_1(\eta/2)K_1(\eta/2)] \end{aligned} \tag{3.35}$$

with I_l, K_l Bessel functions of order l of the first and second type respectively. The correction term $v_{c,corr}^2$ may be evaluated inserting Eq.(3.32) into Eq.(3.33). Using :

$$\frac{\partial k}{\partial\eta} = \frac{k}{2\eta}\left[1 - \frac{k^2(\eta+\eta')}{2\eta'}\right] ,$$

we finally get :

$$v_{c,corr}^2(\eta) = -2^{\beta-5}\eta_c^{-\beta}\pi\alpha(\beta-1)G\Sigma_0 R_d \eta^{\frac{\beta-1}{2}} \mathcal{I}_{disk}(\eta,\beta) \tag{3.36}$$

where it has defined :

$$\mathcal{I}_{disk}(\eta,\beta) = \int_0^\infty \mathcal{F}(\eta,\eta',\beta) k^{3-\beta} \eta'^{\frac{\beta-1}{2}} \mathrm{e}^{-\eta'} d\eta' \tag{3.37}$$

with :

$$\begin{aligned} \mathcal{F} &= 2(\eta+\eta')\,{}_2F_1\left[\left\{\frac{1}{2},\frac{1-\beta}{2}\right\},\{1\},k^2\right] \\ &+ \left[(k^2-2)\eta' + k^2\eta\right] {}_2F_1\left[\left\{\frac{3}{2},\frac{3-\beta}{2}\right\},\{2\},k^2\right] . \end{aligned} \tag{3.38}$$

The function $\mathcal{I}_{disk}(\eta,\beta)$ may not be evaluated analytically, but it is straightforward to estimate it numerically. Note that Eqs.(3.36) and (3.48) can be easily generalized to a different surface density by replacing the term $\mathrm{e}^{-\eta'}$ with $\tilde{\Sigma}(\eta')$ and R_d with R_s, being this latter a typical scale radius of the system, while the function $\mathcal{F}$ remains unaltered.

Table 3.1: Properties of sample galaxies. Explanation of the columns: name of the galaxy, distance in Mpc; disk central surface brightness in the R band (corrected for galactic extinction); disk scalelength in kpc; radius at which the gas surface density equals $1\ \mathrm{M}_\odot/\mathrm{pc}^2$ in arcsec; total HI gas mass in $10^8\ \mathrm{M}_\odot$; Hubble type as reported in the NED database.

Id	D	μ_0	R_d	R_{HI}	M_{HI}	Type
UGC 1230	51	22.6	4.5	101	58.0	Sm
UGC 1281	5.5	22.7	1.7	206	3.2	Sdm
UGC 3137	18.4	23.2	2.0	297	43.6	Sbc
UGC 3371	12.8	23.3	3.1	188	12.2	Im
UGC 4173	16.8	24.3	4.5	178	21.2	Im
UGC 4325	10.1	21.6	1.6	142	7.5	SAm
NGC 2366	3.4	22.6	1.5	439	7.3	IB(s)m
IC 2233	10.5	22.5	2.3	193	13.6	SBd
NGC 3274	6.7	20.2	0.5	225	6.6	SABd
NGC 4395	3.5	22.2	2.3	527	9.7	SAm
NGC 4455	6.8	20.8	0.7	192	5.4	SBd
NGC 5023	4.8	20.9	0.8	256	3.5	Scd
DDO 185	5.1	23.2	1.2	136	1.6	IBm
DDO 189	12.6	22.6	1.2	167	10.5	Im
UGC 10310	15.6	22.0	1.9	130	12.6	SBm

3.4 Low Surface Brightness Spiral Galaxies

3.4.1 Rotation curves: the data

It is easy to understand why LSB rotation curves are ideal tools to test also modified gravity theories. Indeed, successfully fitting the rotation curves of a whatever dark matter dominated system, without resorting to dark matter, should represent a serious evidence arguing in favour of modifications of the standard Newtonian potential. In order to test our model, it has therefore considered a sample of 15 LSB galaxies with well measured HI and Hα rotation curves extracted from a larger sample in [120]. The initial sample contains 26 galaxies, but they have only been considered those galaxies for which data on the rotation curves, the surface photometry in the R band and the gas mass surface density were available[6]. In Table 1, they are reported the quantities one needs for evaluating the theoretical rotation curve referring the reader to [120] for further details and references to retrieve the data[7].

An important remark in in order here. For each LSB galaxy, both HI and Hα data on the rotation curve are available. As yet discussed in [120], the raw data show some scatter mainly due to residuals non circular motions that may lead to ambiguous rotational velocities.

[6]This initial selection reduced indeed the sample to 19 galaxies, but four of them were rejected because of numerical problems when computing the gas rotation curve due to the strong irregularities in the interpolated surface density.

[7]The data on the rotation curves may be also found in the SIMBAD database (`http://cdsweb.u-strasbg.fr`).

However, when deriving mass models from rotation curves, each galaxy is described as an axisymmetric system so that non circular motions do not arise. In order to remove this scatter from the data, it is recommended to use the smoothed rotation curve data derived by a local regression method extensively discussed in [120] and refs. therein. Following these authors, one will adopt the smooth data as input in the fitting procedure. The smoothing procedure may in principle introduce correlations among the data so that it is worth investigating whether this may bias somewhat the results on the model parameters. Moreover, the number of data points on each single rotation curve is reduced and the errors on each point is estimated in a different way than for raw data. As such, it is important to investigate also how this affects the uncertainties on the final estimate of the model parameters.

3.4.2 Modelling LSB galaxies

Since we are interested in fitting rotation curves without any dark matter halo, our model for a generic LSB galaxy is made out of the stellar and gaseous components only.

One can assume the stars are distributed in an infinitely thin and circularly symmetric disk. The surface density $\Sigma(R)$ may be derived from the surface brightness distribution :

$$\mu(R) = -2.5 \log I(R)$$

with $I(R) = \Sigma(R)/\Upsilon_\star$ the light distribution and $\Upsilon_\star$ the stellar mass - to - light (hereafter M/L) ratio. The photometric data (in the R band) are fitted with an exponential model thus allowing to determine the scale length R_d and the central surface brightness μ_0 and hence $I_0 = I(R = 0)$. The only unknown parameter is therefore $\Upsilon_\star$ that makes it possible to convert the central luminosity density I_0 into the central surface mass density Σ_0 entering Eqs.(3.35) and (3.36).

Modelling the gas distribution is quite complicated. Following the standard practice, one assumes the gas is distributed in a infinitely thin and circularly symmetric disk assuming for the surface density $\Sigma(R)$ the profile that has been measured by the HI 21 - cm lines. Since the measurements only cover the range $R_{min} \leq R \leq R_{max}$, one may use a third order interpolation for R in this range, a linear extrapolation between R_{max} and R_{HI}, being this latter a scaling radius defined by $\Sigma(R_{HI}) = 1\ \mathrm{M}_\odot/\mathrm{pc}^2$, while assuming $\Sigma(R) = \Sigma(R_{min})$ for $R \leq R_{min}$. To check if the model works correctly, one can compute the total mass M_{HI} and normalize the model in such a way that this value is the same as that is measured by the total HI 21 - cm emission. Finally, one increases the surface mass density by 1.4 to take into account the helium contribution. It is worth noting that this model is only a crude approximation for R outside the range (R_{min}, R_{max}), while, even in the range (R_{min}, R_{max}), $\Sigma(R)$ gives only an approximated description of the gas distribution since this latter may be quite clumpy and therefore cannot be properly fitted by any analytical expression. However, that the details of the gas distribution are rather unimportant since the rotation curve is dominated everywhere by the stellar disk. The clumpiness of the gas distribution manifests itself in irregularities in the rotation curve that may be easily masked in the fitting procedure, even if this is not strictly needed for our aims.

3.4.3 Fitting the rotation curves

Having modelled a LSB galaxy, Eqs.(3.35) – (3.38) may be straightforwardly used to estimate the theoretical rotation curve as function of three unknown quantities, namely the stellar M/L ratio $\Upsilon_\star$ and the two theory parameters (β, r_c). Actually, the fitting parameters will be $\log r_c$

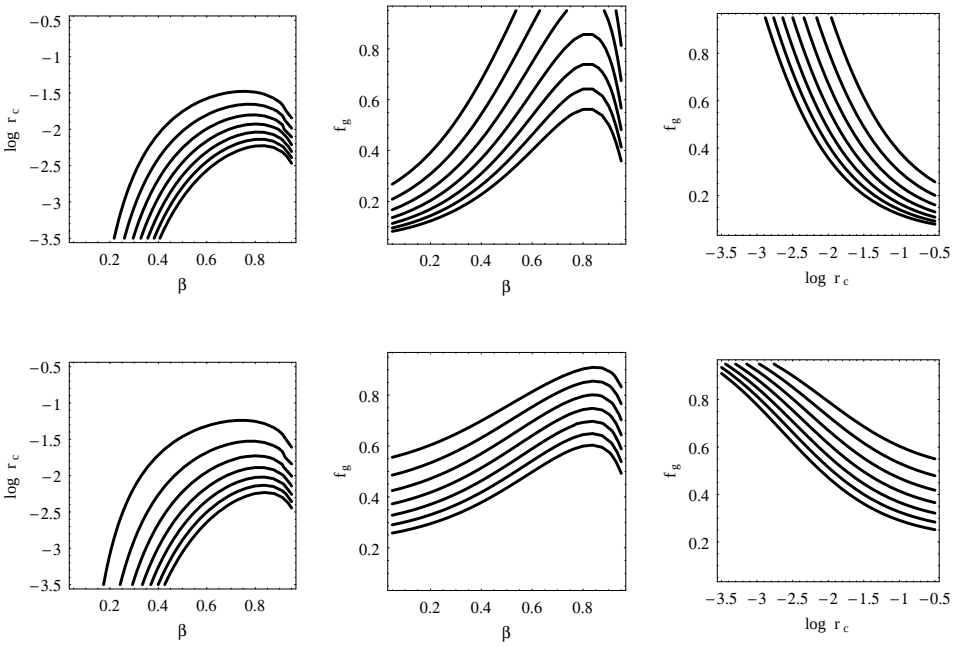

Figure 3.1: Contour plots for $v_c(R_d)$ in the planes $(\beta, \log r_c)$, (left), (β, f_g) (middle), $(\log r_c, f_g)$ (right) with r_c in kpc. The contours are plotted for $v_c(R) = k \times v_{fid}$ with k from 0.7 to 1.3 in steps of 0.1 and $v_{fid} = v_c(R_d)$ for the model with $(\beta, \log r_c, f_g) = (0.61, -2.13, 0.65)$. Upper panels refer to a pointlike system with total mass $m = \Upsilon_\star L_d + M_{HI}$, with L_d the total disk luminosity, M_{HI} the gas mass and $\Upsilon_\star$ given by Eq.(3.39). Lower panels refer to the extended case using as default parameters those of UGC 10310. In each panel, the remaining parameter is set to its fiducial value. Note that similar plots are obtained for values of R other than R_d.

rather than r_c (in kpc) since this is a more manageable quantity that makes it possible to explore a larger range for this theoretically unconstrained parameter. Moreover, we use the gas mass fraction f_g rather than $\Upsilon_\star$ as fitting quantity since the range for f_g is clearly defined, while this is not for $\Upsilon_\star$. The two quantities are easily related as follows :

$$f_g = \frac{M_g}{M_g + M_d} \iff \Upsilon_\star = \frac{(1 - f_g) M_g}{f_g L_d} \tag{3.39}$$

with $M_g = 1.4 M_{HI}$ the gas (HI + He) mass, $M_d = \Upsilon_\star L_d$ and $L_d = 2\pi I_0 R_d^2$ the disk total mass and luminosity.

We use Eq.(3.35) to compute the disk Newtonian rotation curve, while the $v_{c,corr}$ is obtained by integrating numerically Eq.(3.48). For the gas, instead, authors resort to numerical integrations for both the Newtonian rotation curve and the corrective term. The total rotation curve is finally obtained by adding in quadrature these contributions.

To constrain the parameters $(\beta, \log r_c, f_g)$, they minimize the following merit function :

$$\chi^2(\mathbf{p}) = \sum_{i=1}^{N} \left[\frac{v_{c,th}(r_i) - v_{c,obs}(r_i)}{\sigma_i} \right]^2 \tag{3.40}$$

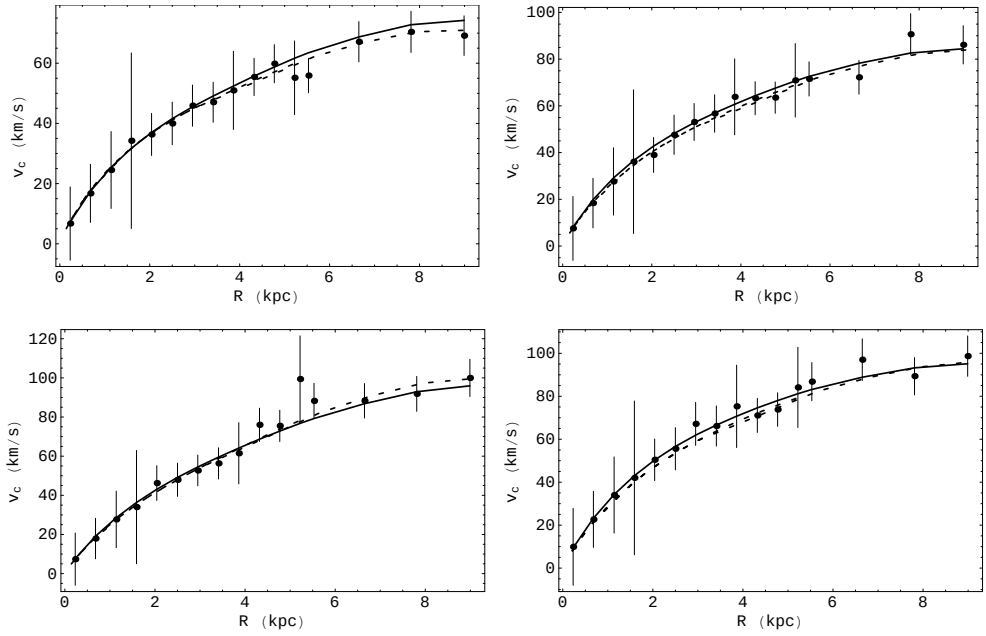

Figure 3.2: Some illustrative examples of simulated rotation curves (smoothing the data for convenience) with overplotted the input theoretical rotation curve (solid line) and the best fit one (short dashed line).

where the sum is over the N observed points. While using the smoothed data helps in better adjusting the theoretical and observed rotation curves, the smoothing procedure implies that the errors σ_i on each point are not Gaussian distributed since they also take into account systematic misalignments between HI and Hα measurements and other effects leading to a conservative overestimate of the true uncertainties (see the discussion in [120] for further details). As a consequence, we do not expect that $\chi^2/dof \simeq 1$ for the best fit model (with $dof = N - 3$ the number of degrees of freedom), but we can still compare different models on the basis of the χ^2 values. In particular, the uncertainties on the model parameters will be estimated exploring the contours of equal $\Delta\chi^2 = \chi^2 - \chi^2_{min}$ in the parameter space.

3.5 LSB: testing the method

The method we have outlined above and the data on LSB galaxies are in principle all what we need to test the viability of R^n gravity. However, there are some subtle issues that can affect in an unpredictable way the outcome of the analysis.

Two main problems worth to be addressed. First, there are three parameters to be constrained, namely the gas mass fraction f_g (related to the stellar M/L ratio $\Upsilon_\star$) and the R^n gravity quantities $(\beta, \log r_c)$. However, although they do not affect the theoretical rotation curve in the same way, there are still some remaining degeneracies hard to be broken. This problem is well illustrated by Fig.,3.1 where they are shown the contours of equal $v_c(R_d)$ in the planes $(\beta, \log r_c)$, (β, f_g) and $(\log r_c, f_g)$ for the pointlike and extended case. Looking, for instance, at right panels, one sees that, for a given β, $\log r_c$ and f_g (and hence $\Upsilon_\star$) have the

same net effect on the rotation curve so that the same value for $v_c(R_d)$ may be obtained for a lower f_g provided one increases $\log r_c$. On the other hand, β and $\log r_c$ have opposite effects on $v_c(R)$: the lower is β, the smaller is $v_c(R)$ for a given R. Since the opposite holds for $\log r_c$, as a result, the same value of $v_c(R_d)$ may be obtained increasing $\log r_c$ and decreasing β. Moreover, while β drives the shape of the rotation curve in the outer region, its effect may be better appreciated if r_c is low so that a further degeneracy arises.

A second issue is related to the authors' decision to use the smooth rather than the raw data. Although [120] claim that this does not affect the results, their analysis is nevertheless performed in the framework of standard theory of gravity with dark matter haloes. It is therefore worth investigating whether this holds also in the case of the R^n gravity we are considering here.

Both these issues may be better investigated through the analysis of simulated rotation curves. To this aim, we take UGC 10310 as input model for the gas surface density and the disk luminosity because its properties are typical of our sample. For given values of the model parameters $(\beta, \log r_c, f_g)$, authors generate observed rotation curves using the same radial sampling of the actual observations. For each r_i, we randomly extract $v_{c,obs}(r_i)$ from a Gaussian distribution centered on the $v_{c,th}(r_i)$. To this point, they attach an error extracted from a second Gaussian distribution centered on the $\varepsilon_i \times v_{c,obs}(r_i)$ with ε_i the percentage error on $v_{c,obs}(r_i)$ in the real sample. The simulated rotation curves thus obtained are quite similar to the raw data so that they use the same smoothing procedure to get simulated smooth data. Both the simulated raw and smooth data are quite similar to the corresponding observed ones so that they represent ideal tools to explore the issues quoted above.

3.5.1 The impact of the parameters degeneracy

As well known, the determination of $\mathcal{N}$ model parameters from the fit to a given data set may be seriously compromised if strong degeneracies exist. Considering for simplicity the case of a pointlike source, the rotation curve may be roughly approximated as:

$$v_c^2(r) \simeq \frac{Gm}{2r} \times \begin{cases} 1 & \text{for } (r/r_c)^\beta << 1 \\ 1 + (1-\beta) & \text{for } (r/r_c)^\beta \simeq 1 \\ (1-\beta)(r/r_c)^\beta & \text{for } (r/r_c)^\beta >> 1 \end{cases} . \tag{3.41}$$

For the typical values of β (~ 0.8) and r_c ($\simeq 0.01$ kpc) they qualitatively estimate from an eyeball fit to the data, it is easy to check that most of the data in the rotation curves mainly probe the region with $(r/r_c)^\beta >> 1$ so that $v_c^2 \simeq Gm/2r_c \times (1-\beta)(r/r_c)^{\beta-1}$. As a result, the theoretical rotation curve mainly depends on the two effective parameters $m_{eff} = m(1-\beta)/2$ and $r_{c,eff} = r_c^\beta$. Moreover, as a further complication, the lower is β, the less v_c^2 depends on r_c since the correction term is more and more negligible. A similar discussion (although less intuitively) also holds in the extended case with the stellar M/L ratio $\Upsilon_\star$ playing the role of the pointlike mass m. Both these problems may be better appreciated looking at Fig. 3.1 as yet discussed above. It is therefore mandatory to explore whether the data are able to break these degeneracies or how they affect the recovering of the model parameters $(\beta, \log r_c, f_g)$.

This task may be ideally tackled fitting the simulated rotation curves generated as described above and comparing the best fit values with the input ones. Indeed, we find that the degeneracy works in a quite dramatic way possibly leading to large discrepancies among the input and best fit values. To better illustrate this point, some typical examples have been reported in Fig. 3.2 where the input theoretical rotation curve (solid line) and the best fit one (short dashed line) are superimposed to the simulated data. Note that we plot smoothed

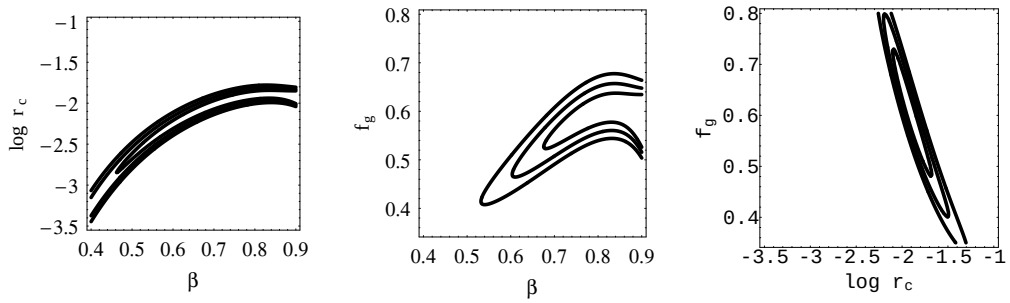

Figure 3.3: Contours of equal $\Delta\chi^2 = \chi^2 - \chi^2_{min}$ projected on the three planes $(\beta, \log r_c)$, (β, f_g), $(\log r_c, f_g)$ for the case of the simulation in the top right panel of Fig. 3.2 with r_c in kpc. In each panel, the remaining parameter is set to its best fit value. The three contours individuate the 1, 2 and 3σ confidence ranges. Open contours mean that no constraints may be obtained.

rather than raw data in order to not clutter the graphic with too many points, but the raw data have been used in the fit. Although the two lines in each panel are always remarkably close so that they can be hardly discriminated by the data, the offset $\Delta p/p = |1 - p_{fit}/p_{sim}|$ may be quite large. Considering, for instance, the parameter β, we get $\Delta\beta/\beta = 24\%$, 11%, 17% and 16% from top left to bottom right clockwise respectively. Similar results are obtained for the full set of simulations, while smaller values of $\Delta p/p$ come out for $p = \log r_c$ and $p = f_g$ (and hence for $\Upsilon_\star$). It is also worth stressing that no significant correlation has been observed between $\Delta p/p$ and p whatever is the parameter p considered.

This exercise also teaches us an important lesson. As it is apparent, better quality data could not be sufficient to break the degeneracy. An instructive example is represented by the top right panel where the two curves almost perfectly overlap. It is clear that reducing the error bars does not help at all so the input and the best fit models are impossible to discriminate notwithstanding a remarkable $\Delta\beta/\beta = 11\%$. In some cases, the two curves start departing from each other for large R so that one could expect that adding more points in this region or extending the data to still higher R efficiently breaks the degeneracy. Unfortunately, the simulated data extend up to $\sim 5R_d$ so that further increasing this coverage with real data is somewhat unrealistic (especially using typical spiral galaxies rather than the gas rich LSBs).

The degeneracy hinted above among the model parameters also dramatically affects the estimated errors on $(\beta, \log r_c, f_g)$. This can be seen in Fig. 3.3 where we report the contours of equal $\Delta\chi^2$ projected on the three planes $(\beta, \log r_c)$, (β, f_g), $(\log r_c, f_g)$ for the case of the simulation in the top right panel of Fig. 3.2. As it is clearly seen, β remains essentially unconstrained, while $\log r_c$ and f_g are only weakly constrained with the 3σ contours still spanning almost the full physical range for f_g. As suggested by the analysis of the pointlike case, these discouraging results are an expected consequence of the dependence of the theoretical rotation curve on the two degenerate quantities $(m_{eff}, r_{c,eff})$ preventing us to efficiently constraint separately the three model parameters.

3.5.2 Breaking the degeneracy among $(\beta, \log r_c, f_g)$

The analysis carried out convincingly shows that the degeneracy among the model parameters can not be broken by the present data on the rotation curves alone. As a result, one has to add

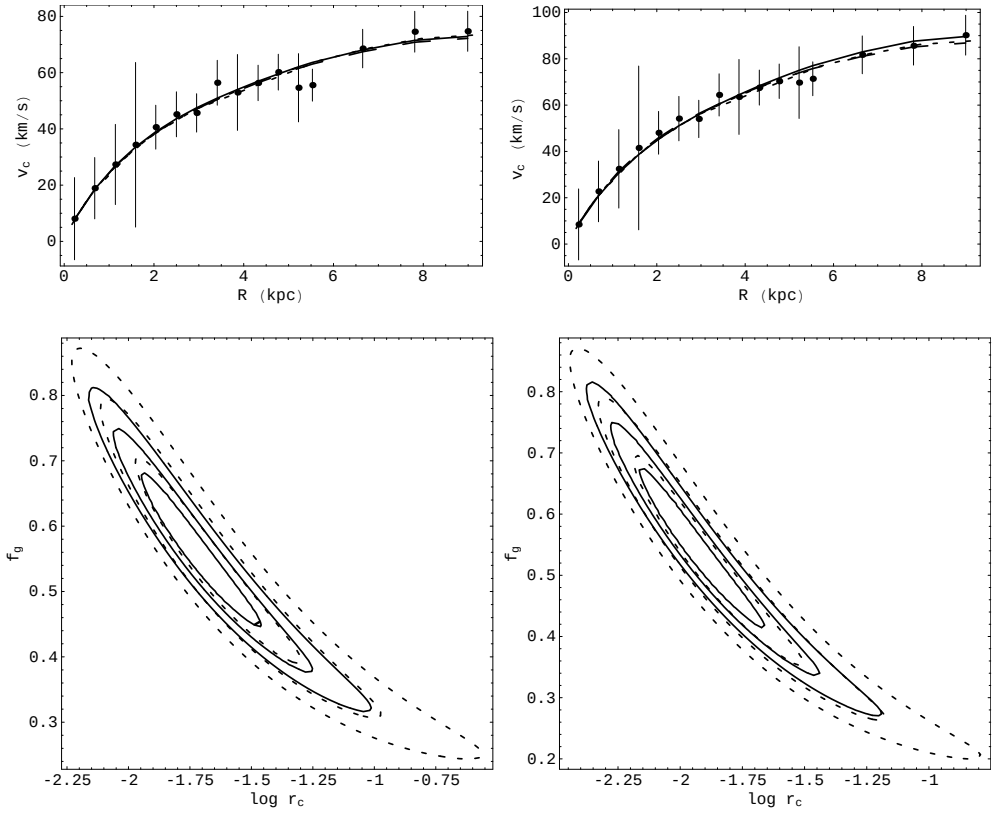

Figure 3.4: *Top panels.* Some illustrative examples of simulated rotation curves (smoothing the data for convenience) with overplotted the input theoretical rotation curve (solid line) and the best fit one from raw (short dashed line) and smooth (long dashed line) data. *Bottom panels.* 1, 2 and 3σ confidence ranges in the plane $(\log r_c, f_g)$ from the fit to raw (solid line) and smooth (short dashed line) data shown in the respective top panels (with r_c in kpc). Note that the two cases reported are representatives of the best (left) and worst (right) situations we find in our sample of simulated rotation curves.

some more constraints coming from different sources in order to set one of the three parameters above thus breaking the degeneracy and correctly recovering the values of the remaining two. Again, the analysis of the simulated rotation curves may help in choosing the best strategy.

As a first possibility, one may resort to stellar population synthesis models in order to set the M/L ratio $\Upsilon_\star$ and hence the gas mass fraction f_g. Although this strategy is not free of problems (see the discussion in Sect. 6), one can ideally correlate the observed colors of the galaxy to the predicted M/L ratio and hence performing the fit to the data with the parameter f_g obtained by Eq.(3.39) so that $(\beta, \log r_c)$ are the only unknown quantities. The fit results to the full set of simulated rotation curves unequivocally show us that this strategy does not work at all. Although we do not report any illustrative examples, we warn the reader that quite similar plots to Fig. 3.2 are obtained. Actually, while $|\Delta \log r_c / \log r_c|$ is reduced to $\sim 10\%$, we still have $|\Delta\beta/\beta| \sim 20\%$ with values as high as 40%. Nevertheless, the input theoretical and the best fit rotation curves overlaps quite well over the range probed by the data.

As in the case with all the parameters free to vary, reducing the errors bars or extending the radial coverage is typically not sufficient for lowering $\Delta\beta/\beta$. Such a result may be anticipated by considering again Eq.(3.41). Setting $\Upsilon_\star$ is the same as choosing m so that one could argue that $(\beta, \log r_c)$ may be determined by the effective quantities $(m_{eff}, r_{c,eff})$ that are constrained by the data. Actually, the situation is much more involved. Indeed, for $\beta << 1$, we are in a quasi Newtonian regime so that $r_{c,eff}$ is very weakly constrained and hence neither β nor r_c may be recovered. On the other hand, if $\beta \simeq 1$ the correction is small and again the constraints on both parameters are weak.

The simple exercise discussed above shows us that also a perfect knowledge of $\Upsilon_\star$ is unable to break the remaining degeneracy between β and $\log r_c$ thus preventing the fit to recover their correct value. As a second possibility, one may resort to the theory itself and decide to set β from the beginning. Actually, this is the same as setting the slope n of the R^n gravity Lagrangian. Since this latter must be the same from the galactic up to the cosmological scales, one may determine n from a different test and then set β from Eq.(3.15). The fit to the data may then be used to estimate $(\log r_c, f_g)$ which, on the contrary, depend on the particular system under examination. Indeed, we find that this strategy works very well. Both $\log r_c$ and f_g are recovered with great accuracy being $|\Delta \log r_c/\log r_c| \sim |\Delta f_g/f_g| \sim 5\%$ and never greater than $\sim 10\%$. Two cases representative of our best and worst situations are shown in Fig. 3.4. In both cases, the input theoretical curve and the best fit one may be hardly distinguished and indeed we get $(\Delta \log r_c/\log r_c, \Delta f_g/f_g) = (-2\%, -3\%)$ for the case in the left panel and $(3\%, 5\%)$ for the one in the right panel.

Considering the intrinsic errors induced by the displacement from the input rotation curve induced by our procedure used to generate the simulated data, we can safely conclude that both $\log r_c$ and f_g are exactly recovered within the expected precision.

It is also interesting to look at the bottom panels in Fig. 3.4 showing the iso - $\Delta\chi^2$ contours in the plane $(\log r_c, f_g)$. Although still covering a large region of the parameter space, the confidence ranges are now closed so that it is possible to extract meaningful constraints on the parameters. Following the usual approach (see, e.g., [120]), 1 and 2σ errors are obtained by projecting on the axes the contours for $\Delta\chi^2 = 1$ and $\Delta\chi^2 = 4$ respectively[8]. A naive propagation of errors on f_g and the use of Eq.(3.39) makes it possible to infer constraints on $\Upsilon_\star$. It is remarkable that the uncertainty on $\log r_c$ remains large (hence rendering r_c known only within an order of magnitude). Reducing the error on $\log r_c$ is, however, quite difficult with the data at hand. As can be easily checked, r_c mainly determines the value of the circular velocity in the outer region with v_c being larger for smaller r_c. For $\beta \simeq 0.8$ as we will adopt later, $(r/r_c)^\beta \simeq 1 - 50$ for r ranging from 10^{-2} to $10^2 r_c$ where most of the data are concentrated. In order to get smaller errors on $\log r_c$, one should increase the number of points (and reducing the measurement uncertainties) in the region $r > 10^3 r_c$. For typical values of $\log r_c \simeq -2$ and $R_d \simeq 2$ kpc, one then needs to measure the rotation curve beyond $r \sim 5R_d$ which is quite unrealistic at the moment.

3.5.3 Raw vs smooth data

In the analysis of the simulated cases described above, we have up to now used the raw data as input to the fitting procedure. Nevertheless, in Sect. 4, we have claimed that the smooth rather than the raw data will be used in the analysis of the observed LSB galaxies rotation

[8]We caution the reader that the contours in Figs. 3.3 and 3.4 refer to 2D confidence ranges so that $\Delta\chi^2 = 2.30, 6.17, 11.8$ respectively. They do not must be confused with those reported in the text which refer to constraints in a 1D parameter space.

curves. As explained above and further discussed in de Blok & Bosma (2002) and references therein, smooth data are better suited to recover constraints on a given theory since they are less sensitive to non axisymmetric features and outliers affected by unpredictable errors.

Any smoothing procedure may potentially introduce some correlation among the data points because of binning the data and averaging the measurements in a given bin. Although the procedure adopted by de Blok & Bosma (2002) and briefly described in Appendix B is quite efficient in reducing these problems, a residual correlation still remains so that it is worth exploring whether this affects the results.

To this aim, we have fitted both the raw and the smooth data with the β parameter set for the reasons discussed above. As a first qualitative test, we have checked that the results are interchangeable, i.e. we may fit equally well the raw data with the best fit curve from the fit to the smooth data and vice versa. This is clearly seen in the top panels of Fig. 3.4 where the long dashed lines (representing the best fit to the smooth data) are hardly distinguished by the short dashed ones (from the fit to the raw data). As a more rigorous test, we have compared the best fit values from the two fits with those used to generate the simulated curve. Indeed, we find a remarkable agreement between the three sets of $(\log r_c, f_g)$ values. What is more interesting, in many cases, $(\Delta p/p)_{smooth} < (\Delta p/p)_{raw}$ thus advocating in favor of the use of the smooth rather than the raw data.

As a final test, we also explore whether the confidence ranges and hence the uncertainties on the model parameters are affected. A nice visual result may be gained looking at the bottom panels in Fig. 3.4 and comparing the solid with the short dashed lines. As it is clear, the confidence regions quite well overlap with no visible offset from one another. Actually, using smooth rather than raw data leads to wider confidence regions and hence larger errors on $(\log r_c, f_g)$. However, this is expected since the smooth dataset contains a lower number of points so that we can roughly expect that the error σ_p on a parameter p increases by a factor $\varepsilon \propto (N_{raw}/N_{smooth})^{1/2}$. This is indeed the case when comparing the estimated errors from projecting the 1D confidence regions on the $(\log r_c, f_g)$ axes.

A final comment is in order. Because of how the measurement uncertainties have been computed, the best fit reduced $\chi^2/d.o.f$ values are not expected to be close to 1. This is indeed the case when dealing with the raw data. However, a further reduction is expected for the smooth data because of the peculiarities of the smoothing procedure used. For instance, we get $(\chi^2/d.o.f.)_{raw} = 0.29$ vs $(\chi^2/d.o.f.)_{smooth} = 0.07$ for the case in the right panel of Fig. 3.4. There are two motivations concurring to the finding of such small reduced χ^2. First, the uncertainties have been conservatively estimated so that the true ones may also be significantly smaller. Should this be indeed the case, $\chi^2/d.o.f.$ turn out to be underestimated. A second issue comes from an intrinsic feature of the smoothing procedure. As discussed in Appendix B, the method we employ is designed to recover the best approximation of an underlying model by a set of sparse data. Since the fit to the smooth data searches for the best agreement between the model and the data, an obvious consequence is that the best fit must be as close as possible to data that are by their own as close as possible to the model. As such, if the best fit model reproduces the data, the χ^2 is forced to be very small hence originating the observed very small values of the reduced χ^2. Note that both these effects are systematics so that they work the same way over the full parameters space. Since we are interested in $\Delta\chi^2$ rather than χ^2_{min}, these systematics cancel out thus not affecting anyway the estimate of the uncertainties on the model parameters.

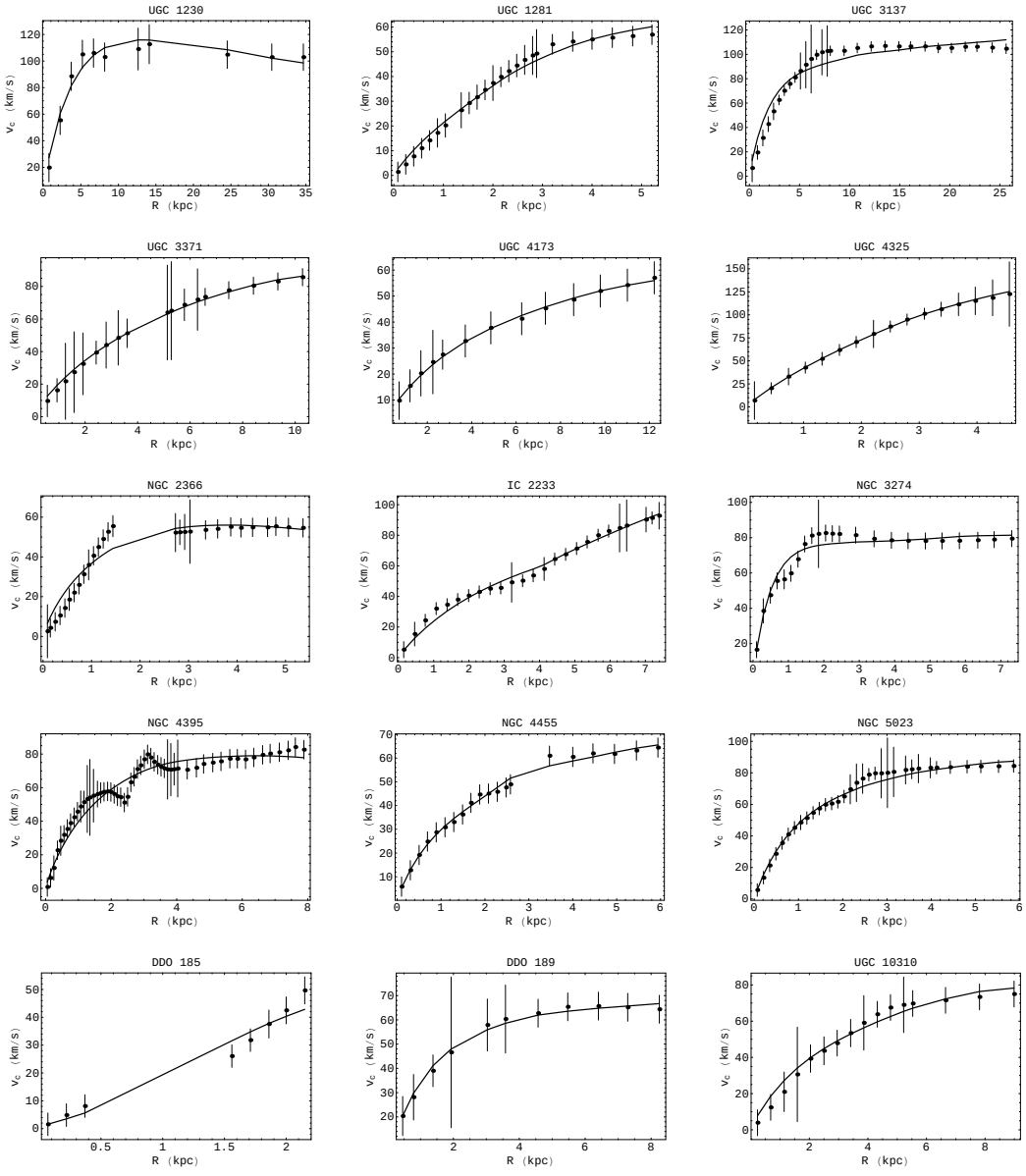

Figure 3.5: Best fit curves superimposed to the data for the sample of 15 LSB galaxies considered. See Table 1 for details on the galaxies and Table 2 for the values of the best fit parameters. A case by case discussion is presented in the Appendix A.

3.6 Low Surface Brightness Galaxies: Results

The extensive analysis of the previous section make it possible to draw two summarizing conclusions. First, we have to set somewhat the slope n of the gravity Lagrangian in order to break the degeneracy the model parameters. Second, we can rely on the smoothed data without introducing any bias in the estimated parameters or on their uncertainties.

A key role is then played by how we set n and hence β. To this aim, one may resort to cosmology. Indeed, R^n gravity has been introduced as a possible way to explain the observed cosmic speed up without the need of any dark energy component. Motivated by the first encouraging results, we have fitted the SNeIa Hubble diagram with a model comprising only baryonic matter, but regulated by modified Friedmann equations derived from the R^n gravity Lagrangian. Indeed, we find that the data are consistent with the hypothesis of no dark energy and dark matter provided $n \neq 1$ is assumed [78]. Unfortunately, the constraints on n are quite weak so that we have decided to set n to its best fit value without considering the large error. This gives $\beta = 0.817$ that we will use throughout the rest of the work. Note that Eq.(3.15) quickly saturates as function of n so that, even if n is weakly constrained, β turns out to be less affected.

A comment is in order here. Setting β to the value derived from data probing cosmological scales, we are implicitly assuming that the slope n of the gravity Lagrangian is the same on all scales. From a theoretical point of view, this is an obvious consistency assumption. However, it should be nicer to derive this result from the analysis of the LSB rotation curves since they probe a different scale. Unfortunately, the parameters degeneracy discussed above prevents us to efficiently perform this quite interesting test. Indeed, an accurate estimate of n from β needs a well determined β since a small offset $\Delta\beta/\beta$ translates in a dramatically large $\Delta n/n$. As a consequence, a possible inconsistency among the estimated β from different galaxies could erroneously lead to the conclusion that the gravity theory is theoretically not self consistent. To validate such a conclusion, however, one should reduce $\Delta\beta/\beta$ to less than 5%. Unfortunately, our analysis of the simulated rotation curves have shown us that this is not possible with the data at hand. It is therefore wiser to opt for a more conservative strategy and look for a consistency[9] between the results from the cosmological and the galactic scales exploring whether the value of β set above allows to fit all the rotation curves with physical values of the remaining two parameters $(\log r_c, f_g)$. This is our aim in this work, while the more ambitious task hinted above will need for a different dataset.

With this caveat in mind, all we need to fit the data is the modelling of LSB galaxies described in Sect. 4.3 and the smoothed data available in literature. The best fit curves thus obtained are shown in Fig. 3.5, while the constraints on $(\log r_c, f_g)$ and on the stellar M/L ratio $\Upsilon_\star$ are reported in Table 2. As a preliminary remark, it is worth noting that three galaxies (namely, NGC 2366, NGC 4395 and DDO 185) may be excluded by further discussion because of problematic data.

Indeed, for NGC 2366 the lack of data in the intermediate region prevents from deriving useful constraints, while the bump and the sink in NGC 4395 clearly signals the effect of local clumps in the gas distribution. Finally, for DDO 185, we have only 8 points separated by a large gap so that the fit is unable to converge. We stress that these cases are problematic

[9] A similar problem also arises when dealing with MOND where the critical acceleration a_0 plays a similar role as n for our theory. In principle, one should leave this quantity free when fitting galactic rotation curves and then check whether the same value is recovered for all galaxies. Unfortunately, model degeneracies prevent to perform such a test so that it is common to set a_0 to its fiducial value $1.2\times10^{-10}\mathrm{m/s^2}$ from the beginning.

whatever is the mass model and the gravity theory adopted so that we will not consider them anymore in the following discussion. A detailed case - by - case analysis of the full sample is presented in Appendix A, while here we mainly dedicate to some general lessons we can draw from the fit results.

Fig. 3.5 shows that, for 11 over 12 cases (the only problematic one being UGC 3137), there is an overall very good agreement between the data and the best fit curve thus suggesting that our modified gravitational potential allows to fit the data without any dark matter halo. Indeed, our model galaxies are based only on what is directly observed (the stellar mass and the gas content) and no exotic component is added. Needless to say, this is not possible in the standard Newtonian theory of gravity, while it is the presence of the additive power law term in the modified gravitational potential that makes it possible to increase the rotation curve in such a way to reproduce what is measured. In order to further substantiate this result, we can compare the constraints on the galactic parameters f_g and $\Upsilon_\star$ with what is expected from astrophysical considerations.

First, we consider the gas mass fraction f_g. Roughly averaging the best fit values for the 11 successfully fitted galaxies, we get $\langle f_g \rangle \simeq 0.51$ with a standard deviation $\sigma_g \simeq 0.18$. Both these values are typical of LSB galaxies thus suggesting that our model galaxies are physically reasonable. As a further check, one could question whether the estimated values of the M/L ratio $\Upsilon_\star$ are reasonable. The stellar M/L is usually obtained by fitting the Newtonian rotation curve of the exponential disk to the observed data in the inner region. However, such an estimate may be seriously biased. On the one hand, one usually add a dark halo contributing also to the inner rotation curve so that less disk mass is needed and hence the M/L ratio could be underestimated. On the other hand, being r_c of order 10^{-2} kpc, using the Newtonian gravitational potential significantly underestimates the *true* rotation curve for a given disk mass so that more mass and hence an artificially higher M/L is needed if the halo is neglected. As a consequence, we cannot rely on the estimates of M/L reported in literature if they have been obtained by studying the inner rotation curve. A possible way out could be to use the relation between broad band colors and M/L [35]. Unfortunately, this relation has been obtained by considering stellar population models that are typical of high surface brightness galaxies that have quite different properties. Moreover, such a relation has been calibrated by fitting the Tully - Fisher law under the hypothesis of maximal disk and Newtonian gravitational potential. Indeed, as a cross check, we have used the Bell & de Jong (2001) formulae with the colors available in the NED database[10] obtaining values of $\Upsilon_\star$ typically much smaller than 1. This is in contrast with the usual claim that $M/L \simeq 1.4$ for LSB galaxies [120], while some suitably chosen population synthesis models predict $\Upsilon_\star$ between 0.5 and 2 [**?**].

Excluding the four problematic galaxies (UGC 3137, NGC 2366, NGC 4395, DDO 185), a direct comparison of the values of $\Upsilon_\star$ in Table 2 with the fiducial range $(0.5, 2.0)$ shows that in 9 over 11 cases the fitted $\Upsilon_\star$ is consistent within 1σ with the fiducial range quoted above. For UGC 1230 and DDO 189, the fitted M/L is unacceptably high so that a residual matter component seems to be needed. Should this missing matter be indeed dark matter, our proposed scenario would fail for these two galaxies. Deferring to Appendix A possible solutions for each single case, we here note that our constraints on $\Upsilon_\star$ comes from those on f_g through Eq.(3.39). Here, an assumption on the helium fraction f_{He} has been assumed to convert the measured HI mass M_{HI} into the total gas mass $M_g = f_{He} M_{HI}$. Although reasonable,

[10] Note that these colors are typically in a different photometric system than that used by Bell & de Jong (2001). Although this introduces a systematic error, it is unlikely that this causes a significant bias in the estimated M/L. For details see the NED database (`http://nedwww.ipac.caltech.edu`).

our choice for the constant conversion factor is affected by an unknown uncertainty that we have not taken into account. Moreover, we have assumed the same f_{He} for all galaxies, while it is conceivable that star evolution related phenomena could make f_{He} mildly galaxy dependent. Should f_{He} be lower, than $\Upsilon_\star$ will be smaller thus lowering the disagreement observed. Moreover, we have not included any molecular gas in the gas budget. Although this is typically a good assumption, it is worth noting that our modified potential may increase the contribution to the total rotation curve of any mass element so that it is possible that the missing matter in UGC 1230 and DDO 189 is represented by unaccounted molecular gas. However, even excluding these two galaxies, we end up with a conservative estimate of 10 over 12 successful fits with plausible astrophysical values of the fitted galactic parameters which is a satisfactory considering the paucity of the sample.

Finally, let us consider the results on $\log r_c$. Different from the case of β, r_c is not a universal constant. Nevertheless, considering the conservative sample of 9 successfully fitted galaxies (thus excluding UGC 1230, UGC 3137, NGC 2366, NGC 4395, DDO 185, DDO 189) and roughly averaging the best fit values, we get $\langle \log r_c \rangle = -2.0 \pm 0.6$. The reasonably low scatter in $\log r_c$ may be qualitatively explained considering that r_c mainly determines the value of the terminal velocity in the rotation curve. Since this quantity has a low scatter for the sample of LSB galaxies we have used, it is expected that the same holds for $\log r_c$.

The constraints on $(\log r_c, f_g)$ summarized in Table 2 have been obtained for $\beta = 0.817$, consistent with the best fit n from the fit to SNela Hubble diagram. However, since the estimate of n is affected by a large uncertainty so that it is worth wondering how this impacts the results presented here. To this aim, we have repeated the fit for UGC 10310 for $n = 2.5$ ($\beta = 0.740$) and $n = 4.5$ ($\beta = 0.858$). For the best fit values, we get :

$$(\log r_c, f_g, \Upsilon_\star) = (-1.85, 0.58, 1.42) \quad for\ \beta = 0.740 \ ,$$

$$(\log r_c, f_g, \Upsilon_\star) = (-1.36, 0.41, 1.62) \quad for\ \beta = 0.858 \ ,$$

to be compared with $(\log r_c, f_g, \Upsilon_\star) = (-1.76, 0.56, 1.55)$. As expected, increasing β, $\log r_c$ and f_g become smaller in order to give the same observed rotation curve, consistent with what expected from Fig. 3.1. Although the shift in the best fit values is significant, the data do not still allow to draw a definitive conclusion. For instance, the 2σ confidence ranges for $\log r_c$ turn out to be :

$$\begin{array}{ll} (-2.16, -1.39) & for\ \beta = 0.740 \\ (-2.05, -1.34) & for\ \beta = 0.817 \\ (-2.04, -1.35) & for\ \beta = 0.858 \end{array} \tag{3.42}$$

which are consistent with each other. Note that further increasing n have no significant effect on the estimate of the parameters since β quickly saturates towards its asymptotic value $\beta = 1$. We are therefore confident that, although the constraints on $(\log r_c, \beta)$ depend on β, our main results are qualitatively unaltered by the choice of n (and hence β).

It is also worth noting that the three values of β considered above all provide quite good fits to the observed rotation curve. This is not surprising given the data at hand and our analysis parameters degeneracies presented in Sect. 5. In order to constrain β from rotation curves leaving it as a free parameter in the fit, therefore, one could explore the possibility to performed a combined χ^2 analysis of the full set of rotation curves. This can eventually be complemented by adding a prior on β, e.g., from the cosmological constraints on n. Exploring this issue is outside our aims here, but should be addressed in a forthcoming work.

Summarizing, the results from the fit and the reasonable agreement between the recovered $\Upsilon_\star$ and that predicted from stellar population synthesis models make us confident that R^n gravity is indeed a possible way to fit the rotation curves of LSB galaxies using only baryonic components (namely, the stellar disk and the interstellar gas) thus escaping the need of any putative dark matter halo.

Table 3.2: Best fit values of the model parameters from minimizing $\chi^2(\beta, \log r_c, f_g)$ with $\beta = 0.817$ corresponding to $n = 3.5$ as obtained from the best fit to the SNeIa data with only baryonic matter. We report 1σ (2σ) confidence ranges on the fitting parameters computed by projecting on the $(\log r_c, f_g)$ axes the contours $\Delta\chi^2 = 1$ $(\Delta\chi^2 = 4)$. The best fit stellar M/L ratio $\Upsilon_\star$ has been obtained evaluating Eq.(3.39) for the best fit f_g, while the uncertainty is obtained by usual propagation of errors symmetrizing the 1σ range of f_g. Note that this procedure is not completely correct since the errors are not Gaussian so that they are likely to be overestimated (especially when giving rise to unphysical negative lower limits for $\Upsilon_\star$). We also give $\chi^2/d.o.f.$ for the best fit model.

Id	$\log r_c$			f_g			$\Upsilon_\star$	χ^2/dof
	bf	1σ	2σ	bf	1σ	2σ		
UGC 1230	-0.38	$(-0.59, -0.13)$	$(-0.78, -0.05)$	0.15	$(0.13, 0.18)$	$(0.10, 0.21)$	$15.9 \pm 3.1 \pm 7.1$	0.33
UGC 1281	-2.12	$(-2.26, -1.95)$	$(-2.38, -1.76)$	0.47	$(0.37, 0.56)$	$(0.29, 0.66)$	$1.36 \pm 0.53 \pm 1.04$	0.22
UGC 3137	-1.67	$(-1.70, -1.63)$	$(-1.73, -0.60)$	0.61	$(0.59, 0.63)$	$(0.57, 0.64)$	$12.0 \pm 0.9 \pm 1.8$	1.80
UGC 3371	-1.78	$(-1.99, -1.52)$	$(-2.16, -1.21)$	0.40	$(0.28, 0.54)$	$(0.20, 0.67)$	$3.5 \pm 1.9 \pm 3.8$	0.03
UGC 4173	-0.74	$(-1.11, -0.16)$	$(-1.39, 0.55)$	0.36	$(0.26, 0.49)$	$(0.20, 0.65)$	$8.9 \pm 5.1 \pm 11.3$	0.01
UGC 4325	-2.81	$(-2.96, -2.62)$	$(-3.07, -2.36)$	0.69	$(0.55, 0.80)$	$(0.40, 0.89)$	$0.51 \pm 0.33 \pm 0.69$	0.01
NGC 2366	0.03	$(-0.47, 1.05)$	$(-0.77, 1.25)$	0.18	$(0.17, 0.20)$	$(0.15, 0.23)$	$14.4 \pm 1.9 \pm 4.4$	1.09
IC 2233	-2.05	$(-2.12, -1.96)$	$(-2.19, -1.87)$	0.60	$(0.55, 0.64)$	$(0.50, 0.68)$	$1.56 \pm 0.29 \pm 0.60$	0.50
NGC 3274	-2.09	$(-2.14, -2.03)$	$(-2.19, -1.98)$	0.49	$(0.47, 0.52)$	$(0.44, 0.55)$	$2.89 \pm 0.30 \pm 0.60$	0.84
NGC 4395	-0.25	$(-0.50, -0.05)$	$(-0.69, 0.23)$	0.093	$(0.090, 0.101)$	$(0.088, 0.110)$	$12.1 \pm 1.6 \pm 2.5$	0.70
NGC 4455	-2.36	$(-2.41, -2.30)$	$(-2.46, -2.24)$	0.85	$(0.82, 0.87)$	$(0.79, 0.89)$	$0.38 \pm 0.08 \pm 0.17$	0.18
NGC 5023	-2.52	$(-2.58, -2.46)$	$(-2.63, -2.40)$	0.52	$(0.49, 0.55)$	$(0.46, 0.58)$	$1.02 \pm 0.12 \pm 0.26$	0.29
DDO 185	-2.74	$(-2.81, -2.52)$	$(-2.87, -2.10)$	0.94	$(0.71, 0.97)$	$(0.41, 1.00)$	$0.12 \pm 0.49 \pm 1.14$	0.83
DDO 189	-1.82	$(-1.85, -1.47)$	$(-2.00, -1.24)$	0.53	$(0.43, 0.62)$	$(0.35, 0.72)$	$6.44 \pm 2.52 \pm 4.90$	0.06
UGC 10310	-1.76	$(-1.92, -1.56)$	$(-2.05, -1.34)$	0.56	$(0.46, 0.65)$	$(0.37, 0.74)$	$1.55 \pm 0.60 \pm 1.16$	0.21

3.6.1 Details on fit results

In Sect. 6, we have discussed the main features of the fit results as a whole, while here we give some few details on the comparison of the model with the rotation curve on a case - by - case basis.

UGC 1230. This is a somewhat problematic case giving a best fit $\Upsilon_\star = 15.9 \pm 3.1$ which is hard to explain in terms of reasonable population synthesis models. High values of M/L are also obtained in the case of maximum disk and dark halo models. For instance, de Blok & Bosma (2002) find $\Upsilon_\star = 6.1$ for both isothermal and NFW dark halo models. It is therefore likely that a problem may reside in the data or in the modelling (e.g., an underestimate of the gas content or a wrong measurement of the distance of the galaxy that could lead to underestimate the total absolute luminosity and hence overestimating $\Upsilon_\star$). Although such a possibility exist, it is worth noting that the value of $\log r_c$ is significantly larger than what is found for the other galaxies thus enhancing the need for an unseen component at odds with our working hypothesis of no dark matter. We have therefore decided to not consider UGC 1230 as a successful fits even if there is a good agreement between the data and the best fit curve.

UGC 1281. This is a typical case with the model nicely reproducing the data and a value of $\Upsilon_\star$ in agreement with population synthesis models. There is only a marginal overestimate of the rotation curve for $R \leq 1$ kpc, but it is well within the errors. To this aim, we remark that a slight overestimate of the theoretical rotation curve for the innermost points is expected for all galaxies since we have artificially assumed the gas surface density is flat in this region where no data are available. Should this not be the actual situation, v_c turns out to be slightly biased high.

UGC 3137. This case is not satisfactory for our approach. Indeed, the reduced χ^2 for the best fit model is anomalously high (~ 2) essentially due to the theoretical curve being higher than the observed one for the innermost points and smaller in the intermediate region. Moreover, the estimated $\Upsilon_\star = 12.0 \pm 1.9$ is too large to be reconciled with population synthesis models. The disagreement is hard to explain given that the data seem to be of good quality and the curve is quite smooth. It is, however, worth noting that it is not possible to achieve a good fit also in the dark matter case whatever is the halo model used (see, e.g., de Blok & Bosma 2002). It has to be remarked that UGC 3137 is an edge - on galaxy so that deriving a disk mass model from the surface brightness involves a series of assumptions that could have introduced some unpredictable systematic error.

UGC 3371. The agreement between the data and the model is extremely good and the estimated values of $(\log r_c, f_g)$ are typical of the sample we have considered. The best fit $\Upsilon_\star$ is somewhat larger than expected on the basis of stellar population model, but the fiducial $\Upsilon_\star = 1.4$ typically used in dark matter fitting is only 1σ smaller. We can therefore consider this fit successfull and physically reasonable.

UGC 4173. Although the agreement between the data and the best fit model is almost perfect, this case is somewhat more problematic than UGC 3371 since we get an anomalously high $\Upsilon_\star$. As such, we could deem this galaxy as a failure for R^n gravity. However, examining the 2D confidence regions in the plane $(\log r_c, f_g)$, it is easy to find out models with typical values of $\log r_c$ and lower $\Upsilon_\star$ that could still agree with the rotation curve within the errors.

Moreover, the uncertainties on the data points are probably overestimated as could be inferred noting that also dark halo models reproduce the observed curve with a very small χ^2 which is a typical signal of too high errors. Given these issues, we include this galaxy in the sample of successful fits.

UGC 4325. The best fit model matches perfectly the observed rotation curve with a typical value of $\log r_c$, but a somewhat small but still reasonable $\Upsilon_\star$. However, since $\log r_c$ and $\Upsilon_\star$ are positively correlated, one could increase $\log r_c$ and hence $\Upsilon_\star$ still achieving a very good fit to the data, even if this is not our final choice.

NGC 2366. This curve is a challenge both for R^n gravity and dark matter models. The very linear rise in the inner part rapidly changes in a flat part at larger radii. Moreover, there are no points in the intermediate region that could give constraints on how the change takes place. As de Blok & Bosma (2002) suggests, it is possible that the outermost points which are based on the HI data alone are underestimated. Another possibility is the presence of non circular motions due to the inner bar - like structure. These uncertainties on the data lead to a very bad fit with large values for both $\log r_c$ and $\Upsilon_\star$. Given this situation, we have not considered anymore this galaxy stressing, however, that this is not an evidence against R^n gravity.

IC 2233. It is quite difficult to get a very good fit to this galaxy rotation curve since, looking at the plot, one sees an abrupt change of concavity for $R \geq 3$ kpc. As a consequence, a perfect matching between the data and the model is not possible. Nevertheless, the best fit model provides a quite good agreement with the data. Moreover, the best fit values of $(\log r_c, f_g)$ are typical of our sample and the estimated $\Upsilon_\star$ nicely agrees with the fiducial one suggested in previous literature. We can therefore consider this galaxy as one of the most remarkable successes of R^n gravity.

NGC 3274. Although the general trend of the curve is well reproduced, there is a certain disagreement in the region $1 \text{ kpc} \leq R \leq 2 \text{ kpc}$ where a change of concavity occurs that is not reproduced by the model. Note that features like this could be related to a clumpiness in the gas distribution that cannot be modeled analytically. Considering, moreover, that the value of $\log r_c$ is quite typical and the estimated M/L ratio is not too difficult to reconcile with population synthesis models (although somewhat high), we conclude that R^n gravity successfully reproduces this curve.

NGC 4395. The rotation curve of this galaxy is strongly affected by the presence of star formation regions that cause an oscillating behaviour for $1.5 \text{ kpc} \leq R \leq 4 \text{ kpc}$ that is not possible to reproduce by any analytical model. Indeed, the best fit model is unable to agree reasonably well with the data so that the results on $(\log r_c, f_g)$ are significantly altered. Given the problems with the modeling, we have therefore decided to exclude this galaxy from the final sample since it is impossible to decide whether a bad fit is a signal of a breakdown for R^n gravity.

NGC 4455. Both the fit and the estimated values of the model parameters are quite satisfactory, although the low $\Upsilon_\star$ may argue in favour of a higher $\log r_c$. Note that there is a hole in the observed rotation curve around ~ 3 kpc. Adding some more data in this region could help in better constraining the parameters with particular regard to $\Upsilon_\star$. It is worth noting that the best fit curve tends to be higher (but well within the measurement errors) in the outer

region. Extending the measurement of this galaxy rotation curve to larger radii could therefore be a crucial test for our paradigm in this particular case. Note, however, that it is also possible that the parameters will be adjusted in such a way to still provide a good fit.

NGC 5023. This edge - on galaxy is, in a certain sense, an ameliorated version of UGC 3137. Indeed, the best fit model underestimates the rotation curve in the region between 2 and 3 kpc, but fits quite well the remaining data. Inspecting the rotation curve, a change of concavity occurs at 2 kpc and it is, indeed, this feature the origin of the disagreement. The similarity with the case of UGC 3137 could suggest to reject this galaxy considering also this fit as an unsuccessful one. However, a closer look shows that, while in the case of UGC 3137 the best fit model works bad both in the inner and the intermediate regions, here the disagreement is limited to the zone where the change of concavity takes place. Moreover, in this case, the best fit $\log r_c$ is typical of our sample and the estimated M/L ratio is quite reasonable so that we have finally decided to retain this galaxy.

DDO 185. This very linear curve is quite difficult to reproduce and, indeed, our best fit model makes a poor job with a too small M/L ratio. However, the overall rotation curve measurements are of very poor quality so that this galaxy can be discarded from further considerations.

DDO 189. There is an almost perfect matching between the data and the best fit model. The estimated values of $(\log r_c, f_g)$ are typical for the LSB galaxies in our sample, but $\Upsilon_\star$ is unexpectedly large. Since f_g takes a completely reasonable value, a possible problem could arise with the conversion from f_g to $\Upsilon_\star$. For instance, should f_{He} be smaller than our fiducial value, then $\Upsilon_\star$ should be revised towards lower values. In order to be conservative, we have however decided to exclude this galaxy from the sample of successful fits even if nothing prevents the reader to take the opposite decision.

UGC 10310. Everything works well for this galaxy. The best fit model provides a good fit to the observed rotation curve with only a modest overestimate (still within the uncertainties) in the innermost region that could be ascribed to our assumptions in the gas modelling. The values of $\log r_c$ and f_g are typical of our sample, while the best fit $\Upsilon_\star$ may be easily reconciled with the predictions from stellar population synthesis models.

3.7 High Surface Brightness Spiral Galaxies

Using the same formalism of the LSB galaxies, the analysis for HSB has done leading to the results reported in Table(3.3).
The total HSB sample is made of two different subsamples:

- the first sample, with 15 galaxies, represents the best available rotation curves to study the mass distribution of luminous and/or dark matter, and it has been used in works concerning modifications of gravity and the core/cusp controversy. This sample includes nearby galaxies of different Surface Brightness: DDO 47 [170]; ESO 116-G12, ESO 287-G13, NGC 7339, NGC 1090 [169]; UGC 8017, UGC 10981, UGC 11455 [380]; M 31, M 33 [114]; IC 2574 [245]; NGC 5585 [115]; NGC 6503 [387]; NGC 2403 [158]; NGC 55 [305];
- a second sample consists of 15 selected objects from [323] that has been used to test

MOND. This sample consists of the following galaxies: UGC 6399, UGC 6983, UGC 6917, NGC 3972, NGC 4085, NGC 4183, NGC 3917, NGC 3949, NGC 4217, NGC 3877, NGC 4157, NGC 3953, NGC 4100 [368, 374]; NGC 300 [304]; UGC 128 [371].

Table 3.3: Properties and parameters of the mass model of the analyzed sample ($\beta = 0.7$) from [162]. From left to right, the columns read: name of the galaxy, Hubble Type as reported in the NED database, adopted distance in Mpc, B-band luminosity in $10^9\, L_{B\odot}$, disk scale length in kpc, gas mass in $10^9\, M_\odot$ until last measured point, gas fraction in %, disk mass in $10^9\, M_\odot$, scale length parameter in kpc, mass-to-light ratio in $\Upsilon^B_\odot$, and chi-square χ^2_{red}.

Id	Type	D	L_B	R_D	M_{gas}	f_{gas}	M_D	r_c	$\Upsilon^B_\star$	χ^2_{red}
DDO 47	IB	4	0.1	0.5	2.2	96 ± 1	0.01	0.005	0.1	0.5
IC 2574	SABm	3	0.8	1.78	0.52	79 ± 12	0.14	0.017 ± 0.003	0.2	0.8
NGC 5585	SABc	6.2	1.5	1.26	1.45	58 ± 3	1	0.038 ± 0.004	0.7	1.4
NGC 55	SBm	1.6	4	1.6	1.3	84 ± 7	0.24	0.024 ± 0.004	0.06	0.14
ESO 116-G12	SBcd	15.3	4.6	1.7	21	50	2.1	0.05 ± 0.01	0.5	1.2
NGC 6503	Sc	6	5	1.74	2.3	18 ± 0.7	10.6	0.21 ± 0.014	2.1	18
M 33	Sc	0.84	5.7	1.4	3.7	53 ± 2	3.3	0.075 ± 0.004	0.58	25
NGC 7339	SABb	17.8	7.3	1.5	6.2	2.8 ± 0.2	22	0.41 ± 0.07	3	2.3
NGC 2403	Sc	3.25	8	2.08	4.46	27 ± 0.9	12.1	0.21 ± 0.015	1.5	19
M 31	Sb	0.78	20	4.5	–	–	180 ± 70	1.53 ± 0.19	9	3.4
ESO 287-G13	Sbc	35.6	30	3.3	14	25 ± 1	41	0.48 ± 0.05	1.4	3.2
NGC 1090	Sbc	36.4	38	3.4	100	18 ± 1	47	0.59 ± 0.04	1.2	0.9
UGC 8017	Sab	102.7	40	2.1	–	–	9.1 ± 0.3	0.01 ± 0.01	0.23	5.2
UGC 11455	Sc	75.4	45	5.3	–	–	74 ± 3	0.14 ± 0.01	1.6	5
UGC 10981	Sbc	155	120	5.4	–	–	460 ± 200	$\sim 10^{11}$	3.8	4.9
UGC 6399	Sm	18.6	1.6	2.4	1	23 ± 3	3.3	0.1 ± 0.03	2	0.1
NGC 300	Scd	1.9	2.3	1.7	1.3	39 ± 4	2	0.052 ± 0.010	0.87	0.43
UGC 6983	SBcd	18.6	4.2	2.7	4.1	24 ± 2	13	0.46 ± 0.1	3.1	0.88
UGC 6917	SBd	18.6	4.4	2.9	2.6	14 ± 1	16	0.71 ± 0.17	3.6	0.47
UGC 128	Sd	60	5.2	6.4	10.7	32 ± 5	23	0.39 ± 0.11	4.4	0.1
NGC 3972	Sbc	18.6	6.7	2	1.5	39 ± 3	2.5	0.025 ± 0.004	0.37	0.1
NGC 4085	Sc	18.6	6.9	1.6	1.3	44 ± 4	1.7	0.014 ± 0.003	0.25	1
NGC 4183	Scd	18.6	9.5	1.4	4.9	60 ± 6	3.2	0.09 ± 0.023	0.3	0.33
NGC 3917	Scd	18.6	11	3.1	2.6	22 ± 1.5	9.2 ± 0.9	0.098 ± 0.014	0.8	1
NGC 3949	Sbc	18.6	19	1.7	4.1	19 ± 2.2	17	0.22 ± 0.06	0.9	0.25
NGC 4217	Sb	18.6	21	2.9	3.3	6.1 ± 0.7	52	0.55 ± 0.15	2.5	0.38
NGC 4100	Sbc	18.6	25	2.5	4.4	13 ± 1.5	28	0.20 ± 0.03	1.1	1.52
NGC 3877	Sc	18.6	27	2.8	1.9	7.3 ± 0.8	24	0.2 ± 0.04	0.9	0.75
NGC 4157	Sb	18.6	30	2.6	12	26 ± 2.6	33	0.25 ± 0.04	1.1	0.53
NGC 3953	SBbc	18.6	41	3.8	4	2.8 ± 0.18	140	1.9 ± 0.5	3.4	0.78

Available photometry and radio observations show that the stars and the gas in the sample of galaxies are distributed in an infinitesimal thin and circular symmetric disk. While the HI surface luminosity density distribution $\Sigma_{gas}(r)$ gives a direct measurement of the gas mass, optical observations show that the stars have an exponential distribution:

$$\Sigma_D(r) = (M_D/2\sigma R_D^2) e^{-r/R_D}, \tag{3.43}$$

where M_D is the disk mass and R_D is the scale length, the latter being measured directly from the optical observations, while M_D is kept as a free parameter of our analysis. The total circular velocity is the sum of each squared contribution from stars and gas, and respectively

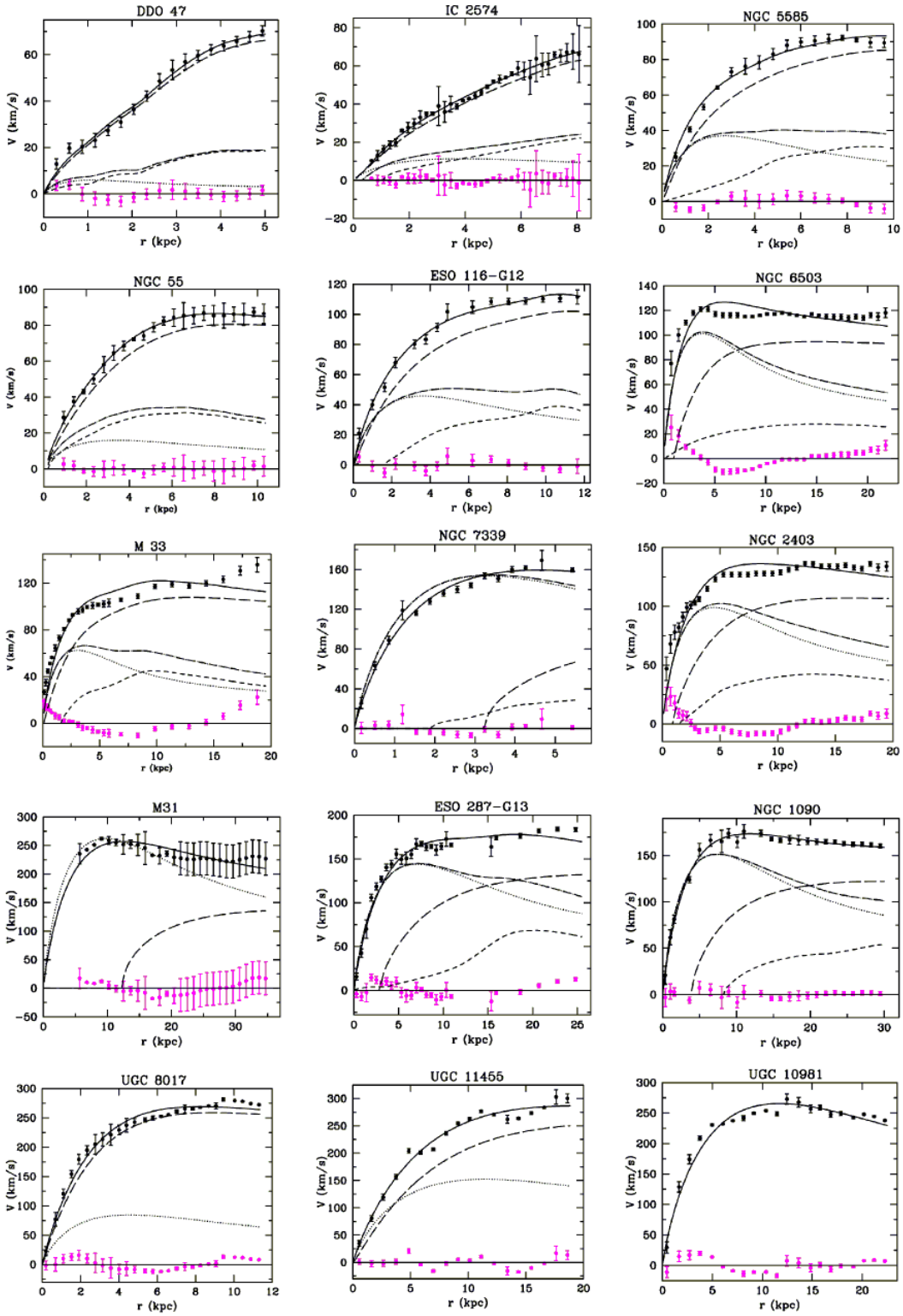

Figure 3.6: The solid line represents the best-fit total circular velocity. The dashed and dotted lines are the Newtonian contribution from gas and the stars, while the dot-dashed represents their sum. The long dashed-line is the non Newtonian contribution of the gas and the stars to the model. Below the rotation curves, we plot the residuals.

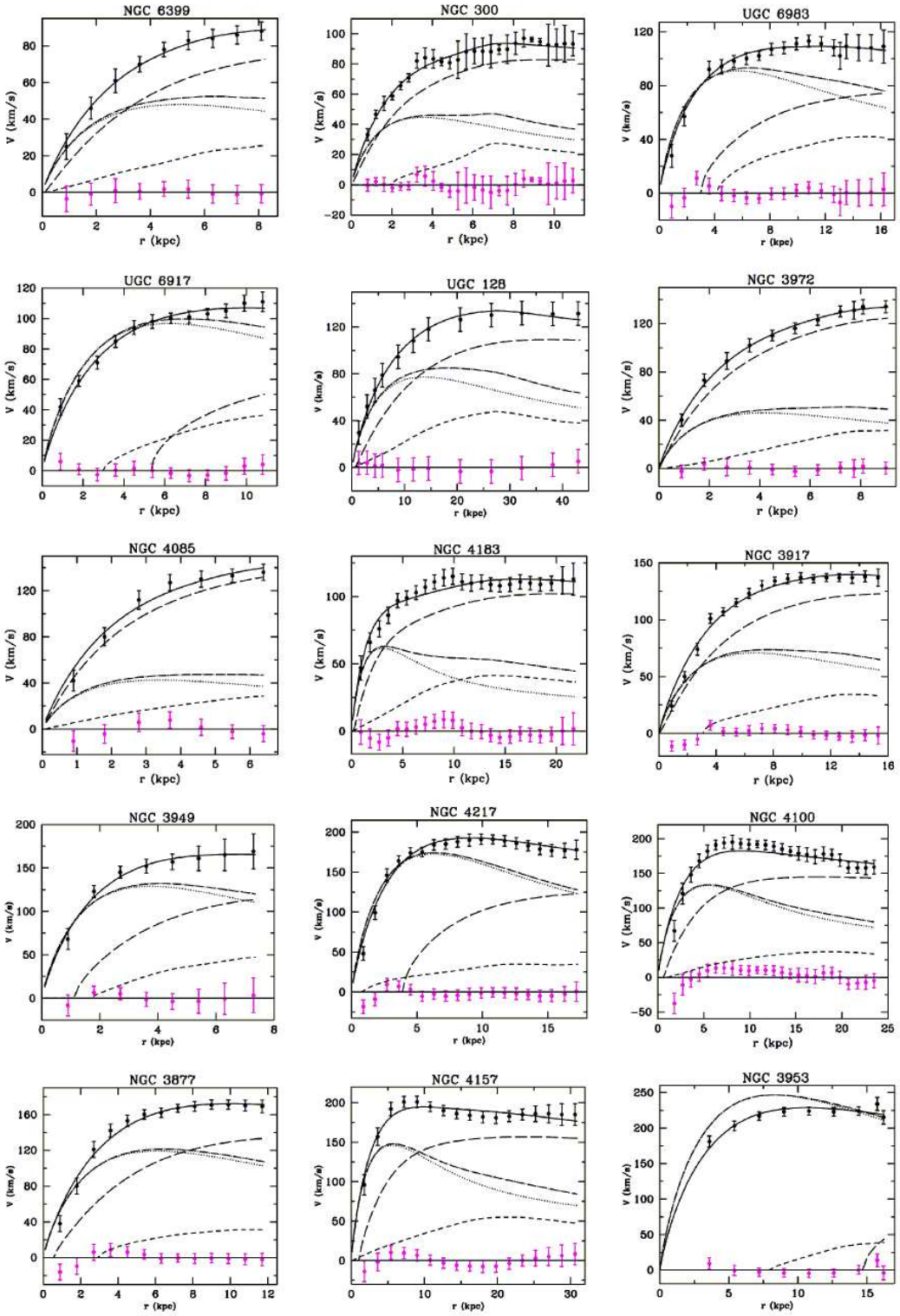

Figure 3.7: Best fit curves superimposed to the data from selected objects from [323]. See Fig.(3.6) for details.

from the Newtonian and corrective term of the extended gravitational potential as given in Eq.(3.34).

In a first step, rotation curves of HSB are χ^2 best fitted with the following free parameters: the slope (β) and the scale length (r_c) of the theory, and the gas mass fraction (f_{gas}) related to the disk mass simply by $M_D = M_{gas}(1 - f_{gas})/f_{gas}$. The errors for the best fit values of the free parameters are calculated at one standard deviation with the $\chi^2_{red} + 1$ rule. From the results of these fits it gets a mean value of

$$\beta_{HSB} = 0.7 \pm 0.25 \ (n \simeq 2.2) \, . \tag{3.44}$$

In the second step it has redone the best-fit fixing the slope parameter at $\beta = 0.7$ keeping as free parameters only r_c and f_{gas}. In the case of LSB a mean value of

$$\beta_{LSB} = 0.58 \pm 0.15 \ (n \simeq 1.7) \, , \tag{3.45}$$

has been obtained, perfectly compatible with this result. This parameter, however, is well constrained from SNela observations to be

$$\beta_{SN} = 0.87 \ (n \simeq 3.5) \, , \tag{3.46}$$

also compatible with these results.
Summarizing the results of this analysis, in general we have:

- the velocity model coming from modified gravitational potential well fits rotation curves;
- acceptable values for the mass-to-light ratios;
- too vast range for values of gas fraction ($0\% < f_{gas} < 100\%$);
- not clear comprehension for the big variation of values for the scale length parameter ($0.005\,\mathrm{kpc} < r_c < 1.53\,\mathrm{kpc}$)

3.8 Burkert haloes

At this point, it is worth wondering whether a link may be found between R^n gravity and the standard approach based on dark matter haloes since both theories fit equally well the same data. The *trait-de-union* between these two different schemes can be found in the modified gravitational potential which induces a correction to the rotation curve in a similar manner as a dark matter halo does. As a matter of fact, it is possible to define an *effective dark matter halo* by imposing that its rotation curve equals the correction term to the Newtonian curve induced by R^n gravity. Mathematically, one can split the total rotation curve derived from R^n gravity as $v_c^2(r) = v_{c,N}^2(r) + v_{c,corr}^2(r)$ where the second term is the correction. Considering, for simplicity a spherical halo embedding a thin exponential disk, one may also write the total rotation curve as $v_c^2(r) = v_{c,disk}^2(r) + v_{c,DM}^2(r)$ with $v_{c,disk}^2(r)$ the Newtonian disk rotation curve and $v_{c,DM}^2(r) = GM_{DM}(r)/r$ the dark matter one, $M_{DM}(r)$ being its mass distribution. Equating the two expressions, one gets:

$$M_{DM}(\eta) = M_{vir} \left(\frac{\eta}{\eta_{vir}} \right) \frac{2^{\beta-5}\eta_c^{-\beta}(1-\beta)\eta^{\frac{\beta-5}{2}}\mathcal{I}_0(\eta) - \mathcal{V}_d(\eta)}{2^{\beta-5}\eta_c^{-\beta}(1-\beta)\eta^{\frac{\beta-5}{2}}\mathcal{I}_0(\eta_{vir}) - \mathcal{V}_d(\eta_{vir})} \, . \tag{3.47}$$

with $\eta = r/R_d$, $\Sigma_0 = \Upsilon_\star i_0$, $\mathcal{V}_d(\eta) = I_0(\eta/2)K_0(\eta/2) \times I_1(\eta/2)K_1(\eta/2)$[11] and :

$$\mathcal{I}_0(\eta,\beta) = \int_0^\infty \mathcal{F}_0(\eta,\eta',\beta) k^{3-\beta} \eta'^{\frac{\beta-1}{2}} \mathrm{e}^{-\eta'} d\eta' \tag{3.48}$$

with $\mathcal{F}_0$ only depending on the geometry of the system and "vir" indicating virial quantities. Eq.(3.47) defines the mass profile of an effective spherically symmetric DM halo whose ordinary rotation curve provides the part of the corrected disk rotation curve due to the addition of the curvature corrective term to the gravitational potential. It is evident that, from an observational viewpoint, there is no way to discriminate between this dark halo model and R^n gravity. Having assumed spherical symmetry for the mass distribution, it is immediate to compute the mass density for the effective dark halo as $\rho_{DM}(r) = (1/4\pi r^2) dM_{DM}/dr$. The most interesting features of the density profile are its asymptotic behaviors that may be quantified by the logarithmic slope $\alpha_{DM} = d\ln\rho_{DM}/d\ln r$ which can be computed only numerically as function of η for fixed values of β (or n). As expected, α_{DM} depends explicitly on β, while (r_c, Σ_0, R_d) enter indirectly through η_{vir}. The asymptotic values at the center and at infinity denoted as α_0 and α_∞ result particularly interesting. It turns out that α_0 almost vanishes so that in the innermost regions the density is approximately constant. Indeed, $\alpha_0 = 0$ is the value corresponding to models having an inner core such as the cored isothermal sphere [43] and the Burkert model [62, 63, 50]. Moreover, it is well known that galactic rotation curves are typically best fitted by cored dark halo models (see, e.g., [171] and references therein). On the other hand, the outer asymptotic slope is between -3 and -2, that are values typical of most dark halo models in literature. In particular, for $\beta = 0.80$ one finds $(\alpha_0, \alpha_\infty) = (-0.002, -2.41)$, which are quite similar to the value for the Burkert model $(0, -3)$. It is worth noting that the Burkert model has been empirically proposed to provide a good fit to the LSB and dwarf galaxies rotation curves. The values of $(\alpha_0, \alpha_\infty)$ that authors find for their best fit effective dark halo therefore suggest a possible theoretical motivation for the Burkert - like models. Due to the construction, the properties of the effective dark matter halo are closely related to the disk one. As such, we do expect some correlation between the dark halo and the disk parameters. To this aim, exploiting the relation between the virial mass and the disk parameters , one can obtain a relation for the Newtonian virial velocity $V_{vir} = GM_{vir}/R_{vir}$:

$$M_d \propto \frac{(3/4\pi\delta_{th}\Omega_m\rho_{crit})^{\frac{1-\beta}{4}} R_d^{\frac{1+\beta}{2}} \eta_c^\beta}{2^{\beta-6}(1-\beta)G^{\frac{5-\beta}{4}}} \frac{V_{vir}^{\frac{5-\beta}{2}}}{\mathcal{I}_0(V_{vir},\beta)} \ . \tag{3.49}$$

Authors have numerically checked that Eq.(3.49) may be well approximated as $M_d \propto V_{vir}^a$ which has the same formal structure as the baryonic Tully - Fisher (BTF) relation $M_b \propto V_{flat}^a$ with M_b the total (gas + stars) baryonic mass and V_{flat} the circular velocity on the flat part of the observed rotation curve. In order to test whether the BTF can be explained thanks to the effective dark matter halo it has been proposing, one should look for a relation between V_{vir} and V_{flat}. This is not analytically possible since the estimate of V_{flat} depends on the peculiarities of the observed rotation curve such as how far it extends and the uncertainties on the outermost points. For given values of the disk parameters, authors therefore simulate theoretical rotation curves for some values of r_c and measure V_{flat} finally choosing the fiducial value for r_c that gives a value of V_{flat} as similar as possible to the measured one. Inserting the relation thus found between V_{flat} and V_{vir} into Eq.(3.49) and averaging over different simulations, they finally get :

$$\log M_b = (2.88 \pm 0.04)\log V_{flat} + (4.14 \pm 0.09) \tag{3.50}$$

[11] Here I_l and K_l, with $l = 1, 2$ are the Bessel functions of first and second type.

while a direct fit to the observed data gives [249] :

$$\log M_b = (2.98 \pm 0.29) \log V_{flat} + (3.37 \pm 0.13) \ . \tag{3.51}$$

The slope of the predicted and observed BTF are in good agreement thus leading further support to our approach. The zero point is markedly different with the predicted one being significantly larger than the observed one, but it is worth stressing, however, that both relations fit the data with similar scatter. A discrepancy in the zero point may be due to the approximate treatment of the effective halo which does not take into account the gas component. Neglecting this term, one should increase the effective halo mass and hence V_{vir} which affects the relation with V_{flat} leading to a higher than observed zeropoint. Indeed, the larger is M_g/M_d, the more the point deviate from our predicted BTF thus confirming our hypothesis. Given this caveat, one may therefore conclude with confidence that R^n gravity offers a theoretical foundation even for the empirically found BTF relation.

3.9 What have we learnt from galaxies?

Rotation curves of spiral galaxies have been considered for a long time the strongest evidence of the existence of dark matter haloes surrounding their luminous components. Notwithstanding the great experimental efforts, up to now there has never been any firm detection of such an exotic dark component that should make up these haloes. It is therefore worth wondering whether dark matter indeed exists or it is actually the signal of the need for a different gravitational physics.

Motivated by these considerations, we have explored here the case of R^n gravity. Since such theories have been demonstrated to be viable alternatives to the dark energy giving rise to scenarios capable of explaining the observed cosmic speed up, it is highly interesting to investigate their consequences also at galactic scales. To this aim, we have solved the vacuum field equations for power - law $f(R)$ theories in the low energy limit thus deriving the gravitational potential of a pointlike source. It turns out that both the potential and the rotation curve are corrected by an additive term scaling as $(r/r_c)^{\beta-1}$ with the scalelength r_c depending on the system physical features (e.g. the mass) and β a function of the slope n of the gravity Lagrangian. In particular, for $n = 1$, our approximated solution reduces to the standard Newtonian one. For $0 < \beta < 1$, the potential is still asymptotically vanishing, but the rotation curve is higher than the Newtonian one. These results still hold when we compute the corrected potential for extended systems with spherical symmetry or thin disk configuration. As a result, we have argued that the rotation curve of spiral galaxies could be fitted using the luminous components only thus eliminating the need for dark matter.

In order to verify this hypothesis, we have considered a sample of 15 LSB galaxies with well measured combined HI and Hα rotation curves extending far beyond the optical edge of the disk. Since these systems are usually claimed to be dark matter dominated, reproducing their rotation curves without the need of any dark matter halo would represent a significant evidence in favour of R^n gravity. Moreover, fitting to rotation curves allows in principle to constrain the theory parameters (β, r_c) and determine the M/L ratio of the stellar component. Unfortunately, extensive simulations have highlighted the need to set a strong prior on β (and hence n) to break the degeneracy among the three fitting parameters $(\beta, \log r_c, f_g)$. To this aim, we have resorted to the results of SNeIAa Hubble diagram fitting without dark matter and dark energy which shows that $n = 3.5$ reproduces the data without the need of any dark sector.

Motivated by this consideration, we have set $n = 3.5$ giving $\beta = 0.817$ in order to check whether R^n gravity may fit both the SNeIa Hubble diagram and the LSB rotation curves without either dark energy on cosmological scales and dark matter on galactic scales with the same value of the slope n. Indeed, we conservatively estimate that 10 of a sample of 12 usable galaxies can be properly fitted by the corrected rotation curves based only on the baryonic components (stars and gas) of the galaxies with values of the M/L ratio which may be reconciled with predictions from stellar population synthesis models. It is worth emphasizing that all the LSB rotation curves have been successfully fitted using the same value of β. Although β has been set from the beginning, this does not guarantee that the full set of curves will be satisfactorily well fitted. Indeed, should we have found that a single rotation curve demands for a different β, this could have been a decisive evidence against R^n gravity. On the contrary, the same β leads to equally good fit for all the 10 successful galaxies. We therefore conclude that the self consistency of the theory has been verified thus leading further support to R^n gravity as a viable alternative to the dark sector on galactic and cosmological scales.

These encouraging results are a strong motivation for investigating R^n gravity further from both observational and theoretical point of views. Still remaining on galactic scales, it was mandatory to extend the analysis of the rotation curves to the case of high surface brightness (HSB) galaxies. Although their structure is more complicated (since one has to include also a bulge component), HSB galaxies are more numerous than LSB ones so that we may perform our test on a larger sample thus increasing the significance of the results. To this aim, it is important to carefully select the sample in order to include systems with well measured and extended rotation curve and not affected by possible non circular motions due to spiral arms or bar - like structures. While this could be a limitation, it is worth stressing that in modeling HSB one may neglect the gas component which has been the most important source of theoretical uncertainty in our study of LSB galaxies. Should the test on HSB be successful as the present one, we could convincingly demonstrate that R^n gravity is a *no dark matter* solution to the long standing problem of the rotation curves of spiral galaxies. As we have verified, HSB galaxies give a positive answer to this question: we remark the relevance of the used sample that contains objects in a large range of luminosity and with very accurate and proper kinematic. At the end there was found in general a reasonable agreement, with some discrepancies, between the HSB and LSB circular velocity model, encouraging further investigations from the theoretical point of view.

Furthermore, if one considers the model parameters settled by the fit over the observational data on LSB rotation curves, it is possible to construct a phenomenological analogous of Dark Matter halo whose shape is similar to the one of Burkert model. Since Burkert model has been empirically introduced to give account of the DM distribution in the case of LSB and dwarf galaxies, this result could represent an interesting achievement since it furnishes a theoretical foundation to such a model. By investigating the relation among dark halo and the disk parameters, we have deduced a relation between M_d and V_{flat} which reproduces the baryonic Tully - Fisher. In fact, exploiting the relation between the virial mass and the disk parameters, one can obtain a relation for the virial velocity which can be satisfactory approximated as $M_d \propto V_{vir}^a$. Even such a result seems very intriguing since it furnishes again a theoretical interpretation for a phenomenological relation. As a matter of fact, although not definitive, these phenomenological issues regarding fourth order gravity can represent a viable approach for future more exhaustive investigations and in particular support the quest for a unified view of the dark side of the Universe.

CHAPTER 4

The Sersic Virial Hyperplane

After having showed how f(R) gravity models can be able to reproduce rotation curves of spiral galaxies and the Tully-Fisher relation which holds for this morphological class of galaxies, we can try to apply the same approach to elliptical galaxies. In this case, before to go to the them dynamics properties (i.e. the dispersion velocity curve, which is their analogous of rotation curves for spiral galaxies), we have found another useful results.

While working on the right way to approach this problem we have found another useful scaling relation which holds for this kind of galaxies. We have called it, *Sersic Virial Hyperplane* and, as we are going to show in this chapter, it is a four dimensional generalization of some more famous and historical relations such as the Fundamental Plane and the Photometric Plane. As we have reproduced the Tully-Fisher relation for spiral galaxies, we expect from future works to reproduce also this relation in the framework of f(R) gravity models. At the same time its importance goes above the gravity model which one applies to it, because it has two values inside. It is a more general relation between the dynamical, cinematical and morphological properties of an elliptical galaxy with respect usual relations, depicting a more comprehensive picture where the evolution of these objects can be better understood. Moreover, giving its narrow intrinsic dispersion respect to the Fundamental and Photometric Planes, it could be used as a new high-sensitivity distance indicator.

4.1 General properties of Elliptical Galaxies

Elliptical and S0 galaxies (hereafter, collectively referred to as early - type galaxies, ETGs) present a striking regularity in their luminosity distribution. The ETG surface brightness is well fitted by the well known $r^{1/4}$ profile [123], while considerable better results are obtained using the Sersic $r^{1/n}$ law [338]. From the photometric point of view, therefore, ETG may be considered as characterized by only three parameters, namely the slope n of the Sersic profile, the effective radius R_e containing half of the total luminosity, and the effective surface

brightness μ_e defined as $\mu_e = \mu(R_e)$, or equivalently the average surface intensity $\langle I_e \rangle = (L_T/2)/(\pi R_e^2)$.

The ETG kinematic may be schematically characterized through its central velocity dispersion σ_0 which, under suitable assumptions on the mass profile, gives information on the mass and hence the mass - to - light (hereafter M/L) ratio. Being a mass tracer, it is reasonable to expect that σ_0 is somewhat correlated to the total luminosity L_T, even if it is difficult to forecast an analytic form for such a correlation, given the subtleties of the luminous and dark components modelling. It is therefore not surprising that empirical searches for such a correlation were early undertaken. A remarkable success was represented by the Faber - Jackson (FJ) $L_T \propto \sigma_0^4$ relation [148]. The large scatter in the FJ law led to the need for higher dimensional representations of ETGs. Considering $n = 4$, there remains just three parameters describing an ETG so that one could wonder whether a relation exist among the photometric quantities $(R_e, \langle I_e \rangle)$ and the kinematical one σ_0. This relation were indeed found [133, 136] and, when expressed in a logarithmic scale, is just a plane soon dubbed the *fundamental plane* (FP). It is worth noting that such a plane was not unexpected. Indeed, a simple application of the virial theorem gives $R_e \propto \sigma_0^2 \langle I_e \rangle^{-1}$, under the hypotheses of constant M/L ratio and structural homology. The observed FP plane is however tilted, i.e. one indeed finds $R_e \propto \sigma_0^\alpha \langle I_e \rangle^{-\beta}$, but with $(\alpha, \beta) = (1.49, 0.75)$ rather than $(2, 1)$ as forecasted before [38]. Such a tilt may be easily explained introducing a power - law correlation $M/L \propto L_T^\gamma$ (with $\gamma \simeq 0.27$), but interpreting the origin of such a relation is a difficult and ambiguous task due to proposals ranging from non - homology [303], to stellar populations effects [136], from systematic variations in kinematical structure [372, 36, 64] to a combination of different terms [365].

Although the de Vaucouleurs profile is a satisfactory fit, it is well known that the Sersic profile has to be preferred [65, 175, 303]. As such, forcing $n = 4$ in the fit may systematically bias the estimate of R_e and $\langle I_e \rangle$ and hence affect the FP. Introducing n increases the number of parameters needed to describe ETGs leading to wonder whether scaling relations exist. Actually, given the observational difficulties in measuring σ_0, it is worth looking for empirical correlations involving only the photometric parameters. Interesting examples are the Kormendy relation (KR) between R_e and μ_e [217] and the scalelength - shape relation between R_e and n [391]. However, just as the FJ relation is a projection of the FP, both the R_e - μ_e and the R_e - n relations may be seen as projections of a more fundamental law among these three photometric parameters. In logarithmic units, such a relation indeed exists and it is a plane referred to as the *photometric plane* (PhP) recently detected in both near infrared [207] and optical [176]. While observationally the PhP is confirmed also at intermediate redshift (La Barbera et al. 2004, 2005), a definitive theoretical interpretation is still lacking. Modelling the stars in ETG as a self - gravitating gas, Lima Neto et al. (1999) have recovered a PhP like relation (referred to as the *entropic plane*) by assuming that the specific entropy (i.e., the entropy for mass unit) is constant for all ETGs. Later, Márquez et al. (2001) derived an *energy - entropy* (or *mass - entropy*) line giving a possible explanation for the structural relations among photometric parameters. Moreover, they also find out that the specific entropy increases as a consequence of merging processes so offering a possible way to test the model against the observed variation of the PhP with redshift.

There are two general lessons to draw from the above short summary. First, two dimensional scaling relations turn out to be projections of a more general three dimensional law. It is therefore worth wondering whether this also holds for the FP and PhP being possible projections of a four parameters law. It is worth noting that a first step towards this direction has been attempted by Graham (2002) fitting a hyperplane (in logarithmic units) to the set of parameters $(n, R_e, \langle I_e \rangle, \sigma_0)$, but it was never prosecuted. On the other hand, from a theoretical point of view, both the entropic plane and the FP are tentatively explained on the implicit

assumption that ETGs are in a state of dynamical equilibrium so that the virial theorem applies and the Boltzmann - Gibbs entropy may be evaluated. Motivated by these considerations, here we investigate whether a four dimensional relation among photometric and kinematic quantities may come out as consequence of the virial theorem and some assumptions on the stellar M/L consistent with stellar population synthesis models. Should such a relation exist, one could thus reconcile both the FP and the PhP under the same theoretical standard thus representing a valid tool to investigate ETG formation theories.

4.2 Modelling Elliptical Galaxies

Although some recent results show the presence of thin discs in inner regions of elliptical galaxies[1], ETGs may be well described as a luminous stellar distribution embedded in a dark matter halo dominating the outer mass profile. In the following, we will assume spherical symmetry for both these components. While this is an acceptable hypothesis for the halo, it is clearly an oversimplification for the elliptical luminous component. Nevertheless, this will allow us to get analytical expressions for the main quantities we are interested in without dramatically affecting the main results.

4.2.1 The Sersic profile

Under the hypothesis of constant M/L, the surface density of the luminous component may be easily obtained as:

$$\Sigma(R) = \Upsilon_\star I(R) \tag{4.1}$$

with $\Upsilon_\star$ the M/L ratio and $I(R)$ the surface luminosity density. As well known, the Sersic $r^{1/n}$ law [338] is best suited to describe the surface brightness distribution of elliptical galaxies [65, 175, 303]. Motivated by these evidences, we will therefore set:

$$I(R) = I_e \exp\left\{-b_n\left[\left(\frac{R}{R_e}\right)^{1/n} - 1\right]\right\} \tag{4.2}$$

with I_e the luminosity density at the effective radius R_e and b_n a constant defined such that the luminosity within R_e is half the total luminosity. It is possible to show that b_n may be found by solving [106]:

$$\Gamma(2n, b_n) = \Gamma(2n)/2 \tag{4.3}$$

where $\Gamma(a, z)$ is the incomplete Γ function and $\Gamma(a)$ the actual Γ function. Useful approximating formulae may be found in Graham & Driver (2005) and references therein, but we will exactly solve Eq.(4.3) in the following.

Assuming cylindrical symmetry, the luminosity profile within R is:

$$L(R) = 2\pi \int_0^R I(R')R'dR' = L_T \times \frac{\gamma(2n, b_n x)}{\Gamma(2n)} \tag{4.4}$$

[1] S0 galaxies contain, by definition, a thin disc, so that, strictly speaking, our following discussion applies only to the bulge component. However, neglecting this disc does not introduce any significant systematic error. Moreover, our sample is mainly dominated by elliptical galaxies so that we confidently neglect the disc component in S0 systems.

with $x \equiv R/R_e$ and

$$L_T = 2\pi n I_e R_e^2 b_n^{-2n} \mathrm{e}^{b_n} \Gamma(2n) \tag{4.5}$$

the total luminosity. The volume luminosity density $j(s)$ may be easily obtained deprojecting $I(R)$. Defining $s = r/R_e$ (with r the radius in spherical coordinates), we get [246]:

$$\nu(s) = -\frac{1}{\pi} \int_s^\infty \frac{di}{dx} \frac{dx}{\sqrt{x^2 - s^2}}$$

with $i(x) = I(R)/I_e$ and $\nu(s) = (R_e/I_e) j(s)$. Some algebra finally leads to the following expressions for the mass density $\rho_\star(s)$ and the mass profile $M_\star(s)$:

$$\rho_\star(s) = \frac{M_\star^T}{4\pi R_e^3} \times \frac{\mathcal{I}_\nu(s)}{\mathcal{I}_M(s)} \ , \tag{4.6}$$

$$M_\star(s) = M_\star^T \times \frac{\mathcal{I}_M(s)}{\mathcal{I}_M(s)} \ , \tag{4.7}$$

where we have denoted with $M_\star^T$ the total stellar mass:

$$M_\star^T = 4(b_n/n) \Upsilon_\star I_e R_e^2 \mathcal{I}_M(\infty) \ , \tag{4.8}$$

having used the abuse of notation

$$f(\infty) = \lim_{y \to \infty} f(y) \ .$$

Finally, to get Eqs.(4.6) and (4.7), we have used the auxiliary functions:

$$\mathcal{I}_\nu(s) = \int_s^\infty \frac{x^{(1-n)/n} \exp\left[-b_n \left(x^{1/n} - 1\right)\right]}{\left(x^2 - s^2\right)^{1/2}} dx \ , \tag{4.9}$$

$$\mathcal{I}_M(s) = \int_0^s \mathcal{I}_\nu(s') s'^2 ds' \ . \tag{4.10}$$

Both these functions cannot be analytically expressed, but are straightforward to be numerically evaluated. Actually, imposing $M_\star^T = \Upsilon_\star L_T$, it is immediate to get:

$$\mathcal{I}_M(\infty) = \frac{\pi n^2 \mathrm{e}^{b_n} \Gamma(2n)}{2 b_n^{2n+1}} \ , \tag{4.11}$$

so that we get an upper limit for $\mathcal{I}_M(s)$.

4.2.2 The dark halo

Most of the kinematical tracers of the total gravitational potential are usually affected by a severe degeneracy between the luminous component and the dark one so that there are different dark halo models able to fit the same data for a given stellar mass profile. It is therefore important to rely on a physical theory of halo formation to select models which are both compatible with the data and also physically well motivated. From this point of view, numerical simulations of galaxy formation in hierarchical CDM scenarios are very helpful since they predict the initial shape of the dark matter distribution. Here, we assume a NFW profile

[266] as initial dark matter halo and neglect the effect of the baryons gravitational collapse. The main features of the NFW model are :

$$\rho_{DM}(r) \equiv \frac{\rho_s}{x\ (1+x)^2}\ ,\ x = r/r_s \tag{4.12}$$

$$M_{DM}(r) = 4\pi\rho_s r_s^3\ f(x) = M_{vir} f(x)/f(c_{NFW})\ , \tag{4.13}$$

$$f(x) \equiv \ln(1+x) - \frac{x}{1+x}\ , \tag{4.14}$$

$$c_{NFW} \equiv r_{vir}/r_s\ , \tag{4.15}$$

$$M_{vir} = \frac{4\pi\delta_{th}}{3}\rho_{crit} r_{vir}^3\ , \tag{4.16}$$

where c is the concentration parameter, M_{vir} the virial mass and r_{vir} the virial radius[2]. The model is fully described by two independent parameters, which we assume to be c_{NFW} and M_{vir}. Numerical simulations, supported by observational data, motivate a correlation between c_{NFW} and M_{vir} so that the NFW model may be considered as a single parameter family. For instance, Bullock et al. (2001) have found :

$$c_{NFW} = 15 - 3.3\log\left(\frac{M_{vir}}{10^{12}h^{-1}\ \mathrm{M}_\odot}\right) \tag{4.17}$$

with a log normal scatter $\delta\log c \simeq 0.11$. An updated version of Eq.(4.17) has been obtained by Napolitano et al. (2005) :

$$c_{NFW} = \frac{16.7}{1+z}\left(\frac{M_{vir}}{10^{11}h^{-1}\ \mathrm{M}_\odot}\right)^{-0.125} \tag{4.18}$$

which is better suited for galaxy scale systems.

The NFW model is not the only model proposed to fit the results of numerical simulations. Some authors [258, 172] have proposed models with a central slope steeper than the NFW one. On the other hand, it is also possible that the inner slope does not reach any asymptotic value with the logarithmic slope being a power - law function of the r [267, 92] or that the deprojected Sersic profile also fits the numerical dark matter haloes [257, 178, 179]. However, the difference between all these models and the NFW one is very small for radii larger than 0.5% - 1% the virial radius so that we will not consider models other than the NFW one.

4.3 The virial theorem

Elliptical galaxies are known to be characterized by scaling relations among their kinematic and structural parameters. In an attempt to investigate whether such empirical laws may be recovered under a single theoretical scheme, we can rely on the hypothesis of statistical equilibrium. In such an assumption, the virial theorem holds :

[2]The virial radius is defined such that the mean density within r_{vir} is δ_{th} times the critical density ρ_{crit}. According to the concordance ΛCDM model, we assume a flat universe with $(\Omega_m, \Omega_\Lambda, h) = (0.3, 0.7, 0.72)$ where $\delta_{th} = 337$.

$$2K + W = 0 \tag{4.19}$$

with K and W the total kinetic and potential energy respectively. Both these quantities may be evaluated given the assumed spherical symmetry as we sketch below, referring the interested reader to Appendix A for further details.

4.3.1 Kinetic and gravitational energy

Neglecting the net rotation velocity of the system (which is reasonable, given the low values of v_c in elliptical galaxies), the total kinetic energy is given as [43] :

$$K = 3\pi \int_0^\infty \Sigma(R)\sigma_{los}^2(R)RdR \tag{4.20}$$

with $\Sigma(R)$ the star surface density and $\sigma_{los}(R)$ the luminosity weighted velocity dispersion projected along the line of sight. Following Mamon & Lokas (2005), for a spherically symmetric system, it is :

$$\begin{aligned} \sigma_{los}^2(R) &= \frac{2G}{I(R)} \int_R^\infty \mathcal{K}(r/R)\rho_\star(r)M(r)r^{-1}dr \\ &= \frac{2G}{I(x)} \int_x^\infty \mathcal{K}(s/x)\rho_\star(s)M(s)s^{-1}ds \end{aligned}$$

with $s = r/R_e$, $x = R/R_e$, $I(R)$ and $\rho_\star(r)$ given by Eqs.(4.2) and (4.6) respectively, the total mass profile reading :

$$M(s) = \frac{M_\star^T}{\mathcal{I}_M(\infty)} \left[\mathcal{I}_M(s) + \frac{M_{vir}}{M_\star^T} \frac{\mathcal{I}_M(\infty)}{f(c_{NFW})} f(s, R_e/r_s) \right] , \tag{4.21}$$

and $\mathcal{K}(s/x)$ a kernel function depending on the assumed anisotropy profile. In order to not increase too much the number of parameters, we will assume constant anisotropy so that it is :

$$\begin{aligned} \mathcal{K}(u) &= \frac{1}{2}u^{2\beta-1} \left[\left(\frac{3}{2} - \beta \right) \sqrt{\pi} \frac{\Gamma(\beta - 1/2)}{\Gamma(\beta)} \right. \\ &+ \left. \beta \, \mathrm{B}\left(\frac{1}{u^2}, \beta + \frac{1}{2}, \frac{1}{2} \right) - \mathrm{B}\left(\frac{1}{u^2}, \beta - \frac{1}{2}, \frac{1}{2} \right) \right] \end{aligned} \tag{4.22}$$

with $B(x, a, b)$ the Beta function. Some tedious algebra makes it possible to finally get :

$$\begin{aligned} \sigma_{los}^2(x) &= \frac{GM_\star^T}{R_e} \frac{4b_n^{2(1+n)}}{pi^2 n^3 \mathrm{e}^{b_n} \Gamma(2n)} \\ &\times \frac{\mathcal{I}_\sigma^\star(x) + (M_{vir}/M_\star^T)[\mathcal{I}_M(\infty)/f(c_{NFW})]\mathcal{I}_\sigma^{DM}(x)}{\exp[-b_n(x^{1/n} - 1)]} \end{aligned} \tag{4.23}$$

having defined the auxiliary functions :

$$\mathcal{I}_\sigma^\star(x, n, \beta) \equiv \int_x^\infty \mathcal{K}(s/x) \frac{\mathcal{I}_\nu(s)\mathcal{I}_M(s)}{s}^{-1} ds ,$$

$$\mathcal{I}_\sigma^{DM}(x,n,R_e/r_s,\beta) \equiv \int_x^\infty \frac{\mathcal{K}(s/x)\mathcal{I}_\nu(s)f(s,R_e/r_s)}{s}^{-1} ds \ .$$

As we will see later, $\sigma^2_{los}(R)$ does not enter the applications we are interested in. Actually, the quantity of interest is rather σ^2_0, i.e. $\sigma^2_{los}(R)$ averaged within a circular aperture of radius $R_e/8$ which is what is measured by the galaxy spectrum. As a general rule, it is :

$$\begin{aligned}\sigma^2_{ap}(R_{ap}) &= \frac{\int_0^{R_{ap}} 2\pi R I(R)\sigma^2_{los}(R)dR}{\int_0^{R_{ap}} 2\pi R I(R)dR} \\ &= \frac{2\pi R_e^2}{L_2(x_{ap})}\int_0^{x_{ap}} I(x)\sigma^2_{los}(x)xdx\end{aligned}$$

with R_{ap} the radius of the circular aperture, $x_{ap} = R_{ap}/R_e$ and we have defined :

$$\begin{aligned}L_2(x_{ap}) &= \int_0^{R_{ap}} 2\pi R I(R)dR \\ &= L_T \times \frac{\gamma(2n, b_n x_{ap}^{1/n})}{\Gamma(2n)} \ .\end{aligned} \tag{4.24}$$

Following the usual notation, we denote with σ_0 the central velocity dispersion obtained by setting $R_{ap} = R_e/8$. Using then Eq.(4.24), it is easy to finally get :

$$\begin{aligned}\sigma^2_0 &= \frac{GM^T_\star}{R_e}\frac{4b_n^{2+4n}}{\pi^2 n^4 \mathrm{e}^{2b_n}\Gamma(2n)} \\ &\times \frac{\mathcal{I}^\star_0 + (M_{vir}/M^T_\star)[\mathcal{I}_M(\infty)/f(c_{NFW})]\mathcal{I}^{DM}_0}{\gamma[2n,(1/8)^{1/n}]}\end{aligned} \tag{4.25}$$

having defined :

$$\mathcal{I}^\star_0(n,\beta) = \int_0^{1/8} \mathcal{I}^\star_\sigma(x,n,\beta)xdx \ , \tag{4.26}$$

$$\mathcal{I}^{DM}_0(n,R_e/r_s,\beta) = \int_0^{1/8} \mathcal{I}^{DM}_\sigma(x,n,R_e/r_s,\beta)xdx \ . \tag{4.27}$$

As a next step, we insert Eq.(4.24) into Eq.(4.20) and, by using Eq.(4.25), we finally obtain :

$$K = \frac{1}{2}M^T_\star\sigma^2_0 \times k(\mathbf{p}) \tag{4.28}$$

with $\mathbf{p}$ denoting the set of parameters

$$\mathbf{p} = (n, R_e, I_e, \beta, \Upsilon_\star, M_{vir}, c_{NFW}) \ ,$$

and $k(\mathbf{p})$ given explicitly in Appendix A. Note that, although I_e and $\Upsilon_\star$ do not explicitly enter the above equations, they are however included as parameters since they determine the total stellar mass $M^T_\star$ because of Eq.(4.8). On the other hand, r_s is not counted as an independent

parameter since it is determined as function of M_{vir} and c. Should we use Eq.(4.17) or (4.18), the virial mass M_{vir} would be the only parameter related to the dark halo properties.

The computation of W may be carried out in a similar way starting from the definition [43] :

$$W = -4\pi G \int_0^\infty \rho_{tot}(r) M_{tot}(r) r dr \ . \tag{4.29}$$

Splitting the total density and mass as the sum of the luminous and dark components, after some algebra, one gets :

$$W = -\frac{G M_\star^{T2}}{R_e^2} \times w(\mathbf{p}) \tag{4.30}$$

with $\mathbf{p}$ denoting the same set of parameters as above but dropping out β. The dimensionless quantity $w(\mathbf{p})$ is given in Appendix A. It is worth noting that, while n and R_e directly enter the integrals defining $w(\mathbf{p})$, $\Upsilon_\star$ and I_e only work as scaling parameters through $M_\star^T$. Moreover, a qualitative analysis shows that, for the stellar component, $w(\mathbf{p})$ reduces to a function of n only.

An important caveat is in order here. Eq.(4.29) refers to the total gravitational energy taking care of the contributions coming from both the stellar component and the dark halo. On the other hand, the kinetic energy computed above only refers to the stellar component as it can be understood noting that the velocity term entering is the one of the stellar particles. As such, when applying the virial theorem, we have to subtract from W the gravitational energy of the dark halo. Although in the following we will still use W (and, in the Appendix, for completeness we compute all the terms involved) to denote the gravitational energy, we stress that we are actually referring to the stellar component only.

4.3.2 Scaling relations from the virial theorem

Inserting Eqs.(4.28) and (4.30) into Eq.(4.19) and solving with respect to σ_0, we get :

$$\sigma_0^2 = \frac{G M_\star^T}{R_e} \frac{w(\mathbf{p})}{k(\mathbf{p})} \ . \tag{4.31}$$

It is then convenient to introduce :

$$\langle I_e \rangle \equiv \frac{L_T/2}{\pi R_e^2} \tag{4.32}$$

so that the total stellar mass is $M_\star^T = \Upsilon_\star L_T = 2\pi \Upsilon_\star \langle I_e \rangle R_e^2$ and the relation above can be recast as :

$$2 \log \sigma_0 = \log \langle I_e \rangle + \log R_e + \log \frac{w(\mathbf{p})}{k(\mathbf{p})} + \log \left(2\pi G \Upsilon_\star\right) \ . \tag{4.33}$$

Let us suppose for a while that it is possible to neglect the dark halo component. Should this be the case, both $k(\mathbf{p})$ and $w(\mathbf{p})$ turn out to be a function of $(n, R_e, \langle I_e \rangle)$, where hereafter we use $\langle I_e \rangle$ rather than I_e as a parameter[3]. Although determining how the ratio $w(\mathbf{p})/k(\mathbf{p})$ depends on $(n, R_e, \langle I_e \rangle)$ needs for a full computation of the integrals involved, we can, as

[3]See, e.g. Graham & Driver (2005), for the relation between I_e and $\langle I_e \rangle$ and other related formulae.

first approximation, suppose that $w(\mathbf{p})/k(\mathbf{p})$ is linear in a logarithmic scale. It is possible, therefore, to write :

$$\log\left[w(\mathbf{p})/k(\mathbf{p})\right] \simeq a\log\langle I_e\rangle + b\log R_e + c\log\left(n/4\right) + d\ . \tag{4.34}$$

From stellar population synthesis models, we know that the stellar M/L ratio may be correlated with the total stellar luminosity L_T. Approximating this relation as a power - law, we can therefore write :

$$\log\Upsilon_\star \simeq \alpha_\star + \beta_\star\log L_T = \alpha_\star + \beta_\star\log\left(2\pi\langle I_e\rangle R_e^2\right)\ . \tag{4.35}$$

Inserting Eqs.(4.34) and (4.35) into Eq.(4.33), one finally gets :

$$\log\sigma_0 = a_T\log\langle I_e\rangle + b_T\log R_e + c_T\log\left(n/4\right) + d_T \tag{4.36}$$

with

$$\left\{\begin{array}{l} a_T = \dfrac{a+\beta_\star+1}{2} \\ \\ b_T = \dfrac{b+2\beta_\star+1}{2} \\ \\ c_T = \dfrac{c}{2} \\ \\ d_T = \dfrac{\alpha_\star}{2} + \dfrac{\beta_\star+1}{2}\log\left(2\pi\right) + \dfrac{1}{2}\log G + d \end{array}\right. . \tag{4.37}$$

As a first remark, let us note that the exact value of d depends on the adopted units. In the following, we will express σ_0 in km/s, $\langle I_e\rangle$ in $\mathrm{L}_\odot/\mathrm{pc}^2$ and R_e in kpc. In particular, having expressed R_e in linear rather than angular units makes d dependent on the distance to the galaxy. A second important caveat is related to our starting hypothesis of having neglected the dark halo component. Actually, we do know that galaxies are embedded in their dark matter haloes. As a consequence, $w(\mathbf{p})/k(\mathbf{p})$ is a function of the halo parameters too. To take into account this dependence, we still assume Eq.(4.34), but let d be an unknown function of (c, M_{vir}) to be determined by the data.

With all these caveats in mind, Eq.(4.36) defines an hyperplane in the logarithmic space allowing to express the kinematic quantity $\log\sigma_0$ as a function of the photometric parameters $\log\langle I_e\rangle$, $\log R_e$, $\log(n/4)$. Since we have recovered it for a Sersic model under the hypothesis of virial equilibrium, we will call it the *Sersic Virial Hyperplane*.

Should our assumptions hold for real elliptical galaxies, the Sersic Virial Hyperplane (hereafter SVH) should represent a tight scaling relations among kinematic and photometric parameters. For an idealized sample of galaxies perfectly satisfying our working hypotheses and all at the same distance, the scatter around this hyperplane should be generated by essentially two terms. First, the halo parameters (c_{NFW}, M_{vir}) may differ on a case - by - case basis. This is the same as saying that the dark matter content in the inner regions or, equivalently, the global M/L ratio (defined as M_{tot}/L_T rather than $M_\star^T/L_T$) is different from one galaxy to another. On the other hand, d_T in Eq.(4.37) may scatter from one galaxy to another because of different values of the parameters (α, β) of the $\Upsilon_\star - L_T$ relation because of different details of the stellar evolution process. Note that this latter effect may also affect the coefficients (a_T, b_T) thus further increasing the scatter on the SVH.

It is worth stressing that the SVH may be seen as a generalization of both the FP and PhP which, from this point of view, reduce to particular cases of the SVH. Indeed, forcing the de Vaucouleurs model to fit the galaxies surface brightness profiles is the same as setting $n = 4$ in Eq.(4.36). Solving with respect to $\log R_e$, we get :

$$\log R_e = a_{FP} \log \sigma_0 + b_{FP} \log \langle I_e \rangle + c_{FP} \tag{4.38}$$

which is indeed the FP with

$$\begin{cases} a_{FP} = 1/b_T \\ b_{FP} = -a_T/b_T \\ c_{FP} = -d_T/b_T \end{cases} . \tag{4.39}$$

Actually, we do not expect that the coefficients of the observed FP are equal to what is predicted by Eq.(4.39) since, assuming $n = 4$ in the fit, can bias the estimate of $(R_e, \langle I_e \rangle)$ in a way that depends on what the true value of n is. Moreover, the departure of n from $n = 4$ introduces a further scatter which is not included in the above expression for c_{FP}. Although these effects have to be carefully quantified, it is nevertheless worth stressing that the FP turns out to be only a projection of the SVH on the plane $\log (n/4) = 0$ so that its coefficients may be (at least, in principle) predicted on the basis of physical considerations.

On the other hand, when solving Eq.(4.36) with respect to $\log R_e$, we can also neglect the dependence on $\log \sigma_0$ assuming this latter is, in a very rough approximation, the same for all galaxies. We thus get :

$$\log R_e = a_{PhP} \log \langle I_e \rangle + b_{PhP} \log (n/4) + c_{PhP} \tag{4.40}$$

with

$$\begin{cases} a_{PhP} = -a_T/b_T \\ b_{PhP} = -c_T/b_T \\ c_{PhP} = (1/b_T) \log \sigma_0 - d_T/b_T \end{cases} . \tag{4.41}$$

which is indeed the PhP. Note that, since $\log \sigma_0$ is obviously not the same for all galaxies, the scatter in the PhP may then be easily interpreted as a scatter in $\log \sigma_0$ and hence in the kinematic structure of the galaxies.

4.3.3 Computing k and w

In previous paragraphs we have used the virial theorem to derive the SVH relation. Here, we give some further details on the computation of the kinetic and gravitational potential energy for the spherically symmetric and isotropic Sersic + NFW model we are considering.

First, let us consider the kinetic energy term which we have finally written as in Eq.(4.28). It is easy to derive the explicit expression for $k(\mathbf{p})$ proceeding as follows. First, we Eq.(4.24) into Eq.(4.20) and then split the integral in two terms, the first one originated by the product $\Sigma(s) \times \mathcal{I}^{\star}_{\sigma}(s)$, and the second one due to $\Sigma(s) \times \mathcal{I}^{DM}_{\sigma}(s)$. By using Eq.(4.25), after some algebra, we finally obtain Eq.(4.28) with :

$$
\begin{aligned}
k(\mathbf{p}) &= \frac{3\gamma(2n, b_n x_{ap}^{1/n})}{\Gamma(2n)} \\
&\times \frac{k_\star + (M_{vir}/M_\star^T)[\mathcal{I}_M(\infty)/f(c_{NFW})]k_{DM}}{\mathcal{I}_0^\star + (M_{vir}/M_\star^T)[\mathcal{I}_M(\infty)/f(c_{NFW})]\mathcal{I}_0^{DM}}
\end{aligned}
\tag{4.42}
$$

with

$$
k_\star(n,\beta) = \int_0^\infty \mathcal{I}_\sigma^\star(x,n,\beta) x dx \ , \tag{4.43}
$$

$$
k_{DM}(n, R_e/r_s, \beta) = \int_0^\infty \mathcal{I}_\sigma^{DM}(x, R_e/r_s, \beta) x dx \ . \tag{4.44}
$$

Let us now reconsider the computation of W which may be carried out in a similar way starting from Eq.(4.29). Splitting the total density and mass as the sum of the luminous and dark components, after some algebra, one arrives at Eq.(4.30) where we have defined :

$$
\begin{aligned}
w(\mathbf{p}) &= w_\star(n) \\
&+ \left(\frac{M_{vir}}{M_\star^T}\right)^2 \left(\frac{R_e}{r_{vir}}\right) w_{DM}(c_{NFW}) \\
&+ \left(\frac{M_{vir}}{M_\star^T}\right) w_\star^{DM}(c_{NFW}, n, R_e/r_s) \\
&+ \left(\frac{M_{vir}}{M_\star^T}\right) w_{DM}^\star(c_{NFW}, n, R_e/r_s) \ .
\end{aligned}
\tag{4.45}
$$

It is then only a matter of algebra to demonstrate that :

$$
w_\star(n) = \frac{1}{\mathcal{I}_M^2(\infty)} \int_0^\infty \mathcal{I}_\nu(s)\mathcal{I}_M(s) s ds \ , \tag{4.46}
$$

$$
w_{DM}(c) = \frac{c^2}{f^2(c)} \int_0^\infty \frac{\ln(1+cy) - cy(1+cy)^{-1}}{(1+cy)^2} dy \ , \tag{4.47}
$$

$$
\begin{aligned}
w_\star^{DM}(c, n, R_e/r_s) &= \frac{1}{\mathcal{I}_M(\infty) f(c)} \\
&\times \int_0^\infty \mathcal{I}_\nu(s) f(s, R_e/r_s) s ds \ ,
\end{aligned}
\tag{4.48}
$$

$$
\begin{aligned}
w_{DM}^\star(c, n, R_e/r_s) &= \frac{1}{\mathcal{I}_M(\infty) f(c)} \left(\frac{R_e}{r_s}\right)^2 \\
&\times \int_0^\infty \left(1 + \frac{R_e}{r_s} s\right) \mathcal{I}_M(s) s ds \ ,
\end{aligned}
\tag{4.49}
$$

where we have dropped the subscript NFW from the concentration parameter to shorten the notation. The analytic expression for w/k may then easily worked out.

We stress that, since we use the stellar velocity dispersion, the kinetic energy computed above is the one of the stellar component only. As a consequence, when resorting to the virial theorem, $2K + W = 0$, we must include in the gravitational energy only the term related to the stellar component, i.e. we must set $w(\mathbf{p}) = w_\star(\mathbf{p}) + w_\star^{DM}(\mathbf{p})$.

4.4 Testing the SVH assumptions

The derivation of the SVH in Eq.(4.36) relies on two main hypothesis which are analytically formalized in Eqs.(4.34) and (4.35). While the relation $\Upsilon_\star \propto L_T^\beta$ may be tested resorting to stellar population synthesis models, checking the validity of Eq.(4.34) needs for a detailed computation of $w(\mathbf{p})/k(\mathbf{p})$ as function of the photometric parameters $(n, \langle I_e \rangle, R_e)$, the anisotropy constant β, the stellar M/L ratio $\Upsilon_\star$ and the halo parameters (c_{NFW}, M_{vir}). In principle, we should therefore compute $w(\mathbf{p})/k(\mathbf{p})$ over a grid in the seven dimensional space defined by the model parameters and then fit Eq.(4.34) to this *dataset* in order to check its validity. However, such an approach could be partially misleading. Indeed, not all the positions in this seven dimensional space are physical, that is to say not all the set $\mathbf{p}$ do describe realistic ETGs. It is, for instance, possible that a given $\mathbf{p}$ corresponds to a galaxy having a dark matter mass fraction within R_e unrealistically low or high. We are obviously not interested in fitting a linear relation to unrealistic models so that we should cut out such unphysical regions of the parameter space before doing the fit. Unfortunately, this is not analytically feasible given the complexity of the parameter space. A more reasonable choice relies on using the distribution of photometric parameters in the observed ETGs as a guidance and a physically motivated recipe to choose the dark halo parameters to sample the physical region of the space $(n, \langle I_e \rangle, R_e, \beta, \Upsilon_\star, c_{NFW}, M_{vir})$. We therefore compute $w(\mathbf{p})/k(\mathbf{p})$ not over the full grid, but only over the region of the parameter space spanned by realistic ETGs. Fitting Eq.(4.34) to these physically viable values makes it possible to both check the validity of such a relation and estimate its coefficients.

4.4.1 The data

As a first step to carry on the approach detailed above, one has to assemble a sample of ETGs as large as possible. To this aim, we have started from the NYU Value-Added Galaxy Catalog (hereafter, VAGC) which is a cross-matched collection of galaxy catalogs maintained for the study of galaxy formation and evolution [45] and mainly based on the SDSS data release 6 [3]. Among the vast amount of available data, we use the *low-redshift* (hereafter, lowZ) catalog of galaxies with estimated comoving distances in the range $10 < D < 150\ h^{-1}\mathrm{Mpc}$. We refer the reader to Blanton et al. (2005) and the VACG website[4] for details on the compilation of the catalog[5].

We shortcut the lowZ catalog only retaining those data we are mainly interested in and rejecting all the galaxies with no measurements of σ_0 leaving us with 43312 out of 49968 objects with magnitudes in the five SDSS filters $u'g'r'i'z'$. In order to select only ETGs, we apply a set of criteria which we briefly details below.

1. A Sersic profile has been fitted to the surface brightness profile of each galaxy using an automated pipeline retrieving the parameters (n, R_e, A) with R_e in $arcsec$ and A the total flux in nanomaggies. As a first criterium, we select only galaxies with $2.5 \leq n \leq 5.5$, where the upper limit is dictated by the code limit $n = 6.0$. This selection is performed using the fit in the i' band since it is less affected by dust without the reduced efficiency of the z' band.

[4] `http://cosmo.nyu.edu/blanton/vagc/`

[5] Note that the version we are using is updated only to the fourth SDSS data release [2] covering an effective survey area of 6670 square degrees.

2. As a second criterium, we impose the cut $R_{90}/R_{50} > 2.6$ [341] with R_{90} and R_{50} the Petrosian radii containing 90% and 50% of the total luminosity as estimated by the data. Note that, although the Petrosian radii do non depend on any fitting, the ratio R_{90}/R_{50} is correlated with n so that the two criteria are somewhat redundant. Removing one of them or changing the order does not alter in a significant way the final sample.

3. We exclude all galaxies with $\sigma_0 < 70\ \mathrm{km/s}$ since the dispersion velocity measurements for these systems may be problematic [40].

4. Elliptical galaxies are segregated in a well defined region of the color - magnitude plane. In order to further restrict our sample, we therefore impose the cut $(g-r)_- \leq g-r \leq (g-r)_+$ with $(g-r)_\pm = pM_r + q \pm \delta$. Here, M_r is the absolute magnitude in the r filter and the parameters (p, q, δ) have been tailored from Fig. 2 in Bernardi et al. (2005) where a different ETG sample has been extracted from the SDSS DR2 [1].

The final sample thus obtained contains 9046 galaxies out of an initial catalog containing 49968 objects. It is worth noting that most of the rejected objects have been excluded by the first three cuts (retaining only 9105 entries), while the fourth cut only removes 59 further galaxies. This is reassuring since the last cut is somewhat qualitative and based on a different set of selection criteria[6] [40].

We then use the data reported in the lowZ catalog for the galaxies in the above sample to collect the quantities listed below.

- *Photometric quantities.* While the Sersic index n and the effective radius R_e in $arcsec$ are directly available in the lowZ catalog, the average effective intensity $\langle I_e \rangle$ is not present. To this aim, we first convert the total flux A (in nanomaggies) reported in the catalog in the apparent total magnitude m_t as [45] :

$$m_t = 22.5 - 2.5 \log A \ .$$

We then use the assumed concordance cosmological model to estimate the total absolute magnitude $\mathcal{M}_t$ as :

$$\begin{aligned} \mathcal{M}_t &= m_t - 5 \log D_L(z) + 5 \log h - 10 \log (1+z) \\ &- K(z) - A_G - 42.38 \end{aligned}$$

where z is the galaxy redshift, D_L the luminosity distance, $K(z)$ the K - correction, A_G the galactic extinction, and the term $10 \log (1+z)$ takes into account the cosmological dimming. While $K(z)$ and A_G are reported in the catalog for each of the five SDSS filters, our use of the luminosity distance makes the estimate of M_t cosmological model dependent. However, for the values of z involved, the dependence on the cosmological model is actually meaningless. We finally estimate :

$$\langle I_e \rangle = 10^{-6} \times \frac{\mathrm{dex}[(\mathcal{M}_t - \mathcal{M}_\odot)/2.5]}{2\pi R_e^2} \tag{4.50}$$

[6] It is worth noting that we cannot use these criteria since the lowZ catalog does not report the parameters which the selection by Bernardi et al. (2005) are based on.

with $\mathrm{dex}(x) \equiv 10^x$, $\mathcal{M}_\odot$ the Sun absolute magnitude in the given filter[7]. We stress that, in Eq.(4.50), R_e is expressed in kpc rather than $arcsec$. To this aim, we simply use :

$$R_e(\mathrm{kpc}) = R_e(arcsec) \times D_A(z)/206265$$

with $D_A(z)$ the angular diameter distance in Mpc.

- *Kinematic quantities.* The lowZ catalog reports the velocity dispersion and its error as determined from the SDSS spectrum of the galaxy. This is measured in a circular aperture of fixed radius $R_{ap} = R_{SDSS} = 1.5\ arcsec$, while σ_0 in Eq.(4.25) has been estimated for $R_{ap} = R_e/8$. To correct for this offset, we follow Jørgensen et al. (1995, 1996) setting :

$$\sigma_0^{obs} = \sigma_0^{lowZ} \times \left(\frac{R_{SDSS}}{R_e/8} \right)^{0.04} \tag{4.51}$$

with σ_0^{lowZ} the value in the catalog and R_e in $arcsec$ here.

- *Auxiliary quantities.* The lowZ catalog contains a wealth of information on each object that we really do not need for our analysis. We do, however, add to our catalog some further quantities that we will use for check. In particular, we include the absolute magnitude $\mathcal{M}_{SDSS}$ as estimated from the image rather than the fit, and the average effective surface brightness computed as [177] :

$$\langle \mu_e \rangle = \langle \mu_e \rangle_{abs} + 10 \log(1+z) + K(z) + A_G$$

with

$$\langle \mu_e \rangle_{abs} = \mathcal{M}_t + 2.5 \log(2\pi R_e^2) + 36.57$$

with R_e in kpc. Note that $\langle \mu_e \rangle$ rather than $\log \langle I_e \rangle$ is often used in the FP and PhP fit.

Although the Sersic law is known to well fit the surface brightness profile of ETGs, it is worth noting that our derivation of $\langle I_e \rangle$ relies on extrapolating the fit results well beyond the visible edge of the galaxy. As such, it is possible that $\mathcal{M}_t$ provides a biased estimate of the actual total absolute magnitude of the galaxy which is better represented by $\mathcal{M}_{SDSS}$. A bias in the estimate of $\mathcal{M}_t$ propagates on the estimates of the colors which may be related to the stellar mass by population synthesis models. In order to reduce as more as possible such a bias, we have studied the histogram of $\Delta col = col_{obs} - col_{est}$, where $col_{obs} = \mathcal{M}_{SDSS,j} - \mathcal{M}_{SDSS,k}$ and $col_{est} = \mathcal{M}_{t,j} - \mathcal{M}_{t,k}$. In principle, all these histograms should be centered at the null value with a small scatter. After removing few outliers, this is indeed the case for $g' - r'$ and $r' - i'$ (with rms values of 0.08 and 0.06 mag respectively), while this is not for $u' - r'$ and $i' - z'$ (having rms values of 0.21 and 0.13 mag). Motivated by this bias, we will use only data in $g'r'i'$ filters when fitting the SVH.

[7] We use $\mathcal{M}_\odot = (5.82, 5.44, 4.52, 4.11, 3.89)$ for the $u'g'r'i'z'$ filters respectively as evaluated from a detailed Sun model reported in `www.ucolick.org/~cnaw/sun.html`

4.4.2 Bayesian parameter estimation

Once a dataset has been assembled, we still have to decide a statistical methodology to check the validity of our linear assumptions for the dependence of $w(\mathbf{p})/k(\mathbf{p})$ on the model parameters. As well known [152, 5, 219], fitting a linear relation in a multiparameter space may seriously depend on the method adopted to get the estimate of the coefficients. Moreover, the choice of the most suitable method also depends on the uncertainties on the model parameters. The Bayesian probabilistic approach offers an ideal way out of these problems. We do not enter in any detail here referring the interested reader to the vast literature available (see, e.g., D' Agostini (2004) and refs. therein).

Let us suppose that a linear relation holds as:

$$y = ax_1 + bx_2 + cx_3 + d \tag{4.52}$$

and let σ_{int} be its intrinsic scatter. If the errors on the variables involved are statistically independent, one can demonstrate that the best fit estimate of the parameters (a, b, c, d) and of the scatter σ_{int} is obtained by minimizing the following merit function [118]:

$$\begin{aligned} -\ln\mathcal{L} &= \frac{1}{2}\sum_{i=1}^{\mathcal{N}} \ln\left(\sigma_{int}^2 + \sigma_{y,i}^2 + a^2\sigma_{1,i}^2 + b^2\sigma_{2,i}^2 + c^2\sigma_{3,i}^2\right) \\ &+ \frac{1}{2}\sum_{i=1}^{\mathcal{N}} \frac{(y_i - ax_{1,i} - bx_{2,i} - cx_{3,i} - d)^2}{\sigma_{int}^2 + \sigma_{y,i}^2 + a^2\sigma_{1,i}^2 + b^2\sigma_{2,i}^2 + c^2\sigma_{3,i}^2} \end{aligned} \tag{4.53}$$

with $\sigma_{y,i}$ and $\sigma_{j,i}$ the errors on y and x_j for the i-th object and the sum is over the $\mathcal{N}$ objects in the sample. It is worth stressing that the minimization with respect to d may be performed analytically, i.e., for given (a, b, c, σ_{int}), the best fit d is given by:

$$d = \frac{\sum_{i=1}^{\mathcal{N}} \frac{y_i - ax_{1,i} - bx_{2,i} - cx_{3,i}}{\sigma_{int}^2 + \sigma_{y,i}^2 + a^2\sigma_{1,i}^2 + b^2\sigma_{2,i}^2 + c^2\sigma_{3,i}^2}}{\sum_{i=1}^{\mathcal{N}} \frac{1}{\sigma_{int}^2 + \sigma_{y,i}^2 + a^2\sigma_{1,i}^2 + b^2\sigma_{2,i}^2 + c^2\sigma_{3,i}^2}} \ . \tag{4.54}$$

With this value of d, one can compute $-\ln\mathcal{L}$ and then find the set of parameters (a, b, c, σ_{int}) that minimizes it, therefore representing the best fit solution. It is worth stressing, however, that Eqs.(4.53) and (4.54) strictly hold if the errors on the variables involved are uncorrelated, i.e. their covariance matrix is diagonal. Actually, this is not the case for our problem because of the correlation between n and R_e introduced by the photometric fitting algorithm. Fortunately, Eqs.(4.53) and (4.54) may be easily adapted to this more general situation by changing the denominator to include a covariance term between the errors on n and R_e.

The final expression depends on which fit one is considering.In our case, $(n, R_e, \langle I_e\rangle)$ are obtained as a result of a fitting procedure which does introduce a correlation among the errors on n and R_e so that Eq.(4.53) does not strictly hold. Nevertheless, the generalization is quite immediate. Indeed, since the errors are uncorrelated from one galaxy to another, it is easy to show that Eq.(4.53) may be simply rewritten as:

$$\begin{aligned} -\ln\mathcal{L} &= \frac{1}{2}\sum_{i=1}^{\mathcal{N}} \ln\left(\sigma_{int}^2 + \sigma_{obs,i}^2 + \sigma_{th,i}^2\right) \\ &+ \frac{1}{2}\sum_{i=1}^{\mathcal{N}} \frac{(y_i - ax_{1,i} - bx_{2,i} - cx_{3,i} - d)^2}{\sigma_{int}^2 + \sigma_{obs,i}^2 + \sigma_{th,i}^2} \end{aligned} \tag{4.55}$$

where σ_{int} is the intrinsic scatter, while $\sigma_{obs,i}$ and $\sigma_{th,i}$ are the errors on y and $y_{th} = ax_1 + bx_2 + cx_3 + d$ respectively for the i - th galaxy. As a useful application, let us consider the SVH. In this case, we have :

$$y = \log \sigma_0 \quad , \quad x_1 = \log \langle I_e \rangle \quad ,$$

$$x_2 = \log R_e \quad , \quad x_3 = \log (n/4) \quad .$$

Dropping for sake of notation the subscript i, the error on y simply reads :

$$\sigma_o bs = \frac{\varepsilon(\sigma_0)}{(\ln 10)\sigma_0}$$

with $\varepsilon(x)$ the measurement error on x. In order to compute σ_{th}, we have first to remember that $\langle I_e \rangle$ is not directly measured, but rather computed using Eq.(4.50) so that its uncertainty must be computed by propagating those on the total absolute magnitude $\mathcal{M}_t$ and the effective radius R_e. Taking also into account the correlation between n and R_e introduced by the fitting procedure, we finally get :

$$\begin{aligned} \sigma^2_{th} &= a^2 \left[\frac{4\varepsilon^2(R_e)}{(\ln 10)^2 R_e^2} + \frac{\varepsilon^2(\mathcal{M}_t)}{(2.5)^2} \right] + \frac{b^2 \varepsilon^2(R_e)}{(\ln 10)^2 \ R_e^2} \\ &+ \frac{c^2 \varepsilon^2(n)}{(\ln 10)^2 \ n^2} + \frac{2bc \ \mathrm{cov}(R_e, n)}{(\ln 10)^2 R_e \ n} \end{aligned}$$

with $\mathrm{cov}(R_e, n)$ the covariance between the parameters R_e and n introduced by the code fitting the observed surface brightness profile. Note that there is no covariance between the total absolute magnitude $\mathcal{M}_t$ and the photometric parameters (n, R_e) since $\mathcal{M}_t$ is directly measured from the image and not the output of the fitting code.

Eq.(4.55) may easily be adapted to all the fit we have considered in the work provided the quantities (y, x_1, x_2, x_3) are correctly identified so that the computation of the errors $(\sigma_{obs}, \sigma_{th})$ may be performed along the lines described above taking correctly into account the covariance between n and R_e when needed.

The general formulae (4.52) – (4.54) may be easily adapted to our problem. Eqs.(4.34) and (4.52) may be identified setting :

$$y = \log (w/k) \ , \ x_1 = \log \langle I_e \rangle \ , x_2 = \log R_e \ , x_3 = \log (n/4)$$

so that we can estimate the coefficients (a, b, c, d) by maximizing the likelihood function. To this aim, we use a Markov Chain Monte Carlo (hereafter MCMC) approach in order to efficiently explore the parameter space (a, b, c, σ_{int}) and estimate both the best fit values and their errors (computed at the 68% and 95% confidence levels). In order to avoid any possible bias in the determination of (a, b, c, σ_{int}), we test for the convergence of the chains using the test proposed in Dunkley et al. (2005) and conservatively cutting out the initial values to skip the burn - in period.

The Bayesian approach here described makes it possible not only to estimate the model parameters, but also to meaningfully compare different models. To this aim, a quick tool is represented by the so called *Akaike Information Criterium* (AIC) defined as [4] :

$$AIC = -2 \ln \mathcal{L}_{max} + 2\mathcal{N}_p \tag{4.56}$$

with $\mathcal{L}_{max}$ the value of the likelihood at maximum and $\mathcal{N}_p$ the number of model parameters. The lower is the AIC value, the better is the model in reproducing the data with the minimal number of parameters. Indeed, typically, models with too few parameters provide a poor fit (i.e., a small value of $\mathcal{L}_{max}$), while the second term penalizes an unnecessary increase of $\mathcal{N}_p$. An alternative tool is provided by the *Bayesian Information Criterium* (BIC) given as [335] :

$$BIC = -2\ln\mathcal{L}_{max} + \mathcal{N}_p \ln\mathcal{N} \tag{4.57}$$

which more strongly penalizes models with large $\mathcal{N}_p$. It is worth noting that, although being implemented for the same task (discriminating among models with different number of parameters), the AIC and BIC have a diverse statistical foundation, which we do not discuss here referring the interested reader to the literature (see, e.g., [230] and refs. therein). It is customary to quantify how much a model is preferred over the other using the Jeffreys scale according to which a value of ΔAIC or ΔBIC of 2 is considered as positive evidence and a difference of 6 as a strong evidence against the model with the larger value [196]. We, however, caution the reader to not trust too much the large values of ΔAIC and ΔBIC we will get later. To understand this point, let us consider an idealized model fitting perfectly the data, i.e. making the numerator in Eq.(4.53) equal to zero for each galaxy. Let us further assume that the denominator in Eq.(4.53) is the same for all galaxies and call σ_c this quantity. In this case, for the best fit model, we would get :

$$-2\ln\mathcal{L}_{max} \simeq 2\mathcal{N}\times\ln\sigma_c \ .$$

A second model also fitting perfectly the data, but more parameters will have approximately the same value of $\mathcal{L}_{max}$ so that we get :

$$\Delta AIC = 2\Delta\mathcal{N}_p \ \ , \ \ \Delta BIC = \Delta\mathcal{N}_p\times\ln\mathcal{N} \ .$$

Since $\ln\mathcal{N} \geq 7$, it is sufficient to have $\Delta\mathcal{N}_p = 1$ to have a difference in BIC values larger than the maximum value of the Jeffreys scale. Still retaining the idealized equality of the errors, we can consider two models with a modest difference in the value of the following pseudo - χ^2 :

$$\chi^2 = \sum_{i=1}^{\mathcal{N}} \frac{(y_i - ax_{1,i} - bx_{2,i} - cx_{3,i} - d)^2}{\sigma_c^2} \ .$$

The values of ΔAIC and ΔBIC will then read :

$$\Delta AIC = \Delta\chi^2 + 2\Delta\mathcal{N}_p \ \ , \Delta AIC = \Delta\chi^2 + \Delta\mathcal{N}_p\times\ln\mathcal{N} \ .$$

Even if $\Delta\mathcal{N}_p = 1$, the ΔBIC values will be quite high also in the idealized case $\Delta\chi^2 = 0$, while it is sufficient to have $\Delta\chi^2 \simeq 1$ to get $\Delta AIC > 2$, i.e. a positive evidence against the model with the larger AIC value. Motivated by these considerations, we hereafter will compare the models based on the AIC and BIC values still considering the one with the lowest AIC and BIC as preferred, but we prefer to not rely on the Jeffreys scale to assess any qualitative ranking.

4.4.3 Setting the model parameters

Even if we have assembled an ETG catalog and chosen the statistical method to deal with it, we are still not able to test our assumption (4.34) since, in order to compute w/k, there are

four further quantities we have to know, namely the anisotropy constant β, the stellar M/L ratio $\Upsilon_\star$ and the NFW halo parameters (c_{NFW}, M_{vir}). To this aim, we can resort to two different constraints. First, assuming the system is virialized, the central velocity dispersion may be estimated both from Eq.(25) and from the virial theorem through Eq.(4.31) so that we can impose the constraint :

$$\begin{aligned} \frac{w(\mathbf{p})}{k(\mathbf{p})} &= \frac{4b_n^{2+4n}}{\pi^2 n^4 \mathrm{e}^{2b_n}\Gamma(2n)} \\ &\times \frac{\mathcal{I}_0^\star + (M_{vir}/M_\star^T)[\mathcal{I}_M(\infty)/f(c_{NFW})]\mathcal{I}_0^{DM}}{\gamma[2n,(1/8)^{1/n}]} \ . \end{aligned} \tag{4.58}$$

Moreover, in order to be reliable, the model must be able to predict a value for σ_0 which is in agreement (within the errors) with the observed one. Needless to say, with only two constraints, it is not possible to set the two stellar quantities $(\beta, \Upsilon_\star)$ and the NFW parameters (c_{NFW}, M_{vir}) so that we have to further narrow the four dimensional parameter space to explore. To this end, we use Eq.(4.18) to link c_{NFW} to M_{vir}. Then, we determine a guess for the stellar M/L ratio proceeding as follows. As a first step, for each observed galaxy, we estimate [166] :

$$\Upsilon_\star^V = 4.0 + 0.38\,[t(z) - 10] \tag{4.59}$$

with $t(z)$ the age (in Gyr) of the galaxy at redshift z computed assuming a formation redshift $z_F = 2$. We then convert to the r' band M/L as :

$$\log \Upsilon_{\star,guess} = \log \Upsilon_\star^V + 0.4\left[(V-r') - (V-r')_\odot\right]$$

with $V - r' = 0.36$ [165]. We further scale down this value by a factor 1.8 to change from the Salpeter IMF used by Fukugita et al. (1998) to the Chabrier IMF. Note that, by using the same value for $V - r'$ for all galaxies, we are neglecting the scatter of this quantity in our ETG sample. Moreover, although reasonable, there is no definitive evidence that all the ETGs in our sample have the same age, i.e. the same value of z_F. Finally, Eq.(4.59) is based on population synthesis models which provide estimates of $\Upsilon_\star^V$ affected by an uncertainty (dependent on the different combinations of model ingredients) that can be as high as a factor 2. In order to qualitatively take into account all these possible systematics, we therefore set :

$$\Upsilon_\star = (\eta/1.8)\times\Upsilon_{\star,guess}$$

with η a new parameter (likely in the range $0.5 - 1.5$) to be determined. To set the three parameters (β, η, M_{vir}), we then use an approximate methodology schematically sketched below.

i. We generate a grid in the space $\eta - \log M_{vir}$ with $0.5 \leq \eta \leq 1.5$ and $10.5 \leq \log M_{vir} \leq 13.5$ and, for each point of this grid, solve Eq.(4.58) with respect to β.

ii. For each triple $(\eta, \log M_{vir}, \beta)$ determined above, we compute the two following quantities :

$$\frac{\Delta\sigma_0}{\varepsilon_{\sigma_0}} = \frac{\sigma_0^{obs} - \sigma_0^{th}(\eta, \log M_{vir}, \beta)}{\varepsilon_{\sigma_0}} \ , \tag{4.60}$$

Table 4.1: Best fit coefficients, intrinsic scatter, AIC and BIC values for all the models discussed in the text for the *In* sample. We use the general fitting formula $\log(w/k) = a\log\langle I_e\rangle + b\log R_e + c\log(n/4) + d\log\Upsilon_\star + e\log M_{vir} + f\log c_{NFW} + g$. A - sign means that parameter being set to 0 in the fit. For each model, we do not report the best fit zero point g since it depends on the assumed filter and mean galaxy distance and has no interest for our discussion.

a	b	c	d	e	f	σ_{int}	AIC	BIC
0.074	0.144	1.421	-	-	-	0.062	4374.48	4394.11
0.029	0.107	1.422	−0.020	-	-	0.058	4533.92	4558.46
0.020	0.112	1.487	−0.075	-	-	0.055	4595.62	4620.16
0.129	0.176	1.877	-	−0.091	-	0.034	5296.96	5321.50
0.087	0.131	1.855	-	−0.081	0.034	0.029	5616.50	5645.95

$$f_e = \left\{1 + \frac{M_\star^T}{M_{vir}}\frac{f(c_{NFW})}{f(R_e/r_s)}\frac{\mathcal{I}_M(s=1)}{\mathcal{I}_M(\infty)}\right\}^{-1}, \tag{4.61}$$

with ε_{σ_0} the measurement error on the observed velocity dispersion, σ_0^{th} given by Eq.(25) or (4.31) and f_e the dark matter mass fraction within the effective radius R_e.

iii. We choose the triple $(\eta, \log M_{vir}, \beta)$ giving the lowest value of $|\Delta\sigma_0/\varepsilon_{\sigma_0}|$ as our best estimate of the model parameters finally retaining only those galaxies with both $|\Delta\sigma_0/\varepsilon_{\sigma_0}| \leq 5$ and $0 \leq f_e \leq 1$.

It is worth stressing that this procedure, although not ideal, is able to provide realistic values of the model parameters. Note that the cuts on $|\Delta\sigma_0/\varepsilon_{\sigma_0}|$ and f_e have been left quite loose to take into account possible systematic errors due to departure from spherical symmetry or virialization. Indeed, the above procedure does not work for all the galaxies in our starting catalog so that we end up with a subsample containing $\simeq 75\%$ of the initial sample. As an encouraging result, we find that the median and rms values of $\Delta\sigma_0/\varepsilon_{\sigma_0}$ are respectively $\simeq -0.25$ and $\simeq 2.0$ indicating that the modelling is quite satisfactory for most of the systems. Moreover, for the selected subsample, we get $f_e \simeq 0.44\pm0.14$ corresponding roughly to $f_e \simeq 0.31$ for a Salpeter IMF in good agreement with previous results in literature. We are therefore confident that, although only approximated, our procedure gives reliable values for the model parameters $(\eta, \log M_{vir}, \beta)$.

4.4.4 Results

Having setted all the model parameters, we are now able to compute $w(\mathbf{p})$, $k(\mathbf{p})$ and $\log(w/k)$ for all the galaxies in our ETG sample surviving our selection cuts on $\Delta\sigma_0/\varepsilon_{\sigma_0}$ and f_e. Note that such a constraints make us confident that the systems we are considering are described reasonably well by our Sersic + NFW model. Should this not be the case, the computed values of $\log(w/k)$ would sample a non physical region of the parameter space thus potentially biasing the fitting in a incorrect way.

With all this staff, we are now able to test the validity of Eq.(4.34) running our MCMC algorithm to determine the fit coefficients (a, b, c, d). As a preliminary step, it is, however,

Table 4.2: Same as Table 1 for the *hn* sample.

a	b	c	d	e	f	σ_{int}	AIC	BIC
-0.003	0.099	0.655	-	-	-	0.122	3216.40	3236.03
-0.021	0.100	0.521	0.237	-	-	0.098	3642.94	3667.47
-0.022	0.083	0.577	0.054	-	-	0.106	3503.94	3528.48
0.094	0.182	0.630	-	-0.082	-	0.092	3762.04	3787.98
0.021	0.108	1.298	-	0.017	0.439	0.189	3542.08	3571.53

worth splitting the sample in two datasets according to the value of n. Indeed, most of the properties of the Sersic model change their correlation with n depending on n being smaller or larger than the canonical $n = 4$ value (see, e.g., Graham & Driver 2005). As such, fitting a single relation to galaxies with $n \leq 4$ and $n \geq 4$ is still possible, but the coefficient of the $\log(n/4)$ term could turn out to be a kind of average of the two eventually different slopes thus possibly biasing the later comparison betwenn the observed and the predicted SVH. In order to investigate this issue, we therefore divide the sample in two subsamples hereafter referred to as the *low n* (*ln*) and *high n* (*hn*) samples depending on n being smaller or larger than $n = 4$. Note that, since n depends on the wavelength, the same galaxy will be included in the *ln* or *hn* sample depending on the filter. However, in all cases, $\sim 80\%$ of the galaxies belong to the *ln* sample as expected since we include galaxies with $n = 4$ in the *ln* subset.

As a preliminary step to run the MCMC algorithm, we have to choose the range for each of the fit coefficients. To this aim, we perform a *direct fit* to our dataset, i.e. we minimize a χ^2 merit function defined artifically setting to 1 the denominator in Eq.(4.53). We then run the MCMC code with each parameter p_i in the range $(0.3, 3)\times p_{i,df}$ with $p_{i,df}$ the result from the direct fit and check the chain convergence using the Dunkley test [138]. The best fit parameters for the different fits we consider in the following are reported in Table 1 (2) for the *ln* (*hn*) sample[8] taking the r filter as the fiducial one[9].

Let us first discuss the results for the *ln* sample. As a mandatory test, we start checking the validity of Eq.(4.34). Fitting this relation to the data, we get :

$$(a, b, c, \sigma_{int}) = (0.074, 0.144, 1.421, 0.062) \tag{4.62}$$

for the best fit parameters, while the median values and 68% confidence ranges after marginalization read :

$$a = 0.071^{+0.009}_{-0.011} \quad , \quad b = 0.140^{+0.012}_{-0.013} \quad ,$$

$$c = 1.428^{+0.034}_{-0.033} \quad , \quad \sigma_{int} = 0.062^{+0.002}_{-0.001} \quad .$$

Note that, hereafter, we will not report the constraint on the zeropoint d since its value depends on the adopted filter, the median distance of the galaxies and the physical units so

[8] Note that, to save computer time, we run the chains using 1000 random galaxies for each subset having checked that the results are unaffected by increasing the sample up to 5000 objects.

[9] The choice of the r filter as fiducial one is motivated by the observation that it is the nearest to the V band used in Eq.(4.59). It is worth stressing, however, that the conclusions presented in this section do not depend at all on this choice.

that it has no interest for our discussion. The small intrinsic scatter and the good fit to the data are strong evidences confirming the validity of our assumption (4.34) thus motivating the SVH approach. It is nevertheless worth investigating which is the effect of taking into account the dependence on w/k on the other model quantities. As a first step, we add a logarithmic term to include the stellar M/L ratio obtaining the results in the second row of Table 1. The inclusion of this further term does not appreciably change the coefficients of the terms $logR_e$ and $\log(n/4)$ having a larger effect on that of the $log\langle I_e\rangle$. What is more important, however, the intrinsic scatter is only modestly reduced thanks to the $\log\Upsilon_\star$ term whose coefficients is quite low. Indeed, both the AIC and BIC values are quite larger than for our reference model thus arguing strongly against the inclusion of $\Upsilon_\star$ as a further parameter.

Up to now, we have only considered parameters related to the visible component, but we know that the dark halo also plays a role. As a first attempt, we therefore try improving the fit by replacing the stellar M/L ratio with the dynamical one defined as [205, 287] :

$$\Upsilon_{dyn} = \frac{M_{dyn}}{L(R_e)} = \frac{(1.65)^2 R_e \sigma_0^2}{G L_T/2} \ ,$$

which thus estimate the global M/L ration within the effective radius also taking into account the dark matter content. As it is evident from the third row in Table 1, although the coefficient of the $\log\Upsilon_{dyn}$ is higher than in the $\Upsilon_\star$ case, the intrinsic scatter is essentially the same so that the same qualitative discussion holds. We can therefore again conclude that the inclusion of this term is disfavoured.

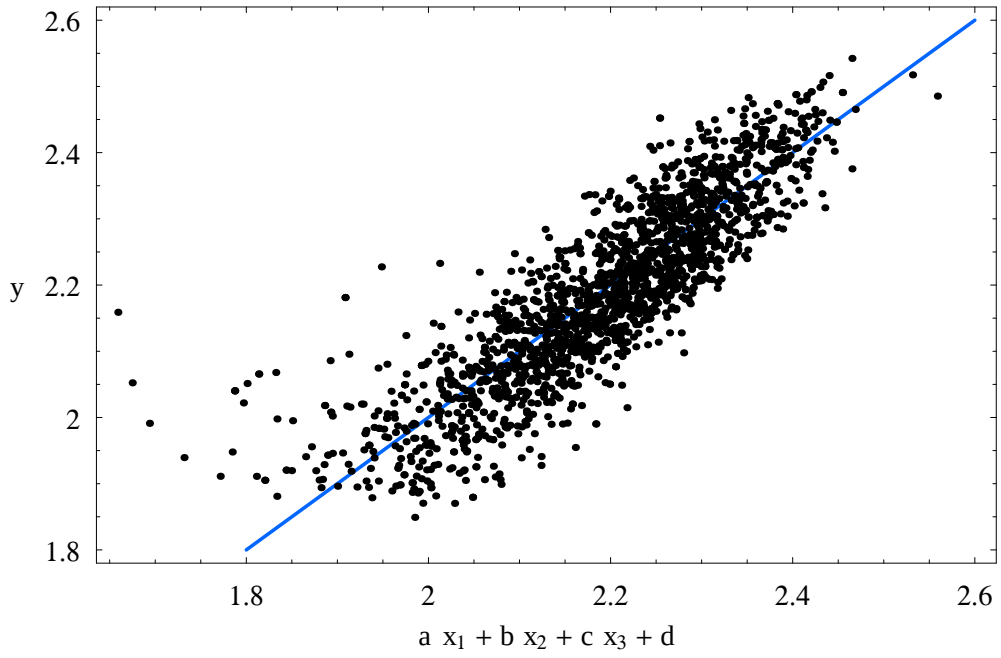

Figure 4.1: The observed SVH for the full ETG sample in the r' filter. On the y - axis, we report $y = \log\sigma_0$, while on the x - axis, the best fit $ax_1 + bx_2 + cx_3 + d$ with $x_1 = \log\langle I_e\rangle$, $x_2 = \log R_e$, $x_3 = \log(n/4)$ and (a, b, c, d) set to their best fit values in Table 3. Note that, to improve the figure readibility, we plot only 2000 randomly selected galaxies.

As a next step, we try dropping out terms related to the (stellar or dynamical) M/L ratio, but explicitly including the dark halo virial mass as a parameter obtaining the results summarized in the fourth row of Table 1. Inserting such a term in the fitting relation have a considerable effect on the coefficients of the $\log\langle I_e\rangle$ and $\log R_e$ also increasing the one of $\log(n/4)$. Moreover, the intrinsic scatter is almost halved thus naively suggesting that such a relation should be preferred. Actually, a reduction in the intrinsic scatter is expected since the dark halo enters the ratio w/k through its effect on the kinetic energy. Although its contribution is typically smaller than the stellar one, it is clear that neglecting it for all galaxies unavoidably increase the scatter since its percentage contribution differs from one galaxy to another. Nevertheless, the values of ΔAIC and ΔBIC are so large that, also not relying on the Jeffreys scale, this relation is statistically disfavoured.

Finally, we try adding also a term related to the dark halo concentration c_{NFW} although this is somewhat redundant given that c_{NFW} is a function of M_{vir} in our modelling procedure. Not surprisingly, the scatter is only modestly reduced and similar considerations as above may be done thus leading again to the exclusion of this model on the basis of the quite high ΔAIC and ΔBIC values.

The same analysis presented for the *ln* sample has been repeated for the *hn* sample too obtaining the results summarized in Table 2. We do not discuss them in detail here since most of the comments above may be referred to this case too. There is, however, an important difference. First, the coefficient of the $\log(n/4)$ term is smaller than the corresponding one for the *ln* case, with typically $c(n \leq 4) \geq 2c(n > 4)$. This may be considered as *a posteriori* validation of our choice of dividing the galaxies in two subsets. Should we have fitted all the galaxies with the same relation, the c coefficient should likely come out as an average of the two values weighted by the different numbers of galaxies with $n \leq 4$ and $n > 4$. As such, the predicted SVH c_T should be overestimated for the $n > 4$ galaxies thus possibly biasing the later comparison between the predicted and observed SVH.

The extensive testing described make us confidently conclude that our assumption (4.34) is indeed well founded thus furnishing a strong theoretical foundation for the SVH.

4.5 The observed SVH

The above analysis has convincingly shown the validity of Eq.(4.34) thus giving a first strong argument in favour of the SVH given by Eq.(4.36). Motivated by this theoretical successful result, we now look for the observed SVH in order to definitively validate our derivation. A preliminary caveat is in order here. As we have seen, the best fit parameters of Eq.(4.34) are different depending on n being smaller or larger than the canonical $n = 4$ value. It is worth stressing, however, that using the parameters obtained for the *ln* sample to fit the *hn* sample does not increase significantly the rms scatter so that we argue that joining the two samples does not introduce any significant bias. There are also some observational motivations to not divide the sample in two subsets. First, the parameter n is affected by its own statistical uncertainty so that it could be difficult to decide whether a galaxy with $n \simeq 4$ should be added to the *ln* or *hn* sample. Moreover, in applications to cluster samples, the number of galaxies with reliable measurement of n is typically quite small (expecially at higher redshift) so that such a splitting gives rise to a too small number to perform any statistical analysis. Motivated by these considerations, we therefore fit the theoretical SVH in Eq.(4.36) to the full catalog paying the price of likely increasing the intrinsic scatter to the advantage of working with a larger dataset.

Table 4.3: Results of the MCMC code for the SVH relation (4.36) using the full sample. (1) Filter id. (2) Values of $(a, b, c, d, \sigma_{int})$ for the best fit relation. (3) - (6) Median value and 68% confidence range for each fit parameter (a, b, c, σ_{int}) obtained after marginalizing over the remaining ones. (7) Root mean square of the best fit residuals.

(1)	(2)	(3)	(4)	(5)	(6)	(7)
Id	$(a, b, c, d, \sigma_{int})_{bf}$	a	b	c	σ_{int}	σ_{rms}
g'	$(0.542, 0.618, 0.223, 0.674, 0.042)$	$0.545^{+0.008}_{-0.007}$	$0.621^{+0.009}_{-0.008}$	$0.226^{+0.013}_{-0.014}$	$0.042^{+0.001}_{-0.001}$	0.065
r'	$(0.518, 0.617, 0.211, 0.734, 0.048)$	$0.520^{+0.008}_{-0.008}$	$0.617^{+0.011}_{-0.008}$	$0.211^{+0.011}_{-0.018}$	$0.048^{+0.001}_{-0.001}$	0.069
i'	$(0.536, 0.610, 0.247, 0.694, 0.047)$	$0.536^{+0.006}_{-0.010}$	$0.611^{+0.007}_{-0.009}$	$0.242^{+0.015}_{-0.021}$	$0.047^{+0.002}_{-0.001}$	0.068

4.5.1 The SVH coefficients

In order to determine the best fit parameters, we run our MCMC code fitting Eq.(4.36) to the full dataset in the r' filter thus getting the best fit curve superimposed to the data in Fig. 4.1. Table 3 reports the best fit and median values and the 68% confidence range for each fit parameter also giving the root mean square of the best fit residuals as a further check on the quality of the fit. It is worth stressing that the best fit relation is obtained for values of (a, b, c, σ_{int}) that do not necessarily coincide with the median values of each single parameter. This is a typical consequence of the degeneracies occuring when fitting a multiparameter relation. Since the full likelihood is not the product of the marginalized likelihoods, it is indeed possible that the best fit relation does not coincide with the one obtained using the median values. Actually, we find only a slight discrepancy among the two set of values and, moreover, the 68% confidence ranges turn out to be quite symmetric around the median value. We therefore argue that the marginalized likelihood functions can be well described by Gaussian and employ in the following this approximation when propagating the errors.

Considering the best fit parameters, we get :

$$\begin{aligned} \log \sigma_0 &= 0.518 \log \langle I_e \rangle + 0.617 \log R_e \\ &+ 0.211 \log (n/4) + 0.704 \end{aligned}$$

with an intrinsic scatter $\sigma_{int} = 0.048$ in the r' filter. As Fig. 4.1 shows, there is a very good one - to - one correspondence between the left and right hand side of Eq.(4.63) as it is also confirmed by the low value of the root mean square of the best fit residuals, being $\sigma_{rms} = 0.069$. Such a remarkable good fit may be considered as the first observational[10] validation of the proposed SVH.

Actually, such a successful test only shows that a SVH - like relation indeed exists. However,

[10]It is worth noting that a first attempt to fit a hyperplane to a small sample of Coma and Fornax galaxies (collected from the literature available at that time) has yet been successfully performed in Graham (2005). However, in that work, the fit was only empirically motivated and the rest of the work gives off the dependence on σ_0 concentrating on the PhP. We can therefore consider the present work as the first theoretically motivated study of the SVH based on a large and homogenous ETG sample.

to fully validate our theoretical derivation, we have to check that the (a, b, c) values[11] derived from the fit are in agreement with the expectations in Eq.(4.37). Let us first start comparing the values of (a_{obs}, b_{obs}) with the predicted ones (a_T, b_T). To this end, one should assume a value for the slope $\beta_\star$ of the $\Upsilon_\star$ - L_T relation. Although this can in principle be estimated from population synthesis models, a simpler and less demanding test may be performed evaluating it from the comparison itself. Solving Eq.(4.37) with respect to $\beta_\star$, we may get two different values for this quantity depending on whether we use the couple (a_{obs}, a) or (b_{obs}, b). In principle, these two estimates should agree if our assumptions are motivated. Employing Gaussian statistics for the reasons explained above, we thus solve for $\beta_\star$ using the median values of (a, b) and (a_{obs}, b_{obs}) quoted above to get central values and use a naive propagation of the errors to get an estimate of the uncertainty. This simple approach gives us the following results :

$$\beta(a, a_{obs}) = -0.03 \pm 0.02 \quad , \quad \beta(b, b_{obs}) = 0.05 \pm 0.01 \quad ,$$

which do not agree at all notwitstanding the quite large errors. It is worth stressing that the values in Eq.(4.37) have been obtained under the simplifying hypothesis of spherical symmetry. As well known [43], for a given total mass, the velocity dispersion may considerably differ between spherically and flattened systems. Quantifying this effect is not possible unless one takes carefully into account the distribution in the intrinsic flattening q which is largely unknown. We can, however, roughly quantify the impact of this systematic error by first writing the *true* velocity dispersion as :

$$\sigma^2_{0,true} = \sigma^2_0 + \sigma^2_{0,sys} = \sigma^2_0 \times \left[1 + \left(\frac{\sigma_{0,sys}}{\sigma_0}\right)^2\right]$$

with $\sigma_{0,sys}$ the term we are neglecting because of the above systematics. Using the SVH for σ^2_0, we get :

$$\begin{aligned} \log \sigma_{0,true} &= a_T \log \langle I_e \rangle + b_T \log R_e + c_T \log (n/4) + d_T \\ &+ \frac{1}{2} \log \left[1 + \left(\frac{\sigma_{0,sys}}{\sigma_0}\right)^2\right] . \end{aligned} \tag{4.63}$$

The fit to the real data is consistent with the existence of the SVH so that we can argue that the last term on the r.h.s. is linear in logarithmic units. In particular, by writing

$$\log \left[1 + \left(\frac{\sigma_{0,sys}}{\sigma_0}\right)^2\right] \propto \delta \log \langle I_e \rangle \tag{4.64}$$

the SVH is recovered provided that we replace a_T with $a_T + \delta/2$. From the values of (a_{obs}, b_{obs}, a, b) and using a similar procedure as above, we finally estimate :

$$\beta = 0.05 \pm 0.01 \quad , \quad \delta = -0.08 \pm 0.02.$$

[11] Hereafter, we will only consider the values of (a, b, c) parameters since d also depends on the galaxy distance. As such, its value is a kind of average distance of the galaxies in the sample and can not be compared to the theoretical prediction. Finally, we remind the reader that the values of (a, b, c, σ_{int}) obtained for the *In* sample will be used as reference one in the comparison between observed and predicted SVH coefficients.

Although such an approach is only qualitative, a more conservative choice for the value of β is indeed given by the one obtained by this procedure. Such a small value of β indicates a quite weak correlation between $\Upsilon_\star$ and L_T. This is qualitatively consistent with the finding of Padmanabhan et al. (2004). Estimating the stellar M/L from the correlation with the D_{4000} strength [205], these authors find $\Upsilon_\star$ to be almost constant with L_T which compares well with our estimated β. Moreover, these same authors also find $\Upsilon_{dyn} \propto L_T^{0.17}$. Writing $\Upsilon_{dyn} \propto (M_{dyn}/M_\star^T)\Upsilon_\star$ and considering that we find $M_{dyn}/M_\star^T \propto L_T^{0.09}$ for our data, we therefore predicts $\Upsilon_{dyn} \propto L_T^\gamma$ with $\gamma = 0.14 \pm 0.01$ in qualitatively satisfactory agreement with the Padmanabhan et al. value. Notwithstanding the encouraging result for β, it is worth stressing that Eq.(4.64) is actually an unmotivated assumption. Nevertheless, we can qualitatively assess whether such a hypothesis is reasonable by a qualitative analogy with spiral galaxies. Some recent works [316, 282] indeed claims that the shape of the rotation curve is determined not only by the total luminosity, but also weakly depends on the mean surface density. Considering σ_0 as the analog of v_c for ETGs, we may qualitatively assume that the power - law relation $\Upsilon_\star - L_T$ describes the dependence of $\sigma_{0,true}$ on L_T, while Eq.(4.64) takes into account a possible effect related to $\langle I_e \rangle$. Although this interpretation is, strictly speaking, unmotivated, the small δ value and the positive match with the Padmanabhan et al. finding make us confident that Eq.(4.64) is not unrealistic.

Actually, there is a further problem when comparing the observed and theoretically expected value of the $\log(n/4)$ term. Indeed, we find $c_{obs} = 0.211 \neq c_T/2 = 0.714$. In principle, we can recover such a tilt by adding a term proportional to $\log(n/4)$ to Eq.(4.64). However, a different route is possible by reconsidering our derivation of the theoretical SVH. Indeed, we have computed the kinetic energy by assuming that the rotational contribution is negligible. Including it, we should replace the $\log(w/k)$ term with a more general $\log[w/(k+k_v)]$ having denoted with k_v the rotational contribute. Noting that

$$\frac{w}{k+k_v} = \left(\frac{k+k_v}{w}\right)^{-1} = \frac{w}{k}\left(1+\frac{k_v}{k}\right)^{-1} ,$$

and assuming as a first reasonable approximation that :

$$\log\left(1+\frac{k_v}{k}\right)^{-1} = a_v \log\langle I_e\rangle + b_v \log R_e + c_v \log(n/4) + d_v \ , \tag{4.65}$$

we still get the SVH with coefficients given as :

$$\begin{cases} a_T = (a + a_v + \beta_\star + \delta + 1)/2 \\ b_T = (b + b_v + 2\beta_\star + 1)/2 \\ c_T = (c + c_v)/2 \end{cases} , \tag{4.66}$$

where we have also separately included the term (4.64). The tilt of the observed SVH with respect to the theoretical one predicted by Eqs.(4.36) and (4.37) may thus be explained assuming that $(\beta_\star, \delta) \simeq (0.05, -0.08)$ and $(a_v, b_v, c_v) \simeq (0, 0, -1)$. Actually, one can also neglect the term (4.64) collectively including its effect in the a_v coefficient thus still obtaining for $\beta_\star$ a value leading to a satisfactory agreement with the Padmanabhan et al. results.

As a final remark, let us make some considerations on the observed scatter. Being $\sigma_{int}/\sigma_{rms} \simeq 0.7$, we see that the intrinsic scatter accounts for most of the observed one. While it is possible that the remaining 30% is simply due to measurement uncertainties, there are also some theoretical hints suggesting why σ_{rms} is larger than σ_{int}. First, on one hand,

σ_{int} only accounts for the scatter in Eq.(4.34), while other possible source of scatter (such as that induced by the conversion from $\Upsilon_\star^V$ to $\Upsilon_\star$ and the one coming from the c_{NFW} - M_{vir} relation) are not considered. Moreover, it is likely that σ_{int} is actually underestimated since we do have forced the galaxies with $n > 4$ to follow the same SVH as the ones with $n \leq 4$ notwithstanding the small difference between their $\log(w/k)$ relations.

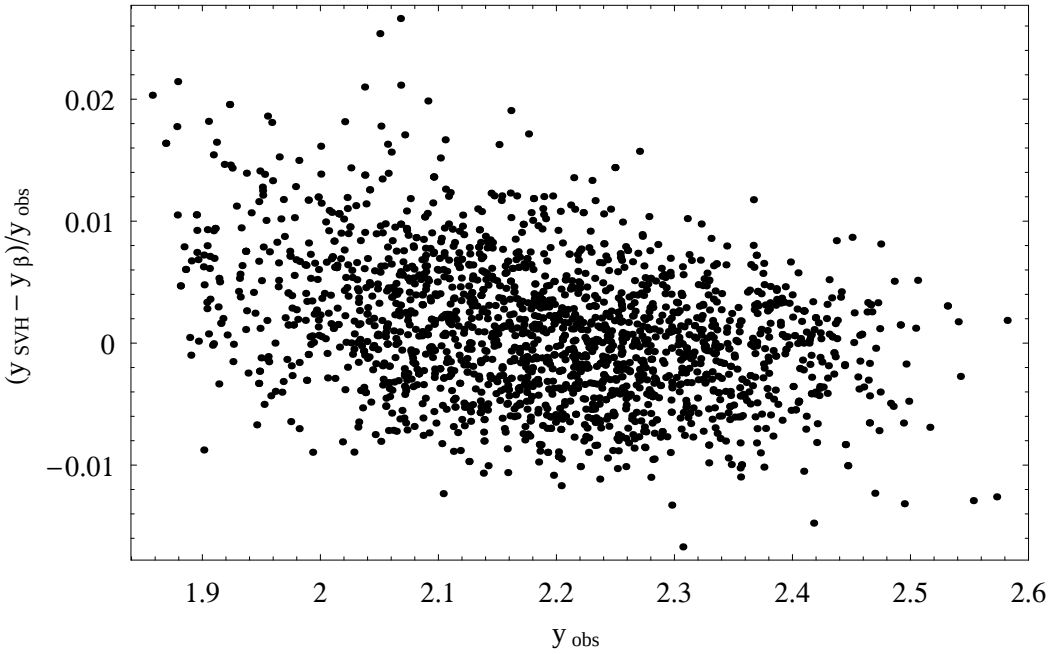

Figure 4.2: The comparison between the standard SVH and its β version for a set of 2000 randomly selected galaxies. On the y - axis, we report the difference $y_{SVH} - y_\beta$ between the values of $y = \log \sigma_0$ as predicted from the standard and β - SVH normalized with respect to the observed value reported on x - axis.

Considering all these encouraging results, we therefore conclude that the theoretically predicted SVH is observationally well founded showing a tilt that can be satisfactory explained in terms of a power - law $\Upsilon_\star - L_T$ relation and of the impact of rotational support.

4.5.2 A two parameter SVH

Although being a three parameter relation, Eq.(4.34) may be simplified noting that an equally satisfactory fit to the $\log(w/k)$ data may be achieved also negleting the terms depending on $\langle I_e \rangle$ and R_e. The SVH then simplifies to :

$$\log \sigma_0 = \frac{\beta_\star + 1}{2} \log \langle I_e \rangle + \frac{2\beta_\star + 1}{2} \log R_e + \frac{c}{2} \log(n/4) + d \qquad (4.67)$$

which we will refer to as the β - *SVH*. Using the same procedure as above, we have fitted this relation to the full sample obtaining an equally good fit to the data as for the standard SVH. Actually, although the coefficients of the different terms in Eqs.(4.36) and (4.67) differ, the

Table 4.4: Results of the MCMC code for the β - SVH relation (4.67) using the full sample. (1) Filter id. (2) Values of $(\beta, c, d, \sigma_{int})$ for the best fit relation. (3) - (5) Median value and 68% confidence range for the fit parameters. (6) Root mean square of the best fit residuals.

(1)	(2)	(3)	(4)	(5)	(6)
Id	$(\beta, c, d, \sigma_{int})_{bf}$	β	c	σ_{int}	σ_{rms}
g'	$(0.118, 0.586, 0.635, 0.047)$	$0.115^{+0.013}_{-0.012}$	$0.587^{+0.038}_{-0.040}$	$0.047^{+0.001}_{-0.002}$	0.084
r'	$(0.112, 0.469, 0.645, 0.050)$	$0.111^{+0.012}_{-0.04}$	$0.463^{+0.048}_{-0.046}$	$0.050^{+0.002}_{-0.002}$	0.084
i'	$(0.098, 0.526, 0.667, 0.049)$	$0.095^{+0.011}_{-0.013}$	$0.527^{+0.097}_{-0.048}$	$0.049^{+0.002}_{-0.002}$	0.072

two relations predict quite similar values for $\log \sigma_0$ as we show in Fig. 4.2. In the r' filter, we get for the best fit relations :

$$(\beta_\star, c, d, \sigma_{int}) = (0.112, 0.469, 0.645, 0.050)$$

with however a notable increase in the rms scatter being now $\sigma_{rms} = 0.084$ instead of $\sigma_{rms} = 0.064$. Such an increase is, however, expected since we have dropped out one parameter. In order to statistically compare the two fits, we resort to the AIC and BIC values finding (for a sample of 2000 randomly extracted galaxies) :

$$AIC(SVH) = 8956.80 \quad , \quad AIC(\beta - SVH) = 8915.40 \ ,$$

$$BIC(SVH) = 8979.20 \quad , \quad AIC(\beta - SVH) = 8931.95 \ .$$

Both the AIC and BIC values indicate a strong preference of the $\beta - SVH$ over the standard SVH which is expected given that the reduction of σ_{rms} and σ_{int} is not so high to claim for a further more parameter.

It is worth noting that using the estimated $\beta_\star$ and the slope of the $M_{dyn}/M^T_\star$ - L_T relation, we get $\Upsilon_{dyn} \propto L_T^\gamma$ with $\gamma \simeq 0.20$ well in agreement with $\gamma = 0.17$ by Padmanabhan et al. (2004). Notwithstanding this remarkable success, we remark that the β - SVH relies on a somewhat unmotivated approximation having neglected the dependence of $\log(w/k)$ on the parameters $(\log\langle I_e\rangle, \log R_e)$. We therefore conclude that, although being statistically preferred, the β - SVH is less theoretically motivated so that the standard SVH should be globally preferred.

4.5.3 The SVH in different filters

Although we have chosen the r' band as the fiducial one, we have also fitted the SVH and β - SVH relations in the g' and i' filters. The best fit values and the estimates for the fitting parameters are reported in Tables 3 and 4 which the interested reader is referred to. Here we do not discuss these results in details, but just highlight some general remarks.

First, it is worth stressing that, within the a given sample, both σ_{int} and σ_{rms} are almost independent on the filter. Such a nice result is a further observational validation of the SVH

since it shows that our theoretical assumptions are indeed verified in all the optical bands we have considered. This is an important test since our derivation of the SVH relies only on physical hypotheses that are not related to the wavelength the observations are taken.

Due to using only three filters, it is not possible to infer any trend of the fit parameters with the wavelength. Actually, considering the best fit values, there is not a clear trend, but rather (a, b, c) seem to be almost the same within the errors. Interpreting this result is not easy. On the one hand, it is known that the photometric parameters $(n, \langle I_e \rangle, R_e)$ depend on the central wavelength used in the fitting, but quantifying this effect is a quite difficult task since one also has to take into account the different signal - to - noise ratio of the different filters. On the other hand, our theoretical derivation rests on the kinetic and gravitational energy which depends on the filter only through $\Upsilon_\star$ needed to conver the observed total luminosity in a total stellar mass. According to our inferred $\beta_\star$ values, $\Upsilon_\star$ is only weakly correlated so that it is likely that the ratio w/k, for fixed values of $(n, \langle I_e \rangle, R_e)$, does not depend on the filter thus giving SVH coefficients independent of the wavelength. Although these subtleties make it difficult to draw a definitive conclusion, we tentatively argue that the nearly independence of the observed SVH coefficients on the filter is a further evidence in favour of our modelling and hypotheses.

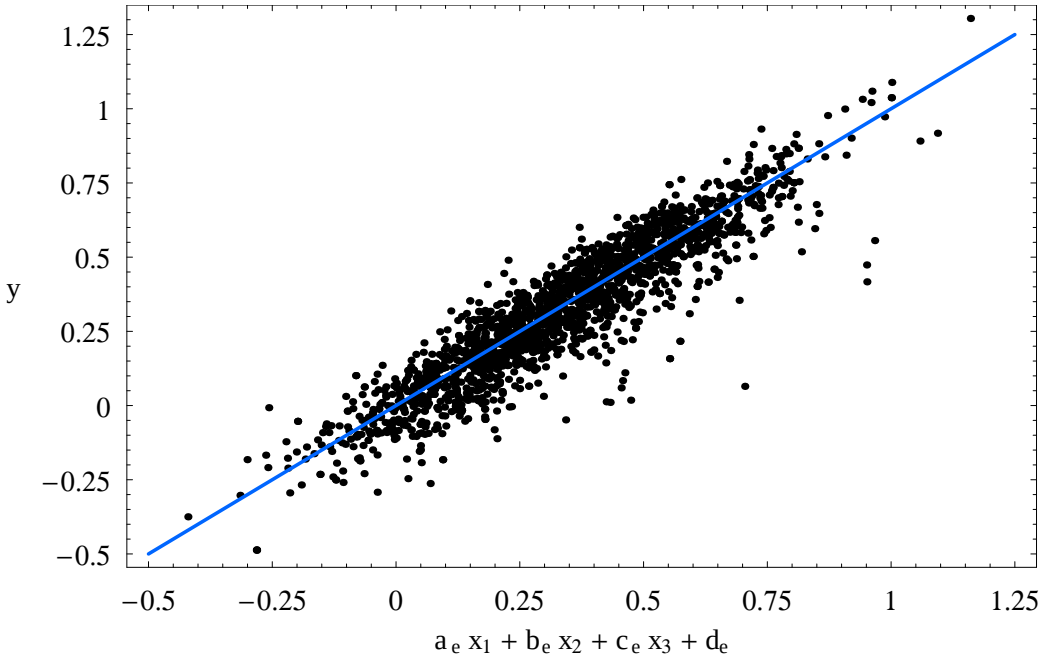

Figure 4.3: The observed inverse SVH for 2000 randomly selected galaxies in the r' filter. On the y - axis, we report $\log R_e$, while on the x - axis, the best fit $a_e x_1 + b_e x_2 + c_e x_3 + d_e$ with $x_1 = \log \sigma_0$, $x_2 = \log \langle I_e \rangle$, $x_3 = \log (n/4)$ and (a_e, b_e, c_e, d_e) as reported in Table 4.

4.5.4 The inverse SVH vs the FP and PhP planes

Being an immediate consequence of the virial theorem and our assumptions (4.34) and (4.35), we have up to now written the SVH as a relation giving the velocity dispersion as a function

Table 4.5: Results of the MCMC code for the inverse - SVH relation (4.68). (1) Filter id. (2) Values of $(a_e, b_e, c_e, d_e, \sigma_{int})$ for the best fit relation. (3) - (6) Median value and 68% confidence range for the fit parameters. (7) Root mean square of the best fit residuals.

(1)	(2)	(3)	(4)	(5)	(6)	(7)
Id	$(a_e, b_e, c_e, d_e, \sigma_{int})_{bf}$	a_e	b_e	c_e	σ_{int}	σ_{rms}
g'	$(1.159, -0.805, -0.157, -0.227, 0.068)$	$1.159^{+0.016}_{-0.023}$	$-0.805^{+0.010}_{-0.006}$	$-0.151^{+0.045}_{-0.018}$	$0.068^{+0.001}_{-0.001}$	0.093
r'	$(1.180, -0.791, -0.180, -0.319, 0.069)$	$1.178^{+0.014}_{-0.017}$	$-0.791^{+0.009}_{-0.007}$	$-0.180^{+0.019}_{-0.022}$	$0.070^{+0.001}_{-0.002}$	0.094
i'	$(1.175, -0.809, -0.166, -0.275, 0.069)$	$1.175^{+0.015}_{-0.015}$	$-0.807^{+0.009}_{-0.007}$	$-0.153^{+0.026}_{-0.023}$	$0.069^{+0.001}_{-0.001}$	0.097

of the photometric parameters. However, we can solve Eq.(4.36) with respect to R_e obtaining what we term the *inverse - SVH*:

$$\log R_e = a_e \log \sigma_0 + b_e \log \langle I_e \rangle + c_e \log (n/4) + d \tag{4.68}$$

with :

$$\begin{cases} a_e = 1/b \\ b_e = -a/b \\ c_e = -c/b \\ d_e = -d/b \end{cases} \tag{4.69}$$

which can be directly evaluated from the best fit values reported above. A most reliable estimate is, however, obtained by fitting Eq.(4.68) to the data using the same MCMC procedure thus obtaining also a value for the intrinsic scatter. The results are summarized in Table 5, while Fig. 4.3 shows how well the data are fitted in the r' band.

It is immediate to see that the values in Table 5 are in strong disagreement with the theoretical expectations based on Eq.(4.69). On the one hand, this is by no means a shortcoming of the model, but rather an expected consequence of the problems with fitting an inverse relation so that we do not discuss anymore this issue. On the other hand, one should worry about the consistency of the inferred values of (a_e, b_e, c_e) with those that can be somewhat predicted by our theoretical assumptions. To this aim, we should compute, for each observed galaxy, the values of σ_0 and its uncertainty and then fit Eq.(4.68) to this simulated measurements in order to predict what values are expected neglecting the correlation $\Upsilon_\star$ - L_T. The comparison between such values and the observed ones should give us an estimate of $\beta_\star$ as we have yet done above from the SVH fit. We do not perform such a test here since the above discussion has yet demonstrated that our theoretical assumptions leads to a SVH in agreement with the observed one so that we do expect a similar conclusion for the inverse - SVH.

It is more interesting to note that both the intrinsic and rms scatter in $\log R_e$ are practically independent on the filter with $\sigma_{rms} \simeq 0.10$ and $\sigma_{int} \simeq 0.07$. As an intriguing result, we find that σ_{rms} is almost the same as the intrinsic scatter in the c_{NFW} - M_{vir} relation predicted by numerical simulations ($\sigma_c = 0.11$). Indeed, while in the FP and the PhP the scatter must be attributed to different causes (such as variation in the halo parameters, non homology and stellar populations), in our model, the main source is just the c_{NFW} - M_{vir} relation with a residual contribution coming from the color based conversion from Υ_V to $\Upsilon_\star$. Actually, our intrinsic scatter is smaller than σ_c since, in our modelling, we use Eq.(4.18) neglecting its scatter so that σ_{int} does not take into account this effect. A more careful analysis is

Table 4.6: Results of the MCMC code for the inverse - SVH relation (4.68) in the r' filter using different cuts on $y = \log \sigma_0$. (1) Cut on y. (2) Values of $(a_e, b_e, c_e, d_e, \sigma_{int})$ for the best fit relation. (3) - (6) Median value and 68% confidence range for the fit parameters.

(1)	(2)	(3)	(4)	(5)	(6)
y	$(a_e, b_e, c_e, d_e, \sigma_{int})_{bf}$	a_e	b_e	c_e	σ_{int}
y_{low} [a]	$(1.197, -0.784, -0.205, -0.398, 0.068)$	$1.203^{+0.068}_{-0.067}$	$-0.784^{+0.010}_{-0.009}$	$-0.207^{+0.028}_{-0.027}$	$0.069^{+0.002}_{-0.002}$
y_{med} [b]	$(1.039, -0.723, 0.003, -0.188, 0.068)$	$1.047^{+0.035}_{-0.041}$	$-0.721^{+0.010}_{-0.011}$	$0.005^{+0.002}_{-0.001}$	$0.068^{+0.003}_{-0.003}$
y_{high} [c]	$(1.008, -0.832, -0.145, 0.206, 0.073)$	$0.998^{+0.046}_{-0.038}$	$-0.835^{+0.012}_{-0.009}$	$-0.142^{+0.030}_{-0.035}$	$0.074^{+0.002}_{-0.002}$

[a] $1.84 \leq y \leq 2.06$
[b] $2.06 \leq y \leq 2.18$
[c] $2.18 \leq y \leq 2.58$

therefore needed to understand whether the c_{NFW} - M_{vir} scatter is indeed the driving term in the determination of both the intrinsic and observational scatter.

It is worth wondering how the inverse SVH (4.68) works as distance indicator. To this aim, we note that the rms scatter in $\log R_e$ translates into a $\ln 10 \times \sigma_{rms} \simeq 22\%$ scatter in the distance estimates for the r' filter. Table 4 in Bernardi et al. (2003) reports a collection from literature of various FP determinations with the corresponding scatter on the distance ranging from 13% to 22% so that, taken at face values, increasing the number of parameters with respect to the FP (4 instead of 3 for the SVH vs the FP) does not ameliorate the performances as distance indicator. However, it is worth stressing that different determinations rely on different fitting methods. A meaningful comparison should be based on the same fitting method and we advocate the use of our Bayesian approach in order to not underestimate the intrinsic scatter. For the best fit FP relation in the r' filter, we get :

$$\log R_e = 1.119 \log \sigma_0 - 0.769 \log \langle I_e \rangle - 0.236$$

with $\sigma_{int} = 0.068$ and $\sigma_{rms} = 0.092$, while the constraints on the parameters are as follows :

$$a = 1.115^{+0.016}_{-0.014} \ , \ b = -0.768^{+0.007}_{-0.006} \ , \ \sigma_{int} = 0.071^{+0.001}_{-0.002} \ .$$

The rms scatter in the distance is indeed now increased to 21%, i.e. almost the same as the one obtained using the inverse - SVH. Such a result should suggest that the introduction of a fourth parameter is meaningless. Nevertheless, both the AIC and BIC statistics indicate that the inverse - SVH has to be preferred with :

$$AIC(\mathrm{inv} - SVH) = 7818.70 < AIC(FP) = 7868.90 \ ,$$

$$BIC(\mathrm{inv} - SVH) = 7841.10 < BIC(FP) = 7885.70 \ .$$

It is somewhat surprising that, although the inverse - SVH performs statistically better than the FP, the rms scatter in distance determination and the intrinsic scatter in $\log R_e$ are essentially the same. However, one should also take into account that our sample is made out of all ETGs in the lowZ catalog without any separation in field or clusters objects. It is therefore

worth reconsidering the fit and hence the scatter using smaller subsamples separated according to their environment. This is outside the aims of this introductory investigation and will be presented elsewhere.

As we have demonstrated in Sect. 3.2, a different projection of the SVH is the PhP so that it is worth comparing how the inverse - SVH performs as a distance indicator compared to the PhP. To this aim, we run the MCMC code to determine the PhP parameters thus obtaining for the best fit relation in the r' filter :

$$\log R_e = -0.552 \log \langle I_e \rangle + 0.303 \log (n/4) + 1.689 \ ,$$

with $\sigma_{int} = 0.175$ and $\sigma_{rms} = 0.178$, while the constraints after marginalization turn out to be :

$$a = -0.552^{+0.013}_{-0.016} \ , \ b = 0.292^{+0.045}_{-0.050} \ , \ \sigma_{int} = 0.175^{+0.003}_{-0.002} \ .$$

Both the PhP intrinsic and rms scatter are significantly larger than the corresponding ones for the inverse - SVH so that we can safely conclude that this latter is clearly preferred. Such a result is not surprising at all. As we have seen in Sect. 3.2, the PhP is obtained from the SVH by *marginalizing* over $\log \sigma_0$ which is the only dynamical quantity, while the FP is obtained by neglecting the difference between the actual Sersic index n and the canonical de Vaucouleurs value $n = 4$. Since $n \simeq 4$ indeed holds for most of ETGs, the term $\log (n/4)$ is typically quite small so that neglecting it does no increase significantly either σ_{int} or σ_{rms}. On the contrary, being σ_0 a tracer of the total mass, neglecting it is the same as assuming that the scaling properties of the system are independent of its mass which is clearly a quite rough approximation leading to the strong increase in σ_{int} and σ_{rms} we find when forcing the inverse - SVH to reduce to the PhP.

4.5.5 Impact of selection criteria

The ETG sample we are using is a subsample of the lowZ SDSS catalog assembled through a set of selection criteria described in Sect. 4.1. Although well motivated, such criteria are however somewhat subjective so that it is worth investigating how they affect the estimate of the SVH coefficients. Actually, we will consider hereafter the inverse SVH since it is a more interesting tool as a distance indicator. Moreover, we will only use the r' filter as fiducial one stressing that the main conclusions are unaffected by this choice.

As a first test, we investigate the impact on the parameter estimation of the selection criteria on the velocity dispersion σ_0. According to our default choice, we have included in the sample all galaxies with $\sigma_0 \geq 70$ km/s. As a check, we divide the ETGs according to the value of σ_0 in three roughly equally populated subsamples. As it is apparent from the results in Table 6, while it is possible to see a trend for the a_e coefficient decreasing with increasing σ_0 range, this is not possible for the remaining two parameters (b_e, c_e). In particular, we find the quite unexplicable result that $c_e \simeq 0$ in the middle σ_0 range. Actually, predicting any quantitative behaviour of the coefficients is quite complicated. It is, however, worth noting that higher velocity dispersion systems are likely to be more massive. As such, it is expected that their dark matter haloes play a major role in the dynamics of the system. Since no dark halo parameters explicitly enter the inverse SVH, (c_{NFW}, M_{vir}) only indirectly affect such a relation through their impact on $\log \sigma_0$. The larger is the cut on σ_0, the higher is the total mass and hence the halo mass. As a consequence, the larger will be the impact of the dark halo on the dynamics thus making less important the value of the photometric quantities. Indeed, a numerical analysis shows that the dominant term in the inverse - SVH is typically

the first one, while the contribution of the other two terms decreases as $\sigma_{0,min}$ increases in agreement with the qualitative trend we expect based on the above discussion. It is, however, worth noting that the intrinsic scatter σ_{int} is, on the contrary, not dependent on the $\log\sigma_0$ range so that we cannot infer any preferred range in σ_0 from the point of view of ameliorating the performances of the inverse - SVH as distance indicator.

There is a more subtle issue worth to be discussed. Even if we have never quoted it, there is an *a priori* selection criterium adopted by the SDSS collaboration. Actually, no galaxy with $m_r > 17.77$ (with m_r the total apparent magnitude in the r' filter) has been chosen as a spectroscopic target. Since r' can be expressed as function of the photometric parameters, this selection may be considered as a prior on the model parameters space. The Bayesian approach allows to include this effect by modifying the merit function as :

$$\mathcal{L} = \mathcal{L}_{data} \times \mathcal{H}[r_{cut} - m_r(\mathbf{p})] \tag{4.70}$$

with $\mathcal{L}_{data}$ given by Eq.(4.53), $\mathcal{H}(x)$ the Heaviside step function, r_{cut} the limiting value for m_r. In Eq.(4.70), m_r is considered as a function of $(\sigma_0, \langle I_e\rangle, n)$ by first expressing the total apparent magnitude as function of the photometric quantities $(n, R_e, \langle I_e\rangle)$ and then using the inverse - SVH to get R_e as function of σ_0. The MCMC code is then runned as usual, but now the parameter d may not be analitycally computed through Eq.(4.54), but must be estimated from the fit. For the best fit relation, we get :

$$(a_e, b_e, c_e, d_e, \sigma_{int})_{bf} = (1.197, -0.784, -0.205, 0.310, 0.068) \ ,$$

with the median and 68% confidence ranges given as :

$$a_e = 1.203^{+0.068}_{-0.067} \quad , \quad b_e = -0.784^{0.010}_{-0.009} \ ,$$

$$c_e = -0.207^{+0.028}_{-0.027} \quad , \quad \sigma_{int} = 0.069^{+0.002}_{-0.002} \ .$$

Taken at face values, the best fit parameters do not agree with the ones in second row of Table 4, obtained neglecting the prior on m_r. However, the difference between the two relations is actually quite small and, moreover, the median values of the (a_e, b_e, c_e) coefficients are consistent within the errors. Finally, the intrinsic scatter σ_{int} is almost exactly the same. We therefore conclude that the selection criterium $m_r < 17.77$ has a meaningful impact on the determination of the inverse - SVH.

4.6 Discussion and conclusions

Early type galaxies may be considered as a homogenous class of objects from many point of views. A further support to this idea is represented by the existence of several interesting scaling relations among their photometric and/or kinematic parameters, the most famous ones being the FP (between $\log\sigma_0$, $\log\langle I_e\rangle$ and $\log R_e$) and the PhP (where $\log\sigma_0$ is replaced by the Sersic index $\log n$). In an attempt to look for a unified description of both these relations, we have presented here the *Sersic Virial Hyperplane* (SVH) expressing a kinematical quantity, namely the velocity dispersion σ_0, as a function of the Sersic photometric parameters $(n, , R_e, \langle I_e\rangle)$. In the usual logarithmic units, such a relation reduces to a hyperplane (i.e., a plane in four dimensions) where all ETGs lay with a small thickness as inferred from the low intrinsic scatter σ_{int}. Just as the FJ relation is a projection of the FP and the KR a projection

of the PhP, thus we find that both the FP and the PhP are projections of the SVH so that the scatter in these well known relations can be ascribed to neglecting one of the SVH variables.

Our derivation of the SVH relies on very few assumptions. First, ETGs are postulated to be in dynamical equilibrium so that the virial theorem applies. Given that ETGs are old systems likely to have formed most of their stellar content and settled their main structural properties at $z \sim 2$ [256], this hypothesis seems to be well founded, at least as a first well motivated approximation. Starting from this premise, the SVH comes out as a consequence of the virial theorem and of Eqs.(4.34) and (4.35). The first one relies on an approximated log-linear relation between the model dependent quantity $w(\mathbf{p})/k(\mathbf{p})$ and the Sersic photometric parameters, while the second one assumes the existence of a power-law relation between the stellar M/L ratio $\Upsilon_\star$ and the total luminosity L_T. Given mass models for the luminous and dark components of a typical ETG, Eq.(4.34) has been verified by computing $\log(w/k)$ for a large ETG sample selected from the low redshift version of the VAGC catalog based on SDSS DR4. Moreover, we have also shown that such a relation is statistically preferred over other possible approximating formulae. On the other hand, the relation $\Upsilon_\star \propto L_T^\beta$ is expected on the basis of stellar populations synthesis models and is also invoked to explain the FP tilt. It is worth stressing, however, that here the tilt of the SVH is due to the dependence of the stellar M/L on L_T, while, in the case of the FP, such a relation involve the global (stellar plus dark) M/L ratio. As a consequence, one has to resort to a mechanism coupling the dark and luminous mass density profiles in order to have $M_{dyn}/L_T \propto L_T^\beta$, while here we only rely on what is predicted by stellar population synthesis models. From this point of view, therefore, the SVH relies only on known physics without the need of any unexplained interaction between baryons and CDM particles.

The discussion in Sect. 5 have observationally validated the SVH and confidently demonstrated that its parameters may be reconciled with our theoretical predictions provided the contribute of the rotational support is taken into account. It is therefore worth wondering how this derivation and the constraints on the fitting parameters can be ameliorated. We have here used the Bayesian approach to infer the estimate of the SVH coefficients and its intrinsic scatter from a dataset based on the lowZ catalog. Such a sample is however affected by known problems. In particular, the automated code used by Blanton et al. (2005) to estimate the Sersic parameters does not work very well. The recovered values of (n, R_e, A) and hence of $\log\langle I_e\rangle$ are biased in a complicated way depending on the values of the parameters themselves. Modeling this bias and taking care of it in the fitting procedure is quite difficult, but we have shown that the estimate of the inverse-SVH coefficients is likely to be not significantly affected. A possible way out of this systematic uncertainty relies on resorting to a different sample. The recently released Millenium Galaxy Catalog [234, 137] contains a detailed bulge/disc decomposition of ~ 10000 nearby galaxies with detailed fitting of the Sersic law to the surface brightness profile [14]. The code is tested and shown not to be biased and the errors on the photometric parameters togetger with their covariance matrix are available. Cross-matching with the SDSS and selecting only the ETGs should provide an ideal sample to test the SVH retrieving a more reliable estimate of its coefficients and scatter thus allowing to reconsider it as a distance indicator.

From a theoretical point of view, it is worth reconsidering our basic assumptions. As discussed above, the tilt of the SVH with respect to the virial theorem predictions may be fully ascribed to a power-law relation between the stellar M/L ratio $\Upsilon_\star$ and the total luminosity L_T. Although estimating the slope $\beta_\star$ from the tilt is, in principle, possible, confronting with an expected value is welcome. To this aim, one can resort to stellar population synthesis models [156, 58, 223, 243] by varying the different ingredients entering the codes and looking (by trial and error) for the combination giving the slope β needed to reproduce the correct

SVH tilt. Should these stellar models be able to reproduce the observed colors of ETG, our derivation of the SVH could be further strengthened.

A fundamental role in the ETG modeling has been played by the choice of the dark halo model. Although the NFW mass density profile is the standard one, it is nevertheless well known that it encounters serious difficulties in explaining the inner rotation curves of low surface brightness galaxies (see, e.g., de Blok 2005 and refs. therein). Moreover, some recent evidences from the planetary nebulae dynamics have put into question the need for a significative amount of dark matter in the inner regions of elliptical galaxies [314, 263]. To overcome this problem, one may resort to a phenomenological ETG model to smoothly interpolate between a constant M/L ratio and a dark matter dominated system [364] thus making it easier to study the impact of changing the dark mass content on the SVH coefficients. A subtle effect, worth to be investigated, is the relation between the concentration c_{NFW} and the virial mass M_{vir} of the halo. Actually, the scatter of this relation concurs in determining the scatter in the SVH. Said in another way, for given M_{vir} and stellar mass parameters, the scatter in the $c_{NFW} - M_{vir}$ relation introduces a scatter on $M_{DM}(R_e)/M_{dyn}(R_e)$ thus contributing to the total SVH scatter. Numerical N - body simulations and semi - analytical galaxy formation models predict different halo models with its own $c_{NFW} - M_{vir}$ relation and scatter. It should be tempting to investigate whether a large ETG sample could be used to discriminate among these different possibilities on the basis of the SVH scatter they predict.

The aim of the present work was mainly to introduce the SVH as a unifying scenario for the ETG scaling relations. If the encouraging results presented here will be further confirmed, both observationally and theoretically, we are confident that the SVH could represent a valid tool to investigate the ETG properties under a single picture.

CHAPTER 5

Modelling clusters of galaxies by $f(R)$-gravity

5.1 Clusters of Galaxies as fundamental bundle of Dark Matter at large scales

Since in previous chapter we have analyzed f(R) gravity applied to galactic system, we are now going up in scale and considering clusters of galaxies. As for rotation curves of galaxies also clusters can be considered as an historical remark for the need of dark components: since the pioneering work by [394], the problem of high mass-to-light ratios of galaxy clusters has been faced by asking for huge amounts of unseen matter in the framework of Newtonian theory of gravity. It is interesting to stress the fact that Zwicky addressed such an issue dealing with *missing matter* and not with *dark matter*.

A fundamental issue is related to clusters and superclusters of galaxies. Such structures, essentially, rule the large scale structure, and are the intermediate step between galaxies and cosmology. As the galaxies, they appear dark-matter dominated but the distribution of dark matter component seems clustered and organized in a very different way with respect to galaxies. It seems that dark matter is ruled by the scale and also its fundamental nature could depend on the scale. For a comprehensive review see [27].

In the philosophy of Extended Theories of Gravity, the issue is now to reconstruct the mass profile of clusters *without* dark matter, i.e. to find out corrections to the Newton potential producing the same dynamics as dark matter but starting from a well motivated theory. This is the goal of this work.

As we will see, the problem is very different with respect to that of galaxies and we need different corrections to the gravitational potential in order to consistently fit the cluster mass profiles.

The Chapter is organized as follows. In Section 5.2, also referring to other results, we discuss the weak field limit of $f(R)$-gravity showing that an $f(R)$ theory is, in principle, quite fair to address the cluster problem [235]. In Section 5.3, starting from the corrected potential previously derived for a point-like masses, we generalize the results to extended spherically symmetric systems as required for well shaped cluster models of the Bautz and Morgan classification [34]. Section 5.4 is devoted to the description of the general properties of galaxy clusters. In Section 5.5, the sample of galaxy clusters which we are going to fit is discussed in details. Results are presented in Section 5.6, while Section 5.7 is devoted to the discussion and the conclusions.

5.2 $f(R)$-gravity

Let us consider the general action:

$$\mathcal{A} = \int d^4x\sqrt{-g}\,[f(R) + \mathcal{X}\mathcal{L}_m]\ , \tag{5.1}$$

where $f(R)$ is an analytic function of the Ricci scalar R, g is the determinant of the metric $g_{\mu\nu}$, $\mathcal{X} = \dfrac{16\pi G}{c^4}$ is the coupling constant and $\mathcal{L}_m$ is the standard perfect-fluid matter Lagrangian. Such an action is the straightforward generalization of the Hilbert-Einstein action of GR obtained for $f(R) = R$. Since we are considering the metric approach, field equations are obtained by varying (5.1) with respect to the metric:

$$f'R_{\mu\nu} - \frac{1}{2}fg_{\mu\nu} - f'_{;\mu\nu} + g_{\mu\nu}\Box f' = \frac{\mathcal{X}}{2}T_{\mu\nu}\,. \tag{5.2}$$

where $T_{\mu\nu} = \frac{-2}{\sqrt{-g}}\frac{\delta(\sqrt{-g}\mathcal{L}_m)}{\delta g^{\mu\nu}}$ is the energy momentum tensor of matter, the prime indicates the derivative with respect to R and $\Box = {}_{;\sigma}{}^{;\sigma}$. We adopt the signature $(+,-,-,-)$.

As discussed in details in [86], we deal with the Newtonian and the post-Newtonian limit of $f(R)$ - gravity on a spherically symmetric background. Solutions for the field equations can be obtained by imposing the spherical symmetry [85]:

$$ds^2 = g_{00}(x^0, r){dx^0}^2 + g_{rr}(x^0, r)dr^2 - r^2 d\Omega \tag{5.3}$$

where $x^0 = ct$ and $d\Omega$ is the angular element.

To develop the post-Newtonian limit of the theory, one can consider a perturbed metric with respect to a Minkowski background $g_{\mu\nu} = \eta_{\mu\nu} + h_{\mu\nu}$. The metric coefficients can be developed as:

$$\begin{cases} g_{tt}(t,r) \simeq 1 + g^{(2)}_{tt}(t,r) + g^{(4)}_{tt}(t,r) \\ g_{rr}(t,r) \simeq -1 + g^{(2)}_{rr}(t,r) \\ g_{\theta\theta}(t,r) = -r^2 \\ g_{\phi\phi}(t,r) = -r^2\sin^2\theta \end{cases}, \tag{5.4}$$

where we put, for the sake of simplicity, $c = 1$, $x^0 = ct \to t$. We want to obtain the most general result without imposing particular forms for the $f(R)$-Lagrangian. We only consider analytic Taylor expandable functions

$$f(R) \simeq f_0 + f_1 R + f_2 R^2 + f_3 R^3 + \dots . \tag{5.5}$$

To obtain the post-Newtonian approximation of $f(R)$ - gravity, one has to plug the expansions (5.4) and (5.5) into the field equations (5.2) and then expand the system up to the orders $O(0)$, $O(2)$ and $O(4)$. This approach provides general results and specific (analytic) Lagrangians are selected by the coefficients f_i in (5.5) [86].

If we now consider the $O(2)$ - order of approximation, the field equations (5.2), in the vacuum case, results to be

$$\begin{cases} f_1 r R^{(2)} - 2 f_1 g^{(2)}_{tt,r} + 8 f_2 R^{(2)}_{,r} - f_1 r g^{(2)}_{tt,rr} + 4 f_2 r R^{(2)} = 0 \\ \\ f_1 r R^{(2)} - 2 f_1 g^{(2)}_{rr,r} + 8 f_2 R^{(2)}_{,r} - f_1 r g^{(2)}_{tt,rr} = 0 \\ \\ 2 f_1 g^{(2)}_{rr} - r[f_1 r R^{(2)} \\ - f_1 g^{(2)}_{tt,r} - f_1 g^{(2)}_{rr,r} + 4 f_2 R^{(2)}_{,r} + 4 f_2 r R^{(2)}_{,rr}] = 0 \\ \\ f_1 r R^{(2)} + 6 f_2 [2 R^{(2)}_{,r} + r R^{(2)}_{,rr}] = 0 \\ \\ 2 g^{(2)}_{rr} + r[2 g^{(2)}_{tt,r} - r R^{(2)} + 2 g^{(2)}_{rr,r} + r g^{(2)}_{tt,rr}] = 0 \end{cases} \tag{5.6}$$

It is evident that the trace equation (the fourth in the system (5.6)), provides a differential equation with respect to the Ricci scalar which allows to solve the system at $O(2)$ - order. One obtains the general solution :

$$\begin{cases} g^{(2)}_{tt} = \delta_0 - \frac{2GM}{f_1 r} - \frac{\delta_1(t) e^{-r\sqrt{-\xi}}}{3\xi r} + \frac{\delta_2(t) e^{r\sqrt{-\xi}}}{6(-\xi)^{3/2} r} \\ \\ g^{(2)}_{rr} = -\frac{2GM}{f_1 r} + \frac{\delta_1(t)[r\sqrt{-\xi}+1] e^{-r\sqrt{-\xi}}}{3\xi r} - \frac{\delta_2(t)[\xi r + \sqrt{-\xi}] e^{r\sqrt{-\xi}}}{6\xi^2 r} \\ \\ R^{(2)} = \frac{\delta_1(t) e^{-r\sqrt{-\xi}}}{r} - \frac{\delta_2(t)\sqrt{-\xi} e^{r\sqrt{-\xi}}}{2\xi r} \end{cases} \tag{5.7}$$

where $\xi \doteq \dfrac{f_1}{6 f_2}$, f_1 and f_2 are the expansion coefficients obtained by the $f(R)$-Taylor series. In the limit $f \to R$, for a point-like source of mass M we recover the standard Schwarzschild solution. Let us notice that the integration constant δ_0 is dimensionless, while the two arbitrary time-functions $\delta_1(t)$ and $\delta_2(t)$ have respectively the dimensions of $lenght^{-1}$ and $lenght^{-2}$; ξ has the dimension $lenght^{-2}$. As extensively discussed in [86], the functions $\delta_i(t)$ $(i = 1, 2)$ are completely arbitrary since the differential equation system (5.6) depends only on spatial derivatives. Besides, the integration constant δ_0 can be set to zero, as in the standard theory of potential, since it represents an unessential additive quantity. In order to obtain the physical prescription of the asymptotic flatness at infinity, we can discard the Yukawa growing mode in (5.7) and then the metric is :

$$\begin{aligned} ds^2 &= \left[1 - \frac{2GM}{f_1 r} - \frac{\delta_1(t)e^{-r\sqrt{-\xi}}}{3\xi r}\right]dt^2 \\ &- \left[1 + \frac{2GM}{f_1 r} - \frac{\delta_1(t)(r\sqrt{-\xi}+1)e^{-r\sqrt{-\xi}}}{3\xi r}\right]dr^2 \\ &- r^2 d\Omega\,. \end{aligned} \tag{5.8}$$

The Ricci scalar curvature is

$$R = \frac{\delta_1(t)e^{-r\sqrt{-\xi}}}{r}\,. \tag{5.9}$$

The solution can be given also in terms of gravitational potential. In particular, we have an explicit Newtonian-like term into the definition. The first of (5.7) provides the second order solution in term of the metric expansion (see the definition (5.4)). In particular, it is $g_{tt} = 1 + 2\phi_{grav} = 1 + g_{tt}^{(2)}$ and then the gravitational potential of an analytic $f(R)$-theory is

$$\phi_{grav} = -\frac{GM}{f_1 r} - \frac{\delta_1(t)e^{-r\sqrt{-\xi}}}{6\xi r}\,. \tag{5.10}$$

Among the possible analytic $f(R)$-models, let us consider the Taylor expansion where the cosmological term (the above f_0) and terms higher than second have been discarded. We rewrite the Lagrangian (5.5) as

$$f(R) \sim a_1 R + a_2 R^2 + ... \tag{5.11}$$

and specify the above gravitational potential (5.10), generated by a point-like matter distribution, as: by a point-like matter distribution, as:

$$\phi(r) = -\frac{3GM}{4a_1 r}\left(1 + \frac{1}{3}e^{-\frac{r}{L}}\right)\,, \tag{5.12}$$

where

$$L \equiv L(a_1, a_2) = \left(-\frac{6a_2}{a_1}\right)^{1/2}\,. \tag{5.13}$$

L can be defined as the *interaction length* of the problem[1] due to the correction to the Newtonian potential. We have changed the notation to remark that we are doing only a specific choice in the wide class of potentials (5.10), but the following considerations are completely general.

5.3 Extended systems

The gravitational potential (5.12) is a point-like one. Now we have to generalize this solution for extended systems. Let us describe galaxy clusters as spherically symmetric systems and

[1] Such a length is function of the series coefficients, a_1 and a_2, and it is not a free independent parameter in the following fit procedure.

then we have to extend the above considerations to this geometrical configuration. We simply consider the system composed by many infinitesimal mass elements dm each one contributing with a point-like gravitational potential. Then, summing up all terms, namely integrating them on a spherical volume, we obtain a suitable potential. Specifically, we have to solve the integral:

$$\Phi(r) = \int_0^\infty r'^2 dr' \int_0^\pi \sin\theta' d\theta' \int_0^{2\pi} d\omega' \; \phi(r') \, . \tag{5.14}$$

The point-like potential (5.12)can be split in two terms. The *Newtonian* component is

$$\phi_N(r) = -\frac{3GM}{4a_1 r} \tag{5.15}$$

The extended integral of such a part is the well-known (apart from the numerical constant $\frac{3}{4a_1}$) expression. It is

$$\Phi_N(r) = -\frac{3}{4a_1}\frac{GM(<r)}{r} \tag{5.16}$$

where $M(<r)$ is the mass enclosed in a sphere with radius r. The *correction* term:

$$\phi_C(r) = -\frac{GM}{4a_1}\frac{e^{-\frac{r}{L}}}{r} \tag{5.17}$$

considering some analytical steps in the integration of the angular part, gives the expression:

$$\Phi_C(r) = -\frac{2\pi G}{4} \cdot L \int_0^\infty dr' r' \rho(r') \cdot \frac{e^{-\frac{|r-r'|}{L}} - e^{-\frac{|r+r'|}{L}}}{r} \tag{5.18}$$

The radial integral is numerically estimated once the mass density is given. We underline a fundamental difference between such a term and the Newtonian one: while in the latter, the matter outside the spherical shell of radius r does not contribute to the potential, in the former external matter takes part to the integration procedure. For this reason we split the corrective potential in two terms:

- if $r' < r$:

$$\begin{aligned}\Phi_{C,int}(r) &= -\frac{2\pi G}{4} \cdot L \int_0^r dr' r' \rho(r') \cdot \frac{e^{-\frac{|r-r'|}{L}} - e^{-\frac{|r+r'|}{L}}}{r} \\ &= -\frac{2\pi G}{4} \cdot L \int_0^r dr' r' \rho(r') \cdot e^{-\frac{r+r'}{L}} \left(\frac{-1+e^{\frac{2r'}{L}}}{r}\right)\end{aligned}$$

- if $r' > r$:

$$\begin{aligned}\Phi_{C,ext}(r) &= -\frac{2\pi G}{4} \cdot L \int_r^\infty dr' r' \rho(r') \cdot \frac{e^{-\frac{|r-r'|}{L}} - e^{-\frac{|r+r'|}{L}}}{r} = \\ &= -\frac{2\pi G}{4} \cdot L \int_r^\infty dr' r' \rho(r') \cdot e^{-\frac{r+r'}{L}} \left(\frac{-1+e^{\frac{2r}{L}}}{r}\right)\end{aligned}$$

The total potential of the spherical mass distribution will be

$$\Phi(r) = \Phi_N(r) + \Phi_{C,int}(r) + \Phi_{C,ext}(r) \tag{5.19}$$

As we will show below, for our purpose, we need the gravitational potential derivative with respect to the variable r; the two derivatives may not be evaluated analytically so we estimate them numerically, once we have given an expression for the *total* mass density $\rho(r)$. While the Newtonian term gives the simple expression:

$$-\frac{\mathrm{d}\Phi_N}{\mathrm{d}r}(r) = -\frac{3}{4a_1}\frac{GM(<r)}{r^2} \tag{5.20}$$

The internal and external derivatives of the corrective potential terms are much longer. We do not give them explicitly for sake of brevity, but they are integral-functions of the form

$$\mathcal{F}(r,r') = \int_{\alpha(r)}^{\beta(r)} dr'\ f(r,r') \tag{5.21}$$

from which one has:

$$\begin{aligned}\frac{\mathrm{d}\mathcal{F}(r,r')}{\mathrm{d}r} = &\int_{\alpha(r)}^{\beta(r)} dr' \frac{\mathrm{d}f(r,r')}{\mathrm{d}r} + \\ &-f(r,\alpha(r))\frac{\mathrm{d}\alpha}{\mathrm{d}r}(r) + f(r,\beta(r))\frac{\mathrm{d}\beta}{\mathrm{d}r}(r)\end{aligned} \tag{5.22}$$

Such an expression is numerically derived once the integration extremes are given. A general consideration is in order at this point. Clearly, the Gauss theorem holds only for the Newtonian part since, for this term, the force law scales as $1/r^2$. For the total potential (5.12), it does not hold anymore due to the correction. From a physical point of view, this is not a problem because the full conservation laws are determined, for $f(R)$-gravity, by the contracted Bianchi identities which assure the self-consistency. For a detailed discussion, see [84, 88, 149].

5.4 Cluster mass profiles

Clusters of galaxies are generally considered self-bound gravitational systems with spherical symmetry and in hydrostatic equilibrium if virialized. The last two hypothesis are still widely used, despite of the fact that it has been widely proved that most clusters show more complex morphologies and/or signs of strong interactions or dynamical activity, especially in their innermost regions ([**?**, 122]).
Under the hypothesis of spherical symmetry in hydrostatic equilibrium, the structure equation can be derived from the collisionless Boltzmann equation

$$\frac{d}{dr}(\rho_{gas}(r)\ \sigma_r^2) + \frac{2\rho_{gas}(r)}{r}(\sigma_r^2 - \sigma_{\theta,\omega}^2) = -\rho_{gas}(r)\cdot\frac{d\Phi(r)}{dr} \tag{5.23}$$

where Φ is the gravitational potential of the cluster, σ_r and $\sigma_{\theta,\omega}$ are the mass-weighted velocity dispersions in the radial and tangential directions, respectively, and ρ is gas mass-density. For an isotropic system, it is

$$\sigma_r = \sigma_{\theta,\omega} \tag{5.24}$$

The pressure profile can be related to these quantities by

$$P(r) = \sigma_r^2 \rho_{gas}(r) \tag{5.25}$$

Substituting Eqs. (5.24) and (5.25) into Eq. (5.23), we have, for an isotropic sphere,

$$\frac{dP(r)}{dr} = -\rho_{gas}(r)\frac{d\Phi(r)}{dr} \tag{5.26}$$

For a gas sphere with temperature profile $T(r)$, the velocity dispersion becomes

$$\sigma_r^2 = \frac{kT(r)}{\mu m_p} \tag{5.27}$$

where k is the Boltzmann constant, $\mu \approx 0.609$ is the mean mass particle and m_p is the proton mass. Substituting Eqs. (5.25) and (5.27) into Eq. (5.26), we obtain

$$\frac{d}{dr}\left(\frac{kT(r)}{\mu m_p}\rho_{gas}(r)\right) = -\rho_{gas}(r)\frac{d\Phi}{dr}$$

or, equivalently,

$$-\frac{d\Phi}{dr} = \frac{kT(r)}{\mu m_p r}\left[\frac{d\ln\rho_{gas}(r)}{d\ln r} + \frac{d\ln T(r)}{d\ln r}\right] \tag{5.28}$$

Now the total gravitational potential of the cluster is:

$$\Phi(r) = \Phi_N(r) + \Phi_C(r) \tag{5.29}$$

with

$$\Phi_C(r) = \Phi_{C,int}(r) + \Phi_{C,ext}(r) \tag{5.30}$$

It is worth underlining that if we consider *only* the standard Newtonian potential, the *total* cluster mass $M_{cl,N}(r)$ is composed by gas mass + mass of galaxies + cD-galaxy mass + dark matter and it is given by the expression:

$$\begin{aligned} M_{cl,N}(r) &= M_{gas}(r) + M_{gal}(r) + M_{CDgal}(r) + M_{DM}(r) \\ &= -\frac{kT(r)}{\mu m_p G} r\left[\frac{d\ln\rho_{gas}(r)}{d\ln r} + \frac{d\ln T(r)}{d\ln r}\right] \end{aligned} \tag{5.31}$$

$M_{cl,N}$ means the standard estimated *Newtonian* mass. Generally the galaxy part contribution is considered negligible with respect to the other two components so we have:

$$M_{cl,N}(r) \approx M_{gas}(r) + M_{DM}(r) \approx$$

$$\approx -\frac{kT(r)}{\mu m_p} r\left[\frac{d\ln\rho_{gas}(r)}{d\ln r} + \frac{d\ln T(r)}{d\ln r}\right]$$

Since the gas-mass estimates are provided by X-ray observations, the equilibrium equation can be used to derive the amount of dark matter present in a cluster of galaxies and its spatial distribution.

Inserting the previously defined *extended-corrected* potential of Eq. (5.29) into Eq. (5.28), we obtain:

$$-\frac{\mathrm{d}\Phi_N}{\mathrm{d}r} - \frac{\mathrm{d}\Phi_C}{\mathrm{d}r} = \frac{kT(r)}{\mu m_p r}\left[\frac{\mathrm{d}\ln\rho_{gas}(r)}{\mathrm{d}\ln r} + \frac{\mathrm{d}\ln T(r)}{\mathrm{d}\ln r}\right] \tag{5.32}$$

from which the *extended-corrected* mass estimate follows:

$$\begin{aligned} M_{cl,EC}(r) + \frac{4a_1}{3G} r^2 \frac{\mathrm{d}\Phi_C}{\mathrm{d}r}(r) = \\ = \frac{4a_1}{3}\left[-\frac{kT(r)}{\mu m_p G} r\left(\frac{d\ln\rho_{gas}(r)}{d\ln r} + \frac{d\ln T(r)}{d\ln r}\right)\right] \end{aligned} \tag{5.33}$$

Since the use of a corrected potential avoids, in principle, the additional requirement of dark matter, the total cluster mass, in this case, is given by:

$$M_{cl,EC}(r) = M_{gas}(r) + M_{gal}(r) + M_{CDgal}(r) \tag{5.34}$$

and the mass density in the Φ_C term is

$$\rho_{cl,EC}(r) = \rho_{gas}(r) + \rho_{gal}(r) + \rho_{CDgal}(r) \tag{5.35}$$

with the density components derived from observations.

In this work, we will use Eq. (5.33) to compare the baryonic mass profile $M_{cl,EC}(r)$, estimated from observations, with the theoretical deviation from the Newtonian gravitational potential, given by the expression $-\frac{4a_1}{3G}r^2\frac{\mathrm{d}\Phi_C}{\mathrm{d}r}(r)$. Our goal is to reproduce the observed mass profiles for a sample of galaxy clusters.

5.5 Galaxy Cluster Sample

The formalism described in § 5.4 can be applied to a sample of 12 galaxy clusters. We shall use the cluster sample studied in [377, 378] which consists of 13 low-redshift clusters spanning a temperature range $0.7 \div 9.0$ keV derived from high quality *Chandra* archival data. In all these clusters, the surface brightness and the gas temperature profiles are measured out to large radii, so that mass estimates can be extended up to r_{500} or beyond.

5.5.1 Gas Density Model

The gas density distribution of the clusters in the sample is described by the analytic model proposed in [378]. Such a model modifies the classical $\beta-$model to represent the characteristic properties of the observed X-ray surface brightness profiles, i.e. the power-law-type cusps of gas density in the cluster center, instead of a flat core and the steepening of the brightness profiles at large radii. Eventually, a second $\beta-$model, with a small core radius, is added to improve the model close to the cluster cores. The analytical form for the particle emission is given by:

$$n_p n_e = n_0^2 \cdot \frac{(r/r_c)^{-\alpha}}{(1+r^2/r_c^2)^{3\beta-\alpha/2}} \cdot \frac{1}{(1+r^\gamma/r_s^\gamma)^{\varepsilon/\gamma}} + \\ + \frac{n_{02}^2}{(1+r^2/r_{c2}^2)^{3\beta_2}} \tag{5.36}$$

which can be easily converted to a mass density using the relation:

$$\rho_{gas} = n_T \cdot \mu m_p = \frac{1.4}{1.2} n_e m_p \tag{5.37}$$

where n_T is the total number density of particles in the gas. The resulting model has a large number of parameters, some of which do not have a direct physical interpretation. While this can often be inappropriate and computationally inconvenient, it suits well our case, where the main requirement is a detailed qualitative description of the cluster profiles.
In [378], Eq. (5.36) is applied to a restricted range of distances from the cluster center, i.e. between an inner cutoff r_{min}, chosen to exclude the central temperature bin ($\approx 10 \div 20$ kpc)

Table 5.1: Column 1: Cluster name. Column2: Richness. Column 3: cluster total mass. Column 4: gas mass. Column 5: galaxy mass. Column 6: cD-galaxy mass. All mass values are estimated at $r = r_{max}$. Column 7: ratio of total galaxy mass to gas mass. Column 8: minimum radius. Column 9: maximum radius.

name	R	$M_{cl,N}$ $(M_\odot)$	M_{gas} $(M_\odot)$	M_{gal} $(M_\odot)$	M_{cDgal} $(M_\odot)$	$\frac{gal}{gas}$	r_{min} (kpc)	r_{max} (kpc)
A133	0	$4.35874 \cdot 10^{14}$	$2.73866 \cdot 10^{13}$	$5.20269 \cdot 10^{12}$	$1.10568 \cdot 10^{12}$	0.23	86	1060
A262	0	$4.45081 \cdot 10^{13}$	$2.76659 \cdot 10^{12}$	$1.71305 \cdot 10^{11}$	$5.16382 \cdot 10^{12}$	0.25	61	316
A383	2	$2.79785 \cdot 10^{14}$	$2.82467 \cdot 10^{13}$	$5.88048 \cdot 10^{12}$	$1.09217 \cdot 10^{12}$	0.25	52	751
A478	2	$8.51832 \cdot 10^{14}$	$1.05583 \cdot 10^{14}$	$2.15567 \cdot 10^{13}$	$1.67513 \cdot 10^{12}$	0.22	59	1580
A907	1	$4.87657 \cdot 10^{14}$	$6.38070 \cdot 10^{13}$	$1.34129 \cdot 10^{13}$	$1.66533 \cdot 10^{12}$	0.24	563	1226
A1413	3	$1.09598 \cdot 10^{15}$	$9.32466 \cdot 10^{13}$	$2.30728 \cdot 10^{13}$	$1.67345 \cdot 10^{12}$	0.26	57	1506
A1795	2	$5.44761 \cdot 10^{14}$	$5.56245 \cdot 10^{13}$	$4.23211 \cdot 10^{12}$	$1.93957 \cdot 10^{12}$	0.11	79	1151
A1991	1	$1.24313 \cdot 10^{14}$	$1.00530 \cdot 10^{13}$	$1.24608 \cdot 10^{12}$	$1.08241 \cdot 10^{12}$	0.23	55	618
A2029	2	$8.92392 \cdot 10^{14}$	$1.24129 \cdot 10^{14}$	$3.21543 \cdot 10^{13}$	$1.11921 \cdot 10^{12}$	0.27	62	1771
A2390	1	$2.09710 \cdot 10^{15}$	$2.15726 \cdot 10^{14}$	$4.91580 \cdot 10^{13}$	$1.12141 \cdot 10^{12}$	0.23	83	1984
MKW4	-	$4.69503 \cdot 10^{13}$	$2.83207 \cdot 10^{12}$	$1.71153 \cdot 10^{11}$	$5.29855 \cdot 10^{11}$	0.25	60	434
RXJ1159	-	$8.97997 \cdot 10^{13}$	$4.33256 \cdot 10^{12}$	$7.34414 \cdot 10^{11}$	$5.38799 \cdot 10^{11}$	0.29	64	568

where the ICM is likely to be multi-phase, and r_{det}, where the X-ray surface brightness is at least 3σ significant. We have extrapolated the above function to values outside this restricted range using the following criteria:

- for $r < r_{min}$, we have performed a linear extrapolation of the first three terms out to $r = 0$ kpc;
- for $r > r_{det}$, we have performed a linear extrapolation of the last three terms out to a distance $\bar{r}$ for which $\rho_{gas}(\bar{r}) = \rho_c$, ρ_c being the critical density of the Universe at the cluster redshift: $\rho_c = \rho_{c,0} \cdot (1+z)^3$. For radii larger than $\bar{r}$, the gas density is assumed constant at $\rho_{gas}(\bar{r})$.

We point out that, in Table 5.1, the radius limit r_{min} is almost the same as given in the previous definition. When the value given by [378] is less than the cD-galaxy radius, which is defined in the next section, we choose this last one as the lower limit. On the contrary, r_{max} is quite different from r_{det}: it is fixed by considering the higher value of temperature profile and not by imaging methods.
We then compute the gas mass $M_{gas}(r)$ and the total mass $M_{cl,N}(r)$, respectively, for all clusters in our sample, substituting Eq. (5.36) into Eqs. (5.37) and (5.31), respectively; the gas temperature profile has been described in details in § 5.5.2. The resulting mass values, estimated at $r = r_{max}$, are listed in Table 5.1.

5.5.2 Temperature Profiles

As stressed in § 5.5.1, for the purpose of this work, we need an accurate qualitative description of the radial behavior of the gas properties. Standard isothermal or polytropic models, or even the more complex one proposed in [378], do not provide a good description of the data at all radii and for all clusters in the present sample. We hence describe the gas temperature profiles using the straightforward X-ray spectral analysis results, without the introduction of any analytic model.

X-ray spectral values have been provided by A. Vikhlinin (private communication). A detailed description of the relative spectral analysis can be found in [377].

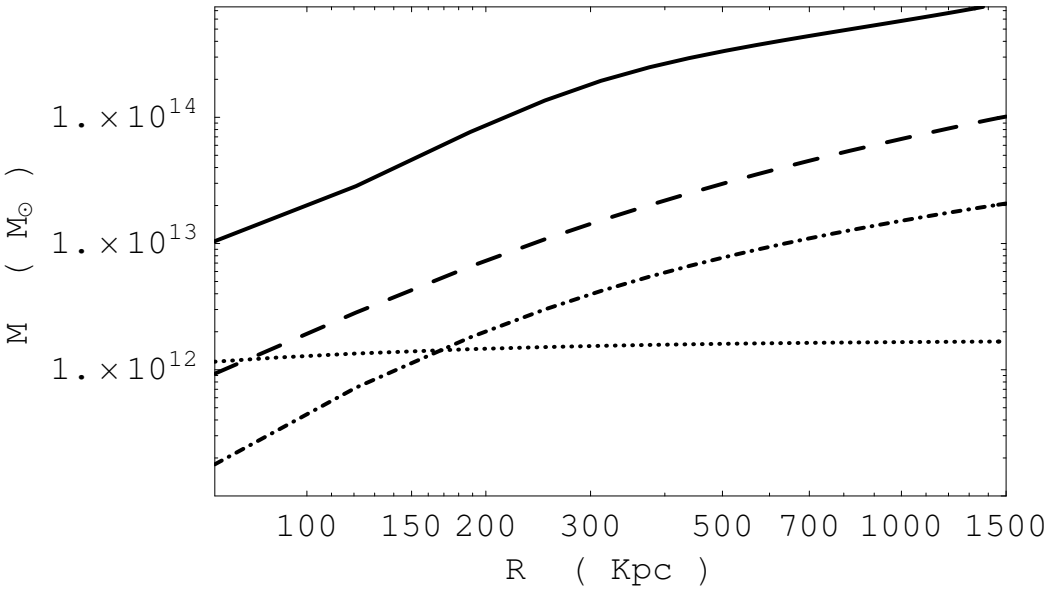

Figure 5.1: Matter components for A478: total Newtonian dynamical mass (continue line); gas mass (dashed line); galactic mass (dotted-dashed line); cD-galaxy mass (dotted line).

5.5.3 Galaxy Distribution Model

The galaxy density can be modelled as proposed by [27]. Even if the galaxy distribution is a *point*-distribution instead of a continuous function, assuming that galaxies are in equilibrium with gas, we can use a $\beta-$model, $\propto r^{-3}$, for $r < R_c$ from the cluster center, and a steeper one, $\propto r^{-2.6}$, for $r > R_c$, where R_c is the cluster core radius (its value is taken from Vikhlinin 2006). Its final expression is:

$$\rho_{gal}(r) = \begin{cases} \rho_{gal,1} \cdot \left[1 + \left(\frac{r}{R_c}\right)^2\right]^{-\frac{3}{2}} & r < R_c \\ \rho_{gal,2} \cdot \left[1 + \left(\frac{r}{R_c}\right)^2\right]^{-\frac{2.6}{2}} & r > R_c \end{cases} \tag{5.38}$$

where the constants $\rho_{gal,1}$ and $\rho_{gal,2}$ are chosen in the following way:

- [27] provides the central number density of galaxies in rich compact clusters for galaxies located within a 1.5 h^{-1}Mpc radius from the cluster center and brighter than $m_3 + 2^m$ (where m_3 is the magnitude of the third brightest galaxy): $n_{gal,0} \sim 10^3 h^3$ galaxies Mpc^{-3}. Then we fix $\rho_{gal,1}$ in the range $\sim 10^{34} \div 10^{36}$ kg/kpc^3. For any cluster obeying the condition chosen for the mass ratio gal-to-gas, we assume a typical elliptical and cD galaxy mass in the range $10^{12} \div 10^{13} M_\odot$.

- the constant $\rho_{gal,2}$ has been fixed with the only requirement that the galaxy density function has to be continuous at R_c.

We have tested the effect of varying galaxy density in the above range $\sim 10^{34} \div 10^{36}$ kg/kpc^3 on the cluster with the lowest mass, namely A262. In this case, we would expect great variations with respect to other clusters; the result is that the contribution due to galaxies and cD-galaxy gives a variation $\leq 1\%$ to the final estimate of fit parameters.
The cD galaxy density has been modelled as described in [332]; they use a Jaffe model of the form:

$$\rho_{CDgal} = \frac{\rho_{0,J}}{\left(\frac{r}{r_c}\right)^2 \left(1 + \frac{r}{r_c}\right)^2} \tag{5.39}$$

where r_c is the core radius while the central density is obtained from $M_J = \frac{4}{3}\pi R_c^3 \rho_{0,J}$. The mass of the cD galaxy has been fixed at $1.14 \times 10^{12}\ M_\odot$, with $r_c = R_e/0.76$, with $R_e = 25$ kpc being the effective radius of the galaxy. The central galaxy for each cluster in the sample is assumed to have approximately this stellar mass.

We have assumed that the total galaxy-component mass (galaxies plus cD galaxy masses) is $\approx 20 \div 25\%$ of the gas mass: in [328], the mean fraction of gas versus the total mass (with dark matter) for a cluster is estimated to be $15 \div 20\%$, while the same quantity for galaxies is $3 \div 5\%$. This means that the relative mean mass ratio gal-to-gas in a cluster is $\approx 20 \div 25\%$. We have varied the parameters $\rho_{gal,1}$, $\rho_{gal,2}$ and M_J in their previous defined ranges to obtain a mass ratio between total galaxy mass and total gas mass which lies in this range. Resulting galaxy mass values and ratios $\frac{\text{gal}}{\text{gas}}$, estimated at $r = r_{max}$, are listed in Table 5.1.

In Fig. (1), we show how each component is spatially distributed. The CD-galaxy is dominant with respect to the other galaxies only in the inner region (below 100 kpc). As already stated in § 5.5.1, cluster innermost regions have been excluded from our analysis and so the contribution due to the cD-galaxy is practically negligible in our analysis. The gas is, as a consequence, clearly the dominant visible component, starting from innermost regions out to large radii, being galaxy mass only $20 \div 25\%$ of gas mass. A similar behavior is shown by all the clusters considered in our sample.

5.5.4 Uncertainties on mass profiles

Uncertainties on the cluster total mass profiles have been estimated performing Monte-Carlo simulations [271]. We proceed to simulate temperature profiles and choose random radius-temperature values couples for each bin which we have in our temperature data given by [377]. Random temperature values have been extracted from a Gaussian distribution centered on the spectral values, and with a dispersion fixed to its 68% confidence level. For the radius, we choose a random value inside each bin. We have performed 2000 simulations for each cluster and perform two cuts on the simulated profile. First, we exclude those profiles that give an unphysical negative estimate of the mass: this is possible when our simulated couples of quantities give rise to too high temperature-gradient. After this cut, we have ≈ 1500 simulations for any cluster. Then we have ordered the resulting mass values for increasing radius values. Extreme mass estimates (outside the $10 \div 90\%$ range) are excluded from the obtained distribution, in order to avoid other high mass gradients which give rise to masses too different from real data. The resulting limits provide the errors on the total mass. Uncertainties on the electron-density profiles has not been included in the simulations, being them negligible with respect to those of the gas-temperature profiles.

Table 5.2: Column 1: Cluster name. Column 2: first derivative coefficient, a_1, of f(R) series. Column3: 1σ confidence interval for a_1. Column 4: second derivative coefficient, a_2, of f(R) series. Column 5: 1σ confidence interval for a_2. Column 6: characteristic length, L, of the modified gravitational potential, derived from a_1 and a_2. Column 7 : 1σ confidence interval for L.

name	a_1	$[a_1-1\sigma,\, a_1+1\sigma]$	a_2 (kpc^2)	$[a_2-1\sigma,\, a_2+1\sigma]$ (kpc^2)	L (kpc)	$[L-1\sigma,\, L+1\sigma]$ (kpc)
A133	0.085	[0.078, 0.091]	$-4.98\cdot10^3$	$[-2.38\cdot10^4,\, -1.38\cdot10^3]$	591.78	[323.34, 1259.50]
A262	0.065	[0.061, 0.071]	-10.63	$[-57.65,\, -3.17]$	31.40	[17.28, 71.10]
A383	0.099	[0.093, 0.108]	$-9.01\cdot10^2$	$[-4.10\cdot10^3,\, -3.14\cdot10^2]$	234.13	[142.10, 478.06]
A478	0.117	[0.114, 0.122]	$-4.61\cdot10^3$	$[-1.01\cdot10^4,\, -2.51\cdot10^3]$	484.83	[363.29, 707.73]
A907	0.129	[0.125, 0.136]	$-5.77\cdot10^3$	$[-1.54\cdot10^4,\, -2.83\cdot10^3]$	517.30	[368.84, 825.00]
A1413	0.115	[0.110, 0.119]	$-9.45\cdot10^4$	$[-4.26\cdot10^5,\, -3.46\cdot10^4]$	2224.57	[1365.40, 4681.21]
A1795	0.093	[0.084, 0.103]	$-1.54\cdot10^3$	$[-1.01\cdot10^4,\, -2.49\cdot10^2]$	315.44	[133.31, 769.17]
A1991	0.074	[0.072, 0.081]	-50.69	$[-3.42\cdot10^2,\, -13]$	64.00	[32.63, 159.40]
A2029	0.129	[0.123, 0.134]	$-2.10\cdot10^4$	$[-7.95\cdot10^4,\, -8.44\cdot10^3]$	988.85	[637.71, 1890.07]
A2390	0.149	[0.146, 0.152]	$-1.40\cdot10^6$	$[-5.71\cdot10^6,\, -4.46\cdot10^5]$	7490.80	[4245.74, 15715.60]
MKW4	0.054	[0.049, 0.060]	-23.63	$[-1.15\cdot10^2,\, -8.13]$	51.31	[30.44, 110.68]
RXJ1159	0.048	[0.047, 0.052]	-18.33	$[-1.35\cdot10^2,\, -4.18]$	47.72	[22.86, 125.96]

5.5.5 Fitting the mass profiles

In the above sections, we have shown that, with the aid of X-ray observations, modelling theoretically the galaxy distribution and using Eq. (5.33), we obtain an estimate of the baryonic content of clusters.
We have hence performed a best-fit analysis of the theoretical Eq. (5.33)

$$M_{bar,th}(r)=\frac{4a_1}{3}\left[-\frac{kT(r)}{\mu m_p G}r\left(\frac{d\ln\rho_{gas}(r)}{d\ln r}+\frac{d\ln T(r)}{d\ln r}\right)\right]+ -\frac{4a_1}{3G}r^2\frac{\mathrm{d}\Phi_C}{\mathrm{d}r}(r) \tag{5.40}$$

versus the observed mass contributions

$$M_{bar,obs}(r)=M_{gas}(r)+M_{gal}(r)+M_{CDgal}(r) \tag{5.41}$$

Since not all the data involved in the above estimate have measurable errors, we cannot perform an *exact* χ-square minimization: Actually, we can minimize the quantity:

$$\chi^2=\frac{1}{N-n_p-1}\cdot\sum_{i=1}^{N}\frac{(M_{bar,obs}-M_{bar,theo})^2}{M_{bar,theo}} \tag{5.42}$$

where N is the number of data and $n_p=2$ the free parameters of the model. We minimize the χ-square using the Markov Chain Monte Carlo Method (MCMC). For each cluster, we have run various chains to set the best parameters of the used algorithm, the Metropolis-Hastings one: starting from an initial parameter vector $\mathbf{p}$ (in our case $\mathbf{p}=(a_1,a_2)$), we generate a new trial point $\mathbf{p}'$ from a tested proposal density $q(\mathbf{p}',\mathbf{p})$, which represents the conditional probability to get $\mathbf{p}'$, given $\mathbf{p}$. This new point is accepted with probability

$$\alpha(\mathbf{p},\mathbf{p}')=min\left\{1,\frac{L(\mathbf{d}|\mathbf{p}')P(\mathbf{p}')q(\mathbf{p}',\mathbf{p})}{L(\mathbf{d}|\mathbf{p})P(\mathbf{p})q(\mathbf{p},\mathbf{p}')}\right\}$$

where $\mathbf{d}$ are the data, $L(\mathbf{d}|\mathbf{p}') \propto \exp(-\chi^2/2)$ is the likelihood function, $P(\mathbf{p})$ is the prior on the parameters. In our case, the prior on the fit parameters is related to Eq. (5.13): being L a length, we need to force the ratio a_1/a_2 to be positive. The proposal density is Gaussian symmetric with respect of the two vectors $\mathbf{p}$ and $\mathbf{p}'$, namely $q(\mathbf{p}, \mathbf{p}') \propto \exp(-\Delta p^2/2\sigma^2)$, with $\Delta\mathbf{p} = \mathbf{p} - \mathbf{p}'$; we decide to fix the dispersion σ of any trial distribution of parameters equal to 20% of trial a_1 and a_2 at any step. This means that the parameter α reduces to the ratio between the likelihood functions.

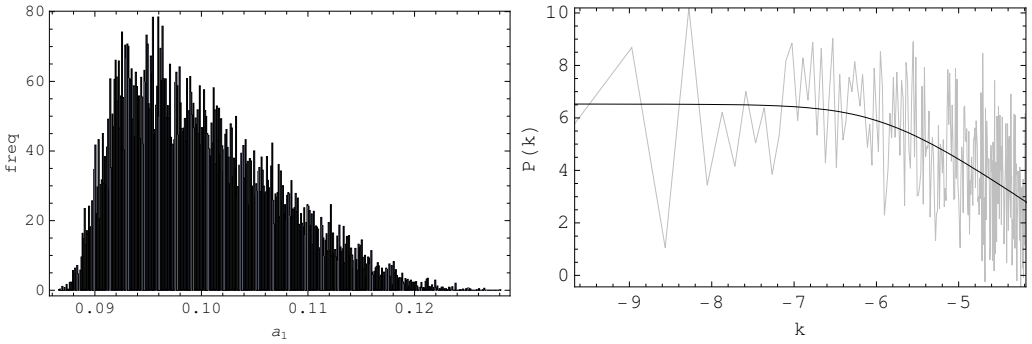

Figure 5.2: Left panel: histogram of the sample points for parameter a_1 in Abell 383 coming out the MCMC implementation used to estimate best fit values and errors for our fitting procedure as described in § 5.5.5. Binning (horizontal axis) and relative frequencies (vertical axis) are given by automatic procedure from Mathematica6.0. Right panel: power spectrum test on sample chain for parameter a_1 using the method described in § 5.5.5. Black line is the logarithm of the analytical template Eq. (5.45) for power spectrum; gray line is the discrete power spectrum obtained using Eq. (5.43) - (5.44).

We have run one chain of 10^5 points for every cluster; the convergence of the chains has been tested using the power spectrum analysis from [138]. The key idea of this method is, at the same time, simple and powerful: if we take the *power spectra* of the MCMC samples, we will have a great correlation on small scales but, when the chain reaches convergence, the spectrum becomes flat (like a white noise spectrum); so that, by checking the spectrum of just one chain (instead of many parallel chains as in Gelmann-Rubin test) will be sufficient

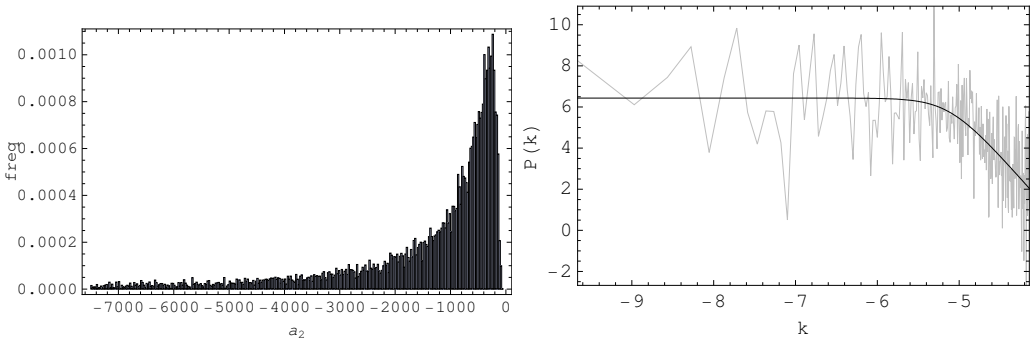

Figure 5.3: Abell 383: histogram (left) and power spectrum test (right) on sample chain for parameter a_2.

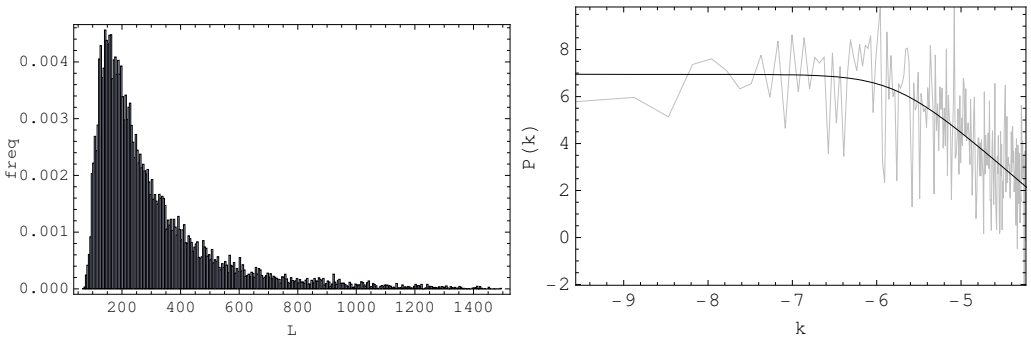

Figure 5.4: Abell 383: histogram (left) and power spectrum test (right) on sample chain for parameter L.

to assess the reached convergence. Remanding to [138] for a detailed discussion of all the mathematical steps. Here we calculate the discrete power spectrum of the chains:

$$P_j = |a_N^j|^2 \tag{5.43}$$

with

$$a_N^j = \frac{1}{\sqrt{N}} \sum_{n=0}^{N-1} x_n \exp\left[i \frac{2\pi j}{N} n\right] \tag{5.44}$$

where N and x_n are the length and the element of the sample from the MCMC, respectively, $j = 1, \ldots, \frac{N}{2} - 1$. The wavenumber k_j of the spectrum is related to the index j by the relation $k_j = \frac{2\pi j}{N}$. Then we fit it with the analytical template:

$$P(k) = P_0 \frac{(k^*/k)^\alpha}{1 + (k^*/k)^\alpha} \tag{5.45}$$

or in the equivalent logarithmic form:

$$\ln P_j = \ln P_0 + \ln\left[\frac{(k^*/k_j)^\alpha}{1 + (k^*/k_j)^\alpha}\right] - \gamma + r_j \tag{5.46}$$

where $\gamma = 0.57216$ is the Euler-Mascheroni number and r_j are random measurement errors with $< r_j >= 0$ and $< r_i r_j >= \delta_{ij}\pi^2/6$. From the fit, we estimate the two fundamental parameters, P_0 and j^* (the index corresponding to k^*). The first one is the value of the power spectrum extrapolated for $k \to 0$ and, from it, we can derive the convergence ratio from $r \approx \frac{P_0}{N}$; if $r < 0.01$, we can assume that the convergence is reached. The second parameter is related to the turning point from a power-law to a flat spectrum. It has to be > 20 in order to be sure that the number of points in the sample, coming from the convergence region, are more than the noise points. If these two conditions are verified for all the parameters, then the chain has reached the convergence and the statistics derived from MCMC well describes the underlying probability distribution (typical results are shown in Figs. (2)-(3)). Following [138] prescriptions, we perform the fit over the range $1 \leq j \leq j_{max}$, with $j_{max} \sim 10j^*$, where a first estimation of j^* can be obtained from a fit with $j_{max} = 1000$, and then performing a second iteration in order to have a better estimation of it. Even if the convergence is achieved after few thousand steps of the chain, we have decided to run longer chains of 10^5 points

to reduce the noise from the histograms and avoid under- or over- estimations of errors on the parameters. The $i-\sigma$ confidence levels are easily estimated deriving them from the final sample the 15.87-th and 84.13-th quantiles (which define the 68% confidence interval) for $i=1$, the 2.28-th and 97.72-th quantiles (which define the 95% confidence interval) for $i=2$ and the 0.13-th and 99.87-th quantiles (which define the 99% confidence interval) for $i=3$.

After the description of the method, let us now comment on the achieved results.

5.6 Results

The numerical results of our fitting analysis are summarized in Table 2; we give the best fit values of the independent fitting parameters a_1 and a_2, and of the gravitational length L, considered as a function of the previous two quantities. In Figs. (3)- (5), we give the typical results of fitting, with histograms and power spectrum of samples derived by the MCMC, to assess the reached convergence (flat spectrum at large scales).

The goodness and the properties of the fits are shown in Figs. (6)- (17). The main property of our results is the presence of a *typical scale* for each cluster above which our model works really good (typical relative differences are less than 5%), while for lower scale there is a great difference. It is possible to see, by a rapid inspection, that this turning-point is located at a radius ≈ 150 kpc. Except for very large clusters, it is clear that this value is independent of the cluster, being approximately the same for any member of the considered sample.

There are two main independent explanations that could justify this trend: limits due to a break in the state of hydrostatic equilibrium or limits in the series expansion of the $f(R)$-models.

If the hypothesis of hydrostatic equilibrium is not correct, then we are in a regime where the fundamental relations Eqs. (5.23)- (5.28), are not working. As discussed in [377], the central (70 kpc) region of every cluster is strongly affected by radiative cooling and thus it cannot directly be related to the depth of the cluster potential well. This means that, in this region, the gas is not in hydrostatic equilibrium but in a multi-phase, turbulent state, mainly driven by some astrophysical, non-gravitational interaction. In this case, the gas cannot be used as a good standard tracer.

We have also to consider another limit of our modelling: the requirement that the $f(R)$-function is Taylor expandable. The corrected gravitational potential which we have considered is derived in the weak field limit, which means

$$R - R_0 << \frac{a_1}{a_2} \tag{5.47}$$

where R_0 is the background value of the curvature. If this condition is not satisfied, the approach does not work (see [86] for a detailed discussion of this point). Considering that a_1/a_2 has the dimension of $length^{-2}$ this condition defines the *length scale* where our series approximation can work. In other words, this indicates the limit in which the model can be compared with data.

For the considered sample, the fit of the parameters a_1 and a_2, spans the length range $\{19; 200\}$ kpc (except for the biggest cluster). It is evident that every galaxy cluster has a *proper* gravitational length scale. It is worth noticing that a similar situation, but at completely different scales, has been found out for low surface brightness galaxies modelled by $f(R)$-gravity [84].

Considering the data at our disposal and the analysis which we have performed, it is not possible to quantify exactly the quantitative amount of these two different phenomena (i.e.

the radiative cooling and the validity of the weak field limit). However, they are not mutually exclusive but should be considered in details in view of a more refined modelling [2].

Similar issues are present also in [56]: they use the the Metric - Skew - Tensor - Gravity (MSTG) as a generalization of the Einstein General Relativity and derive the gas mass profile of a sample of clusters with gas being the only baryonic component of the clusters. They consider some clusters included in our sample (in particular, A133, A262, A478, A1413, A1795, A2029, MKW4) and they find the same different trend for $r \leq 200$ kpc, even if with a different behavior with respect of us: our model gives lower values than X-ray gas mass data while their model gives higher values with respect to X-ray gas mass data. This stresses the need for a more accurate modelling of the gravitational potential.

However, our goal is to show that potential (5.12) is suitable to fit the mass profile of galaxy clusters and that it comes from a self-consistent theory.

In general, it can be shown that the weak field limit of extended theories of gravity has Yukawa-like corrections [355, 206]. Specifically, given theory of gravity of order $(2n+2)$, the Yukawa corrections to the Newtonian potential are n [306]. This means that if the effective Lagrangian of the theory is

$$\mathcal{L} = f(R, \Box R, ..\Box^k R, ..\Box^n R)\sqrt{-g} \tag{5.48}$$

we have

$$\phi(r) = -\frac{GM}{r}\left[1 + \sum_{k=1}^{n} \alpha_k e^{-r/L_k}\right] . \tag{5.49}$$

Standard General Relativity, where Yukawa corrections are not present, is recovered for $n = 0$ (second order theory) while the $f(R)$-gravity is obtained for $n = 1$ (fourth-order theory). Any $\Box$ operator introduces two further derivation orders in the field equations. This kind of Lagrangian comes out when quantum field theory is formulated on curved spacetime [44]. In the series (5.49), G is the value of the gravitational constant considered at infinity, L_k is the interaction length of the k-th component of the non-Newtonian corrections. The amplitude α_k of each component is normalized to the standard Newtonian term; the sign of α_k tells us if the corrections are attractive or repulsive (see [388] for details). Moreover, the variation of the gravitational coupling is involved. In our case, we are taking into account only the first term of the series. It is the the leading term. Let us rewrite (5.12) as

$$\phi(r) = -\frac{GM}{r}\left[1 + \alpha_1 e^{-r/L_1}\right] . \tag{5.50}$$

The effect of non-Newtonian term can be parameterized by $\{\alpha_1, L_1\}$ which could be a useful parameterisation which respect to our previous $\{a_1, a_2\}$ or $\{G_{eff}, L\}$ with $G_{eff} = 3G/(4a_1)$. For large distances, where $r \gg L_1$, the exponential term vanishes and the gravitational coupling is G. If $r \ll L_1$, the exponential becomes 1 and, by differentiating Eq.(5.50) and comparing with the gravitational force measured in laboratory, we get

$$G_{lab} = G\left[1 + \alpha_1\left(1 + \frac{r}{L_1}\right)e^{-r/L_1}\right] \simeq G(1 + \alpha_1) , \tag{5.51}$$

[2] Other secondary phenomena as cooling flows, merger and asymmetric shapes have to be considered in view of a detailed modelling of clusters. However, in this work, we are only interested to show that extended gravity could be a valid alternative to dark matter in order to explain the cluster dynamics.

where $G_{lab} = 6.67 \times 10^{-8}$ g^{-1}cm^{3}s^{-2} is the usual Newton constant measured by Cavendish-like experiments. Of course, G and G_{lab} coincide in the standard Newtonian gravity. It is worth noticing that, asymptotically, the inverse square law holds but the measured coupling constant differs by a factor $(1 + \alpha_1)$. In general, any correction introduces a characteristic length that acts at a certain scale for the self-gravitating systems as in the case of galaxy cluster which we are examining here. The range of L_k of the kth-component of non-Newtonian force can be identified with the mass m_k of a pseudo-particle whose effective Compton's length can be defined as

$$L_k = \frac{\hbar}{m_k c}\,. \tag{5.52}$$

The interpretation of this fact is that, in the weak energy limit, fundamental theories which attempt to unify gravity with the other forces introduce, in addition to the massless graviton, particles *with mass* which also carry the gravitational interaction [173]. See, in particular, [90] for $f(R)$-gravity. These masses are related to effective length scales which can be parameterized as

$$L_k = 2 \times 10^{-5} \left(\frac{1\,\text{eV}}{m_k}\right) \text{cm}\,. \tag{5.53}$$

There have been several attempts to experimentally constrain L_k and α_k (and then m_k) by experiments on scales in the range $1\,\text{cm} < r < 1000\,\text{km}$, using different techniques [157, 348, 143]. In this case, the expected masses of particles which should carry the additional gravitational force are in the range $10^{-13}\text{eV} < m_k < 10^{-5}\,\text{eV}$. The general outcome of these experiments, even retaining only the term $k = 1$, is that *geophysical window* between the laboratory and the astronomical scales has to be taken into account. In fact, the range

$$|\alpha_1| \sim 10^{-2}\,, \qquad L_1 \sim 10^2 \div 10^3\ \text{m}\,, \tag{5.54}$$

is not excluded at all in this window. An interesting suggestion has been given by Fujii [163], which proposed that the exponential deviation from the Newtonian standard potential could arise from the microscopic interaction which couples the nuclear isospin and the baryon number.

The astrophysical counterparts of these non-Newtonian corrections seemed ruled out till some years ago due to the fact that experimental tests of General Relativity seemed to predict the Newtonian potential in the weak energy limit, "inside" the Solar System. However, as it has been shown, several alternative theories seem to evade the Solar System constraints (see [90] and the reference therein for recent results) and, furthermore, indications of an anomalous, long–range acceleration revealed from the data analysis of Pioneer 10/11, Galileo, and Ulysses spacecrafts (which are now almost outside the Solar System) makes these Yukawa–like corrections come again into play [19]. Besides, it is possible to reproduce phenomenologically the flat rotation curves of spiral galaxies considering the values

$$\alpha_1 = -0.92\,, \qquad L_1 \sim 40\ \text{kpc}\,. \tag{5.55}$$

The main hypothesis of this approach is that the additional gravitational interaction is carried by some ultra-soft boson whose range of mass is $m_1 \sim 10^{-27} \div 10^{-28}$eV. The action of this boson becomes efficient at galactic scales without the request of enormous amounts of dark matter to stabilize the systems [322].

Furthermore, it is possible to use a combination of two exponential correction terms and give a detailed explanation of the kinematics of galaxies and galaxy clusters, again without dark matter model [143].

It is worthwhile to note that both the spacecrafts measurements and galactic rotation curves indications come from "outside" the usual Solar System boundaries used up to now

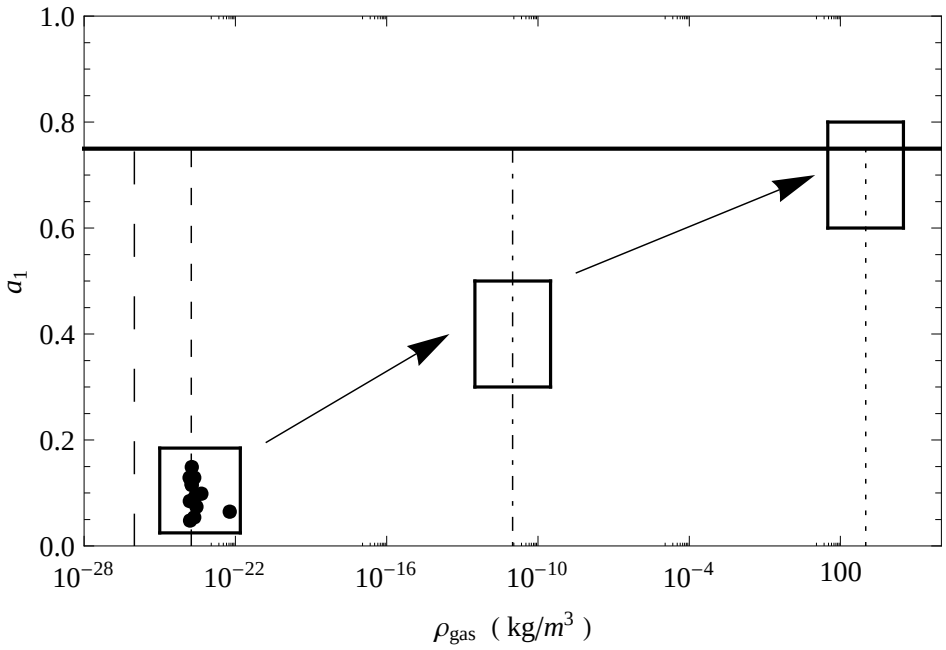

Figure 5.5: Density vs a_1: predictions on the behavior of a_1. The horizontal black bold line indicates the Newtonian-limit, $a_1 \to 3/4$ which we expect to be realized on scales comparable with Solar System. Vertical lines indicate typical approximated values of matter density (without dark matter) for different gravitational structures: universe (large dashed) with critical density $\rho_{crit} \approx 10^{-26}\ \mathrm{kg/m^3}$; galaxy clusters (short dashed) with $\rho_{cl} \approx 10^{-23}\ \mathrm{kg/m^3}$; galaxies (dot-dashed) with $\rho_{gal} \approx 10^{-11}\ \mathrm{kg/m^3}$; sun (dotted) with $\rho_{sun} \approx 10^{3}\ \mathrm{kg/m^3}$. Arrows and boxes show the predicted trend for a_1.

to test General Relativity. However, the above results *do not come* from any fundamental theory to explain the outcome of Yukawa corrections. In their contexts, these terms are phenomenological.

Another important remark in this direction deserves the fact that some authors [248] interpret also the experiments on cosmic microwave background like the experiment BOOMERANG and WMAP [119, 349] in the framework of *modified Newtonian dynamics* again without invoking any dark matter model.

All these facts point towards the line of thinking that also corrections to the standard gravity have to be seriously taken into account beside dark matter searches.

In our case, the parameters $a_{1,2}$, which determine the gravitational correction and the gravitational coupling, come out "directly" from a field theory with the only requirement that the effective action of gravity could be more general than the Hilbert-Einstein theory $f(R) = R$. This main hypothesis comes from fundamental physics motivations due to the fact that any unification scheme or quantum field theory on curved space have to take into account higher order terms in curvature invariants [44]. Besides, several recent results point out that such corrections have a main role also at astrophysical and cosmological scales. For a detailed discussion, see [273, 88, 149].

With this philosophy in mind, we have plotted the trend of a_1 as a function of the density in

Fig.5.5. As one can see, its values are strongly constrained in a narrow region of the parameter space, so that a_1 can be considered a "tracer" for the size of gravitational structures. The value of a_1 range between $\{0.8 \div 0.12\}$ for larger clusters and $\{0.4 \div 0.6\}$ for poorer structures (i.e. galaxy groups like MKW4 and RXJ1159). We expect a particular trend when applying the model to different gravitational structures. In Fig. 5.5, we give characteristic values of density which range from the biggest structure, the observed Universe (large dashed vertical line), to the smallest one, the Sun (vertical dotted line), through intermediate steps like clusters (vertical short dashed line) and galaxies (vertical dot-dashed line). The bold black horizontal line represents the Newtonian limit $a_1 = 3/4$ and the boxes indicate the possible values of a_1 that we obtain by applying our theoretical model to different structures.

Similar considerations hold also for the characteristic gravitational length L directly related to both a_1 and a_2. The parameter a_2 shows a very large range of variation $\{-10^6 \div -10\}$ with respect to the density (and the mass) of the clusters. The value of L changes with the sizes of gravitational structure (see Fig. 5.6), so it can be considered, beside the Schwarzschild radius, a sort of additional gravitational radius. Particular care must be taken when considering Abell 2390, which shows large cavities in the X-ray surface brightness distribution, and whose central region, highly asymmetric, is not expected to be in hydrostatic equilibrium. All results at small and medium radii for this cluster could hence be strongly biased by these effects [378]; the same will hold for the resulting exceptionally high value of L. Fig. 5.6 shows how observational properties of the cluster, which well characterize its gravitational potential (such as the average temperature and the total cluster mass within r_{500}, plotted in the left and right panel, respectively), well correlate with the characteristic gravitational length L.

For clusters, we can define a gas-density-weighted and a gas-mass-weighted mean, both depending on the series parameters $a_{1,2}$. We have:

$$\begin{aligned} < L >_\rho &= 318 \text{ kpc} \qquad < a_2 >_\rho = -3.40 \cdot 10^4 \\ < L >_M &= 2738 \text{ kpc} \qquad < a_2 >_M = -4.15 \cdot 10^5 \end{aligned} \tag{5.56}$$

It is straightforward to note the correlation with the sizes of the cluster cD-dominated-central region and the "gravitational" interaction length of the whole cluster. In other words, the parameters $a_{1,2}$, directly related to the first and second derivative of a given analytic $f(R)$-model determine the characteristic sizes of the self gravitating structures.

5.7 What have we learnt from clusters?

In this work we have investigated the possibility that the high observational mass-to-light ratio of galaxy clusters could be addressed by $f(R)$- gravity without assuming huge amounts of dark matter. We point out that this proposal comes out from the fact that, up to now, no definitive candidate for dark-matter has been observed at fundamental level and then alternative solutions to the problem should be viable. Furthermore, several results in $f(R)$-gravity seem to confirm that valid alternatives to ΛCDM can be achieved in cosmology. Besides, as discussed in the Introduction, the rotation curves of spiral galaxies can be explained in the weak field limit of $f(R)$-gravity. Results of our analysis go in this direction.

We have chosen a sample of relaxed galaxy clusters for which accurate spectroscopic temperature measurements and gas mass profiles are available. For the sake of simplicity, and considered the sample at our disposal, every cluster has been modelled as a self bound gravitational system with spherical symmetry and in hydrostatic equilibrium. The mass distribution has been described by a corrected gravitational potential obtained from a generic analytic

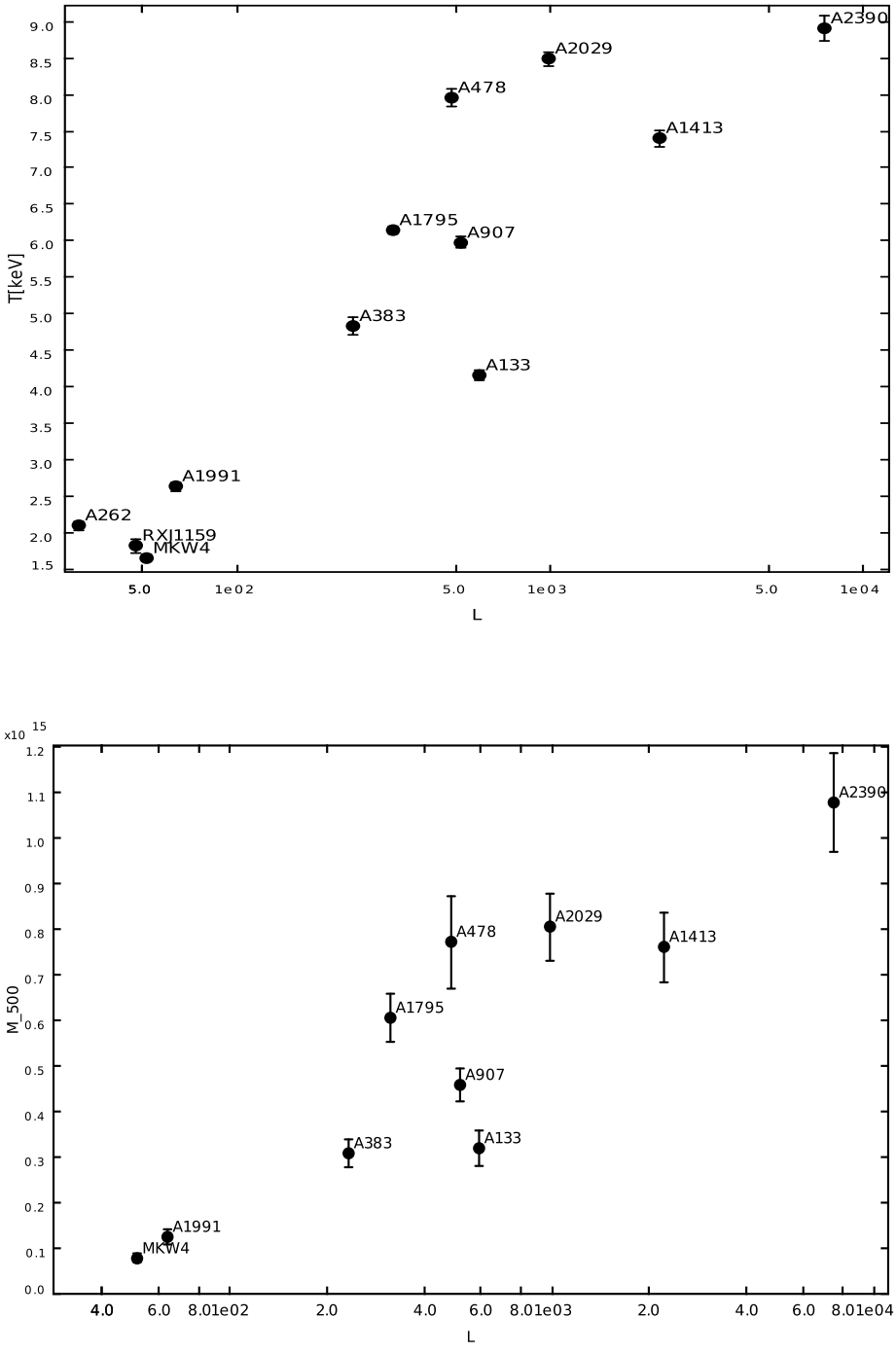

Figure 5.6: Single temperature fit to the total cluster spectrum (left panel) and total cluster mass within r_{500} (given as a function of $M_\odot$) (right panel) are plotted as a function of the characteristic gravitational length L. Temperature and mass values are from [378].

$f(R)$-theory. In fact, as soon as $f(R) \neq R$, Yukawa-like exponential corrections emerge in the weak field limit while the standard Newtonian potential is recovered only for $f(R) = R$, the Hilbert-Einstein theory.

Our goal has been to analyze if the dark-matter content of clusters can be addressed by these correction potential terms. As discussed in detail in the previous section and how it is possible to see by a rapid inspection of Figs. **??**- **??**, all the clusters of the sample are consistent with the proposed model at 1σ confidence level. This shows, at least *qualitatively*, that the high mass-to-light ratio of clusters can be explained by using a modified gravitational potential. The good agreement is achieved on distance scales starting from 150 kpc up to 1000 kpc. The differences observed at smaller scales can be ascribed to non-gravitational phenomena, such as cooling flows, or to the fact that the gas mass is not a good tracer at this scales. The remarkable result is that we have obtained a consistent agreement with data only using the corrected gravitational potential in a large range of radii. In order to put in evidence this trend, we have plotted the baryonic mass vs radii considering, for each cluster, the scale where the trend is clearly evident.

In our knowledge, the fact that $f(R)$-gravity could work at these scales has been only supposed but never achieved by a direct fitting with data (see [235] for a review). Starting from the series coefficients a_1 and a_2, it is possible to state that, at cluster scales, two characteristic sizes emerge from the weak field limit of the theory. However, at smaller scales, e.g. Solar System scales, standard Newtonian gravity has to be dominant in agreement with observations.

In conclusion, if our considerations are right, gravitational interaction depends on the scale and the *infrared limit* is led by the series coefficient of the considered effective gravitational Lagrangian. Roughly speaking, we expect that starting from cluster scale to galaxy scale, and then down to smaller scales as Solar System or Earth, the terms of the series lead the clustering of self-gravitating systems beside other non-gravitational phenomena. In our case, the Newtonian limit is recovered for $a_1 \to 3/4$ and $L(a_1, a_2) \gg r$ at small scales and for $L(a_1, a_2) \ll r$ at large scales. In the first case, the gravitational coupling has to be redifined, in the second $G_\infty \simeq G$. In these limits, the linear Ricci term is dominant in the gravitational Lagrangian and the Newtonian gravity is restored [306]. Reversing the argument, this could be the starting point to achieve a theory capable of explaining the strong segregation in masses and sizes of gravitationally-bound systems.

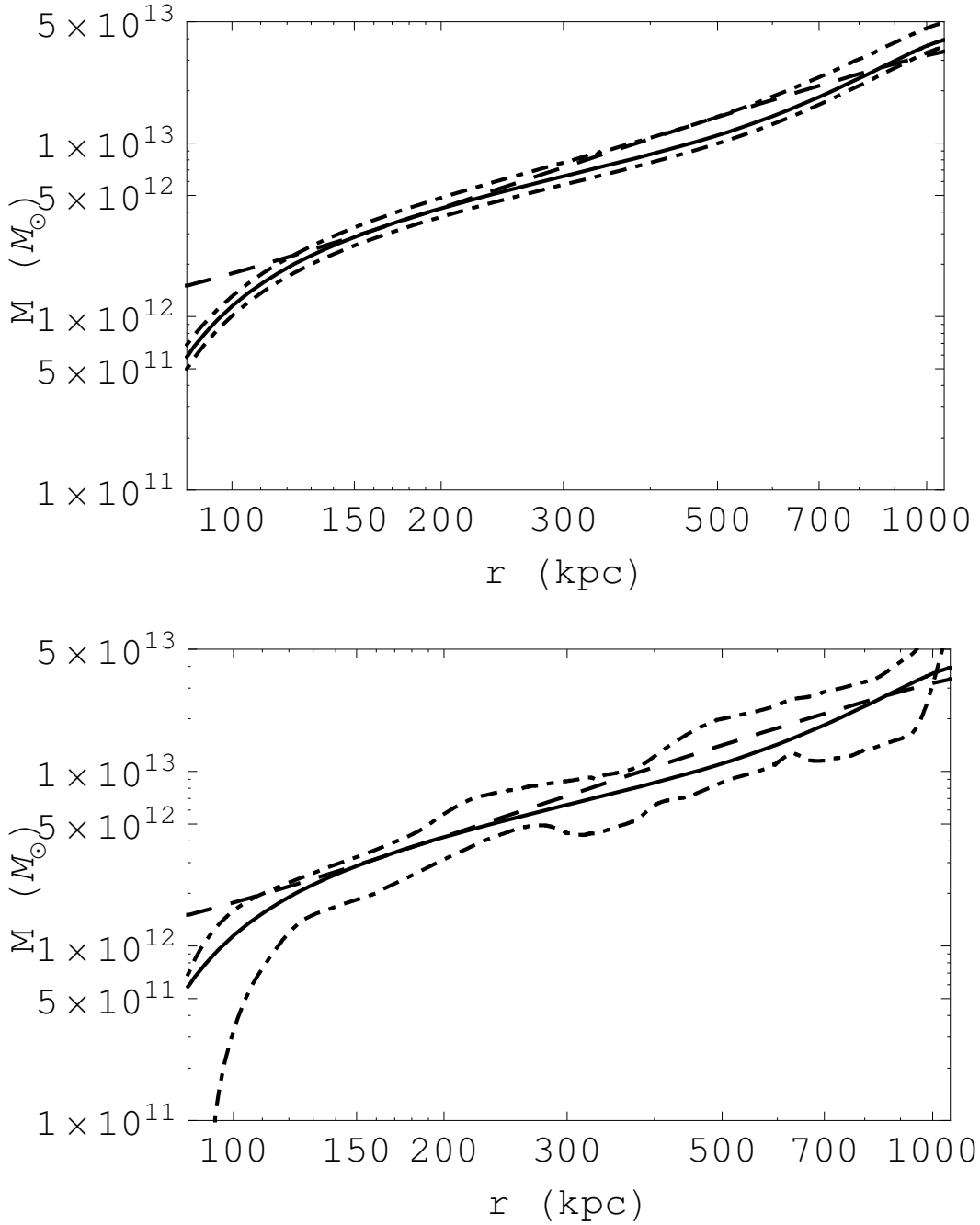

Figure 5.7: Baryonic mass vs radii for Abell A133. Dashed line is the experimental-observed estimation Eq. (5.41) of baryonic matter component (i.e. gas, galaxies and cD-galaxy); solid line is the theoretical estimation Eq. (5.40) for baryonic matter component. Dotted lines are the 1-σ confidence levels given by errors on fitting parameters in the left panel; and from fitting parameter plus statistical errors on mass profiles as discussed in § 5.5.4 in the right panel.

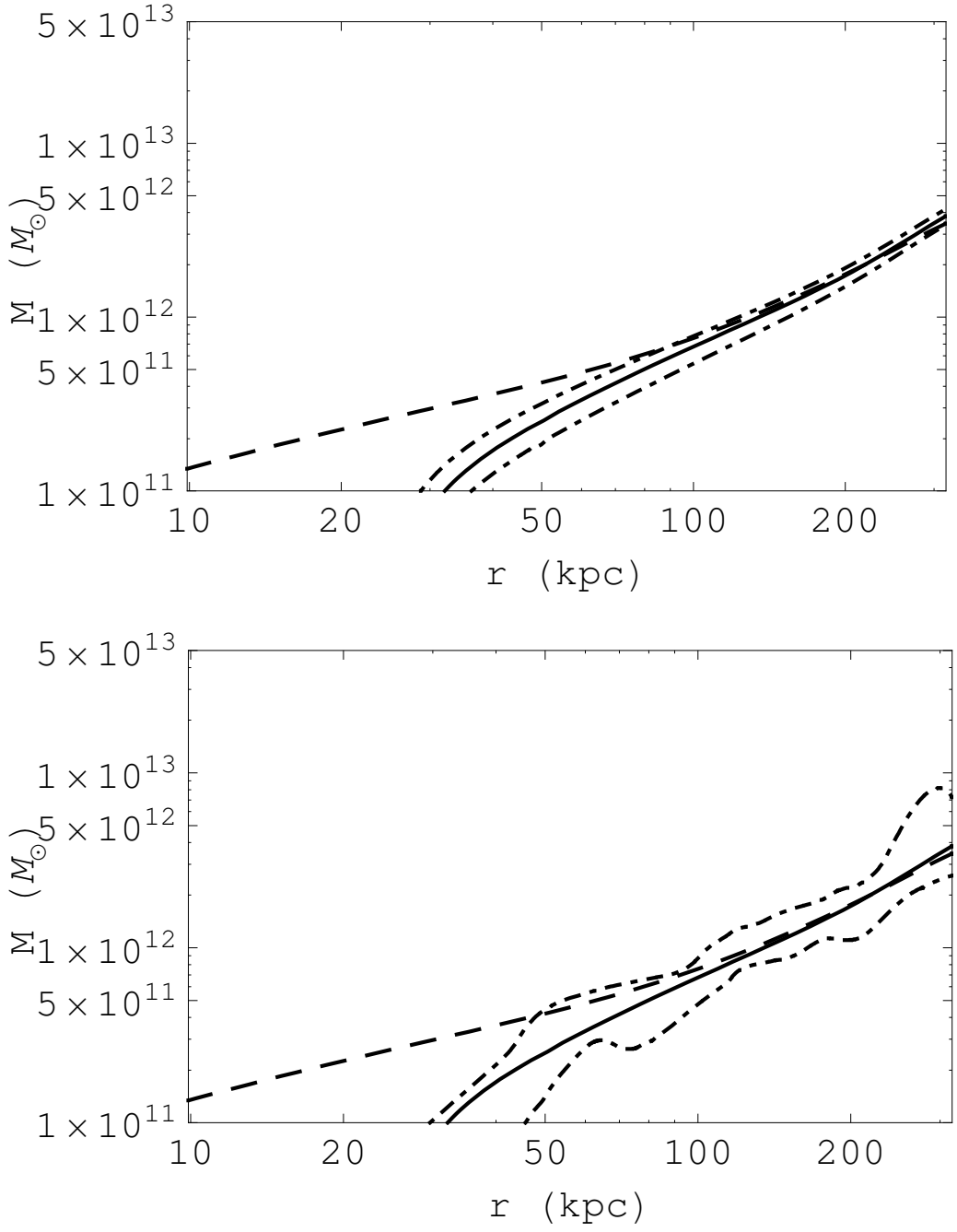

Figure 5.8: Same of Fig.2 but for cluster Abell 262.

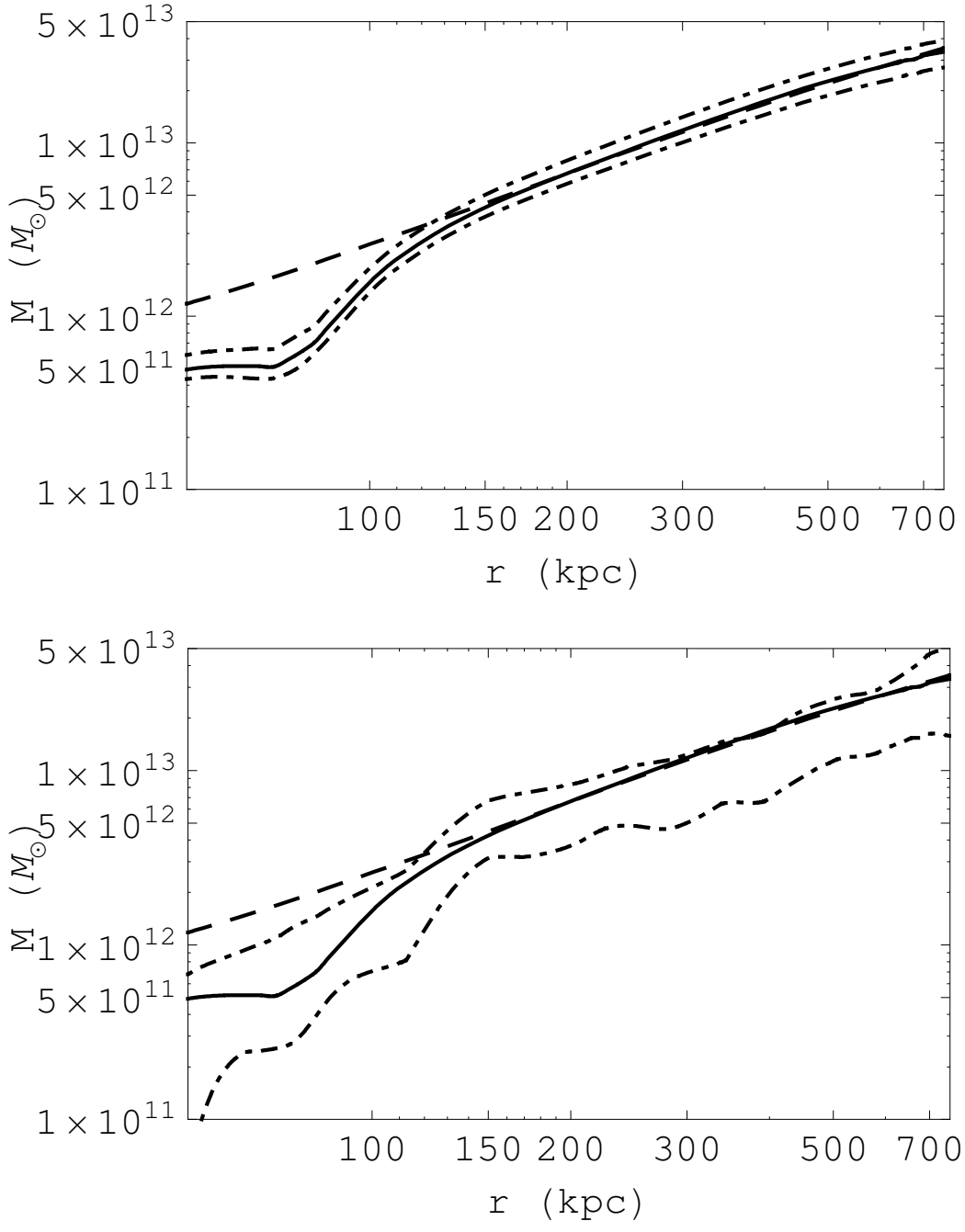

Figure 5.9: Same of Fig.2 but for cluster Abell 383.

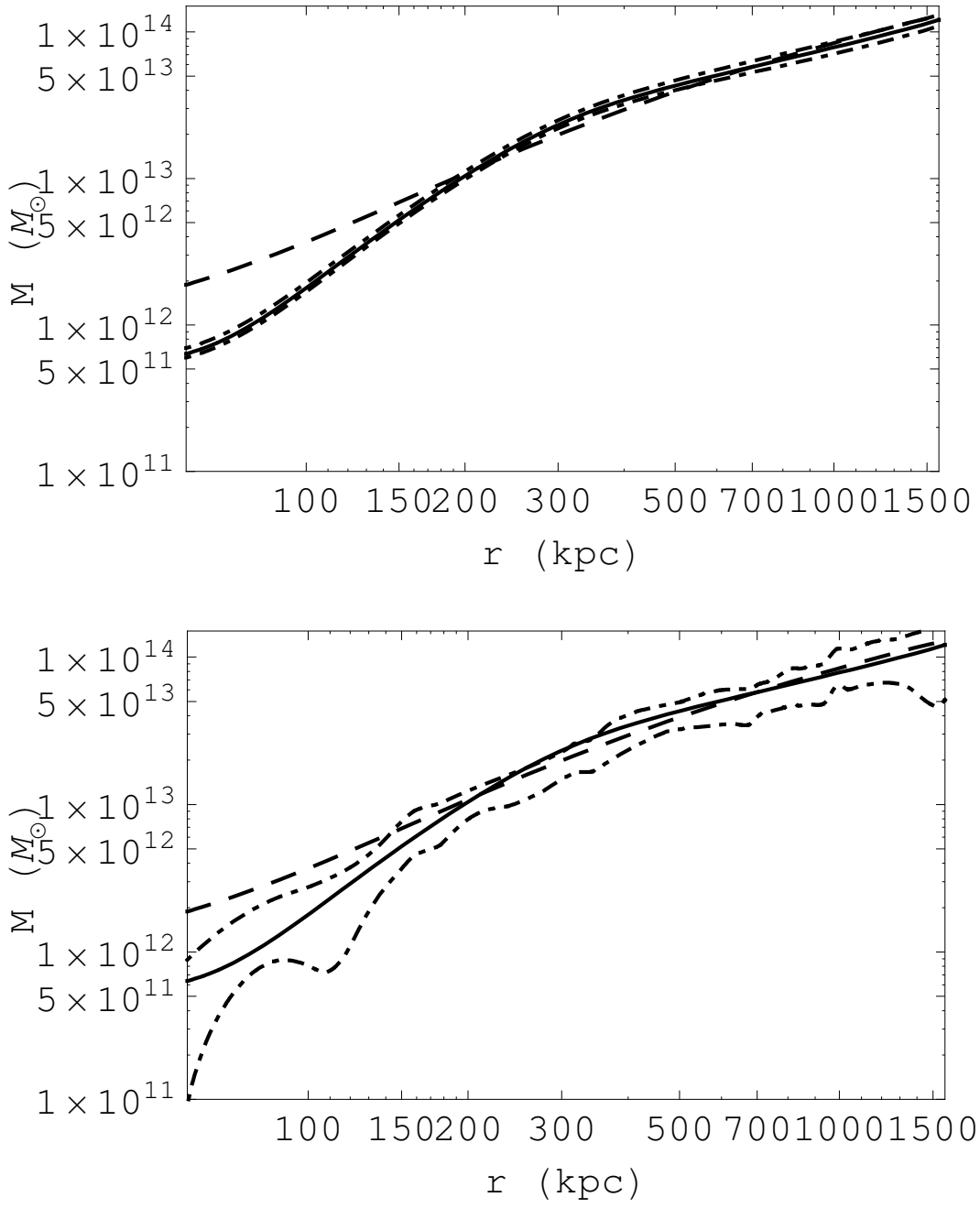

Figure 5.10: Same of Fig.2 but for cluster Abell 478.

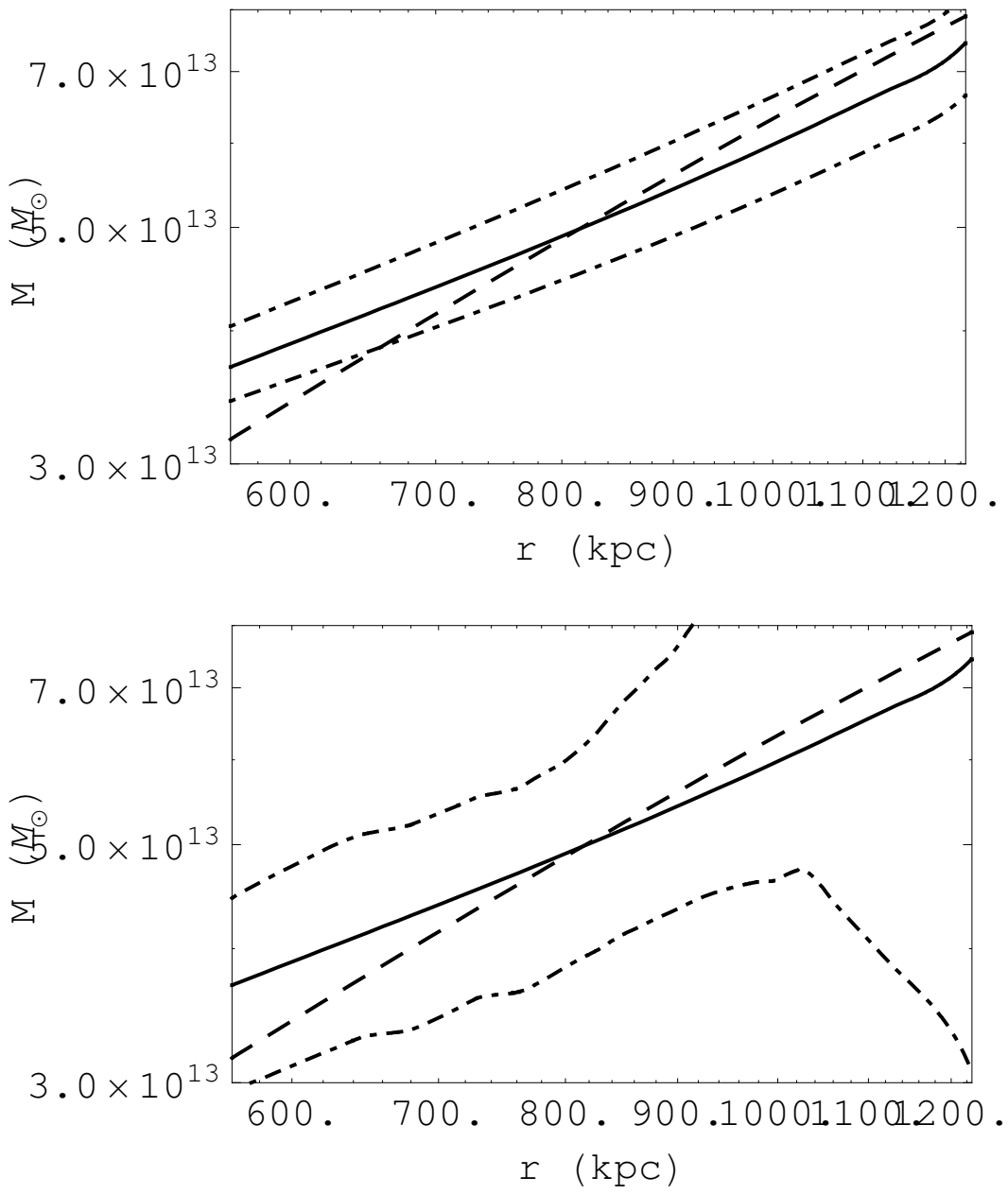

Figure 5.11: Same of Fig.2 but for cluster Abell 907.

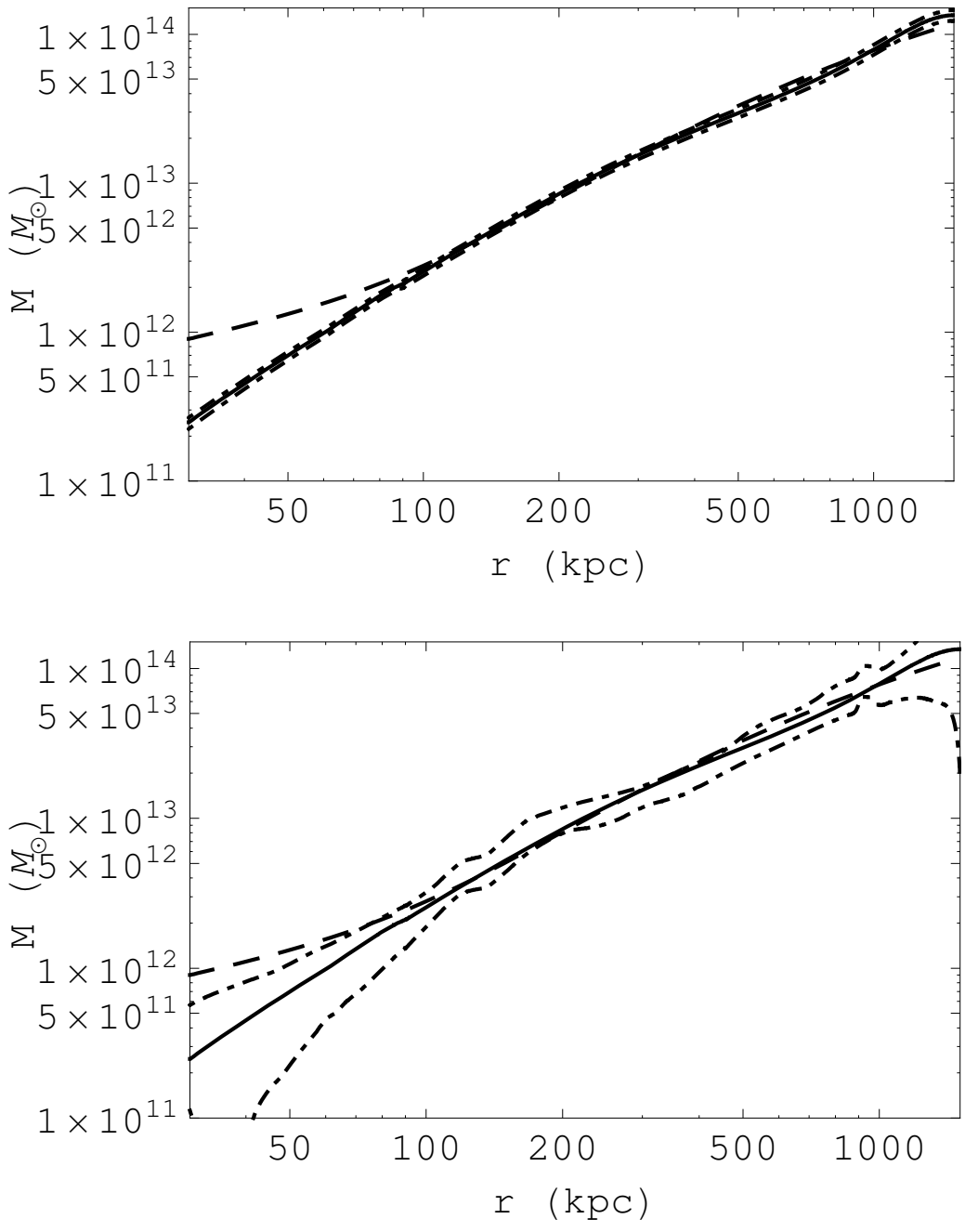

Figure 5.12: Same of Fig.2 but for cluster Abell 1413.

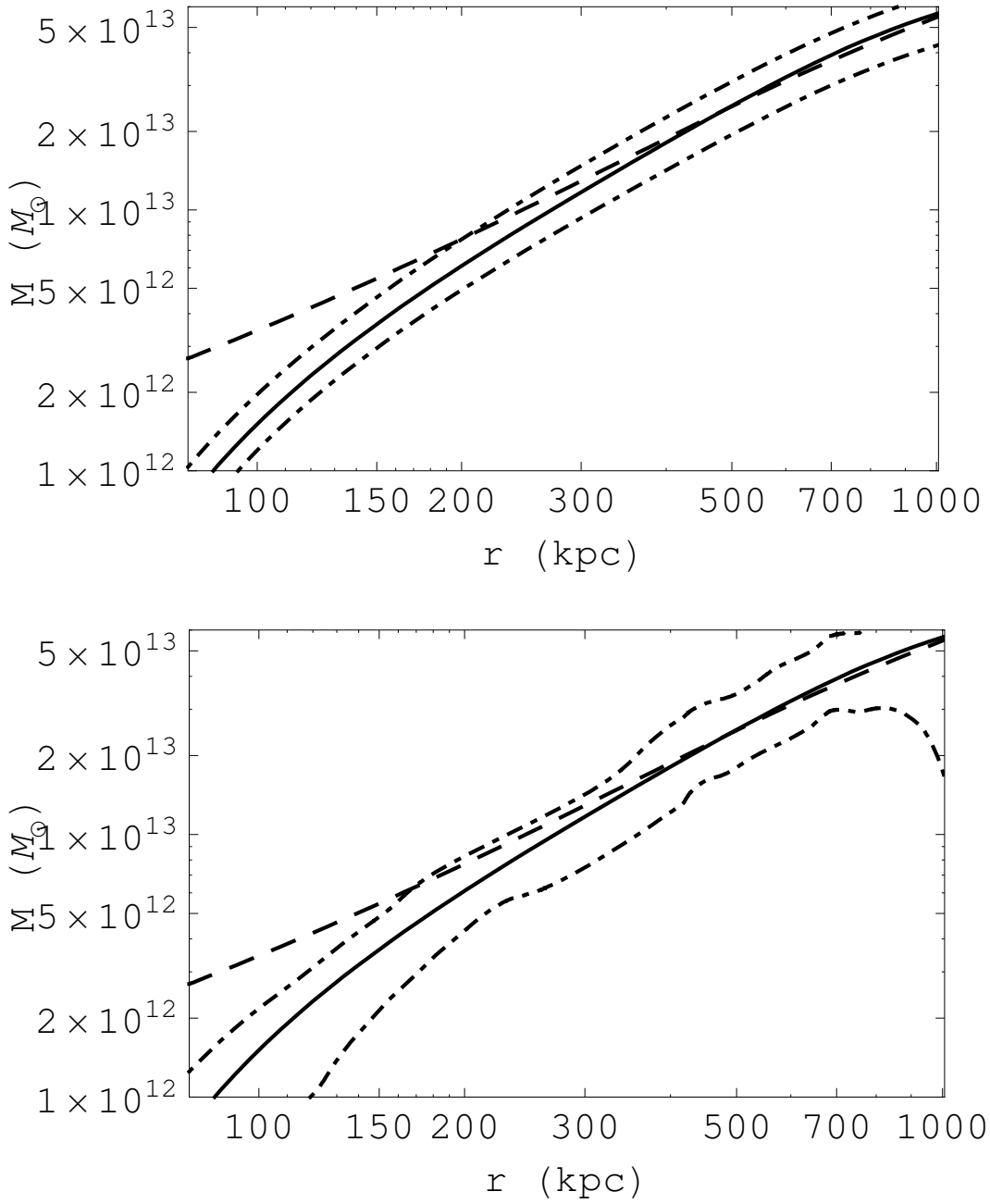

Figure 5.13: Same of Fig.2 but for cluster Abell 1795.

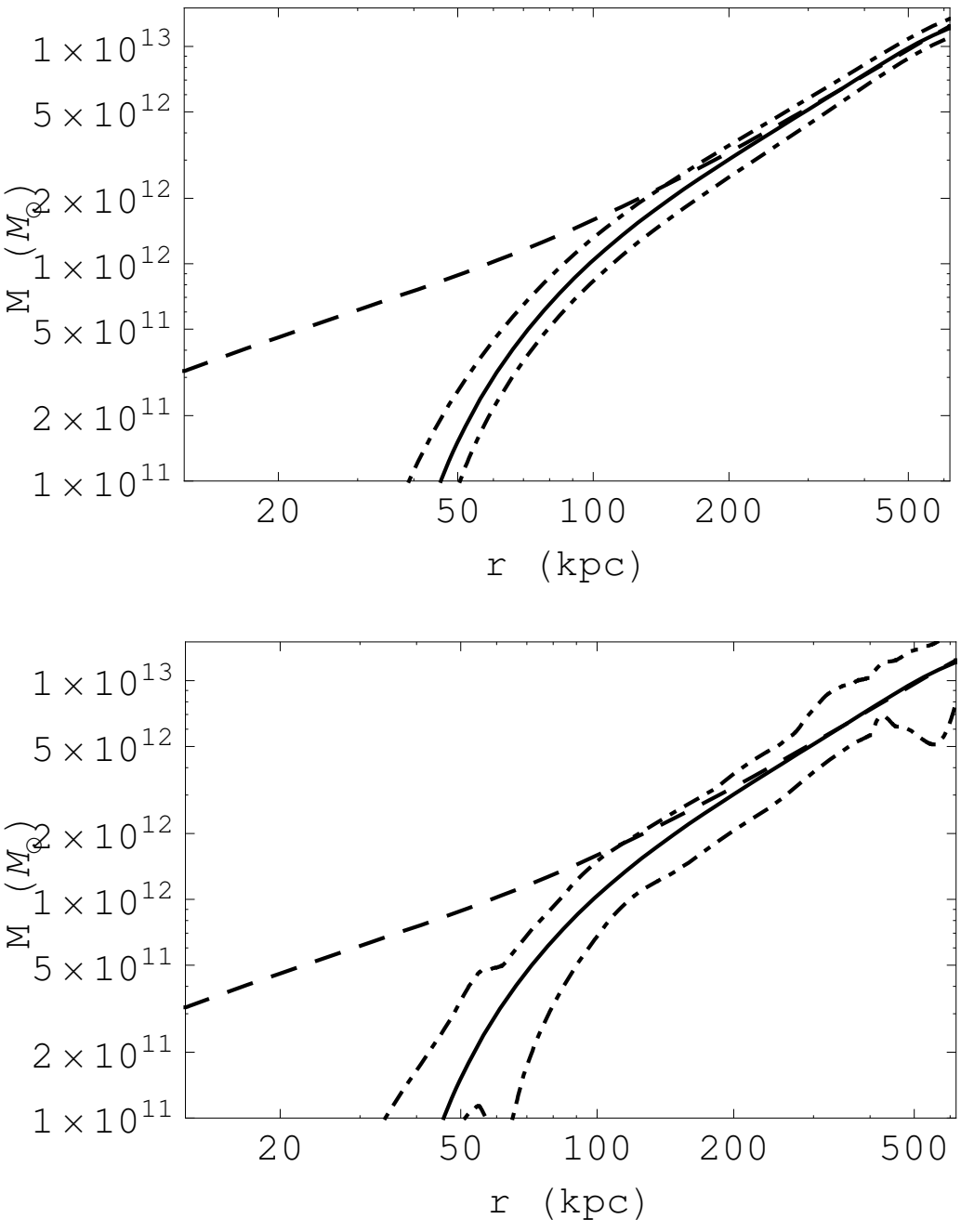

Figure 5.14: Same of Fig.2 but for cluster Abell 1991.

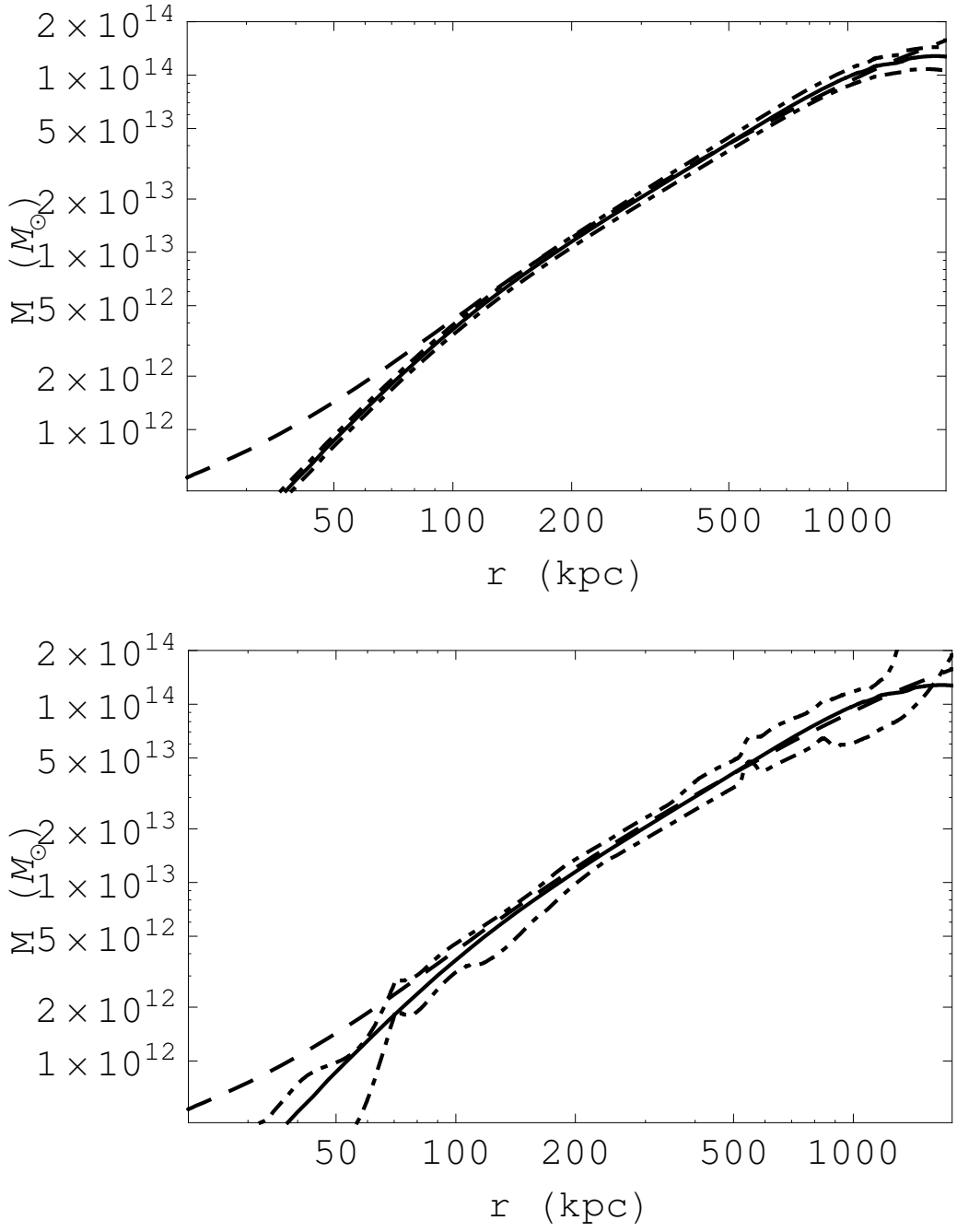

Figure 5.15: Same of Fig.2 but for cluster Abell 2029.

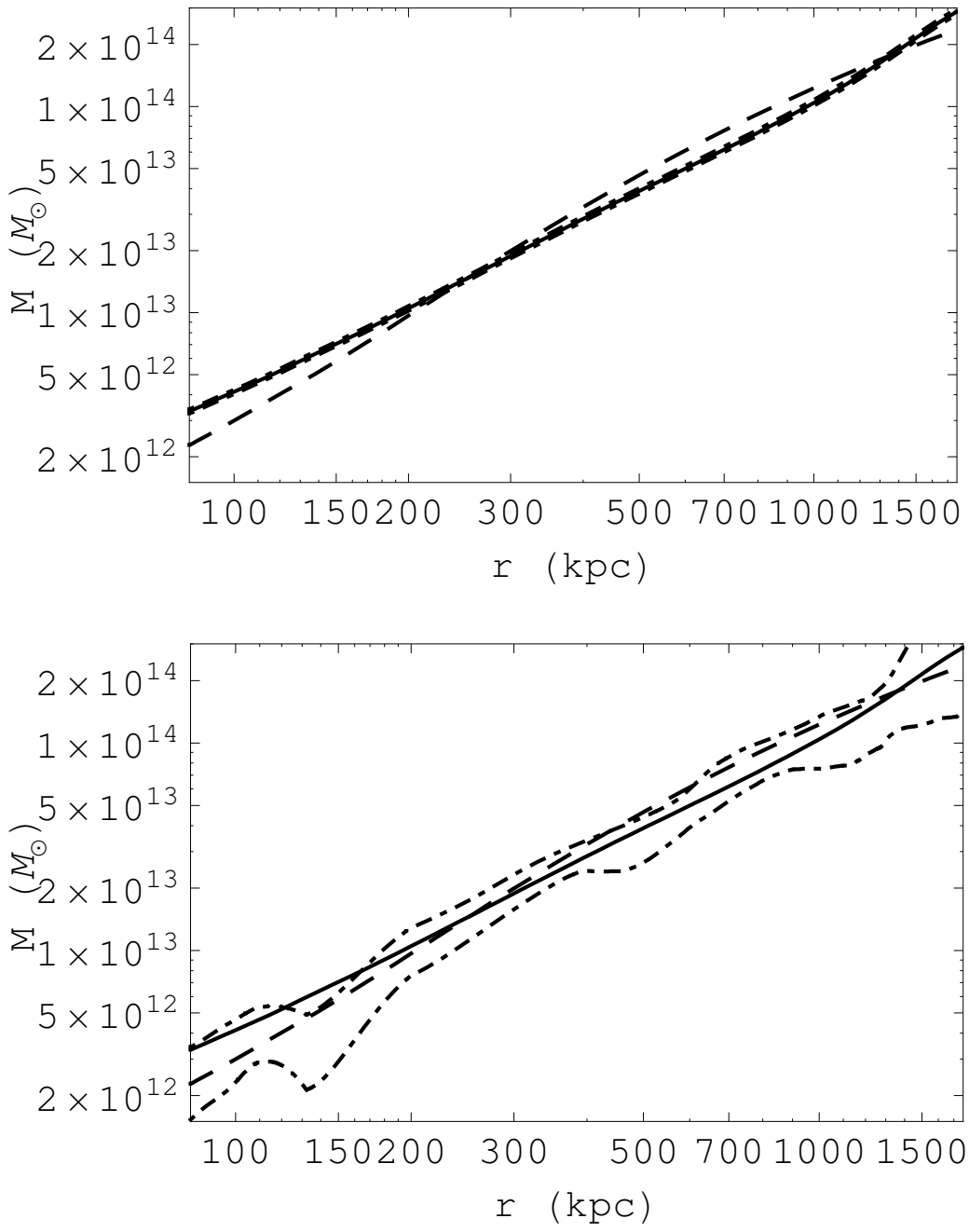

Figure 5.16: Same of Fig.2 but for cluster Abell 2390.

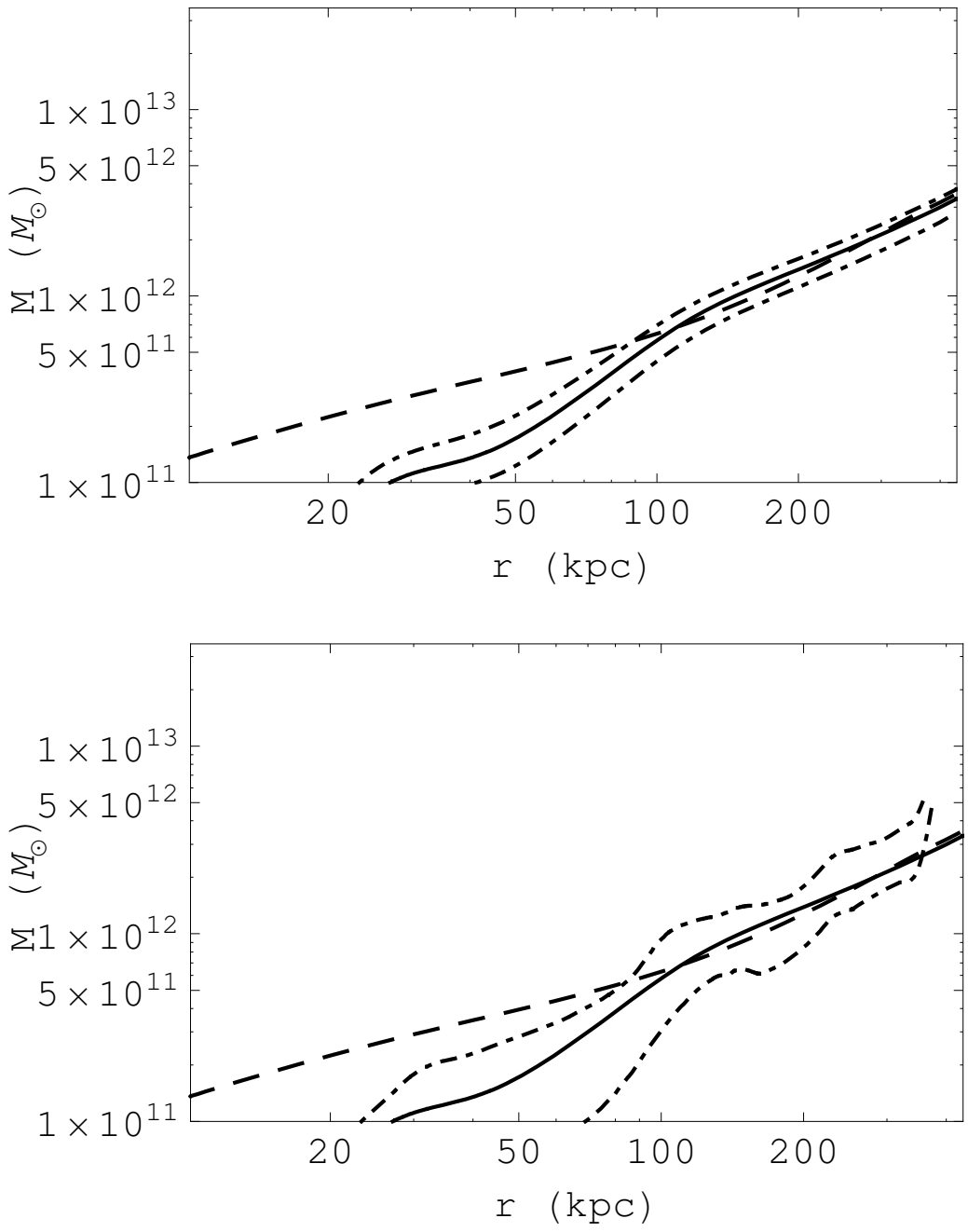

Figure 5.17: Same of Fig.2 but for cluster MKW4.

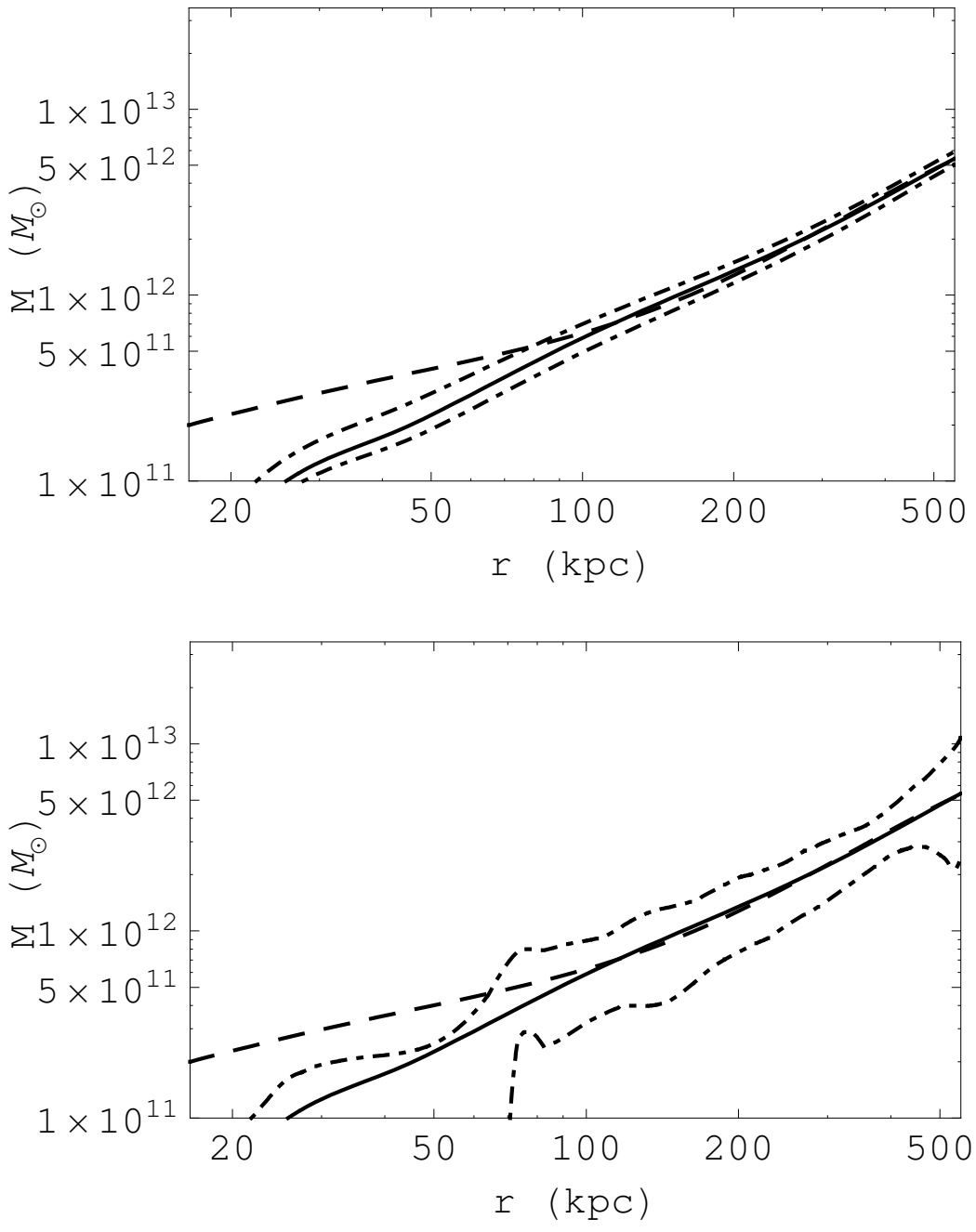

Figure 5.18: Same of Fig.2 but for cluster RXJ1159.

Part III
Cosmography

CHAPTER 6

Cosmography vs $f(R)$

As soon as astrophysicists realized that Type Ia Supernovae (SNeIa) were standard candles, it appeared evident that their high luminosity should make it possible to build a Hubble diagram, i.e. a plot of the distance - redshift relation, over some cosmologically interesting distance ranges. Motivated by this attractive consideration, two independent teams started SNeIa surveys leading to the unexpected discovery that the universe expansion is speeding up rather than decelerating [291, 292, 311, 329, 167]. This surprising result has now been strengthened by more recent data coming from SNeIa surveys [213, 363, 30, 312, 313, 24, 390, 126], large scale structure [134, 290, 357, 185, 298] and cosmic microwave background (CMBR) anisotropy spectrum [119, 356, 269, 308, 37, 349, 351]. This large dataset coherently points toward the picture of a spatially flat universe undergoing an accelerated expansion driven by a dominant negative pressure fluid, typically referred to as *dark energy* [112].

While there is a wide consensus on the above scenario depicted by such good quality data, there is a similarly wide range of contrasting proposals to solve the dark energy puzzle. Surprisingly, the simplest explanation, namely the cosmological constant Λ [97, 319], is also the best one from a statistical point of view [360, 361, 336]. Unfortunately, the well known coincidence and 120 orders of magnitude problems render Λ a rather unattractive solution from a theoretical point of view. Inspired by the analogy with inflation, a scalar field ϕ, dubbed *quintessence* [289, 286], has then been proposed to give a dynamical Λ term in order to both fit the data and avoid the above problems. However, such models are still plagued by difficulties on their own, such as the almost complete freedom in the choice of the scalar field potential and the fine tuning of the initial conditions. Needless to say, a plethora of alternative models are now on the market all sharing the main property to be in agreement with observations, but relying on completely different physics.

Notwithstanding their differences, all the dark energy based theories assume that the observed acceleration is the outcome of the action of an up to now undetected ingredient to be added to the cosmic pie. In terms of the Einstein equations, $G_{\mu\nu} = \chi T_{\mu\nu}$, such models are simply modifying the right hand side including in the stress - energy tensor something more

than the usual matter and radiation components.

As a radically different approach, one can also try to leave unchanged the source side, but rather modifying the left hand side. In a sense, one is therefore interpreting cosmic speed up as a first signal of the breakdown of the laws of physics as described by the standard General Relativity (GR). Since this theory has been experimentally tested only up to the Solar System scale, there is no a priori theoretical motivation to extend its validity to extraordinarily larger scales such as the cosmological ones (e.g. the last scattering surface!). Extending GR, not giving up to its positive results, opens the way to a large class of alternative theories of gravity ranging from extra - dimensions [140, 141, 142, 236, 237] to nonminimally coupled scalar fields [164, 93, 294, 130]. In particular, we will be interested here in fourth order theories [69, 87, 72, 77, 94, 211, 272, 274, 275, 96, 11] based on replacing the scalar curvature R in the Hilbert–Einstein action with a generic analytic function $f(R)$ which should be reconstructed starting from data and physically motivated issues. Also referred to as $f(R)$ gravity, these models have been shown to be able to both fit the cosmological data and evade the Solar System constraints in several physically interesting cases [190, 354, 21, 277, 367].

It is worth noting that both dark energy models and modified gravity theories have shown to be in agreement with the data. As a consequence, unless higher precision probes of the expansion rate and the growth of structure will be available, these two rival approaches could not be discriminated. This confusion about the theoretical background suggests that a more conservative approach to the problem of cosmic acceleration, relying on as less model dependent quantities as possible, is welcome. A possible solution could be to come back to the cosmography [386] rather than finding out solutions of the Friedmann equations and testing them. Being only related to the derivatives of the scale factor, the cosmographic parameters make it possible to fit the data on the distance - redshift relation without any *a priori* assumption on the underlying cosmological model: in this case, the only assumption is that the metric is the Robertson - Walker one (and hence not relying on the solution of cosmic equations). Almost a century after Hubble discovery of the expansion of the universe, we could now extend cosmography beyond the search for the value of the Hubble constant. The SNeIa Hubble diagram extends up to $z = 1.7$ thus invoking the need for, at least, a fifth order Taylor expansion of the scale factor in order to give a reliable approximation of the distance - redshift relation. As a consequence, it could be, in principle, possible to estimate up to five cosmographic parameters, although the still too small dataset available does not allow to get a precise and realistic determination of all of them.

Once these quantities have been determined, one could use them to put constraints on the models. In a sense, we are reverting the usual approach consisting in deriving the cosmographic parameters as a sort of byproduct of an assumed theory. Here, we follow the other way around expressing the model characterizing quantities as a function of the cosmographic parameters. Such a program is particularly suited for the study of fourth order theories of gravity. As is well known, the mathematical difficulties entering the solution of fourth order field equations make it quite problematic to find out analytical expressions for the scale factor and hence predict the values of the cosmographic parameters. A key role in $f(R)$ gravity is played by the choice of the $f(R)$ function. Under quite general hypotheses, we will derive useful relations among the cosmographic parameters and the present day value of $f^{(n)}(R) = d^n f/dR^n$, with $n = 0, \ldots, 3$, whatever $f(R)$ is[1]. Once the cosmographic parameters will be determined, this method will allow us to investigate the cosmography of $f(R)$ theories.

[1]As an important remark, we stress that our derivation will rely on the metric formulation of $f(R)$ theories, while we refer the reader to [299, 300] for a similar work in the Palatini approach.

It is worth stressing that the definition of the cosmographic parameters only relies on the assumption of the Robertson - Walker metric. As such, it is however difficult to state a priori to what extent the fifth order expansion provides an accurate enough description of the quantities of interest. Actually, the number of cosmographic parameters to be used depends on the problem one is interested in. As we will see later, we are here concerned only with the SNeIa Hubble diagram so that we have to check that the distance modulus $\mu_{cp}(z)$ obtained using the fifth order expansion of the scale factor is the same (within the errors) as the one $\mu_{DE}(z)$ of the underlying physical model. Being such a model of course unknown, one can adopt a phenomenological parameterization for the dark energy[2] EoS and look at the percentage deviation $\Delta\mu/\mu_{DE}$ as function of the EoS parameters. We have carried out such exercise using the CPL model introduced later and verified that $\Delta\mu/\mu_{DE}$ is an increasing function of z (as expected), but still remains smaller than 2% up to $z\sim 2$ over a wide range of the CPL parameter space. On the other hand, halting the Taylor expansion to a lower order may introduce significant deviation for $z>1$ that can potentially bias the analysis if the measurement errors are as small as those predicted for future SNeIa surveys. We are therefore confident that our fifth order expansion is both sufficient to get an accurate distance modulus over the redshift range probed by SNeIa and necessary to avoid dangerous biases.

6.1 Apparatus

The key rule in cosmography is the Taylor series expansion of the scale factor with respect to the cosmic time. To this aim, it is convenient to introduce the following functions:

$$H(t)\equiv+\frac{1}{a}\frac{da}{dt}\,, \tag{6.1}$$

$$q(t)\equiv-\frac{1}{a}\frac{d^2a}{dt^2}\frac{1}{H^2}\,, \tag{6.2}$$

$$j(t)\equiv+\frac{1}{a}\frac{d^3a}{dt^3}\frac{1}{H^3}\,, \tag{6.3}$$

$$s(t)\equiv+\frac{1}{a}\frac{d^4a}{dt^4}\frac{1}{H^4}\,, \tag{6.4}$$

$$l(t)\equiv+\frac{1}{a}\frac{d^5a}{dt^5}\frac{1}{H^5}\,, \tag{6.5}$$

which are usually referred to as the *Hubble*, *deceleration*, *jerk*, *snap* and *lerk* parameters, respectively. It is then a matter of algebra to demonstrate the following useful relations:

$$\dot{H}=-H^2(1+q)\,, \tag{6.6}$$

$$\ddot{H}=H^3(j+3q+2)\,, \tag{6.7}$$

$$d^3H/dt^3=H^4\left[s-4j-3q(q+4)-6\right]\,, \tag{6.8}$$

$$d^4H/dt^4=H^5\left[l-5s+10(q+2)j+30(q+2)q+24\right]\,, \tag{6.9}$$

where a dot denotes derivative with respect to the cosmic time t. Eqs.(6.6) - (6.9) make it possible to relate the derivative of the Hubble parameter to the other cosmographic parameters. The distance - redshift relation may then be obtained starting from the Taylor expansion of $a(t)$ along the lines described in [379, 385, 100].

[2]Note that one can always use a phenomenological dark energy model to get a reliable estimate of the scale factor evolution even if the correct model is a fourth order one.

6.1.1 Scale factor series

With these definitions the series expansion to the 5th order in time of the scale factor will be:

$$a(t)=a(t_0)\left\{H_0(t-t_0)-\frac{q_0}{2}H_0^2(t-t_0)^2+\frac{j_0}{3!}H_0^3(t-t_0)^3+\frac{s_0}{4!}H_0^4(t-t_0)^4+\right.$$
$$\left.+\frac{l_0}{5!}H_0^5(t-t_0)^5+O[(t-t_0)^6]\right\} \tag{6.10}$$

$$\frac{a(t)}{a(t_0)}=1+H_0(t-t_0)-\frac{q_0}{2}H_0^2(t-t_0)^2+\frac{j_0}{3!}H_0^3(t-t_0)^3+\frac{s_0}{4!}H_0^4(t-t_0)^4$$
$$+\frac{l_0}{5!}H_0^5(t-t_0)^5+O[(t-t_0)^6] \tag{6.11}$$

It's easy to see that Eq.(6.11) is the inverse of redshift z, being the redshift defined by:

$$1+z=\frac{a(t_0)}{a(t)}$$

The physical distance travelled by a photon that is emitted at time t_* and absorbed at the current epoch t_0 is

$$D=c\int dt=c(t_0-t_*)$$

Assuming $t_*=t_0-\frac{D}{c}$ and inserting in Eq.(6.11) we have:

$$1+z=\frac{a(t_0)}{a(t_0-\frac{D}{c})}=$$

$$=\frac{1}{1-\frac{H_0}{c}D-\frac{q_0}{2}\left(\frac{H_0}{c}\right)^2D^2-\frac{j_0}{6}\left(\frac{H_0}{c}\right)^3D^3+\frac{s_0}{24}\left(\frac{H_0}{c}\right)^4D^4-\frac{l_0}{120}\left(\frac{H_0}{c}\right)^5D^5+O[(\frac{H_0D}{c})^6]} \tag{6.12}$$

The inverse of this expression will be:

$$\begin{aligned}1+z &= 1+\frac{H_0}{c}D+\left(1+\frac{q_0}{2}\right)\left(\frac{H_0}{c}\right)^2D^2+\left(1+q_0+\frac{j_0}{6}\right)\left(\frac{H_0}{c}\right)^3D^3+\\ &+ \left(1+\frac{3}{2}q_0+\frac{q_0^2}{4}+\frac{j_0}{3}-\frac{s_0}{24}\right)\left(\frac{H_0}{c}\right)^4D^4+\left(1+2q_0+\frac{3}{4}q_0^2+\right.\\ &+ \left.\frac{q_0j_0}{6}+\frac{j_0}{2}-\frac{s}{12}+l_0\right)\left(\frac{H_0}{c}\right)^5D^5+O\left[\left(\frac{H_0D}{c}\right)^6\right]\end{aligned} \tag{6.13}$$

Then we reverse the series $z(D)\rightarrow D(z)$ to have the physical distance D expressed as function of redshift z:

$$z(D)=\mathcal{Z}_D^1\left(\frac{H_0D}{c}\right)+\mathcal{Z}_D^2\left(\frac{H_0D}{c}\right)^2+\mathcal{Z}_D^3\left(\frac{H_0D}{c}\right)^3+\mathcal{Z}_D^4\left(\frac{H_0D}{c}\right)^4+\mathcal{Z}_D^5\left(\frac{H_0D}{c}\right)^5+$$
$$+O\left[\left(\frac{H_0D}{c}\right)^6\right] \tag{6.14}$$

with:

$$\mathcal{Z}_D^1{=}1 \tag{6.15}$$
$$\mathcal{Z}_D^2{=}1+\frac{q_0}{2} \tag{6.16}$$
$$\mathcal{Z}_D^3{=}1+q_0+\frac{j_0}{6} \tag{6.17}$$
$$\mathcal{Z}_D^4{=}1+\frac{3}{2}q_0+\frac{q_0^2}{4}+\frac{j_0}{3}-\frac{s_0}{24} \tag{6.18}$$
$$\mathcal{Z}_D^5{=}1+2q_0+\frac{3}{4}q_0^2+\frac{q_0 j_0}{6}+\frac{j_0}{2}-\frac{s}{12}+l_0 \tag{6.19}$$

From this we have:

$$D(z) \quad = \quad \frac{cz}{H_0}\left\{\mathcal{D}_z^0+\mathcal{D}_z^1\ z+\mathcal{D}_z^2\ z^2+\mathcal{D}_z^3\ z^3+\mathcal{D}_z^4\ z^4+O(z^5)\right\} \tag{6.20}$$

with:

$$\mathcal{D}_z^0{=}1 \tag{6.21}$$
$$\mathcal{D}_z^1{=}{-}\left(1+\frac{q_0}{2}\right) \tag{6.22}$$
$$\mathcal{D}_z^2{=}1+q_0+\frac{q_0^2}{2}-\frac{j_0}{6} \tag{6.23}$$
$$\mathcal{D}_z^3{=}{-}\left(1+\frac{3}{2}q_0+\frac{3}{2}q_0^2+\frac{5}{8}q_0^3-\frac{1}{2}j_0-\frac{5}{12}q_0 j_0-\frac{s_0}{24}\right) \tag{6.24}$$
$$\mathcal{D}_z^4{=}1+2q_0+3q_0^2+\frac{5}{2}q_0^3+\frac{7}{2}q_0^4-\frac{5}{3}q_0 j_0-\frac{7}{8}q_0^2 j_0-\frac{1}{8}q_0 s_0-j_0+\frac{j_0^2}{12}-\frac{s_0}{6}-\frac{l_0}{120} \tag{6.25}$$
$$\tag{6.26}$$

In typical applications, one is not interested in the physical distance $D(z)$, but other definitions:

- the luminosity distance:
$$d_L=\frac{a(t_0)}{a(t_0-\frac{D}{c})}\,(a(t_0)r_0) \tag{6.27}$$
- the angular-diameter distance:
$$d_A=\frac{a(t_0-\frac{D}{c})}{a(t_0)}\,(a(t_0)r_0) \tag{6.28}$$

where $r_0(D)$ is:

$$r_0(D)=\begin{cases}\sin(\int_{t_0-\frac{D}{c}}^{t_0}\frac{c\ \mathrm{d}t}{a(t)}) & k=+1;\\ \int_{t_0-\frac{D}{c}}^{t_0}\frac{c\ \mathrm{d}t}{a(t)} & k=0;\\ \sinh(\int_{t_0-\frac{D}{c}}^{t_0}\frac{c\ \mathrm{d}t}{a(t)}) & k=-1.\end{cases} \tag{6.29}$$

If we make the expansion for short distances, namely if we insert the series expansion of $a(t)$ in $r_0(D)$, we have:

$$r_0(D){=}\int_{t_0-\frac{D}{c}}^{t_0}\frac{c\ \mathrm{d}t}{a(t)}=\int_{t_0-\frac{D}{c}}^{t_0}\frac{c\ \mathrm{d}t}{a_0}\left\{1+H_0(t_0-t)+\left(1+\frac{q_0}{2}\right)H_0^2(t_0-t)^2+\right.$$

$$+\left(1+q_0+\frac{j_0}{6}\right)H_0^3(t_0-t)^3+\left(1+\frac{3}{2}q_0+\frac{q_0^2}{4}+\frac{j_0}{3}-\frac{s_0}{24}\right)H_0^4(t_0-t)^4+$$
$$+\left(1+2q_0+\frac{3}{4}q_0^2+\frac{q_0j_0}{6}+\frac{j_0}{2}-\frac{s}{12}+l_0\right)H_0^5(t_0-t)^5+O[(t_0-t)^6]\Bigg\}=$$
$$=\frac{D}{a_0}\left\{1+\frac{1}{2}\frac{H_0D}{c}+\left[\frac{2+q_0}{6}\right]\left(\frac{H_0D}{c}\right)^2+\left[\frac{6+6q_0+j_0}{24}\right]\left(\frac{H_0D}{c}\right)^3+\right.$$
$$+\left[\frac{24+36q_0+6q_0^2+8j_0-s_0}{120}\right]\left(\frac{H_0D}{c}\right)^4+$$
$$+\left[\frac{12+24q_0+9q_0^2+2q_0j_0+6j_0-s_0+12l_0}{72}\right]\left(\frac{H_0D}{c}\right)^5+$$
$$\left.+O\left[\left(\frac{H_0D}{c}\right)^6\right]\right\} \tag{6.30}$$

To convert from physical distance travelled to *r* coordinate traversed we have to consider that the Taylor series expansion of $\sin$-$\sinh$ functions is:

$$r_0(D)=\left[\int_{t_0-\frac{D}{c}}^{t_0}\frac{c\,\mathrm{d}t}{a(t)}\right]-\frac{k}{3!}\left[\int_{t_0-\frac{D}{c}}^{t_0}\frac{c\,\mathrm{d}t}{a(t)}\right]^3+O\left(\left[\int_{t_0-\frac{D}{c}}^{t_0}\frac{c\,\mathrm{d}t}{a(t)}\right]^5\right) \tag{6.31}$$

so that Eq.(6.11) with curvature k term becomes:

$$r_0(D)=\frac{D}{a_0}\left\{\mathcal{R}_D^0+\mathcal{R}_D^1\frac{H_0D}{c}+\mathcal{R}_D^2\left(\frac{H_0D}{c}\right)^2+\mathcal{R}_D^3\left(\frac{H_0D}{c}\right)^3+\right.$$
$$\left.+\mathcal{R}_D^4\left(\frac{H_0D}{c}\right)^4+\mathcal{R}_D^5\left(\frac{H_0D}{c}\right)^5+O\left[\left(\frac{H_0D}{c}\right)^6\right]\right\} \tag{6.32}$$

with:

$$\mathcal{R}_D^0=1 \tag{6.33}$$
$$\mathcal{R}_D^1=\frac{1}{2} \tag{6.34}$$
$$\mathcal{R}_D^2=\frac{1}{6}\left[2+q_0-\frac{kc^2}{H_0^2a_0^2}\right] \tag{6.35}$$
$$\mathcal{R}_D^3=\frac{1}{24}\left[6+6q_0+j_0-6\frac{kc^2}{H_0^2a_0^2}\right] \tag{6.36}$$
$$\mathcal{R}_D^4=\frac{1}{120}\left[24+36q_0+6q_0^2+8j_0-s_0-\frac{5kc^2(7+2q_0)}{a_0^2H_0^2}\right] \tag{6.37}$$
$$\mathcal{R}_D^5=\frac{1}{144}\left[24+48q_0+18q_0^2+4q_0j_0+12j_0-2s_0+24l_0-\frac{3kc^2(15+10q_0+j_0)}{a_0^2H_0^2}\right] \tag{6.38}$$

Using these one for luminosity distance we have:

$$d_L(z)=\frac{cz}{H_0}\left\{\mathcal{D}_L^0+\mathcal{D}_L^1\,z+\mathcal{D}_L^2\,z^2+\mathcal{D}_L^3\,z^3+\mathcal{D}_L^4\,z^4+O(z^5)\right\} \tag{6.39}$$

with:

$$\mathcal{D}_L^0 = 1 \tag{6.40}$$

$$\mathcal{D}_L^1 = -\frac{1}{2}\left(-1 + q_0\right) \tag{6.41}$$

$$\mathcal{D}_L^2 = -\frac{1}{6}\left(1 - q_0 - 3q_0^2 + j_0 + \frac{kc^2}{H_0^2 a_0^2}\right) \tag{6.42}$$

$$\mathcal{D}_L^3 = \frac{1}{24}\left(2 - 2q_0 - 15q_0^2 - 15q_0^3 + 5j_0 + 10q_0 j_0 + s_0 + \frac{2kc^2(1+3q_0)}{H_0^2 a_0^2}\right) \tag{6.43}$$

$$\mathcal{D}_L^4 = \frac{1}{120}\left[-6 + 6q_0 + 81q_0^2 + 165q_0^3 + 105q_0^4 - 110q_0 j_0 - 105q_0^2 j_0 - 15q_0 s_0 + \right. \tag{6.44}$$

$$\left. - 27j_0 + 10j^2 - 11s_0 - l_0 - \frac{5kc^2(1 + 8q_0 + 9q_0^2 - 2j_0)}{a_0^2 H_0^2}\right] \tag{6.45}$$

While for the angular diameter distance it is:

$$d_A(z) = \frac{cz}{H_0}\left\{\mathcal{D}_A^0 + \mathcal{D}_A^1\, z + \mathcal{D}_A^2\, z^2 + \mathcal{D}_A^3\, z^3 + \mathcal{D}_A^4\, z^4 + O(z^5)\right\} \tag{6.46}$$

with:

$$\mathcal{D}_A^0 = 1 \tag{6.47}$$

$$\mathcal{D}_A^1 = -\frac{1}{2}\left(3 + q_0\right) \tag{6.48}$$

$$\mathcal{D}_A^2 = \frac{1}{6}\left[11 + 7q_0 + 3q_0^2 - j_0 - \frac{kc^2}{H_0^2 a_0^2}\right] \tag{6.49}$$

$$\mathcal{D}_A^3 = -\frac{1}{24}\left[50 + 46q_0 + 39q_0^2 + 15q_0^3 - 13j_0 - 10q_0 j_0 - s_0 - \frac{2kc^2(5+3q_0)}{H_0^2 a_0^2}\right] \tag{6.50}$$

$$\mathcal{D}_A^4 = \frac{1}{120}\left[274 + 326q_0 + 411q_0^2 + 315q_0^3 + 105q_0^4 - 210q_0 j_0 - 105q_0^2 j_0 - 15q_0 s_0 + \right. \tag{6.51}$$

$$\left. - 137j_0 + 10j^2 - 21s_0 - l_0 - \frac{5kc^2(17 + 20q_0 + 9q_0^2 - 2j_0)}{a_0^2 H_0^2}\right] \tag{6.52}$$

If we want to use the same notation of [100], we define $\Omega_0 = 1 + \frac{kc^2}{H_0^2 a_0^2}$, which can be considered a purely cosmographic parameter, or $\Omega_0 = 1 - \Omega_k = \Omega_{m,0} + \Omega_{r,0} + \Omega_{X,0}$ if we consider the dynamics of the universe. With this parameter Eqs.(26)-(28) become:

$$\mathcal{D}_{L,y}^0 = 1 \tag{6.53}$$

$$\mathcal{D}_{L,y}^1 = -\frac{1}{2}\left(-3 + q_0\right) \tag{6.54}$$

$$\mathcal{D}_{L,y}^2 = -\frac{1}{6}\left(12 - 5q_0 + 3q_0^2 - j_0 - \Omega_0\right) \tag{6.55}$$

$$\mathcal{D}_{L,y}^3 = \frac{1}{24}\left[52 - 20q_0 + 21q_0^2 - 15q_0^3 - 7j_0 + 10q_0 j_0 + s_0 - 2\Omega_0(1+3q_0)\right] \tag{6.56}$$

$$\mathcal{D}_{L,y}^4 = \frac{1}{120}\left[359 - 184q_0 + 186q_0^2 - 135q_0^3 + 105q_0^4 + 90q_0 j_0 - 105q_0^2 j_0 - 15q_0 s_0 + \right. \tag{6.57}$$

$$\left. - 57j_0 + 10j^2 + 9s_0 - l_0 - 5\Omega_0(17 - 6q_0 + 9q_0^2 - 2j_0)\right] \tag{6.58}$$

and

$$\mathcal{D}^0_{A,y}=1 \tag{6.59}$$

$$\mathcal{D}^1_{A,y}=-\frac{1}{2}\left(1+q_0\right) \tag{6.60}$$

$$\mathcal{D}^2_{A,y}=-\frac{1}{6}\left[-q_0-3q_0^2+j_0+\Omega_0\right] \tag{6.61}$$

$$\mathcal{D}^3_{A,y}=-\frac{1}{24}\left[-2q_0+3q_0^2+15q_0^3-j_0-10q_0j_0-s_0+2\Omega_0\right] \tag{6.62}$$

$$\mathcal{D}^4_{A,y}=-\frac{1}{120}\left[1-6q_0+9q_0^2-15q_0^3-105q_0^4+10q_0j_0+105q_0^2j_0+15q_0s_0+\right. \tag{6.63}$$

$$\left.-3j_0-10j^2+s_0+l_0+5\Omega_0\right] \tag{6.64}$$

Previous relations in this section have been derived for any value of the curvature parameter; but since in the following we will assume a flat universe, we will used the simplified versions for $k=0$. Now, since we are going to use supernovae data, it will be useful to give as well the Taylor series of the expansion of the luminosity distance at it enters the modulus distance, which is the quantity about which those observational data inform. The final expression for the modulus distance based on the Hubble free luminosity distance, $\mu(z)=5\log_{10}d_L(z)$, is:

$$\mu(z)=\frac{5}{\log 10}\cdot\left(\log z+\mathcal{M}^1z+\mathcal{M}^2z^2+\mathcal{M}^3z^3+\mathcal{M}^4z^4\right)\,, \tag{6.65}$$

with

$$\mathcal{M}^1=-\frac{1}{2}\left[-1+q_0\right]\,, \tag{6.66}$$

$$\mathcal{M}^2=-\frac{1}{24}\left[7-10q_0-9q_0^2+4j_0\right]\,, \tag{6.67}$$

$$\mathcal{M}^3=\frac{1}{24}\left[5-9q_0-16q_0^2-10q_0^3+7j_0+8q_0j_0+s_0\right]\,, \tag{6.68}$$

$$\mathcal{M}^4=\frac{1}{2880}\left[-469+1004q_0+2654q_0^2+3300q_0^3+1575q_0^4+200j_0^2-1148j_0+\right.$$

$$\left.--2620q_0j_0-1800q_0^2j_0-300q_0s_0-324s_0-24l_0\right]\,. \tag{6.69}$$

6.1.2 Redshift series

Now we want to derive a different approach to data analysis. If we consider the definition of the luminosity distance, Eq.(6.27), and of the angular-diameter distance, Eq.(6.28), we can rearrange them in the alternative way::

$$d_L(z)=c\,(1+z)\,\int_0^z \mathrm{d}z'\frac{1}{H(z')} \tag{6.70}$$

$$d_L(z)=\frac{c}{1+z}\,\int_0^z \mathrm{d}z'\frac{1}{H(z')} \tag{6.71}$$

It is interesting to study the possibility to obtain the same final expressions for the two defined distances starting from a Taylor series expansion od the Hubble factor instead of the scale factor, namely:

$$H(z) = H_0 + \left.\frac{dH}{dz}\right|_{z=0} z + \frac{1}{2!}\left.\frac{d^2H}{dz^2}\right|_{z=0} z^2 + \frac{1}{3!}\left.\frac{d^3H}{dz^3}\right|_{z=0} z^3 + \frac{1}{4!}\left.\frac{d^4H}{dz^4}\right|_{z=0} z^4 + O(z^5) \quad (6.72)$$

To derive all the terms of this series we have to take in mind the derivation rules (for a more clear notation we will suppress redshift dependence of Hubble factor using $H \equiv H(z)$):

$$\frac{d}{dt} = -(1+z)H\frac{d}{dz} \quad (6.73)$$

$$\frac{d^2}{dt^2} = (1+z)H\left[H + (1+z)\frac{dH}{dz}\right]\frac{d}{dz} + (1+z)^2H^2\frac{d^2}{dz^2} \quad (6.74)$$

$$\frac{d^3}{dt^3} = -(1+z)H\left\{H^2 + (1+z)^2\left(\frac{dH}{dz}\right)^2 + (1+z)H\left[4\frac{dH}{dz} + (1+z)\frac{d^2H}{dz^2}\right]\right\}\frac{d}{dz} +$$
$$-3(1+z)^2H^2\left[H + (1+z)\frac{dH}{dz}\right]\frac{d^2}{dz^2} - (1+z)^3H^3\frac{d^3}{dz^3} \quad (6.75)$$

$$\frac{d^4}{dt^4} = (1+z)H\left[H^2 + 11(1+z)H^2\frac{dH}{dz} + 11(1+z)H\frac{dH}{dz} + (1+z)^3\left(\frac{dH}{dz}\right)^3 + \right.$$
$$\left. + 7(1+z)^2H\frac{d^2H}{dz^2} + 4(1+z)^3H\frac{dH}{dz}\frac{d^2H}{d^2z} + (1+z)^3H^2\frac{d^3H}{d^3z}\right]\frac{d}{dz} +$$
$$+(1+z)^2H^2\left[7H^2 + 22H\frac{dH}{dz} + 7(1+z)^2\left(\frac{dH}{dz}\right)^2 + 4H\frac{d^2H}{dz^2}\right]\frac{d^2}{dz^2} +$$
$$+6(1+z)^3H^3\left[H + (1+z)\frac{dH}{dz}\right]\frac{d^3}{dz^3} + (1+z)^4H^4\frac{d^4}{dz^4} \quad (6.76)$$

Finally using these ones with Eqs.(6.6)-(6.9) we obtain:

$$\frac{dH}{dz} = \frac{H}{1+z}(1+q) \quad (6.77)$$

$$\frac{d^2H}{dz^2} = \frac{H}{(1+z)^2}(-q^2+j) \quad (6.78)$$

$$\frac{d^3H}{dz^3} = \frac{H}{(1+z)^3}(3q^2+3q^3-4qj-3j-s) \quad (6.79)$$

$$\frac{d^4H}{dz^4} = \frac{H}{(1+z)^4}(-12q^2-24q^3-15q^4+32qj+25q^2j+7qs+12j-4j^2+8s+l) \quad (6.80)$$

Starting from the definition of luminosity distance, after integrating, and Taylor expanding the final result, we obtain the luminosity distance formula given by Eq.(6.39). And the same is verified for the angular-diameter distance.

It will be useful also the expansion series of the square Hubble factor, H^2. It is a simple and only long matter of algebra to derive its derivatives so that final results are:

$$\frac{d(H^2)}{dz} = \frac{2H^2}{1+z}(1+q) \quad (6.81)$$

$$\frac{d^2(H^2)}{dz^2}=\frac{2H^2}{(1+z)^2}(1+2q+j) \tag{6.82}$$

$$\frac{d^3(H^2)}{dz^3}=\frac{2H^2}{(1+z)^3}(-qj-s) \tag{6.83}$$

$$\frac{d^4(H^2)}{dz^4}=\frac{2H^2}{(1+z)^4}(4qj+3qs+3q^2j-j^2+4s+l) \tag{6.84}$$

6.2 $f(R)$ derivatives vs Cosmography

6.2.1 $f(R)$ preliminaries

Much interest has been recently devoted to a form of quintessence induced by curvature according to which the present universe is filled by pressureless dust matter only and the acceleration is the result of the modified Friedmann equations obtained by replacing the Ricci curvature scalar R with a generic function $f(R)$ in the gravity action [**?**, **?**]. Under the assumption of a flat universe, the Hubble parameter is therefore determined by[3] :

$$H^2=\frac{1}{3}\left[\frac{\rho_m}{f'(R)}+\rho_{curv}\right] \tag{6.85}$$

where the prime denotes derivative with respect to R and ρ_{curv} is the energy density of an *effective curvature fluid*[4] :

$$\rho_{curv}=\frac{1}{f'(R)}\left\{\frac{1}{2}\left[f(R)-Rf'(R)\right]-3H\dot{R}f''(R)\right\} . \tag{6.86}$$

Assuming there is no interaction between the matter and the curvature terms (we are in the so-called *Jordan frame*), the matter continuity equation gives the usual scaling $\rho_M=\rho_M(t=t_0)a^{-3}=3H_0^2\Omega_M a^{-3}$, with Ω_M the present day matter density parameter. The continuity equation for ρ_{curv} then reads :

$$\dot{\rho}_{curv}+3H(1+w_{curv})\rho_{curv}=\frac{3H_0^2\Omega_M\dot{R}f''(R)}{\left[f'(R)\right]^2}a^{-3} \tag{6.87}$$

with

$$w_{curv}=-1+\frac{\ddot{R}f''(R)+\dot{R}\left[\dot{R}f'''(R)-Hf''(R)\right]}{\left[f(R)-Rf'(R)\right]/2-3H\dot{R}f''(R)} \tag{6.88}$$

the barotropic factor of the curvature fluid. It is worth noticing that the curvature fluid quantities ρ_{curv} and w_{curv} only depends on $f(R)$ and its derivatives up to the third order. As a consequence, considering only their present day values (which may be naively obtained

[3] We use here natural units such that $8\pi G=1$.

[4] Note that the name *curvature fluid* does not refer to the FRW curvature parameter k, but only takes into account that such a term is a geometrical one related to the scalar curvature R.

by replacing R with R_0 everywhere), two $f(R)$ theories sharing the same values of $f(R_0)$, $f'(R_0)$, $f''(R_0)$, $f'''(R_0)$ will be degenerate from this point of view[5].

Combining Eq.(6.87) with Eq.(6.85), one finally gets the following *master equation* for the Hubble parameter:

$$\dot{H}=-\frac{1}{2f'(R)}\left\{3H_0^2\Omega_M a^{-3}+\ddot{R}f''(R)+ \right. \\ \left. +\dot{R}\left[\dot{R}f'''(R)-Hf''(R)\right]\right\} . \tag{6.89}$$

Expressing the scalar curvature R as function of the Hubble parameter as:

$$R=-6\left(\dot{H}+2H^2\right) \tag{6.90}$$

and inserting the result into Eq.(6.89), one ends with a fourth order nonlinear differential equation for the scale factor $a(t)$ that cannot be easily solved also for the simplest cases (for instance, $f(R)\propto R^n$). Moreover, although technically feasible, a numerical solution of Eq.(6.89) is plagued by the large uncertainties on the boundary conditions (i.e., the present day values of the scale factor and its derivatives up to the third order) that have to be set to find out the scale factor.

6.2.2 $f(R)$ derivatives with Cosmography

Motivated by these difficulties, we approach now the problem from a different viewpoint. Rather than choosing a parameterized expression for $f(R)$ and then numerically solving Eq.(6.89) for given values of the boundary conditions, we try to relate the present day values of its derivatives to the cosmographic parameters (q_0, j_0, s_0, l_0) so that constraining them in a model independent way gives us a hint for what kind of $f(R)$ theory could be able to fit the observed Hubble diagram[6].

As a preliminary step, it is worth considering again the constraint equation (6.90). Differentiating with respect to t, we easily get the following relations:

$$\begin{aligned}\dot{R}&=-6\left(\ddot{H}+4H\dot{H}\right)\\ \ddot{R}&=-6\left(d^3H/dt^3+4H\ddot{H}+4\dot{H}^2\right)\\ d^3R/dt^3R&=-6\left(d^4H/dt^4+4Hd^3H/dt^3+12\dot{H}\ddot{H}\right)\end{aligned} \quad . \tag{6.91}$$

Evaluating these at the present time and using Eqs.(6.6) - (6.9), one finally gets:

[5] One can argue that this is not strictly true since different $f(R)$ theories will lead to different expansion rate $H(t)$ and hence different present day values of R and its derivatives. However, it is likely that two $f(R)$ functions that exactly match each other up to the third order derivative today will give rise to the same $H(t)$ at least for $t\simeq t_0$ so that $(R_0, \dot{R}_0, \ddot{R}_0)$ will be almost the same.

[6] Note that a similar analysis, but in the context of the energy conditions in $f(R)$, has yet been presented in [39]. However, in that work, the author give an expression for $f(R)$ and then compute the snap parameter to be compared to the observed one. On the contrary, our analysis does not depend on any assumed functional expression for $f(R)$.

$$R_0 = -6H_0^2(1-q_0) \ , \tag{6.92}$$

$$\dot{R}_0 = -6H_0^3(j_0 - q_0 - 2) \ , \tag{6.93}$$

$$\ddot{R}_0 = -6H_0^4\left(s_0 + q_0^2 + 8q_0 + 6\right) \ , \tag{6.94}$$

$$d^3R_0/dt^3 = -6H_0^5\left[l_0 - s_0 + 2(q_0+4)j_0 - 6(3q_0+8)q_0 - 24\right] \ , \tag{6.95}$$

which will turn out to be useful in the following.

Let us now come back to the expansion rate and master equations (6.85) and (6.89). Since they have to hold along the full evolutionary history of the universe, they naively hold also at the present day. As a consequence, we may evaluate them in $t = t_0$ thus easily obtaining:

$$H_0^2 = \frac{H_0^2\Omega_M}{f'(R_0)} + \frac{f(R_0) - R_0f'(R_0) - 6H_0\dot{R}_0f''(R_0)}{6f'(R_0)} \ , \tag{6.96}$$

$$-\dot{H}_0 = \frac{3H_0^2\Omega_M}{2f'(R_0)} + \frac{\dot{R}_0^2f'''(R_0) + \left(\ddot{R}_0 - H_0\dot{R}_0\right)f''(R_0)}{2f'(R_0)} \ . \tag{6.97}$$

Using Eqs.(6.6) - (6.9) and (6.92) - (6.95), we can rearrange Eqs.(6.96) and (6.97) as two relations among the Hubble constant H_0 and the cosmographic parameters (q_0, j_0, s_0), on one hand, and the present day values of $f(R)$ and its derivatives up to third order. However, two further relations are needed in order to close the system and determine the four unknown quantities $f(R_0)$, $f'(R_0)$, $f''(R_0)$, $f'''(R_0)$. A first one may be easily obtained by noting that, inserting back the physical units, the rate expansion equation reads:

$$H^2 = \frac{8\pi G}{3f'(R)}\left[\rho_m + \rho_{curv}f'(R)\right]$$

which clearly shows that, in $f(R)$ gravity, the Newtonian gravitational constant G is replaced by an effective (time dependent) $G_{eff} = G/f'(R)$. On the other hand, it is reasonable to assume that the present day value of G_{eff} is the same as the Newtonian one so that we get the simple constraint:

$$G_{eff}(z=0) = G \rightarrow f'(R_0) = 1 \ . \tag{6.98}$$

In order to get the fourth relation we need to close the system, we first differentiate both sides of Eq.(6.89) with respect to t. We thus get:

$$\begin{aligned}\ddot{H} = &\frac{\dot{R}^2f'''(R) + \left(\ddot{R} - H\dot{R}\right)f''(R) + 3H_0^2\Omega_Ma^{-3}}{2\left[\dot{R}f''(R)\right]^{-1}\left[f'(R)\right]^2} - \frac{\dot{R}^3f^{(iv)}(R) + \left(3\dot{R}\ddot{R} - H\dot{R}^2\right)f'''(R)}{2f'(R)} \\ &- \frac{\left(d^3R/dt^3 - H\ddot{R} + \dot{H}\dot{R}\right)f''(R) - 9H_0^2\Omega_MHa^{-3}}{2f'(R)} \ ,\end{aligned} \tag{6.99}$$

with $f^{(iv)}(R) = d^4f/dR^4$. Let us now suppose that $f(R)$ may be well approximated by its third order Taylor expansion in $R - R_0$, i.e. we set :

$$f(R) = f(R_0) + f'(R_0)(R - R_0) + \frac{1}{2}f''(R_0)(R - R_0)^2 + \frac{1}{6}f'''(R_0)(R - R_0)^3 \quad (6.100)$$

In such an approximation, it is $f^{(n)}(R) = d^nf/R^n = 0$ for $n \geq 4$ so that naively $f^{(iv)}(R_0) = 0$. Evaluating then Eq.(6.99) at the present day, we get :

$$\begin{aligned}\ddot{H}_0 =& \frac{\dot{R}_0^2 f'''(R_0) + \left(\ddot{R}_0 - H_0\dot{R}_0\right) f''(R_0) + 3H_0^2\Omega_M}{2\left[\dot{R}_0 f''(R_0)\right]^{-1}\left[f'(R_0)\right]^2} - \frac{\left(3\dot{R}_0\ddot{R}_0 - H\dot{R}_0^2\right) f'''(R_0)}{2f'(R_0)} \\ &- \frac{\left(d^3R_0/dt^3 - H_0\ddot{R}_0 + \dot{H}_0\dot{R}_0\right) f''(R_0) - 9H_0^3\Omega_M}{2f'(R_0)} \ . \end{aligned} \quad (6.101)$$

We can now schematically proceed as follows. Evaluate Eqs.(6.6) - (6.9) at $z = 0$ and plug these relations into the left hand sides of Eqs.(6.96), (6.97), (6.101). Insert Eqs.(6.92) - (6.95) into the right hand sides of these same equations so that only the cosmographic parameters (q_0, j_0, s_0, l_0) and the $f(R)$ related quantities enter both sides of these relations. Finally, solve them under the constraint (6.98) with respect to the present day values of $f(R)$ and its derivatives up to the third order. After some algebra, one ends up with the desired result :

$$\frac{f(R_0)}{6H_0^2} = -\frac{\mathcal{P}_0(q_0, j_0, s_0, l_0)\Omega_M + \mathcal{Q}_0(q_0, j_0, s_0, l_0)}{\mathcal{R}(q_0, j_0, s_0, l_0)} \ , \quad (6.102)$$

$$f'(R_0) = 1 \ , \quad (6.103)$$

$$\frac{f''(R_0)}{(6H_0^2)^{-1}} = -\frac{\mathcal{P}_2(q_0, j_0, s_0)\Omega_M + \mathcal{Q}_2(q_0, j_0, s_0)}{\mathcal{R}(q_0, j_0, s_0, l_0)} \ , \quad (6.104)$$

$$\frac{f'''(R_0)}{(6H_0^2)^{-2}} = -\frac{\mathcal{P}_3(q_0, j_0, s_0, l_0)\Omega_M + \mathcal{Q}_3(q_0, j_0, s_0, l_0)}{(j_0 - q_0 - 2)\mathcal{R}(q_0, j_0, s_0, l_0)} \ , \quad (6.105)$$

where we have defined :

$$\begin{aligned}\mathcal{P}_0 =& (j_0 - q_0 - 2)l_0 - (3s_0 + 7j_0 + 6q_0^2 + 41q_0 + 22)s_0 - \left[(3q_0 + 16)j_0 + 20q_0^2 + 64q_0 + \right. \\ &\left. + 12\right] j_0 - \left(3q_0^4 + 25q_0^3 + 96q_0^2 + 72q_0 + 20\right) \ , \end{aligned} \quad (6.106)$$

$$\begin{aligned}\mathcal{Q}_0 =& (q_0^2 - j_0q_0 + 2q_0)l_0 + \left[3q_0s_0 + (4q_0 + 6)j_0 + 6q_0^3 + 44q_0^2 + 22q_0 - 12\right] s_0 \\ &+ \left[2j_0^2 + (3q_0^2 + 10q_0 - 6)j_0 + 17q_0^3 + 52q_0^2 + 54q_0 + 36\right] j_0 + 3q_0^5 + 28q_0^4 + 118q_0^3 + \\ &+ 72q_0^2 - 76q_0 - 64 \ , \end{aligned} \quad (6.107)$$

$$\mathcal{P}_2 = 9s_0 + 6j_0 + 9q_0^2 + 66q_0 + 42 \ , \quad (6.108)$$

$$\mathcal{Q}_2 = -\left\{6(q_0+1)s_0 + [2j_0 - 2(1-q_0)]\, j_0 + 6q_0^3 + 50q_0^2 + 74q_0 + 32\right\} \ , \quad (6.109)$$

$$\mathcal{P}_3 = 3l_0 + 3s_0 - 9(q_0+4)j_0 - (45q_0^2 + 78q_0 + 12) \ , \quad (6.110)$$

$$\mathcal{Q}_3 = -\left\{2(1+q_0)l_0 + 2(j_0+q_0)s_0 - \left(2j_0 + 4q_0^2 + 12q_0 + 6\right) j_0 - (30q_0^3 + 84q_0^2 + 78q_0 + 24)\right\} \ , \quad (6.111)$$

$$\mathcal{R} = (j_0 - q_0 - 2)l_0 - (3s_0 - 2j_0 + 6q_0^2 + 50q_0 + 40)s_0 + \left[(3q_0+10)j_0 + 11q_0^2 + 4q_0 + - 18\right] j_0 - (3q_0^4 + 34q_0^3 + 246q_0 + 104) \ . \quad (6.112)$$

Eqs.(6.102) - (6.112) make it possible to estimate the present day values of $f(R)$ and its first three derivatives as function of the Hubble constant H_0 and the cosmographic parameters (q_0, j_0, s_0, l_0) provided a value for the matter density parameter Ω_M is given. This is a somewhat problematic point. Indeed, while the cosmographic parameters may be estimated in a model independent way, the fiducial value for Ω_M is usually the outcome of fitting a given dataset in the framework of an assumed dark energy scenario. However, it is worth noting that different models all converge towards the concordance value $\Omega_M \simeq 0.25$ which is also in agreement with astrophysical (model independent) estimates from the gas mass fraction in galaxy clusters. On the other hand, it has been proposed that $f(R)$ theories may avoid the need for dark matter in galaxies and galaxy clusters [73, 78, 84, 162, 343, 254, 46]. In such a case, the total matter content of the universe is essentially equal to the baryonic one. According to the primordial elements abundance and the standard BBN scenario, we therefore get $\Omega_M \simeq \omega_b/h^2$ with $\omega_b = \Omega_b h^2 \simeq 0.0214$ [209] and h the Hubble constant in units of $100\mathrm{km/s/Mpc}$. Setting $h = 0.72$ in agreement with the results of the HST Key project [159], we thus get $\Omega_M = 0.041$ for a baryons only universe. We will therefore consider in the following both cases when numerical estimates are needed.

It is worth noticing that H_0 only plays the role of a scaling parameter giving the correct physical dimensions to $f(R)$ and its derivatives. As such, it is not surprising that we need four cosmographic parameters, namely (q_0, j_0, s_0, l_0), to fix the four $f(R)$ related quantities $f(R_0)$, $f'(R_0)$, $f''(R_0)$, $f'''(R_0)$. It is also worth stressing that Eqs.(6.102) - (6.105) are linear in the $f(R)$ quantities so that (q_0, j_0, s_0, l_0) uniquely determine the former ones. On the contrary, inverting them to get the cosmographic parameters as function of the $f(R)$ ones, we do not get linear relations. Indeed, the field equations in $f(R)$ theories are nonlinear fourth order differential equations in the scale factor $a(t)$ so that fixing the derivatives of $f(R)$ up to third order makes it possible to find out a class of solutions, not a single one. Each one of these solutions will be characterized by a different set of cosmographic parameters thus explaining why the inversion of Eqs.(6.102) - (6.112) does not give a unique result for (q_0, j_0, s_0, l_0).

As a final comment, we reconsider the underlying assumptions leading to the above derived relations. While Eqs.(6.96) and (6.97) are exact relations deriving from a rigorous application of the field equations, Eq.(6.101) heavily relies on having approximated $f(R)$ with its third order Taylor expansion (6.100). If this assumption fails, the system should not be closed since a fifth unknown parameter enters the game, namely $f^{(iv)}(R_0)$. Actually, replacing $f(R)$ with its Taylor expansion is not possible for all class of $f(R)$ theories. As such, the above results

only hold in those cases where such an expansion is possible. Moreover, by truncating the expansion to the third order, we are implicitly assuming that higher order terms are negligible over the redshift range probed by the data. That is to say, we are assuming that :

$$f^{(n)}(R_0)(R-R_0)^n << \sum_{m=0}^{3} \frac{f^{(m)}(R_0)}{m!}(R-R_0)^m \quad \text{for } n \geq 4 \tag{6.113}$$

over the redshift range probed by the data. Checking the validity of this assumption is not possible without explicitly solving the field equations, but we can guess an order of magnitude estimate considering that, for all viable models, the background dynamics should not differ too much from the ΛCDM one at least up to $z \simeq 2$. Using then the expression of $H(z)$ for the ΛCDM model, it is easily to see that R/R_0 is a quickly increasing function of the redshift so that, in order Eq.(6.113) holds, we have to assume that $f^{(n)}(R_0) << f'''(R_0)$ for $n \geq 4$. This condition is easier to check for many analytical $f(R)$ models.

Once such a relation is verified, we have still to worry about Eq.(6.98) relying on the assumption that the *cosmological* gravitational constant is *exactly* the same as the *local* one. Although reasonable, this requirement is not absolutely demonstrated. Actually, the numerical value usually adopted for the Newton constant G_N is obtained from laboratory experiments in settings that can hardly be considered homogenous and isotropic. As such, the spacetime metric in such conditions has nothing to do with the cosmological one so that matching the two values of G is strictly speaking an extrapolation. Although commonly accepted and quite reasonable, the condition $G_{local} = G_{cosmo}$ could (at least, in principle) be violated so that Eq.(6.98) could be reconsidered. Indeed, as we will see, the condition $f'(R_0) = 1$ may not be verified for some popular $f(R)$ models recently proposed in literature. However, it is reasonable to assume that $G_{eff}(z=0) = G(1+\varepsilon)$ with $\varepsilon << 1$. When this be the case, we should repeat the derivation of Eqs.(6.102) - (6.105) now using the condition $f'(R_0) = (1+\varepsilon)^{-1}$. Taylor expanding the results in ε to the first order and comparing with the above derived equations, we can estimate the error induced by our assumption $\varepsilon = 0$. The resulting expressions are too lengthy to be reported and depend in a complicated way on the values of the matter density parameter Ω_M, the cosmographic parameters (q_0, j_0, s_0, l_0) and ε. However, we have numerically checked that the error induced on $f(R_0)$, $f''(R_0)$, $f'''(R_0)$ are much lower than 10% for value of ε as high as an unrealistic $\varepsilon \sim 0.1$. We are confident that our results are reliable also for these cases.

6.3 $f(R)$ derivatives and CPL models

A determination of $f(R)$ and its derivatives in terms of the cosmographic parameters need for an estimate of these latter from the data in a model independent way. Unfortunately, even in the nowadays era of *precision cosmology*, such a program is still too ambitious to give useful constraints on the $f(R)$ derivatives, as we will see later. On the other hand, the cosmographic parameters may also be expressed in terms of the dark energy density and EoS parameters so that we can work out what are the present day values of $f(R)$ and its derivatives giving the same (q_0, j_0, s_0, l_0) of the given dark energy model. To this aim, it is convenient to adopt a parameterized expression for the dark energy EoS in order to reduce the dependence of the results on any underlying theoretical scenario. Following the prescription of the Dark Energy Task Force [9], we will use the Chevallier - Polarski - Linder (CPL) parameterization for the EoS setting [103, 233] :

$$w = w_0 + w_a(1-a) = w_0 + w_a z(1+z)^{-1} \tag{6.114}$$

so that, in a flat universe filled by dust matter and dark energy, the dimensionless Hubble parameter $E(z) = H/H_0$ reads:

$$E^2(z) = \Omega_M(1+z)^3 + \Omega_X(1+z)^{3(1+w_0+w_a)}\mathrm{e}^{-\frac{3w_a z}{1+z}} \tag{6.115}$$

with $\Omega_X = 1-\Omega_M$ because of the flatness assumption. In order to determine the cosmographic parameters for such a model, we avoid integrating $H(z)$ to get $a(t)$ by noting that $d/dt = -(1+z)H(z)d/dz$. We can use such a relation to evaluate $(\dot{H}, \ddot{H}, d^3H/dt^3, d^4H/dt^4)$ and then solve Eqs.(6.6) - (6.9), evaluated in $z = 0$, with respect to the parameters of interest. Some algebra finally gives:

$$q_0 = \frac{1}{2} + \frac{3}{2}(1-\Omega_M)w_0 \ , \tag{6.116}$$

$$j_0 = 1 + \frac{3}{2}(1-\Omega_M)\left[3w_0(1+w_0) + w_a\right] \ , \tag{6.117}$$

$$\begin{aligned} s_0 = & -\frac{7}{2} - \frac{33}{4}(1-\Omega_M)w_a - \frac{9}{4}(1-\Omega_M)\left[9 + (7-\Omega_M)w_a\right]w_0 \\ & -\frac{9}{4}(1-\Omega_M)(16-3\Omega_M)w_0^2 - \frac{27}{4}(1-\Omega_M)(3-\Omega_M)w_0^3 \ , \end{aligned} \tag{6.118}$$

$$\begin{aligned} l_0 = & \frac{35}{2} + \frac{1-\Omega_M}{4}\left[213 + (7-\Omega_M)w_a\right]w_a + \frac{1-\Omega_M)}{4}\left[489 + 9(82-21\Omega_M)w_a\right]w_0 + \\ & + \frac{9}{2}(1-\Omega_M)\left[67 - 21\Omega_M + \frac{3}{2}(23-11\Omega_M)w_a\right]w_0^2 + \frac{27}{4}(1-\Omega_M)(47-24\Omega_M)w_0^3 + \\ & + \frac{81}{2}(1-\Omega_M)(3-2\Omega_M)w_0^4 \ . \end{aligned} \tag{6.119}$$

Inserting Eqs.(6.116) - (6.119) into Eqs.(6.102) - (6.112), we get lengthy expressions (which we do not report here) giving the present day values of $f(R)$ and its first three derivatives as function of (Ω_M, w_0, w_a). It is worth noting that the $f(R)$ model thus obtained is not dynamically equivalent to the starting CPL one. Indeed, the two models have the same cosmographic parameters only today. As such, for instance, the scale factor is the same between the two theories only over the time period during which the fifth order Taylor expansion is a good approximation of the actual $a(t)$. It is also worth stressing that such a procedure does not select a unique $f(R)$ model, but rather a class of fourth order theories all sharing the same third order Taylor expansion of $f(R)$.

6.3.1 The ΛCDM case

With these caveats in mind, it is worth considering first the ΛCDM model which is obtained by setting $(w_0, w_a) = (-1, 0)$ in the above expressions thus giving:

$$\begin{cases} q_0 = \dfrac{1}{2} - \dfrac{3}{2}\Omega_M \\ j_0 = 1 \\ s_0 = 1 - \dfrac{9}{2}\Omega_M \\ l_0 = 1 + 3\Omega_M + \dfrac{27}{2}\Omega_M^2 \end{cases} . \tag{6.120}$$

When inserted into the expressions for the $f(R)$ quantities, these relations give the remarkable result :

$$f(R_0) = R_0 + 2\Lambda \quad , \quad f''(R_0) = f'''(R_0) = 0 \ , \tag{6.121}$$

so that we obviously conclude that the only $f(R)$ theory having exactly the same cosmographic parameters as the ΛCDM model is just $f(R) \propto R$, i.e. GR. It is worth noticing that such a result comes out as a consequence of the values of (q_0, j_0) in the ΛCDM model. Indeed, should we have left (s_0, l_0) undetermined and only fixed (q_0, j_0) to the values in (6.120), we should have got the same result in (6.121). Since the ΛCDM model fits well a large set of different data, we do expect that the actual values of (q_0, j_0, s_0, l_0) do not differ too much from the ΛCDM ones. Therefore, we plug into Eqs.(6.102) - (6.112) the following expressions :

$$q_0 = q_0^\Lambda \times (1 + \varepsilon_q) \quad , \quad j_0 = j_0^\Lambda \times (1 + \varepsilon_j) \quad ,$$

$$s_0 = s_0^\Lambda \times (1 + \varepsilon_s) \quad , \quad l_0 = l_0^\Lambda \times (1 + \varepsilon_l) \quad ,$$

with $(q_0^\Lambda, j_0^\Lambda, s_0^\Lambda, l_0^\Lambda)$ given by Eqs.(6.120) and $(\varepsilon_q, \varepsilon_j, \varepsilon_s, \varepsilon_l)$ quantifyin the deviations from the ΛCDM values allowed by the data. A numerical estimate of these quantities may be obtained, e.g., from a Markov chain analysis, but this is outside our aims. Since we are here interested in a theoretical examination, we prefer to consider an idealized situation where the four quantities above all share the same value $\varepsilon << 1$. In such a case, we can easily investigate how much the corresponding $f(R)$ deviates from the GR one considering the two ratios $f''(R_0)/f(R_0)$ and $f'''(R_0)/f(R_0)$. Inserting the above expressions for the cosmographic parameters into the exact (not reported) formulae for $f(R_0)$, $f''(R_0)$ and $f'''(R_0)$, taking their ratios and then expanding to first order in ε, we finally get :

$$\eta_{20} = \frac{64 - 6\Omega_M(9\Omega_M + 8)}{[3(9\Omega_M + 74)\Omega_M - 556]\,\Omega_M^2 + 16} \times \frac{\varepsilon}{27} \ , \tag{6.122}$$

$$\eta_{30} = \frac{6\,[(81\Omega_M - 110)\Omega_M + 40]\,\Omega_M + 16}{[3(9\Omega_M + 74)\Omega_M - 556]\,\Omega_M^2 + 16} \times \frac{\varepsilon}{243\Omega_M^2} \ , \tag{6.123}$$

having defined $\eta_{20} = f''(R_0)/f(R_0) \times H_0^4$ and $\eta_{30} = f'''(R_0)/f(R_0) \times H_0^6$ which, being dimensionless quantities, are more suited to estimate the order of magnitudes of the different terms. Inserting our fiducial values for Ω_M, we get :

$$\begin{cases} \eta_{20} \simeq 0.15 \times \varepsilon \quad \text{for} \quad \Omega_M = 0.041 \\ \eta_{20} \simeq -0.12 \times \varepsilon \text{for} \quad \Omega_M = 0.250 \end{cases} ,$$

$$\begin{cases} \eta_{30} \simeq 4 \times \varepsilon \qquad \text{for} \;\; \Omega_M = 0.041 \\ \eta_{30} \simeq -0.18 \times \varepsilon \text{for} \;\; \Omega_M = 0.250 \end{cases} .$$

For values of ε up to 0.1, the above relations show that the second and third derivatives are at most two orders of magnitude smaller than the zeroth order term $f(R_0)$. Actually, the values of η_{30} for a baryon only model (first row) seems to argue in favor of a larger importance of the third order term. However, we have numerically checked that the above relations approximates very well the exact expressions up to $\varepsilon \simeq 0.1$ with an accuracy depending on the value of Ω_M, being smaller for smaller matter density parameters. Using the exact expressions for η_{20} and η_{30}, our conclusion on the negligible effect of the second and third order derivatives are significantly strengthened.

Such a result holds under the hypotheses that the narrower are the constraints on the validity of the ΛCDM model, the smaller are the deviations of the cosmographic parameters from the ΛCDM ones. It is possible to show that this indeed the case for the CPL parametrization we are considering. On the other hand, we have also assumed that the deviations $(\varepsilon_q, \varepsilon_j, \varepsilon_s, \varepsilon_l)$ take the same values. Although such hypothesis is somewhat ad hoc, we argue that the main results are not affected by giving it away. Indeed, although different from each other, we can still assume that all of them are very small so that Taylor expanding to the first order should lead to additional terms into Eqs.(6.122) - (6.123) which are likely of the same order of magnitude. We may therefore conclude that, if the observations confirm that the values of the cosmographic parameters agree within $\sim 10\%$ with those predicted for the ΛCDM model, we must conclude that the deviations of $f(R)$ from the GR case, $f(R) \propto R$, should be vanishingly small.

It is worth stressing, however, that such a conclusion only holds for those $f(R)$ models satisfying the constraint (6.113). It is indeed possible to work out a model having $f(R_0) \propto R_0$, $f''(R_0) = f'''(R_0) = 0$, but $f^{(n)}(R_0) \neq 0$ for some n. For such a (somewhat ad hoc) model, Eq.(6.113) is clearly not satisfied so that the cosmographic parameters have to be evaluated from the solution of the field equations. For such a model, the conclusion above does not hold so that one cannot exclude that the resulting (q_0, j_0, s_0, l_0) are within 10% of the ΛCDM ones.

6.3.2 The constant EoS model

Let us now take into account the condition $w = -1$, but still retains $w_a = 0$ thus obtaining the so called *quiessence* models. In such a case, some problems arise because both the terms $(j_0 - q_0 - 2)$ and $\mathcal{R}$ may vanish for some combinations of the two model parameters (Ω_M, w_0). For instance, we find that $j_0 - q_0 - 2 = 0$ for $w_0 = (w_1, w_2)$ with :

$$w_1 = \frac{1}{1 - \Omega_M + \sqrt{(1 - \Omega_M)(4 - \Omega_M)}} ,$$

$$w_2 = -\frac{1}{3}\left[1 + \frac{4 - \Omega_M}{\sqrt{(1 - \Omega_M)(4 - \Omega_M)}}\right] .$$

On the other hand, the equation $\mathcal{R}(\Omega_M, w_0) = 0$ may have different real roots for w depending on the adopted value of Ω_M. Denoting collectively with $\mathbf{w}_{null}$ the values of w_0 that, for a given

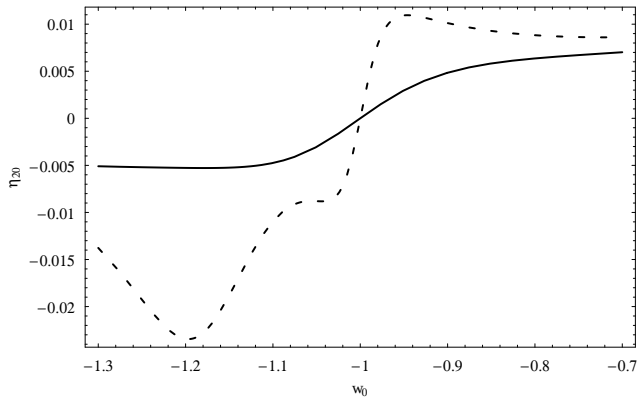

Figure 6.1: The dimensionless ratio between the present day values of $f''(R)$ and $f(R)$ as function of the constant EoS w_0 of the corresponding quiessence model. Short dashed and solid lines refer to models with $\Omega_M = 0.041$ and 0.250 respectively.

Ω_M, make $(j_0 - q_0 - 2)\mathcal{R}(\Omega_M, w_0)$ taking the null value, we individuate a set of quiessence models whose cosmographic parameters give rise to divergent values of $f(R_0$, $f''(R_0)$ and $f'''(R_0)$. For such models, $f(R)$ is clearly not defined so that we have to exclude these cases from further consideration. We only note that it is still possible to work out a $f(R)$ theory reproducing the same background dynamics of such models, but a different route has to be used.

Since both q_0 and j_0 now deviate from the ΛCDM values, it is not surprising that both $f''(R_0)$ and $f'''(R_0)$ take finite non null values. However, it is more interesting to study the two quantities η_{20} and η_{30} defined above to investigate the deviations of $f(R)$ from the GR case. These are plotted in Figs. 6.1 and 6.2 for the two fiducial Ω_M values. Note that the range of w_0 in these plots have been chosen in order to avoid divergences, but the lessons we will draw also hold for the other w_0 values.

As a general comment, it is clear that, even in this case, $f''(R_0)$ and $f'''(R_0)$ are from two to three orders of magnitude smaller that the zeroth order term $f(R_0)$. Such a result could be yet guessed from the previous discussion for the ΛCDM case. Actually, relaxing the hypothesis $w_0 = -1$ is the same as allowing the cosmographic parameters to deviate from the ΛCDM values. Although a direct mapping between the two cases cannot be established, it is nonetheless evident that such a relation can be argued thus making the outcome of the above plots not fully surprising. It is nevertheless worth noting that, while in the ΛCDM case, η_{20} and η_{30} always have opposite signs, this is not the case for quiessence models with $w > -1$. Indeed, depending on the value of Ω_M, we can have $f(R)$ theories with both η_{20} and η_{30} positive. Moreover, the lower is Ω_M, the higher are the ratios η_{20} and η_{30} for a given value of w_0. This can be explained qualitatively noticing that, for a lower Ω_M, the density parameter of the curvature fluid (playing the role of an effective dark energy) must be larger thus claiming for higher values of the second and third derivatives (see also [74] for a different approach to the problem).

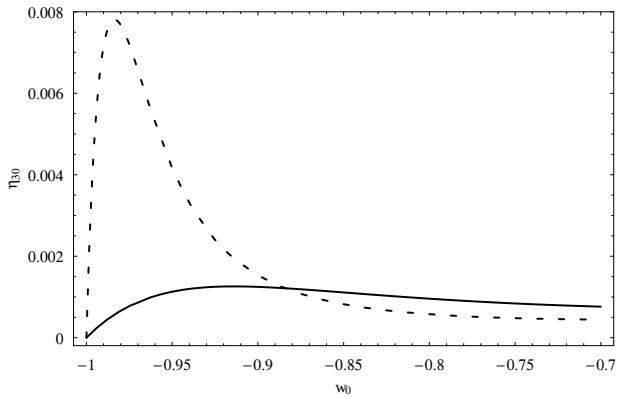

Figure 6.2: The dimensionless ratio between the present day values of $f'''(R)$ and $f(R)$ as function of the constant EoS w_0 of the corresponding quiessence model. Short dashed and solid lines refer to models with $\Omega_M = 0.041$ and 0.250 respectively.

6.3.3 The general case

Finally, we consider evolving dark energy models with $w_a \neq 0$. Needless to say, varying three parameters allows to get a wide range of models that cannot be discussed in detail. Therefore, we only concentrate on evolving dark energy models with $w_0 = -1$ in agreement with some most recent analysis. The results on η_{20} and η_{30} are plotted in Figs. 6.3 and 6.4 where these quantities as functions of w_a. Note that we are considering models with positive w_a so that $w(z)$ tends to $w_0 + w_a > w_0$ for $z \to \infty$ so that the EoS dark energy can eventually approach the dust value $w = 0$. Actually, this is also the range favored by the data. We have, however, excluded values where η_{20} or η_{30} diverge. Considering how they are defined, it is clear that these two quantities diverge when $f(R_0) = 0$ so that the values of (w_0, w_a) making (η_{20}, η_{30}) to diverge may be found solving :

$$\mathcal{P}_0(w_0, w_a)\Omega_M + \mathcal{Q}_0(w_0, w_a) = 0$$

where $\mathcal{P}_0(w_0, w_a)$ and $\mathcal{Q}_0(w_0, w_a)$ are obtained by inserting Eqs.(6.116) - (6.119) into the defintions (6.106) - (6.107). For such CPL models, there is no any $f(R)$ model having the same cosmographic parameters and, at the same time, satisfying all the criteria needed for the validity of our procedure. Actually, if $f(R_0) = 0$, the condition (6.113) is likely to be violated so that higher than third order must be included in the Taylor expansion of $f(R)$ thus invalidating the derivation of Eqs.(6.102) - (6.105).

Under these caveats, Figs. 6.3 and 6.4 demonstrate that allowing the dark energy EoS to evolve does not change significantly our conclusions. Indeed, the second and third derivatives, although being not null, are nevertheless negligible with respect to the zeroth order term thus arguing in favour of a GR - like $f(R)$ with only very small corrections. Such a result is, however, not fully unexpected. From Eqs.(6.116) and (6.117), we see that, having setted $w_0 = -1$, the q_0 parameter is the same as for the ΛCDM model, while j_0 reads $j_0^\Lambda + (3/2)(1 - \Omega_M)w_a$. As we have stressed above, the Hilbert - Einstein Lagrangian $f(R) = R + 2\Lambda$ is recovered when $(q_0, j_0) = (q_0^\Lambda, j_0^\Lambda)$ whatever the values of (s_0, l_0) are. Introducing a $w_a \neq 0$ makes (s_0, l_0) to differ from the ΛCDM values, but the first two cosmographic parameters are only mildly

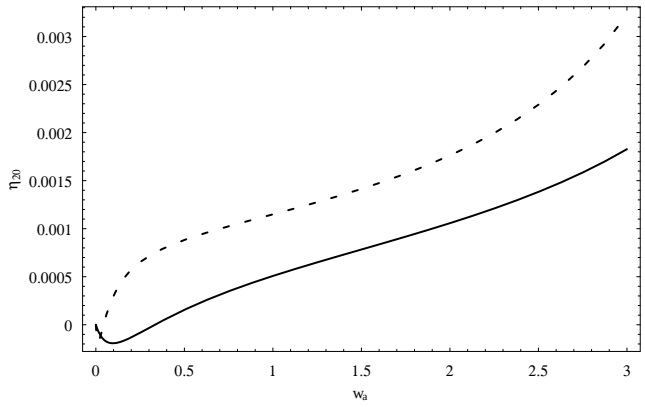

Figure 6.3: The dimensionless ratio between the present day values of $f''(R)$ and $f(R)$ as function of the w_a parameter for models with $w_0 = -1$. Short dashed and solid lines refer to models with $\Omega_M = 0.041$ and 0.250 respectively.

affected. Such deviations are then partially washed out by the complicated way they enter in the determination of the present day values of $f(R)$ and its first three derivatives.

6.4 Constraining $f(R)$ parameters

In the previous section, we have worked an alternative method to estimate $f(R_0)$, $f''(R_0)$, $f'''(R_0)$ resorting to a model independent parameterization of the dark energy EoS. However, in the ideal case, the cosmographic parameters are directly estimated from the data so that Eqs.(6.102) - (6.112) can be used to infer the values of the $f(R)$ related quantities. These latter can then be used to put constraints on the parameters entering an assumed fourth order theory assigned by a $f(R)$ function characterized by a set of parameters $\mathbf{p} = (p_1, \ldots, p_n)$ provided that the hypotheses underlying the derivation of Eqs.(6.102) - (6.112) are indeed satisfied. We show below two interesting cases which clearly highlight the potentiality and the limitations of such an analysis.

6.4.1 Double power law Lagrangian

As a first interesting example, we set :

$$f(R) = R\left(1 + \alpha R^n + \beta R^{-m}\right) \tag{6.124}$$

with n and m two positive real numbers (see, for example, [280] for some physical motivations). The following expressions are immediately obtained :

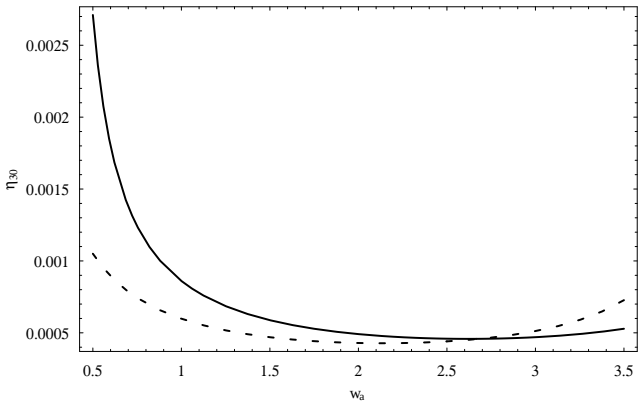

Figure 6.4: The dimensionless ratio between the present day values of $f'''(R)$ and $f(R)$ as function of the w_a parameter for models with $w_0 = -1$. Short dashed and solid lines refer to models with $\Omega_M = 0.041$ and 0.250 respectively.

$$\begin{cases} f(R_0) &= R_0\left(1+\alpha R_0^n+\beta R_0^{-m}\right) \\ f'(R_0) &= 1+\alpha(n+1)R_0^n-\beta(m-1)R_0^{-m} \\ f''(R_0) &= \alpha n(n+1)R_0^{n-1}+\beta m(m-1)R_0^{-(1+m)} \\ f'''(R_0) &= \alpha n(n+1)(n-1)R_0^{n-2} \\ & \quad -\beta m(m+1)(m-1)R_0^{-(2+m)} \end{cases} .$$

Denoting by ϕ_i (with $i = 0, \ldots, 3$) the values of $f^{(i)}(R_0)$ determined through Eqs.(6.102) - (6.112), we can solve :

$$\begin{cases} f(R_0) &= \phi_0 \\ f'(R_0) &= \phi_1 \\ f''(R_0) &= \phi_2 \\ f'''(R_0) &= \phi_3 \end{cases}$$

which is a system of four equations in the four unknowns (α, β, n, m) that can be analytically solved proceeding as follows. First, we solve the first and second equation with respect to (α, β) obtaining :

$$\begin{cases} \alpha = \dfrac{1-m}{n+m}\left(1-\dfrac{\phi_0}{R_0}\right)R_0^{-n} \\ \beta = -\dfrac{1+n}{n+m}\left(1-\dfrac{\phi_0}{R_0}\right)R_0^{m} \end{cases} , \tag{6.125}$$

while, solving the third and fourth equations, we get :

$$\begin{cases} \alpha = \dfrac{\phi_2 R_0^{1-n}\left[1+m+(\phi_3/\phi_2)R_0\right]}{n(n+1)(n+m)} \\ \beta = \dfrac{\phi_2 R_0^{1+n}\left[1-n+(\phi_3/\phi_2)R_0\right]}{m(1-m)(n+m)} \end{cases} . \tag{6.126}$$

Equating the two solutions, we get a systems of two equations in the two unknowns (n, m), namely :

$$\begin{cases} \dfrac{n(n+1)(1-m)\left(1-\phi_0/R_0\right)}{\phi_2 R_0\left[1+m+(\phi_3/\phi_2)R_0\right]} = 1 \\ \dfrac{m(n+1)(m-1)\left(1-\phi_0/R_0\right)}{\phi_2 R_0\left[1-n+(\phi_3/\phi_2)R_0\right]} = 1 \end{cases} . \tag{6.127}$$

Solving with respect to m, we get two solutions, the first one being $m = -n$ which has to be discarded since makes (α, β) goes to infinity. The only acceptable solution is :

$$m = -\left[1-n+(\phi_3/\phi_2)R_0\right] \tag{6.128}$$

which, inserted back into the above system, leads to a second order polynomial equation for n with solutions :

$$n = \frac{1}{2}\left[1+\frac{\phi_3}{\phi_2}R_0 \pm \frac{\sqrt{\mathcal{N}(\phi_0,\phi_2,\phi_3)}}{\phi_2 R_0(1+\phi_0/R_0)}\right] \tag{6.129}$$

where we have defined :

$$\begin{aligned} \mathcal{N}(\phi_0,\phi_2,\phi_3) = & \left(R_0^2\phi_0^2 - 2R_0^3\phi_0 + R_0^4\right)\phi_3^2 \\ & +6\left(R_0\phi_0^2 - 2R_0^2\phi_0 + R_0^3\right)\phi_2\phi_3 \\ & +9\left(\phi_0^2 - 2R_0\phi_0 + R_0^2\right)\phi_2^2 \\ & +4\left(R_0^2\phi_0 - R_0^3\right)\phi_2^3 . \end{aligned} \tag{6.130}$$

Depending on the values of (q_0, j_0, s_0, l_0), Eq.(6.129) may lead to one, two or any acceptable solution, i.e. real positive values of n. This solution has then to be inserted back into Eq.(6.128) to determine m and then into Eqs.(6.125) or (6.126) to estimate (α, β). If the final values of (α, β, n, m) are physically viable, we can conclude that the model in Eq.(6.124) is in agreement with the data giving the same cosmographic parameters inferred from the data themselves. Exploring analytically what is the region of the (q_0, j_0, s_0, l_0) parameter space which leads to acceptable (α, β, n, m) solutions is a daunting task far outside the aim of the present work.

6.4.2 HS model

One of the most pressing problems of $f(R)$ theories is the need to escape the severe constraints imposed by the Solar System tests. A successful model has been recently proposed by Hu and Sawicki [190] (HS) setting[7] :

[7] Note that such a model does not pass the matter instability test so that some viable generalizations [278, 109, 279] have been proposed.

$$f(R) = R - R_c \frac{\alpha (R/R_c)^n}{1 + \beta (R/R_c)^n} \ . \tag{6.131}$$

As for the double power law model discussed above, there are four parameters which we can be expressed in terms of the cosmographic parameters (q_0, j_0, s_0, l_0).

As a first step, it is trivial to get :

$$\begin{cases} f(R_0) &= R_0 - R_c \dfrac{\alpha R_{0c}^n}{1 + \beta R_{0c}^n} \\ f'(R_0) &= 1 - \dfrac{\alpha n R_c R_{0c}^n}{R_0 (1 + \beta R_{0c}^n)^2} \\ f''(R_0) &= \dfrac{\alpha n R_c R_{0c}^n \left[(1-n) + \beta (1+n) R_{0c}^n \right]}{R_0^2 (1 + \beta R_{0c}^n)^3} \\ f'''(R_0) &= \dfrac{\alpha n R_c R_{0c}^n (An^2 + Bn + C)}{R_0^3 (1 + \beta R_{0c}^n)^4} \end{cases} \tag{6.132}$$

with $R_{0c} = R_0 / R_c$ and :

$$\begin{cases} A = -\beta^2 R_{0c}^{2n} + 4 \beta R_{0c}^n - 1 \\ B = 3 (1 - \beta^2 R_{0c}^{2n}) \\ C = -2 (1 - \beta R_{0c}^n)^2 \end{cases} \ . \tag{6.133}$$

Equating Eqs.(6.132) to the four quantities $(\phi_0, \phi_1, \phi_2, \phi_3)$ defined as above, we could, in principle, solve this system of four equations in four unknowns to get (α, β, R_c, n) in terms of $(\phi_0, \phi_1, \phi_2, \phi_3)$ and then, using Eqs.(6.102) - (6.112) as functions of the cosmographic parameters. However, setting $\phi_1 = 1$ as required by Eq.(6.103) gives the only trivial solution $\alpha n R_c = 0$ so that the HS model reduces to the Einstein - Hilbert Lagrangian $f(R) = R$. In order to escape this problem, we can relax the condition $f'(R_0) = 1$ to $f'(R_0) = (1 + \varepsilon)^{-1}$. As we have discussed in Sect. IV, this is the same as assuming that the present day effective gravitational constant $G_{eff,0} = G_N / f'(R_0)$ only slightly differs from the usual Newtonian one which seems to be a quite reasonable assumption. Under this hypothesis, we can analytically solve for (α, β, R_c, n) in terms of $(\phi_0, \varepsilon, \phi_2, \phi_3)$. The actual values of (ϕ_0, ϕ_2, ϕ_3) will be no more given by Eqs.(6.102) - (6.105), but we have checked that they deviate from those expressions[8] much less than 10% for ε up to 10% well below any realistic expectation.

With this caveat in mind, we first solve

$$f(R_0) = \phi_0 \quad , \quad f''(R_0) = (1 + \varepsilon)^{-1}$$

to get :

$$\alpha = \frac{n (1 + \varepsilon)}{\varepsilon} \left(\frac{R_0}{R_c} \right)^{1-n} \left(1 - \frac{\phi_0}{R_0} \right)^2 \ ,$$

[8] Note that the correct expressions for (phi_0, ϕ_2, ϕ_3) may still formally be written as Eqs.(6.102) - (6.105), but the polynomials entering them are now different and also depend on powers of ε.

$$\beta=\frac{n(1+\varepsilon)}{\varepsilon}\left(\frac{R_0}{R_c}\right)^{-n}\left[1-\frac{\phi_0}{R_0}-\frac{\varepsilon}{n(1+\varepsilon)}\right] .$$

Inserting these expressions in Eqs.(6.132), it is easy to check that R_c cancels out so that we can no more determine its value. Such a result is, however, not unexpected. Indeed, Eq.(6.131) can trivially be rewritten as:

$$f(R)=R-\frac{\tilde{\alpha}R^n}{1+\tilde{\beta}R^n}$$

with $\tilde{\alpha}=\alpha R_c^{1-n}$ and $\tilde{\beta}=\beta R_c^{-n}$ which are indeed the quantities that are determined by the above expressions for (α,β). Reversing the discussion, the present day values of $f^{(i)}(R)$ depend on (α,β,R_c) only through the two parameters $(\tilde{\alpha},\tilde{\beta})$. As such, the use of cosmographic parameters is unable to break this degeneracy. However, since R_c only plays the role of a scaling parameter, we can arbitrarily set its value without loss of generality.

On the other hand, this degeneracy allows us to get a consistency relation to immediately check whether the HS model is viable or not. Indeed, solving the equation $f''(R_0)=\phi_2$, we get:

$$n=\frac{(\phi_0/R_0)+[(1+\varepsilon)/\varepsilon](1-\phi_2R_0)-(1-\varepsilon)/(1+\varepsilon)}{1-\phi_0/R_0} ,$$

which can then be inserted into the equations $f'''(R_0)=\phi_3$ to obtain a complicated relation among (ϕ_0,ϕ_2,ϕ_3) which we do not report for sake of shortness. Solving such a relation with respect to ϕ_3/ϕ_0 and Taylor expanding to first order in ε, the constraint we get reads:

$$\frac{\phi_3}{\phi_0}\simeq-\frac{1+\varepsilon}{\varepsilon}\frac{\phi_2}{R_0}\left[R_0\left(\frac{\phi_2}{\phi_0}\right)+\frac{\varepsilon\phi_0^{-1}}{1+\varepsilon}\left(1-\frac{2\varepsilon}{1-\phi_0/R_0}\right)\right] .$$

If the cosmographic parameters (q_0,j_0,s_0,l_0) are known with sufficient accuracy, one could compute the values of $(R_0,\phi_0,\phi_2.\phi_3)$ for a given ε (eventually using the expressions obtained for $\varepsilon=0$) and then check if they satisfied this relation. If this is not the case, one can immediately give off the HS model also without the need of solving the field equations and fitting the data. Actually, given the still large errors on the cosmographic parameters, such a test only remains in the realm of (quite distant) future applications. However, the HS model works for other tests as shown in [190] and so a consistent cosmography analysis has to be combined with them.

6.5 Constraints on $f(R)$ derivatives from the data

Eqs.(6.102) - (6.112) relate the present day values of $f(R)$ and its first three derivatives to the cosmographic parameters (q_0,j_0,s_0,l_0) and the matter density Ω_M. In principle, therefore, a measurement of these latter quantities makes it possible to put constraints on $f^{(i)}(R_0)$, with $i=\{0,\ldots,3\}$, and hence on the parameters of a given fourth order theory through the method shown in the previous section. Actually, the cosmographic parameters are affected by errors which obviously propagate onto the $f(R)$ quantities. Actually, the covariance matrix for the cosmographic parameters is not diagonal so that one has also take care of this to estimate the final errors on $f^{(i)}(R_0)$. A similar discussion also holds for the errors on the dimensionless ratios η_{20} and η_{30} introduced above. As a general rule, indicating with $g(\Omega_M,\mathbf{p})$ a generic $f(R)$

related quantity depending on Ω_M and the set of cosmographic parameters $\mathbf{p}$, its uncertainty reads:

$$\sigma_g^2 = \left|\frac{\partial g}{\partial \Omega_M}\right|^2 \sigma_M^2 + \sum_{i=1}^{i=4} \left|\frac{\partial g}{\partial p_i}\right|^2 \sigma_{p_i}^2 + \sum_{i\neq j} 2\frac{\partial g}{\partial p_i}\frac{\partial g}{\partial p_j} C_{ij} \tag{6.134}$$

where C_{ij} are the elements of the covariance matrix (being $C_{ii} = \sigma_{p_i}^2$), we have set $(p_1, p_2, p_3, p_4) = (q_0, j_0, s_0, l_0)$. and assumed that the error σ_M on Ω_M is uncorrelated with those on $\mathbf{p}$. Note that this latter assumption strictly holds if the matter density parameter is estimated from an astrophysical method (such as estimating the total matter in the universe from the estimated halo mass function). Alternatively, we will assume that Ω_M is constrained by the CMBR related experiments. Since these latter mainly probes the very high redshift universe ($z \simeq z_{lss} \simeq 1089$), while the cosmographic parameters are concerned with the present day cosmo, one can argue that the determination of Ω_M is not affected by the details of the model adopted for describing the late universe. Indeed, we can reasonably assume that, whatever is the dark energy candidate or $f(R)$ theory, the CMBR era is well approximated by the standard GR with a model comprising only dust matter. As such, we will make the simplifying (but well motivated) assumption that σ_M may be reduced to very small values and is uncorrelated with the cosmographic parameters.

Under this assumption, the problem of estimating the errors on $g(\Omega_M, \mathbf{p})$ reduces to estimating the covariance matrix for the cosmographic parameters given the details of the data set used as observational constraints. We address this issue by computing the Fisher information matrix (see, e.g., [359] and references therein) defined as:

$$F_{ij} = \left\langle \frac{\partial^2 L}{\partial\theta_i \partial\theta_j} \right\rangle \tag{6.135}$$

with $L = -2\ln\mathcal{L}(\theta_1, \ldots, \theta_n)$, $\mathcal{L}(\theta_1, \ldots, \theta_n)$ the likelihood of the experiment, $(\theta_1, \ldots, \theta_n)$ the set of parameters to be constrained, and $\langle \ldots \rangle$ denotes the expectation value. Actually, the expectation value is computed by evaluating the Fisher matrix elements for fiducial values of the model parameters $(\theta_1, \ldots, \theta_n)$, while the covariance matrix $\mathbf{C}$ is finally obtained as the inverse of $\mathbf{F}$.

A key ingredient in the computation of $\mathbf{F}$ is the definition of the likelihood which depends, of course, of what experimental constraint one is using. To this aim, it is worth remembering that our analysis is based on fifth order Taylor expansion of the scale factor $a(t)$ so that we can only rely on observational tests probing quantities that are well described by this truncated series. Moreover, since we do not assume any particular model, we can only characterize the background evolution of the universe, but not its dynamics which, being related to the evolution of perturbations, unavoidably need the specification of a physical model. As a result, the SNeIa Hubble diagram is the ideal test[9] to constrain the cosmographic parameters. We therefore defined the likelihood as:

$$\begin{aligned} &\mathcal{L}(H_0, \mathbf{p}) \propto \exp -\chi^2(H_0, \mathbf{p})/2 \\ &\chi^2(H_0, \mathbf{p}) = \textstyle\sum_{n=1}^{\mathcal{N}_{SNeIa}} \left[\dfrac{\mu_{obs}(z_i) - \mu_{th}(z_n, H_0, \mathbf{p})}{\sigma_i(z_i)}\right]^2 , \end{aligned} \tag{6.136}$$

where the distance modulus to redshift z reads:

[9] See the conclusions for further discussion on this issue.

$$\mu_{th}(z, H_0, \mathbf{p}) = 25 + 5\log(c/H_0) + 5\log d_L(z, \mathbf{p}) \ , \tag{6.137}$$

and $d_L(z)$ is the Hubble free luminosity distance:

$$d_L(z) = (1+z)\int_0^z \frac{dz}{H(z)/H_0} \ . \tag{6.138}$$

Using the fifth order Taylor expansion of the scale factor, we get for $d_L(z, \mathbf{p})$ an analytical expression (reported in Appendix A) so that the computation of F_{ij} does not need any numerical integration (which makes the estimate faster). As a last ingredient, we need to specify the details of the SNeIa survey giving the redshift distribution of the sample and the error on each measurement. Following [208], we adopt[10]:

$$\sigma_(z) = \sqrt{\sigma_{sys}^2 + \left(\frac{z}{z_{max}}\right)^2 \sigma_m^2}$$

with z_{max} the maximum redshift of the survey, σ_{sys} an irreducible scatter in the SNeIa distance modulus and σ_m to be assigned depending on the photometric accuracy.

In order to run the Fisher matrix calculation, we have to set a fiducial model which we set according to the ΛCDM predictions for the cosmographic parameters. For $\Omega_M = 0.3$ and $h = 0.72$ (with h the Hubble constant in units of $100\mathrm{km/s/Mpc}$), we get:

$$(q_0, j_0, s_0, l_0) = (-0.55, 1.0, -0.35, 3.11) \ .$$

As a first consistency check, we compute the Fisher matrix for a survey mimicking the recent database in [126] thus setting $(\mathcal{N}_{SNeIa}, \sigma_m) = (192, 0.33)$. After marginalizing over h (which, as well known, is fully degenerate with the SNeIa absolute magnitude $\mathcal{M}$), we get for the uncertainties:

$$(\sigma_1, \sigma_2, \sigma_3, \sigma_4) = (0.38, 5.4, 28.1, 74.0)$$

where we are still using the indexing introduced above for the cosmographic parameters. These values compare reasonably well with those obtained from a cosmographic fitting of the Gold SNeIa dataset[11] [197, 198]:

$$q_0 = -0.90 \pm 0.65 \ \ , \ \ j_0 = 2.7 \pm 6.7 \ \ ,$$

$$s_0 = 36.5 \pm 52.9 \ \ , \ \ l_0 = 142.7 \pm 320 \ \ .$$

[10] Note that, in [208], the authors assume the data are separated in redshift bins so that the error becomes $\sigma^2 = \sigma_{sys}^2/\mathcal{N}_{bin} + \mathcal{N}_{bin}(z/z_{max})^2\sigma_m^2$ with $\mathcal{N}_{bin}$ the number of SNeIa in a bin. However, we prefer to not bin the data so that $\mathcal{N}_{bin} = 1$.

[11] Actually, such estimates have been obtained computing the mean and the standard deviation from the marginalized likelihoods of the cosmographic parameters. As such, the central values do not represent exactly the best fit model, while the standard deviations do not give a rigorous description of the error because the marginalized likelihoods are manifestly non - Gaussian. Nevertheless, we are mainly interested in an order of magnitude estimate so that we do not care about such statistical details.

Because of the Gaussian assumptions it relies on, the Fisher matrix forecasts are known to be lower limits to the accuracy a given experiment can attain on the determination of a set of parameters. This is indeed the case with the comparison suggesting that our predictions are quite optimistic. It is worth stressing, however, that the analysis in [197, 198] used the Gold SNeIa dataset which is poorer in high redshift SNeIa than the [126] one we are mimicking so that larger errors on the higher order parameters (s_0, l_0) are expected.

Rather than computing the errors on $f(R_0)$ and its first three derivatives, it is more interesting to look at the precision attainable on the dimensionless ratios $(\eta_{20}, \eta_{30}$ introduced above since they quantify how much deviations from the linear order are present. For the fiducial model we are considering, both η_{20} and η_{30} vanish, while, using the covariance matrix for a present day survey and setting $\sigma_M/\Omega_M \simeq 10\%$, their uncertainties read :

$$(\sigma_{20}, \sigma_{30}) = (0.04, 0.04) \ .$$

As an application, we can look at Figs. 6.1 and 6.2 showing how (η_{20}, η_{30}) depend on the present day EoS w_0 for $f(R)$ models sharing the same cosmographic parameters of a dark energy model with constant EoS. As it is clear, also considering only the 1σ range, the full region plotted is allowed by such large constraints on (η_{20}, η_{30}) thus meaning that the full class of corresponding $f(R)$ theories is viable. As a consequence, we may conclude that the present day SNeIa data are unable to discriminate between a Λ dominated universe and this class of fourth order gravity theories.

As a next step, we consider a SNAP - like survey [10] thus setting $(\mathcal{N}_{SNeIa}, \sigma_m) = (2000, 0.02)$. We use the same redshift distribution in Table 1 of [208] and add 300 nearby SNeIa in the redshift range $(0.03, 0.08)$. The Fisher matrix calculation gives for the uncertainties on the cosmographic parameters :

$$(\sigma_1, \sigma_2, \sigma_3, \sigma_4) = (0.08, 1.0, 4.8, 13.7) \ .$$

The significant improvement of the accuracy in the determination of (q_0, j_0, s_0, l_0) translates in a reduction of the errors on (η_{20}, η_{30}) which now read :

$$(\sigma_{20}, \sigma_{30}) = (0.007, 0.008)$$

having assumed that, when SNAP data will be available, the matter density parameter Ω_M has been determined with a precision $\sigma_M/\Omega_M \sim 1\%$. Looking again at Figs. 6.1 and 6.2, it is clear that the situation is improved. Indeed, the constraints on η_{20} makes it possible to narrow the range of allowed models with low matter content (the dashed line), while models with typical values of Ω_M are still viable for w_0 covering almost the full horizontal axis. On the other hand, the constraint on η_{30} is still too weak so that almost the full region plotted is allowed.

Finally, we consider an hypothetical future SNeIa survey working at the same photometric accuracy as SNAP and with the same redshift distribution, but increasing the number of SNeIa up to $\mathcal{N}_{SNeIa} = 6\times10^4$ as expected from, e.g., DES [358], PanSTARRS [202], SKYMAPPER [330], while still larger numbers may potentially be achieved by ALPACA [113] and LSST [370]. Such a survey can achieve :

$$(\sigma_1, \sigma_2, \sigma_3, \sigma_4) = (0.02, 0.2, 0.9, 2.7)$$

so that, with $\sigma_M/\Omega_M \sim 0.1\%$, we get :

$$(\sigma_{20}, \sigma_{30}) = (0.0015, 0.0016) \ .$$

Fig. 6.1 shows that, with such a precision on η_{20}, the region of w_0 values allowed essentially reduces to the ΛCDM value, while, from Fig. 6.2, it is clear that the constraint on η_{30} definitively excludes models with low matter content further reducing the range of w_0 values to quite small deviations from the $w_0 = -1$. We can therefore conclude that such a survey will be able to discriminate between the concordance ΛCDM model and all the $f(R)$ theories giving the same cosmographic parameters as quiessence models other than the ΛCDM itself.

A similar discussion may be repeated for $f(R)$ models sharing the same (q_0, j_0, s_0, l_0) values as the CPL model even if it is less intuitive to grasp the efficacy of the survey being the parameter space multivalued. For the same reason, we have not explored what is the accuracy on the double power - law or HS models, even if this is technically possible. Actually, one should first estimate the errors on the present day value of $f(R)$ and its three time derivatives and then propagate them on the model parameters using the expressions obtained in Sect. VI. The multiparameter space to be explored makes this exercise quite cumbersome so that we leave it for a furthcoming work where we will explore in detail how these models compare to the present and future data.

6.6 Conclusions

The recent amount of good quality data have given a new input to the observational cosmology. As often in science, new and better data lead to unexpected discoveries as in the case of the nowadays accepted evidence for cosmic acceleration. However, a fierce and strong debate is still open on what this cosmic speed up implies for theoretical cosmology. The equally impressive amount of different (more or less) viable candidates have also generated a great confusion so that model independent analyses are welcome. A possible solution could come from the cosmography of the universe rather than assuming *ad hoc* solutions of the cosmological Friedmann equations. Present day and future SNeIa surveys have renewed the interest in the determination of the cosmographic parameters so that it is worth investigating how these quantities can constrain cosmological models.

Motivated by this consideration, in the framework of metric formulation of $f(R)$ gravity, we have here derived the expressions of the present day values of $f(R)$ and its first three derivatives as function of the matter density parameter Ω_M, the Hubble constant H_0 and the cosmographic parameters (q_0, j_0, s_0, l_0). Although based on a third order Taylor expansion of $f(R)$, we have shown that such relations hold for a quite large class of models so that they are valid tools to look for viable $f(R)$ models without the need of solving the mathematically difficult nonlinear fourth order differential field equations.

Notwithstanding the common claim that we live in the era of *precision cosmology*, the constraints on (q_0, j_0, s_0, l_0) are still too weak to efficiently apply the program we have outlined above. As such, we have shown how it is possible to establish a link between the popular CPL parameterization of the dark energy equation of state and the derivatives of $f(R)$, imposing that they share the same values of the cosmographic parameters. This analysis has lead to the quite interesting conclusion that the only $f(R)$ function able to give the same values of (q_0, j_0, s_0, l_0) as the ΛCDM model is indeed $f(R) = R + 2\Lambda$. If future observations will tell us that the cosmographic parameters are those of the ΛCDM model, we can therefore rule out all $f(R)$ theories satisfying the hypotheses underlying our derivation of Eqs.(6.102) - (6.105). Actually, such a result should not be considered as a no way out for higher order gravity. Indeed, one could still work out a model with null values of $f''(R_0)$ and $f'''(R_0)$ as required by the above constraints, but non - vanishing higher order derivatives. One could well argue that such a contrived model could be rejected on the basis of the Occam's razor, but nothing

prevents from still taking it into account if it turns out to be both in agreement with the data and theoretically well founded.

If new SNeIa surveys will determine the cosmographic parameters with good accuracy, acceptable constraints on the two dimensionless ratios $\eta_{20} \propto f''(R_0)/f(R_0)$ and $\eta_{30} \propto f'''(R_0)/f(R_0)$ could be obtained thus allowing to discriminate among rival $f(R)$ theories. To investigate whether such a program is feasible, we have pursued a Fisher matrix based forecasts of the accuracy future SNeIa surveys can achieve on the cosmographic parameters and hence on (η_{20}, η_{30}). It turns out that a SNAP - like survey can start giving interesting (yet still weak) constraints allowing to reject $f(R)$ models with low matter content, while a definitive improvement is achievable with future SNeIa survey observing $\sim 10^4$ objects thus making it possible to discriminate between ΛCDM and a large class of fourth order theories. It is worth stressing, however, that the measurement of Ω_M should come out as the result of a model independent probe such as the gas mass fraction in galaxy clusters which, at present, is still far from the 1% requested precision. On the other hand, one can also rely on the Ω_M estimate from the CMBR anisotropy and polarization spectra even if this comes to the price of assuming that the physics at recombination is strictly described by GR so that one has to limit its attention to $f(R)$ models reducing to $f(R) \propto R$ during that epoch. However, such an assumption is quite common in many $f(R)$ models available in literature so that it is not a too restrictive limitation.

A further remark is in order concerning what kind of data can be used to constrain the cosmographic parameters. The use of the fifth order Taylor expansion of the scale factor makes it possible to not specify any underlying physical model thus relying on the minimalist assumption that the universe is described by the flat Robertson - Walker metric. While useful from a theoretical perspective, such a generality puts severe limitations to the dataset one can use. Actually, we can only resort to observational tests depending only on the background evolution so that the range of astrophysical probes reduces to standard candles (such as SNeIa and possibly Gamma Ray Bursts) and standard rods (such as the angular size - redshift relation for compact radiosources). Moreover, pushing the Hubble diagram to $z \sim 2$ may rise the question of the impact of gravitational lensing amplification on the apparent magnitude of the adopted standard candle. The magnification probability distribution function depends on the growth of perturbations [187, 188, 191, 161, 111] so that one should worry about the underlying physical model in order to estimate whether this effect biases the estimate of the cosmographic parameters. However, it has been shown [313, 199, 181, 283, 324] that the gravitational lensing amplification does not alter significantly the measured distance modulus for $z \sim 1$ SNeIa. Although such an analysis has been done for GR based models, we can argue that, whatever is the $f(R)$ model, the growth of perturbations finally leads to a distribution of structures along the line of sight that is as similar as possible to the observed one so that the lensing amplification is approximately the same. We can therefore argue that the systematic error made by neglecting lensing magnification is lower than the statistical ones expected by the future SNeIa surveys. On the other hand, one can also try further reducing this possible bias using the method of flux averaging [384] even if, in such a case, our Fisher matrix calculation should be repeated accordingly. It is also worth noting that the constraints on the cosmographic parameters may be tigthened by imposing some physically motivated priors in the parameter space. For instance, we can impose that the Hubble parameter $H(z)$ stays always positive over the full range probed by the data or that the transition from past deceleation to present acceleration takes place over the range probed by the data (so that we can detect it). Such priors should be included in the likelihood definition so that the Fisher matrix should be recomputed which is left for a forthcoming work.

Although the present day data are still too limited to efficiently discriminate among rival

$f(R)$ models, we are confident that an aggressive strategy aiming at a very precise determination of the cosmographic parameters could offer stringent constraints on higher order gravity without the need of solving the field equations or addressing the complicated problems related to the growth of perturbations. Almost 80 years after the pioneering distance - redshift diagram by Hubble, the old cosmographic approach appears nowadays as a precious observational tool to investigate the new developments of cosmology.

CHAPTER 7

Conclusions and Perspectives

What is the main lesson we can derive from this dissertation?

At the present stage we think that there is one irrefutable reality: the Standard Cosmological Model based on General Relativity has some clearly evident difficulties. These ones first of all rely on a theoretical background; but then they convert in difficulties in interpreting observational data. We could say that *we have a book, but not the alphabet*.

We think it is also clear that nowadays there two big blocks in science which are confronting each other. On a side there are scientists which solve difficulties in the Standard Cosmological Model assuming that General Relativity is right, but then we need some new, exotic, invisible kinds of energy and matter to explain all its problematics. On the other side there are scientists which think that probably the question is that General Relativity is not the most general theory of Gravity, and that we can't extend our limited knowledge of it to ranges which we are not able (and probably we will not be able ever) to reach, so that it may be that we need an extension of General Relativity to a more comprehensive gravity theory.

Unfortunately, in this case there is not a Sixth Patriarch (as in the epigraph of this thesis) which comes and solves (if it solves...) the debate. To some extent this could be seen as a philosophical or even a metaphysical debate. Instead there are possibilities to move the question to a mathematical and physical (in one word: scientific) point of view.

We think that it is probably useless to underline and discuss what is the approach we have chosen to explore and which we believe in.

But it surely important to underline some useful points.

It is not important if f(R)-gravity models *are* the solution to all the problems. We don't think they are. But they are surely one of the most easy and fruitful approaches (toy models) to understand something more about gravity. As we have shown in the previous pages, in the same years Einstein formulated his General Relativity, many authors (and Einstein himself) started to explore *other possibilities*. At the beginning these explorations were made only for mathematical reasons. But when observations showed some interesting and puzzling properties of universe dynamics (i.e. accelerating expansion), these explorations also acquired strong

physical motivations.

At the end: what have we shown in these pages?

As we have just said it seems impossible, or, better, nowadays we have not the right instrumental possibilities to discriminate between alternative gravity models and traditional ones (dark energy, dark matter).

But is there a way to do this? In this vein we have started to work and study cosmography with deeper attention with respect past works. Cosmography may be a useful instrument in discriminating gravity theories because of it is a model independent approach: anyone of its parameters can be estimated without giving any cosmological model. So it is possible to use them in two ways:

- We can use them to discriminate between general relativity and f(R) models. But we have seen that in this case its potentiality depends very much on our technical and instrumental possibilities. We need some minimum sensibility and errors requirements on data survey (such as SNeIa ones) to expect to solve this question. At the moment we have not them and we are not able to do this;
- We can use the cosmographic parameters as constraints one any cosmological model without regarding to its original theoretical background. Being these parameters model independent, their estimations are unavoidable milestones that any theory has to satisfy.

Of course the application of Cosmography is not so simple. In our works we have explored what is the better way to use it and its limits.

Because of we think that it can be a useful instrument in exploring universe dynamics we are just now working trying to extend it in such a way we can use many different data (not only SNeIa which we have used intensively, but also CMB, BAO and gamma ray bursts). This also means that we are studying a way to evade its main limitation (it is founded on a Taylor series of scale factor with respect of cosmic time, or redshift), to make it a more general probe.

Then we have also shown that extended theories of gravity (in particular we have worked with f(R) models) can be successfully applied to a wide range of cosmological and astrophysical fields: they can reproduce SNeIa Hubble diagram, rotation curves of spiral galaxies and (one of the original parts of this thesis) to clusters of galaxies.

In this last case we have found out two important results.

We were able to define a *scale-dependent* gravity, where any gravitational scale as its own gravitational length. In this way we could successfully explain the problem of dark matter on astrophysical scales and its different profiles when passing from galaxies to clusters of galaxies. But it is matter of future works to understand on what theoretical ground this dependence can be established.

But what is more important is that we were able to extract a strong predictive power from this sketch. We have now some hypothetical results ranging from small scale gravitational systems (solar system), to biggest astrophysical scales (galaxies), to the smallest cosmological scales (clusters of galaxies), up to the entire universe. We have only checked one of these ranges. Future works will be devoted to verify our predicitions on galaxies's scale and first of all on solar system, which give more stringent and important constraint on the gravity theory.

Bibliography

[1] Abazajian, K., Adelman - McCarthy, J.K., Agüeros, M.A., Allam, S.S., Anderson, K.S.J., Anderson, S.F. et al. 2004, AJ, 128, 502

[2] Adelman - McCarthy, J.K., Agüeros, M.A., Allam, S.S., Anderson, K.S.J., Anderson, S.F. et al. 2006, ApJS, 162, 38

[3] Adelman - McCarthy, J.K., Agüeros, M.A., Allam, S.S., Allende Prieto, C., Anderson, K.S.J., Anderson, S.F., Annis, J., Bahcall, N.A. et al. 2007, ApJS, 175, 297

[4] Akaike, H. 1974, IEEE Trans. Auto. Control., 19, 716

[5] Akritas, M.G., Bershady, M.A. 1996, ApJ, 470, 706

[6] Abell, G. O. 1975, Galaxies and the Universe, 601

[7] Abell, G. O., 1989, ApJS, 70, 1

[8] Alam, U., Sahni, V., Saini, T.D., Starobinsky, A.A., 2003, MNRAS, 344, 1057

[9] Albrecht et al., *Dark energy task force final report*, FERMILAB-FN-0793-A, astro-ph/0609591, 2006

[10] Aldering G. et al., astro - ph/0405232, 2004; see also `snap.lbl.gov`

[11] Allemandi, G., Borowiec, A., Francaviglia, M., 2004, Phys. Rev. D 70, 103503

[12] Allemandi, G., Francaviglia, M., Ruggiero, M., Tartaglia, A. 2005, Gen. Rel. Grav., 37, 1891

[13] Allemandi, G., Capone, M., Capozziello, S., Francaviglia, M., 2006, *Gen. Relativ. Grav.* **38**, 33

[14] Allen, P.D., Driver, S.P., Graham, A.W., Cameron, E., Liske, J., de Propris, R. 2006, MNRAS, 371, 2

[15] Amendola, L., Capozziello, S., Litterio, M., Occhionero, F., 1992, *Phys. Rev.* **D 45**, 417

[16] Amendola, L., Battaglia-Mayer, A., Capozziello, S., Gottlöber, S., Müller, V., Occhionero, F., Schmidt, H.-J., 1993, *Class. Quantum Grav.* **10**, L43

[17] Amendola, L., Gannouji, R., Polarski, D., Tsujikawa, S., 2007, *Phys. Rev.* **D75**, 083504

[18] Amendola, L., Polarski, D., Tsujikawa, S., 2007, *Phys. Rev. Lett.* **98**, 131302

[19] Anderson, J.D., et al., 2002, *Phys. Rev.* **D 65**, 082004

[20] Appelquist, T., Chodos, A., Freund, P.G.O., *Modern Kaluza-Klein Theories*, Addison-Wesley, Reading (1987)

[21] Appleby, S.A., Battye, R.A., 2007, Phys. Lett. B, 654, 7

[22] Arnaud, M., Neumann, D. M., Aghanim, N., Gastaud, R., Majerowicz, S., Hughes J. P., 2001, A&A, 365, L80

[23] Arnold, V.I., *Mathematical Methods of Classical Mechanics*, Springer-Verlag, Berlin (1978)

[24] Astier, P. et al., 2006, A&A, 447, 31

[25] Bahcall N. A., 1977, Ann. Rev. Astron. Astrophys., 15, 505

[26] Bahcall N. A., 1988, Ann. Rev. Astron. Astrophys., 26, 631

[27] Bahcall N. A., 1996, in "Formation of structure in the universe, 1995, Jerusalem Winter School", astro-ph/9611148,

[28] Bahcall, N.A. et al. 2003, ApJ, 585, 182

[29] Bahcall, N.A., Bode, P. 2003, ApJ, 588, 1

[30] Barris, B.J., et al., 2004, ApJ, 602, 571

[31] Barrow, J., Ottewill, A.C., 1983, *J. Phys. A: Math. Gen.* **16**, 2757

[32] Bassett, B.A., Kunz, M., Parkinson, D., Ungarelli, C., Phys. Rev. D, 68, 043504, 2003

[33] Battaglia-Mayer, A., Schmidt, H.-J., 1993, *Class. Quantum Grav.* **10**, 2441

[34] Bautz, L. P., Morgan, W. W., 1970, ApJ, 162, L149

[35] Bell, E.F., de Jong, R.S. 2001, ApJ, 550, 212

[36] Bender, R., Burstein, D., Faber, S.M. 1992, ApJ, 399, 462

[37] Bennett C.L. et al., 2003, ApJS, 148, 1

[38] Bernardi, M., Sheth, R.K., Annis, J., Burles, S., Eisenstein, D.J. et al. 2003, AJ, 125, 1866

[39] Perez Bergliaffa, S.E., 2006, Phys. Lett. B, 642, 311

[40] Bernardi, M., Sheth, R.K., Nichol, R.C., Schneider, D.P., Brinkmann, J. 2005, AJ, 129, 61

[41] Bertolami, O., Böhmer, Ch.G., Lobo, F.S.N., (2007) gr-qc/0704.1733

[42] Bertotti B., Iess L., Tortora P., Nature **425**, 374 (2003)

[43] Binney, J., Tremaine, S. 1987, *Galactic dynamics*, Princeton University Books, Princeton (USA)

[44] Birrell, N.D. and Davies, P.C.W., 1982, Quantum Fields in Curved Space, Cambridge Univ. Press, Cambridge

[45] Blanton, M.R., Schlegel, D.J., Strauss, M.A., Brinkmann, J., Finkbeiner, D. et al. 2005, AJ, 129, 2562

[46] Boehmer, C.G., Harko, T., Lobo, F.S.N., arXiv:0709.0046 [gr-qc]

[47] Bondi, H., *Cosmology*, Cambridge Univ. Press, Cambridge (1952)

[48] Boughn, S., Crittenden, R., *Nature* (London) **427**, 45, 2004

[49] Borowiec, A., Godlowski, W., Szydlowski, M. 2006, Phys. Rev. D, 74, 043502

[50] Borriello, A., Salucci, P., 2001, Mont. Not. Roy. Astron. Soc., 323, 285

[51] Brans C., Dicke, R.H., *Phys. Rev.* **124**, 925 (1961)

[52] Brill, D.R., Gowdy, R.H., 1970, Rep. Prog. Phys., 33, 413

[53] Brodbeck, O., Straumann, N. 1993, J. Math. Phys., 34, 6

[54] Bronnikov, K., Melnikov, V. 1994, Gen. Rel. Grav., 27, 465

[55] Brownstein, J. R., Moffat, J. W., 2006, ApJ, 636, 721

[56] Brownstein, J. R., Moffat, J. W., 2006, MNRAS, 367, 527

[57] Brownstein, J. R., Moffat, astro-ph/0702146

[58] Bruzual, G., Charlot, S. 2003, MNRAS, 344, 1000

[59] Buchbinder, I.L., Odintsov, S.D., Shapiro, I.L., *Effective Action in Quantum Gravity*, IOP Publishing (1992) Bristol

[60] Buchdahl, H.A., J. Phys. A **12** (8) (1979), 1229

[61] Bullock, J.S., Kolatt, T.S., Sigad, Y., Somerville, R.S., Kravtsov, A.V., Klypin, A., Primack, J.P., Dekel, A. 2001, MNRAS, 321, 559

[62] Burkert, A., 1995, Astroph. Journ., 447, L25

[63] Burkert, A., Silk, J., 1997, Astroph. Journ., 488, L55

[64] Busarello. G., Capaccioli, M., Capozziello, S., Longo, G., Puddu, E. 1997, A&A, 320, 415

[65] Caon, N., Capaccioli, M., D' Onofrio, M. 1993, MNRAS, 265, 1013

[66] Capolupo, A., Capozziello, S., Vitiello, G. *Phys. Lett.* **A 363** (2007) 53

[67] Capozziello, S., de Ritis, P., Rubano, C., Scudellaro, P. *La Rivista del Nuovo Cimento* **4** (1996) 1

[68] Capozziello, S., de Ritis, R., Marino, A.A. *Gen. Relativ. Grav.* **30**, 1247, (1998)

[69] Capozziello, S. 2002, Int. J. Mod. Phys. D, 11, 483

[70] Capozziello, S., Cardone, V.F., Piedipalumbo, E., Sereno, M., Troisi, A., Int. J. Mod. Phys. D, 12, 381, 2003

[71] Capozziello, S., Cardone, V.F., Piedipalumbo, E., Rubano, C., Class. Quant. Grav. **23**, 1205 (2006)

[72] Capozziello, S., Cardone, V.F., Carloni, S., Troisi, A. 2003, Int. J. Mod. Phys. D, 12, 1969

[73] Capozziello, S., Cardone, V.F., Carloni, S., Troisi, A. 2004, Phys. Lett. A, 326, 292

[74] Capozziello, S., Cardone, V.F., Elizalde, E., Nojiri, S., Odintsov, S.D., 2006, Phys. Rev. D 73, 043512

[75] Capozziello, S., Cardone, V.F., Francaviglia, M. 2006, Gen. Rel. Grav., 38, 711

[76] Capozziello, S., Cardone, V.F., Funaro, M., Andreon, S., *Phys. Rev.* **D 70**, (2004) 123501

[77] Capozziello, S., Cardone, V.F., Troisi, A. 2005, Phys. Rev. D, 71, 043503

[78] Capozziello, S., Cardone, V.F., Troisi, A. 2006, JCAP, 0608, 001

[79] Capozziello, S., gr-qc/0412088

[80] Capozziello, S., Cardone, V. F., Troisi, A., 2006a, Jou. Cosm. and Astrop. Phys., 8, 001

[81] Capozziello, S., Cardone, V. F., Troisi, A., 2006b, Physical Review D, 73, 104019

[82] Capozziello, S., Nojiri, S., Odintsov, S.D., *Phys. Lett.* **B 634**, 93 (2006)

[83] Capozziello , S., Nojiri, S., Odintsov, S.D., Troisi, A., 2006, Phys. Lett. B (2006) 135.

[84] Capozziello, S., Cardone, V. F., Troisi, A., 2007, MNRAS, 375, 1423

[85] Capozziello, S., Stabile A., Troisi, A., 2007, Class. quant. grav., 24, 2153

[86] Capozziello, S., Stabile, A., Troisi, A., 2008, Physical Review D, 76, 104019

[87] Capozziello, S., Carloni, S., Troisi, A. 2003, Rec. Res. Devel. Astronomy. & Astrophys., 1, 625, astro - ph/0303041

[88] Capozziello S. and Francaviglia M., 2008, Gen. Rel. Grav.: Special Issue on Dark Energy 40, 357.

[89] Capozziello, S., Troisi, A. 2005, Phys. Rev. D, 72, 044022

[90] Capozziello, S., De Laurentis, M., Nojiri, S., Odintsov, S.D., 2008, arXiv:0808.1335 [hep-th]

[91] Cardone, V.F., Troisi, A., Capozziello, S., Phys. Rev. D, 69, 083517, 2004

[92] Cardone, V.F., Piedipalumbo, E., Tortora, C. 2005, MNRAS, 358, 1325

[93] Caresia, P., Matarrese, S., Moscardini, L., 2004, ApJ, 605, 21

[94] Carloni, S., Dunsby, P.K.S., Capozziello, S., Troisi, A. 2005, Class. Quantum Grav. 22, 2839

[95] Carloni, S., Troisi, A., Dunsby, P.K.S., gr-qc/0706.0452 (2007)

[96] Carroll, S.M., Duvvuri, V., Trodden, M., Turner, M.S. 2004, Phys. Rev. D, 70, 043528

[97] Carroll, S.M., Press, W.H., Turner, E.L. 1992, ARA&A, 30, 499

[98] Cartan, E., *Ann. Ec. Norm.* **42** (1925) 17

[99] Catinella, B., Giovanelli, R., Haynes, M.P. 2006, ApJ, 640, 751

[100] Cattoen, C., Visser, M., 2007, Class. Quant. Grav., 24, 5985

[101] Cembranos, J.A.R. 2006, Phys. Rev. D, 73, 064029

[102] Chen, G., Rathra, B., ApJ, 582, 586, 2003;

[103] Chevallier, M., Polarski, D., 2001, Int. J. Mod. Phys. D, 10, 213

[104] Chiba, T. 2003, Phys. Lett. B, 575, 1

[105] Christensen, N., Meyer, R., Knox, L., Luey, B., 2001, Class. Quant. Grav., 18, 2677

[106] Ciotti, L. 1991, A&A, 249, 99

[107] Clifton, T., Barrow, J.D. 2005, Phys. Rev. D, 72, 103005

[108] Clocchiati, A. et al. 2006, APJ, 642, 1

[109] Cognola, G., Elizalde, E., Nojiri, S., Odintsov, S.D., Sebastiani, L., Zerbini, S., 2008, Phys. Rev. D, 77, 046009

[110] Cole, S. et al. 2005, MNRAS, 362, 505

[111] Cooray, A., Huterer, D., Holz, D.E., 2006, Phys. Rev. Lett., 96, 021301

[112] Copeland E.J., Sami M., Tsujikawa S., 2006, Int. J. Mod. Phys. D 15, 1753

[113] Corasaniti, P.S., LoVerde, M., Crotts, A. et al., 2006, MNRAS, 369, 798

[114] Corbelli, E., Salucci, P., 2007, MNRAS 374(3), 1051

[115] Côté, S., Carignan, C., Sancisi, R., 1991, AJ. 102(3), 904

[116] Croft, R.A.C., Hu, W., Dave, R. 1999, Phys. Rev. Lett., 83, 1092

[117] D'Agostini, G. 2004, physics/0412148

[118] D'Agostini, G. 2005, physics/0511182

[119] de Bernardis, P. et al. 2000, Nature, 404, 955

[120] de Blok, W.J.G., Bosma, A., 2002, A&A, 385, 816

[121] de Blok, W.J.G. 2005, ApJ, 634, 227

[122] De Filippis, E., Sereno, M., Bautz, Longo G., M. W., 2005, ApJ, 625, 108

[123] de Vaucouleurs, G. 1948, Ann. d' Astroph., 11, 247

[124] Daly, R.A., Djorgovsky, S.G., 2004, Astrophys. J., 612, 652

[125] Damour, T., Esposito-Farèse, G., 1992 *Class. Quantum Grav.* **9** 2093

[126] Davis, T., et al., 2007, ApJ, 666, 716

[127] Dabrowski, M.P., 2005, Phys. Lett. B, 625, 184

[128] Dabrowski, M.P., Stachowiak, T., 2006, Annals of Physics, 321, 771

[129] Dabrowski, M.P., 2006, Annalen der Physik, 15, 352

[130] Demianski, M., Piedipalumbo, E., Rubano, C., Tortora, C., 2006, A&A, 454, 55

[131] Dick, R. 2004, Gen. Rel. Grav., 36, 217

[132] Dicke, R. H., 1962 *Phys. Rev.* **125** 2163

[133] Djorgovski, S., Davis, M. 1987, ApJ, 313, 59

[134] Dodelson S. et al., 2002, ApJ, 572, 140

[135] Dolgov, A.D., Kawasaki, M. 2003, Phys. Lett. B, 573, 1

[136] Dressler, A., Lynden - Bell, D., Burstein, D., Davies, R.L., Faber, S.M., Terlevich, R.J., Wegner, G. 1987, ApJ, 313, 42

[137] Driver, S.P., Allen, P.D., Graham, A.W., Cameron, E., Liske, J. 2006, MNRAS, 368, 414

[138] Dunkley, J., Bucher, M., Ferreira, P.G., Moodley, K., Skordis, C. 2005, MNRAS, 356, 925

[139] Duruisseau, J.P., Kerner, R., Gen. Rel. Grav. 15, 797-807 (1983)

[140] Dvali, G.R., Gabadadze G., Porrati M., 2000, Phys. Lett. B, 485, 208

[141] Dvali, G.R., Gabadadze, G., Kolanovic, M., Nitti, F., 2001, Phys. Rev. D, 64, 084004

[142] Dvali, G.R., Gabadadze, G., Kolanovic, M., Nitti, F., 2002, Phys. Rev. D, 64, 024031

[143] Eckhardt, D.H., 1993 Phys. Rev. **48 D**, 3762

[144] Einstein, A., *Sitzung-ber. Preuss. Akad. Wiss.*, 414 (1925)

[145] Eisenstein, D. et al. 2005, ApJ, 633, 560

[146] Eke, V.R., Cole, S., Frenk, C.S., Petrick, H.J. 1998, MNRAS, 298, 1145

[147] Ettori, S., Fabian, A. C., Allen, S. W., Johnstone, R. M., 2002, MNRAS, 331, 635

[148] Faber, S., Jackson, R. 1976, ApJ, 317, 1

[149] Faraoni, V., *Cosmology in Scalar-Tensor Gravity*, Kluwer Academic, Dordrecht (2004)

[150] Faraoni, V., *Class. Quantum Grav.* **22**, 32352 (2005)

[151] Fasalba, P., Gaztanaga, E., MNRAS **350**, L37 (2004)

[152] Feigelson, E.D., Babu, G.J. 1992, ApJ, 397, 55

[153] Ferraris, M., Francaviglia, M., Magnano, G., 1988 *Class. Quantum Grav.* **5** L95

[154] Ferraris, M., Francaviglia, M., Reina, C., *Gen. Relativ. Grav.* **14**, 243 (1982)

[155] Ferraris, M., Francaviglia, M., Volovich, I. ,*Class. Quantum Grav.* **11**, 1505 (1994)

[156] Fioc, M., Rocca - Volmerange, B. 1997, A&A, 326, 950

[157] E. Fischbach, E., Sudarsky, D., Szafer, A., Talmadge, C. and Aroson, S.H., 1986, Phys. Rev. Lett. **56**, 3

[158] Fraternali, F., et al., 2002, AJ, 123, 3124

[159] Freedman, W.L. et al., 2001, ApJ, 553, 47

[160] Freese, K., Lewis, M., Phys. Lett. B, 540, 1, 2002

[161] Frieman, J.A., 1997, Comments Astrophys., 18, 323

[162] Frigerio Martins C. and Salucci P., 2007, MNRAS, 381, 1103

[163] Y. Fujii, Y., 1988, Phys. Lett. **B 202**, 246

[164] Fujii, I., Maeda, K., *The scalar - tensor theory of gravity*, Cambridge University Press, Cambridge (UK), 2003

[165] Fukugita, M., Shimasaku, K., Ichikawa, T. 1995, PASP, 107, 945

[166] Fukugita, M., Hogan, C.J., Peebles, P.J.E. 1998, ApJ, 503, 518

[167] Garnavich P.M. et al., 1998, ApJ, 509, 74

[168] Gasperini, M., Veneziano, G., *Phys. Lett.* **277B** (1992) 256

[169] Gentile, G. et al., 2004, MNRAS 351, 903

[170] Gentile, G. et al., 2005, ApJ 234, L145

[171] Gentile, G., Salucci, P., 2004, Mon. Not. Roy. Astron. Soc., 351, 953

[172] Ghigna, S., Moore, B., Governato, F., Lake, G., Quinn, T., Stadel, J. 2000, ApJ, 544, 616

[173] G.W. Gibbons, G.W. and Whiting, B.F., 1981, *Nature* **291**, 636

[174] Gottlöber, S., Schmidt, H.-J., Starobinsky, A.A., *Class. Quantum Grav.* **7**, 893 (1990)

[175] Graham, A.W., Colless, M. 1997, MNRAS, 287, 221

[176] Graham, A.W. 2002, MNRAS, 334, 859

[177] Graham, A.W., Driver, S.P. 2005, PASA, 22, 118

[178] Graham, A.W., Merritt, D., Moore, B., Diemand, J., Terzic, B. 2006a, AJ, 132, 2701

[179] Graham, A.W., Merritt, D., Moore, B., Diemand, J., Terzic, B. 2006b, AJ, 132, 2711

[180] Green, M.B., Schwarz, J.H., Witten, E., *Superstring Theory*, Cambridge Univ. Press, Cambridge (1987)

[181] Gunnarsson, C., Dahlen, T., Goobar, A., Jönsson, J., Mörtsell, E., 2006, ApJ, 640, 417

[182] Guth, A., *Phys. Rev.* **D 23**, 347 (1981)

[183] Hannestad, S., Mortsell, E., Phys. Rev. D **66**, 0635088 (2002)

[184] Hannestad, S., Mortsell, E., JCAP **0409**, 001 (2004)

[185] Hawkins E. et al., 2003, MNRAS, 346, 78

[186] Hinshaw, G., et al. *Ap. J.* ApJS, **148**, 135 (2003)

[187] Holz, D.E., Wald, R.M., 1998, Phys. Rev. D, 58, 063501

[188] Holz, D.E., Linder, E.V., 2005, ApJ, 631, 678

[189] Hradecky, V., Jones, C., Donnelly, R. H., Djorgovski, S. V., Gal, R. R., Odewahn, S. C., 2000, ApJ, 543, 521

[190] Hu, W., Sawicki, I., 2007, Phys. Rev. D, 76, 064004

[191] Hui, L., Greene, P.B., 2006, Phys. Rev. D, 73, 123526

[192] Hwang, J.C., Noh, H., 1996, Phys. Rev. D, 54, 1460

[193] Hwang, J.C., Noh, H., 2001, Phys. Lett. B, 506, 13

[194] Ikebe, Y., Böhringer, H., Kitayama, T., 2004, ApJ, 611, 175

[195] Isham, C.J., in "Quantum Gravity 2: A second Oxford Symposium", Clarendon Press, Oxford, 1981

[196] Jeffreys, H. 1961, *Theory of probability*, 3rd edition, Oxford University Press, Oxford, UK

[197] John, M.V., 2004, ApJ, 614, 1

[198] John, M.V., 2005, ApJ, 630, 667

[199] Jönsson, J., Dahlen, T., Goobar, A., Gunnarsson, C., Mörtsell, E., Lee, K., 2006, ApJ, 639, 991

[200] Jørgensen, I., Franx, M., Kjærgaard, P. 1995, MNRAS, 273, 1097

[201] Jørgensen, I., Franx, M., Kjærgaard, P. 1996, MNRAS, 280, 167

[202] Kaiser N. and the PanSTARRS Team, in *Bullettin of the Americal Astronomical Society*, page 1049, 2005

[203] Kaku, M., *Quantum Field Theory*, Oxford Univ. Press, Oxford (1993)

[204] Kamenshchik, A., Moschella, U., Pasquier, V., Phys. Lett. B, 511, 265, 2001

[205] Kauffman, G., Heckman, T.M., White, S.D.M., Charlot, S., Tremonti, C. et al. 2003, MNRAS, 341, 33

[206] M. Kenmoku, M., Okamoto, Y. and Shigemoto, K., 1993, *Phys. Rev.* **48 D**, 578

[207] Khosroshahi, H.G., Wadadekar, Y., Kembhavi, A., Mobasher, B. 2000, ApJ, 531, L103

[208] Kim, A.G., Linder, E.V., Miquel, R., Mostek, N., 2004, MNRAS, 347, 909

[209] Kirkman, D., Tyler, D., Suzuki, N., O'Meara, J.M., Lubin, D., 2003, ApJS, 149, 1

[210] Klein, O., *New Theories in Physics*, 77, Intern.Inst. of Intellectual Co-operation, League of Nations (1938)

[211] Kleinert H., Schmidt, H.-J., 2002, Gen. Rel. Grav. 34, 1295

[212] Kluske, S., Schmidt, H.J. 1996, Astron. Nachr., 37, 337

[213] Knop R.A. et al., 2003, ApJ, 598, 102

[214] Koivisto, T., *Phys. Rev.* **D 73**, 083517 (2006)

[215] Krauss, L.M., White, M., *Ap. J.* **397** (1992) 357

[216] Koivisto T., 2007, Phys.Rev.D76, 043527

[217] Kormendy, J. 1977, ApJ, 218, 333

[218] La, D., Steinhardt, P.J., *Phys. Rev. Lett.* **62** (1989) 376

[219] La Barbera, F., Busarello, G., Capaccioli, M. 2000, A&A, 362, 851

[220] La Barbera, F., Merluzzi, P., Busarello, G., Massarotti, M., Mercurio, A. 2004, A&A, 425, 797

[221] La Barbera, F., Covone, G., Busarello, G., Capaccioli, M., Haines, C.P., Mercurio, A., Merluzzi, P. 2005, MNRAS, 358, 1116

[222] Lahav O., et al., 2002, MNRAS, 333, 961

[223] Le Borgne, D., Rocca - Volmerange, B., Prugniel, P., Lancon, A., Fioc, M., Soubiran, C. 2005, A&A, 425, 881

[224] Levi-Civita, T., *The Absolute Differential Calculus*, Blackie and Son, London (1929)

[225] Lewis, A., Bridle, S., 2002, Phys. Rev. D, 66 103511

[226] Li B., Barrow, J.D., Phys. Rev. D75, 084010 (2007)

[227] Li, B., Barrow, J.D., Mota, D.F., submitted to Phys. Rev. D, gr-qc/0705.3795

[228] Li, B., Chu, M.C., Phys. Rev. D74, 104010 (2006).

[229] Li, B., Chan, K.C., Chu, M.C., Phys. Rev. D,in press, astro-ph/0610794 (2006)

[230] Liddle, A.R. 2004, MNRAS, 351, L49

[231] Liddle, A.R., Mukherjee, P., Parkinson, D. 2006, Astron. Geophys., 47, 4.30

[232] Lima Neto, G.B., Gerbal, D., Márquez, I. 1999, MNRAS, 309, 481

[233] Linder, E.V., 2003, Phys. Rev. Lett., 90, 091301

[234] Liske, J., Lemon, D.J., Driver, S.P., Cross, N.J.G., Couch, W.J. 2003, MNRAS, 344, 307

[235] Lobo F.S.N., arXiv: 0807.1640[gr-qc] (2008)

[236] Lue, A., Scoccimarro, R., Starkman, G., 2004, Phys. Rev. D, 69, 044005

[237] Lue, A., Scoccimarro, R., Starkman, G., 2004, Phys. Rev. D, 69, 124015

[238] MacKay, D. J. C., 2002, http://www.inference.phy.cam.ac.uk/mackay/itprnn/book.html

[239] Maeda, K., *Phys. Rev.* **D 39**, 3159 (1989)

[240] Magnano, G., Ferraris, M., Francaviglia, M., *Gen. Relativ. Grav.* **19**, 465 (1987)

[241] Magnano G., SokoLowski, L.M., Phys. Rev. D50, 5039 (1994)

[242] Mannheim, P.D., Kazanas, D., *Ap. J.* **342** (1989) 635

[243] Maraston, C. 2005, MNRAS, 362, 799

[244] Márquez, I., Lima Neto, G.B., Capelato, H., Durret, F., Lanzoni, B., Gerbal, D. 2001, A&A, 379, 767

[245] Martimbeau, N., Carignan, C., Roy, J., 1994, AJ 107(2), 543

[246] Mazure, A., Capelato, H.V. 2002, A&A, 383, 384

[247] McDonald, P. et al. 2005, ApJ, 635, 761

[248] McGaugh, S.S., 2000, Ap. J. Lett. **541**, L33

[249] McGaugh, S.S., 2005, Astroph. Journ., 632, 859

[250] McGaugh, S. S., de Blok, W. J. G., 1998, ApJ, 499, 41

[251] McGaugh, S. S., de Blok, W. J. G., 1998, ApJ, 499, 66

[252] McGaugh, S. S., de Blok, W. J. G., 1998, ApJ, 508, 132

[253] Melchiorri, A., Mersini, L., Odman, C.J., Trodden, M., Phys. Rev. D **68**, 043509 (2003)

[254] Mendoza S. and Rosas-Guevara Y.M., 2007, Astron. Astrophys. 472, 367

[255] Meng X., Wang, P., GRG 36 (8), 1947 (2004); GRG 36 (12), 2673 (2004)

[256] Merlin, E., Chiosi, C. 2006, A&A, 457, 437

[257] Merritt, D., Graham, A.W., Moore, B., Diemand, J., Terzic, B., 2005, astro-ph/0509417 (AJ in press)

[258] Moore, B., Governato, F., Quinn, T., Stadel, J. 1998, ApJ, 499, L5

[259] Moore, B., Ghigna, S., Governato, F., Lake, G., Quinn, T., Stadel, J., Tozzi, P., 1999, ApJ, 524, L19

[260] Mukhanov V.F., Feldman H.A., Brandenberger R.H., 1992, Phys. Rept. 215, 203

[261] Mukherjee, P., Parkinson, D., Liddle, A.R. 2006, ApJ, 638, L51

[262] Multamaki T., Vilja, I., *Phys. Rev. D*, **73**, 024018, 2006

[263] Napolitano, N.R., Capaccioli, M., Romanowsky, A.J., Douglas, N.G., Merrifield, M.R., Kuijken, K., Arnaboldi, M., Gerhard, O., Freeman, K.C. 2005, MNRAS, 357, 691

[264] Navarro, J. F., Frenk, C. S., White S. D. M., 1995, MNRAS, 275, 720

[265] Navarro, J. F., Frenk, C. S., White S. D. M., 1996, ApJ, 462, 563

[266] Navarro, J.F., Frenk, C.S., White, S.D.M. 1997, ApJ, 490, 493

[267] Navarro, J.F., Hayashi, E., Power, C., Jenkins, A.R., Frenk, C.S. et al. 2004, MNRAS, 349, 1039

[268] Navarro, I., van Acoleyen, K. 2005, Phys. Lett. B, 622, 1

[269] Netterfield C.B. et al., 2002, ApJ, 571, 604

[270] Neville, D. 1980, Phys. Rev. D, 21 ,10

[271] Neumann., D. M., Böhringer, H., 1995, Astron. Astrophys., 301, 865

[272] Nojiri, S., Odintsov, S.D. 2003, Phys. Lett. B, 576, 5

[273] Nojiri S. and Odintsov S.D., Int. J. Geom. Meth. Mod. Phys. 4, 115 (2007)

[274] Nojiri S., Odintsov, S.D., 2003, Mod. Phys. Lett. A, 19, 627

[275] Nojiri S., Odintsov, S.D., 2003, Phys. Rev. D, 68, 12352

[276] Nojiri S., Odintsov, S.D., hep-th/06012113 (2006)

[277] Nojiri, S., Odintsov, S.D., 2007, Phys. Lett. B, 652, 343

[278] Nojiri, S., Odintsov, S.D., 2007, Phys. Lett. B, 657, 238

[279] Nojiri S., Odintsov, S.D., Phys. Rev. D accepted (arXiv:0710.1738 [hep-th]) 2007

[280] Nojiri, S., Odintsov, S. D., arXiv:0801.4843 [astro-ph] 2008

[281] Nolta, M. R., et al. *Ap. J.* **608**, 10 (2004)

[282] Noordermeer, E., van der Hulst, J.M., Sancisi, R., Swaters, R.S., van Albada, T.S. 2007, astro-ph/0701731

[283] Nordin, J., Goobar, A., Jönsson, J., 2008, JCAP, 02, 008

[284] Olmo, G.J. 2005, Phys. Rev. D, 72, 083505

[285] Padmanabhan, T., Phys. Rev. D, 66, 021301, 2002

[286] Padmanabhan, T. 2003, Phys. Rept., 380, 235

[287] Padmanabhan, N., Seljak, U., Strauss, M.A., Blanton, M.R., Kauffman, G. et al. 2004, New Astron., 9, 329

[288] Palatini, A., *Rend. Circ. Mat. Palermo* **43** (1919), 203

[289] Peebles, P.J.E., Rathra, B. 2003, Rev. Mod. Phys., 75, 559

[290] Percival W.J. et al., 2002, MNRAS, 337, 1068

[291] Perlmutter S. et al., 1997, ApJ, 483, 565

[292] Perlmutter S. et al., 1999, ApJ, 517, 565

[293] Persic, M., Salucci, P., Stel, F. 1996, MNRAS, 281, 27

[294] Pettorino, V., Baccigalupi, C., Mangano, G., 2005, JCAP, 0501, 014

[295] Pointecouteau, E., Arnaud, M., Kaastra, J., de Plaa, J., 2004, A&A, 423, 33

[296] Pointecouteau, E., Arnaud, M., Pratt, G.W., 2005, A&A, 435, 1

[297] Podariu, S., Daly, R.A., Mory, M.P., Rathra, B., ApJ, 584, 577, 2003

[298] Pope, A.C. et al. 2005, ApJ, 607, 655

[299] Poplawski, N., 2006, Phys. Lett. B, 640, 135

[300] Poplawski, N., 2007, Class. Quant. Grav., 24, 3013

[301] Pratt, G. W., Arnaud, M., 2002, A&A, 394, 375

[302] Pratt, G. W., Arnaud, M., 2005, A&A, 429, 791

[303] Prugniel, Ph., Simien, F. 1997, A&A, 321, 111

[304] Puche, D., Carignan, C., Bosma, A., 1990, AJ, 100(5), 1468

[305] Puche, D., Carignan, C., Wainscoat, R.J., 1991, AJ, 101(2), 447

[306] Quandt, I., Schmidt H. J., 1991, Astron. Nachr., 312, 97

[307] Ramaswamy, S., Yasskin, P.B. 1979, Phys. Rev. D, 19, 2264

[308] Rebolo R. et al., 2004, MNRAS, 353, 747

[309] Refregier, A. 2003, ARA&A, 41, 645

[310] Reiprich, T. H. 2007, Exploring the Cosmic Frontier, ESO Astrophysics Symposia European Southern Observatory, Volume . ISBN 978-3-540-39755-7. Springer, 2007, p. 113, 113

[311] Riess A.G. et al., 1998, AJ, 116, 1009

[312] Riess, A.G. et al., 2004, ApJ, 607, 665

[313] Riess, A.G. et al., 2007, ApJ, 659, 98

[314] Romanowsky, A.J., Douglas, N.G., Arnaboldi, M., Kuijken, K., Merrifield, M.R., Napolitano, N.R.; Capaccioli, M., Freeman, K.C. 2003, Science, 301, 1696

[315] Rosati, P. Borgani, S., Norman, C., 2002, Ann. Rev. Astron. Astrophys., 40, 539

[316] Roscoe, D.F. 1999, A&A, 343, 788

[317] Rubano, C., Scudellaro, P., *Gen. Relativ. Grav.* **37**, 521 (2005)

[318] Ruzmaikina, T.V., Ruzmaikin, A.A., *JETP*, **30**, 372 (1970)

[319] Sahni, V., Starobinski, A. 2000, Int. J. Mod. Phys. D, 9, 373

[320] Sahni, V., Saini, T.D., Starobinsky, A.A., Alam, U., 2003, JETP Lett., 77, 201

[321] Sanchez, A.G. et al. 2006, MNRAS, 366, 189

[322] Sanders, R.H., *Ann. Rev. Astr. Ap.* **2** (1990) 1

[323] Sanders, R. H., McGaugh S. S., 2002, ARA&A, 40, 263

[324] Sarkar, D., Amblard, A., Holz, D.E., Cooray, A., 2008, ApJ, 678, 1

[325] Sciama, D.W., *Mon. Not. R. Ast. Soc.* **113**, 34 (1953)

[326] Schmidt, H.-J., *Class. Quantum Grav.* **7**, 1023 (1990)

[327] Schindler, S., 1999, A&A, 349, 435

[328] Schindler, S., astro-ph/0212104

[329] Schmidt B.P. et al., 1998, ApJ, 507, 46

[330] Schmidt, B.P., Keller, S.C., Francis P.J. et al., *Bullettin of the Americal Astronomical Society*, 37, 457, 2005

[331] Schmidt, H.J. 2004, *Lectures on mathematical cosmology*, gr-qc/0407095

[332] Schmidt, R. W., Allen S. W., astro-ph/0610038, submitted to MNRAS

[333] Schneider, P., Ehlers, J., Falco, E.E., *Gravitational Lenses* Springer–Verlag (1992) Berlin

[334] Schombert, J.M., McGaugh, S.S., Eder, J.A. 2001, AJ, 121, 2420

[335] Schwarz, G. 1978, Annals of Statistics, 5, 461

[336] Seljak, U. et al. 2005, Phys. Rev. D, 71, 103515

[337] Sereno, M., De Filippis, E., Longo G., Bautz, M. W., 2006, ApJ, 645, 170

[338] Sersic, J.L. 1968, *Atlas de Galaxies Australes*, Observatorio Astronomico de Cordoba

[339] Shapiro I.I., in *General Relativity and Gravitation 12*, Ashby N., *et al.*, Eds. Cambridge University Press (1993)

[340] Shapiro S.S., *et al.*, Phys. Rev. Lett. **D 92**, 121101 (2004)

[341] Shimasaku, K., Fukugita, M., Doi, M., Hamabe, M., Ichikawa, T. et al., 2001, AJ 122, 1238

[342] Smith, G. P., Kneib J. P., Ebeling H., Czoske O., Smail I., 2001, ApJ, 552, 493

[343] Sobouti, Y. 2006, astro-ph/0603302

[344] Sofue, Y., Rubin, V. 2001, ARA&A, 39, 137

[345] Sokolowski, L. M., 1989 *Class. Quantum Grav.* **6** 2045

[346] Song, Y., Hu, W., Sawicki, I., *Phys. Rev.* **D 75**, 044004 (2007)

[347] Sotiriou, T.P. 2006, Gen. Rel. Grav., 38, 1407

[348] Speake, C.C. and Quinn, T.J., 1988, Phys. Rev. Lett. **61**, 1340

[349] Spergel, D.N. et al. 2003, ApJS, 148, 175

[350] Spergel, D.N., et al. astro-ph/0603449 (2006)

[351] Spergel, D.N. et al., 2007, ApJS, 170, 377

[352] Starobinsky, A.A. 1980, Phys. Lett. B, 91, 99

[353] Starobinsky, A.A., astro-ph/0706.2041 (2007)

[354] Starobinsky, A.A., 2007, JETP Lett., 86, 157

[355] Stelle, K., 1978, Gen. Relat. Grav., 9, 353

[356] Stompor R. et al., 2001, ApJ, 561, L7

[357] Szalay A.S. et al., 2003, ApJ, 591, 1

[358] The Dark Energy Survey Collaboration, astro - ph/0510346, 2005

[359] Tegmark, M., Taylor, A.N., Heavens, A.F., 2007, ApJ, 4802, 22

[360] Tegmark, M. et al. 2004, Phys. Rev. D, 69, 103501

[361] Tegmark M. et al., 2006, Phys. Rev. D, 74, 123507

[362] Teyssandier P., Tourrenc, Ph., *J. Math. Phys.* **24**, 2793 (1983)

[363] Tonry J.L. et al., 2003, ApJ, 594, 1

[364] Tortora, C., Cardone, V.F., Piedipalumbo, E. 2007, A&A, 463, 105

[365] Trujillo, I., Bukert, A., Bell, E.F. 2004, ApJ, 600, L39

[366] Tsujikawa, S., astro-ph/0705.1032 (2007)

[367] Tsujikawa, S., arXiv:0709.1391 [astro-ph], `to appear in Physical Review D.`

[368] Tully, R.B., et al., 1996, AJ, 112, 2471

[369] Turyshev S.G., Shao M., K.L. Nordtvedt K.L., pre-print: gr-qc/0601035

[370] Tyson, J.A. in *Survey and Other Telescope Technologies and Discoveries*, ed. J.A. Tyson and S.Wolff, page 10, Sidney, 2002

[371] van der Hulst, J.M., et al., 1993, AJ, 106(2), 548

[372] van der Marel, R. 1991, MNRAS, 253, 710

[373] van Waerbecke, L. et al. 2001, A&A, 374, 757

[374] Verheijen, M.A.W., Sancisi, R., 2001, A&A, 370, 765

[375] Viana, P.T.P., Nichol, R.C., Liddle, A.R. 2002, ApJ, 569, 75

[376] Vilkovisky, G., *Class. Quantum Grav.* **9**, 895 (1992)

[377] Vikhlinin, A., Markevitch, M., Murray, S. S., Jones, C., Forman, W., Van Speybroeck, L., 2005, ApJ, 628, 655

[378] Vikhlinin, A., Kravtsov, A., Forman, W., Jones, C., Markevitch, M., Murray, S. S., Van Speybroeck, L., 2006, ApJ, 640, 691

[379] Visser, M., 2004, Class. Quant. Grav., 21, 2603

[380] Vogt, N. P., et al., 2004, Astron. J., 127, 3273

[381] Vollick, D.N., Phys. Rev. D68, 063510 (2003)

[382] Wambsganss, J., Cen, R., Gu, X., Ostriker, J.P., 1997, ApJ, 475, L81

[383] Wands, D., *Class. Quantum Grav.* **11**, 269 (1994)

[384] Wang, Y., ApJ, 536, 531

[385] Wang, Y., Mukherejee, P., 2004, ApJ, 606, 654

[386] Weinberg, S., *Gravitation and cosmology*, Wiley, New York, 1972

[387] Wevers, B.M.H.R., van der Kruit, P.C., Allen, R.J., 1986, A&A, 4, 86

[388] Will, C.M., *Theory and Experiments in Gravitational Physics* (1993) Cambridge Univ. Press, Cambridge

[389] Williams J.G., *et al.*, Phys. Rev. **D 53**, 6730 (1996)

[390] Wood - Vasey, W.M., et al., 2007, ApJ, 666, 694

[391] Young, C.K., Currie, M.J. 1994, MNRAS, 268, L11

[392] Zhang P., 2006, Phys. Rev. D, 73, 123504

[393] Zhang, P., Liguori, M., Bean, R., Dodelson, S., astro-ph/0704.1932, (2007)

[394] Zwicky, F., 1933, Helv. Phys. Acta, 6, 110